UNIVERSITÀ DEGLI STUDI DI CAMERINO

School of Advanced Studies

DOCTORAL COURSE IN

CHEMICAL AND PHARMACEUTICAL SCIENCES AND BIOTECHNOLOGY

XXXVI cycle

ORGANIC-BASED FUNCTIONALIZATION OF COMPOSITE MATERIALS AS A CASE STUDY TO ACHIEVE MATERIALS INNOVATION

PhD Student

Tommaso Compagnucci

Supervisors

Prof. Enrico Marcantoni

Prof. Serena Gabrielli

Dr. Savina Pianesi

"Mancte nova virtute puer

sic itur ad astra"

Virgilio, Aen., IX 641

Author's Declaration

I declare that the work in this dissertation was carried out in accordance with the requirements of the University's Regulations and Code of Practice for School of Advanced Studies, and that it has not been submitted for any other academic award. Except where indicated by specific reference in the text, the work is the candidate's own work. Works done in collaboration with, or with the assistance of others, is indicated as such. Any views expressed in the dissertation are those of the author.

Acknowledgements

This PhD manuscript is the result of three years of work in different laboratories. In this period, I had the opportunity to meet and work with many remarkable people. Without their support, this experience would have been completely impossible, therefore I want to properly thank those people.

First of all, I would like to express my heartfelt thanks to my tutors:

- Professor Dr. Enrico Marcantoni, for the opportunity to perform my PhD in his research group and for the exceptional chance to develop myself as a researcher. Thanks to your support, I was able to acquire unique experiences in my life and that will definitely help me in the rest of my career.
- Dr. Savina Pianesi, for welcoming me like a member of the family of Delta. The friendly atmosphere you created made me feel at home from the first day and it is an important reason why I could finish this thesis. Moreover, I highly appreciate all the times you involved me in industrial projects and valued my opinion in these.
- Professor Dr. Serena Gabrielli, for your advices and suggestions. You often took the time to explain everything in full detail and you made sure I left your office with something new to think about. Nevertheless, I would like to thank you for encouraging my research and for allowing me to grow as a chemist.

Next, I would like to express my special thanks and appreciation to professor dr. Johan Winne. I am immensely grateful for the period I spent in Ghent in your research groups, which made me grow significantly on a professional and human level. You have been an inspiring mentor for me and it has been an honour to work with you.

Of course, I cannot forget all the members of the Marcantoni's research group. Genny, Dario, Martina, Roberto, Vishn, Francesca, Edoardo and Gabriele, you made my life in the lab a lot easier and more enjoyable.

At the same level, I would like to thanks all the "family" of Delta, in particular Claudio, Samuele, Federica, Francesco, Filippo, Alice, Cristiana, Daniele and Riccardo. Moreover, I cannot forget my dearest friend, Francesco Lanero: we worked together for a short period, but it was very important in my PhD experience. Thank you for all your hard work, the beers, jokes and so much more. I will always remember the laughs we shared.

Nevertheless, I would like to express my immense thanks to the Winne's research group. Thank you, Kevin: without you, doing research in lab would be so much more difficult. Moreover, I sincerely appreciate your help, especially in the NMR interpretation, and your availability, even if sometimes

I left the hood a little messy. Thank you, Amjad: I cannot describe in a few sentences how important your part was in my period in Ghent. I will always remember all the amazing experiences we had, my dearest friend. Thank you, Mishi: I really appreciated your kindness and your sunny disposition. Thank you, Didi: your availability was disarming; it was a great honour to work with you. At the same level, I would like to thank Bram, Elias, Ellen, Hilde and Marvin. You made my experience unforgettable.

Finally, I would like to thank my parents, Gabriela and Mauro, my brother Giacomo, my grandmother Adriana and all my family for always being supportive and taking an interest in what I was doing. It was not always easy to explain what I was working on, but nevertheless thanks to your support and your listening ear, you made it all a bit easier. Also, a big thanks to all my friends.

And last, but not least, I would like to take the opportunity to thank the most important person in my life: Irene. Since we first met more than 10 years ago, you completely changed my life. With your love and your endless support, bad moments disappeared with a single smile while sharing the good moments made it even more special. You are the biggest reason that I was able to finish this thesis and I will love you forever.

Preface

Nowadays, it is almost impossible to imagine an advanced human society without polymer materials, since they probably afford the best balance of mechanical, technical and economical properties among all the materials. At the same time, it is clearly alarming all the side-effects deriving from an excessive and unregulated industrialization, that lead to a "barbarian" plundering of all the priceless materials that the Earth offers us, including plastics and polymers.

For this reason, the development of innovative properties in polymer materials has becoming a topic of great interest and many organic chemistry approaches can be effectively developed in order to achieve the desired innovation. In this context, intriguing targets are polymers and polymer-matrix composites because these materials have an exceptional versatility and they find application in an endless list of manufactures and products.

One common way to achieve the wanted innovation is to use an adequate additive. Anyhow, some problems could arise from the simple integration of additives in polymers, such as the migration or the incompatibility. An effective way to tackle these problems is to promote a stronger interaction between the polymer matrix and the additive, such as the formation of a covalent bond. Moreover, considering polymer-matrix composites, the heterogeneity of the two distinct phases can lead to different ways of innovations, since it is possible to develop both functionalized fillers or organic additives. Additionally, the polymer matrix is itself another source of possible innovation, since it can be developed to possess an event-triggered (e.g., temperature-triggered) structure that can achieve the desired advanced property.

The work herein proposed was carried out in the Prof. Marcantoni's research group, at the University of Camerino (Italy) with the collaboration of Delta s.r.l. company, from December 2020 to October 2023. The study had the objective to develop innovative properties in polymer-based materials through the use of organic chemistry approaches.

Taking into account the photocatalytic activity of TiO_2 nanoparticles, in *Chapter 1* it is proposed the coating-free functionalization of the surface of polymer materials with titania (TiO_2) through the development of a "Safer-by-Design" (SbD) approach. The concept of SbD is related to the reduction of hazardous side-effects linked to the use of nanomaterials, such as the release of nanoparticles. In this way, the development of a photocatalytic pre-polymer enabled both an efficient integration of nanoparticles in polymer materials and a surface migration of the photocatalyst, necessary to achieve the desired innovation. Therefore, polymethylmethacrylate-based composites (PMMA/TiO_2 and PMMA/SiO_2/TiO_2) were effectively produced and the photocatalytic activity of their surfaces tested

through the degradation of methylene blue (MB), in accordance to ISO 10678:2010. In this sense, it was observed sufficient photo-activity in prototypes having only 0.45% of TiO_2, while greater results were achieved with 0.9%. Moreover, the SEM-EDX analysis confirmed the presence of titanium (Ti) on the surfaces of PMMA/TiO_2 and PMMA/SiO_2/TiO_2 prototypes.

In *Chapter 2*, it is described the development of polyurethane (PU) and polyurethane-acrylate (PUA) materials functionalized with quaternary ammonium salts (QAS). The latter is a common and effective antimicrobial agent and its incorporation in polymer materials is a promising way to achieve antimicrobial polymers. In this way, different approaches were tested. The most promising one was based on the initial quaternization of isoserinol through a stepwise reaction with 1-iododecane and iodomethane. The obtained QAS was effectively characterized through NMR analysis and it was used as a minor component during the synthesis of many PUAs, casting functionalized PUA films.

The last work (*Chapter 3*) was performed during the semester as an exchange PhD student at University of Ghent (Belgium), under the supervision of prof. Winne. In this period, I had the opportunity to study click chemistry approaches with the chemistry and reactivity of triazolinediones (TADs). In this way, the proposed work described a novel reactivity of TAD reagents with activated aryl system, in particular with *ortho*-hindered-*para*-substituted phenols. At the beginning, the reactivity was studied with low molecular weight reagents, demonstrating the formation of Alder-ene products at room temperature and using acetonitrile as solvent. In order to (almost) exclusively form the Alder-ene product, it was found as mandatory the presence of an alkyl group (e.g.,methyl) in position 4 and hindered groups (i.e., *tert*-butyl) in position 2 and 6 of the phenol ring. After these initial experiments, it was explored the reactivity in polymer applications. In this way, a large number of AA-BB copolymers were synthesized. In all cases, the thermo-reversibility of the formed covalent bond was checked through "transclick" reactions. Finally, it was demonstrated the efficiency of Alder-ene adducts to act as thermal-triggered cross-linker in the formation of polymer films starting from natural vegetable oil, generating so new materials starting from renewable feedstock.

Table of contents

Chapter 1: Superficial photocatalytic activity in minnovative materials

1.1. Photocatalytic degradation of pollutants and microorganisms

The worldwide increase of industrialization and overall population are ones of the most important social factors that are influencing human beings and human society. From the last two centuries, the change of customs caused by the transition from a rural to an industrialized society has affected also the interaction of humans with natural environments and the matter rounding them. Besides the incalculable benefits, nowadays, tremendously serious concerns about all the negative aspects that industrialization intrinsically entails, such as the environmental pollution due to anthropic activities and the increase of the number and the concentration of hazardous, toxic and carcinogenic substances, are exponentially raising.

Therefore, the importance of developing smart and eco-friendly technologies to fight both organic and inorganic pollutants, present in air or in wastewater, and pathogenic microorganism, present in wastewater or over materials surfaces, is the motor for a large number of researches. To further emphasize the topic, the World Health Organization (WHO) published a report where it is estimated that 816,000 deaths were caused by water pollution in 2012. Moreover, a 2014-dated WHO report states that 7 million deaths globally were connected from air pollution, 60% of which due to indoor pollution, 53% were from outdoor pollution, and the overlap was from a combination of the two.[1] Additionally, more than 200 organic pollutants were found in the Songhua River, among which Polycyclic Aromatic Hydrocarbons (PAHs), benzenes and pesticides.[2] These pollutants are heavily responsible for the destruction of aquatic ecosystems by increasing the Biochemical Oxygen Demand (BOD) and many of them are classified as hazardous to humans. Similarly, the prolonged persistence of pathogens in wastewater and surfaces is another crucial point. Indeed, it was reported that SARS-CoV-1 virus can be present in hospital wastewater for long times and it is still active after two weeks at 4°C, while at 20°C is inactive after two days. Moreover, even SARS-CoV-2 virus affects drainage systems and it can be present there for long times.[3]

With this view, Advanced Oxidation Processes (AOPs) can afford the best balance between efficiency of target compound degradation and (eco-)sustainability. One of the most important AOPs is the heterogeneous semiconductor photocatalysis, in which powerful oxidizing species are formed after the interaction of light with a semiconductor. The main advantage claimed by photocatalysis is the complete degradation of organic pollutants present in aqueous and gas phases, through

mineralization. This pathway leads to no secondary pollution, since H_2O, CO_2 and inorganic salts are the main products.[4]

Even though the organic substrate can influence the photocatalyst performance, most of the degradation reactions are oxidations caused by the pollutant-independent formation of strongly oxidizing species, namely Reactive Oxygen Species (ROS). Anyway, radical-mediated reductions, like reductive dehalogenation of halo-compounds and reductive metallization of metal ions, are also important processes to achieve the degradation of target compounds and the removal of heavy metals ions from wastewater streams, respectively.[5]

The same photo-induced radical processes and ROS species are involved in the photocatalytic degradation of biological pollutants. Hence, heterogeneous photocatalysis is an effective and innovative way of sterilization, overcoming important drawbacks of traditional methods like chlorination, UV irradiation and ozone treatments.[3] During chlorination disinfection, mutagenetic and hazardous by-product are formed. The formation of hazardous by-products is also noticed during ozone sterilization; moreover, it requires high operating costs. Instead, the UV-treatment is deficient against UV-resistant viruses and it generally suffers of inappropriate penetration power.

In conclusion, important benefits that heterogeneous photocatalysis can offer are eco-friendly sterilization, effective degradation of pollutants in wastewater treatment, efficient air purification, prolonged photocatalytic efficiency over time and the recyclability of the photocatalyst.

1.1.1. History of heterogeneous photocatalysis

The starting point of photocatalytic processes is unequivocally recognized in the work published by Fujishima and Honda.[6] They were the first to develop the electrochemical photo-splitting of water to produce stoichiometric amount of molecular oxygen and hydrogen, giving so a crucial boost in the production of green hydrogen fuel.

The PhotoElectroChemical (PEC) cell used in this work were basically composed by a photo-anode, made of single-crystal rutile TiO_2, and a H_2 electrode (cathode), made of platinum (Pt). When the photo-anode is irradiated by an enough energetic radiation, the photo-excitation of electrons starts to happen in the semiconductor. These electrons are transferred to the acidic aqueous solution through the Pt cathode, that acts as an electron conductor. Hence, photo-excited electrons (e^-) enable the reduction to H_2 at the cathode; meanwhile, at the anode, O_2 is produced by the reaction of water with electron lacunes or holes (h^+), photo-generated in the photocatalyst after the e^- excitation.

Basically, the energy needed to promote these endothermic redox reactions was ensured by the application of an adequate light source to a semiconductor, such as TiO_2. The mechanism of water photo-splitting can be summarized as follows (*Equations 1-4*):

1) e^-/h^+ formation (at TiO_2 photo-anode): $SC + h\nu \rightarrow e^-_{(CB)} + h^+_{(VB)}$

2) Oxidation (at TiO_2 photo-anode): $2\ H_2O + 4\ h^+_{(VB)} \rightarrow O_2 + 4\ H^+$

3) Reduction (at Pt cathode): $2\ H^+ + 2\ e^-_{(CB)} \rightarrow H_2$

4) Overall redox reaction: $2\ H_2O + 4\ h^+_{(VB)} + 4\ e^-_{(CB)} \rightarrow 2H_2 + O_2$

Equations 1-4

SC = semiconductor, CB = conduction band of semiconductor; VB = valence band of semiconductor.

Further studies on PEC cells have proven that the presence of organics with electron donor groups like carboxylic acids, alcohols or saccharides can improve the H_2 production, since they act as sacrificial reductants and hole traps, reacting with photo-generated h^+ at the photo-anode.[7]

Therefore, the possibility to photo-degrade organic substrates concretely emerged. In this regard, a notable. example is the photo-oxidation reaction of CN^-, added in the photo-anode aqueous solution of the PEC cell, to OCN^-, conducted by Bard and Frank.[8] Approximatively in the same years (70s), the first investigations on photo-oxidation of organic compounds with a single semiconductor were conducted. An interesting example, is the 1976-dated work of Carey *et al.* on the use of TiO_2 nanoparticles to promote the dechlorination of polychlorinated biphenyl compounds under UV light irradiation.[9] Moreover, pioneering studies on photocatalytic processes for the water disinfection have settled the basis for many photocatalytic-based antimicrobial materials. As example, it could be interesting to cite the work of Matsunaga, where platinum-loaded TiO_2 photocatalyst were effectively used to inactivate and/or kill various microorganism.[10]

From these initial works, the investigation on photocatalysts and photocatalytic reactions is continuously booming up to the present day. The widening of researches has matched with the expansion of heterogeneous photocatalysis applicability. In this sense, the most relevant applications are water photo-splitting, treatment of wastewaters, air purification, water and/or surfaces disinfection and photo-catalysed reduction of CO_2 (to produce carbon-based chemical in a sustainable way). From all these aspects, it is clear that photocatalysis incorporates a large number of concepts from different disciplines, like semiconductors physic, surface science, photo-chemistry, physical-chemistry, material science and chemical engineering.

Modern studies are focused on the development and optimization of photocatalytic systems, aiming to promote a wider and wider industrial application of this technology by fixing the main problems still affecting heterogeneous photocatalysis. In this regard, important topics to further

investigate and optimize are the photocatalyst efficiency and the semiconductor activation by visible light. These topics will be discussed in *Chapter 1.1.4*.

1.1.2. Mechanism of semiconductor photocatalysis

SemiConductors (SCs) are a class of materials characterized by a band structure, where a Valence Band (VB) and a Conduction Band (CB) are separated by a forbidden gap (band gap). At the normal state, electrons are mostly located in the VB, while the CB is almost completely unoccupied. However, a source of energy, enough intense to overcame the band gap, can promote the electron jump from the VB to the CB.

When the energy is provided by photons, the process is called photo-excitation and, to be effective, the photon energy has to be higher than the band gap. Hence, knowing the band gap energy of the semiconductor, it is possible to calculate the light wavelength required to promote the electron jump. For example, anatase TiO_2 has a band gap of around 3.2 eV. By applying the Planck-Einstein equation (*Equation 5*):

5) $$E = \frac{hc}{\lambda} = \frac{1240}{\lambda}$$

Equation 5

E = band gap energy (eV); h = Planck's constant; c = speed of light constant; λ = exciting light wavelength (nm).

it is possible to calculate that a wavelength lower than 387.5 nm (UV-A region) is required to photo-excite TiO_2.

In the semiconductor, photo-excited electrons ($e^-_{(CB)}$) move to the CB and they leave electron holes ($h^+_{(VB)}$) in the VB, resulting in the photo-generation of charge carrier couples h^+/e^-. Charge carriers are temporary species, defined by an excitation lifetime. To be effective, they should have enough time to diffuse toward the photocatalyst surface and to interact with adsorbed molecules, like O_2 or H_2O, through interfacial charge transfer.[11] However, during the diffusion, recombination processes are quite prominent. The most important recombination path is the relaxation of photo-excited electrons to the VB, with release of energy as heat or luminescence. This relaxation process is caused by the strong Coulomb's force that attracts photo-excited e^- to the lacune and an intuitive comparison could be the attraction effect played by the Earth gravitational field (lacune) to a person during a jump (electron).[12] Moreover, other radiative and non-radiative recombination ways are due to h^+ or e^- traps, in turn linked to crystal structure defects and grain boundaries.[13]

Once reached the semiconductor surface, h^+/e^- couples are involved in redox reactions, forming primary radicals. These radicals further react with other species, forming secondary radicals. Among

them, strongly oxidizing species, commonly indicated as ROS, are the responsible of the photocatalytic mineralization of organic pollutants.[4]

The overall mechanism can be schematized as follows (*Equations 6-10*):

6) Photo-generation of charge carriers: $SC + h\nu \rightarrow e^-_{(CB)} + h^+_{(VB)}$

7) Reduction: $O_2 + e^- \rightarrow O_2^{-\bullet}$

8) Oxidation: $H_2O/OH^- + h^+ \rightarrow \cdot OH$

9) ROS formation: $O_2^{-\bullet} + H_2O \rightarrow HO_2^{-\bullet} + OH^-$

$2\ HO_2^{-\bullet} \rightarrow O_2 + H_2O_2$

$H_2O_2 + e^- \rightarrow \cdot OH + OH^-$

$OH^- + h^+ \rightarrow \cdot OH$

10) Mineralization: $\cdot OH\ /\ O_2^{-\bullet}\ /\ HO_2^{-\bullet}\ /\ H_2O_2 + OP \rightarrow CO_2 + H_2O$

Equations 6-10

The photocatalysis mechanism for anatase TiO_2 is shown in *Figure 1*.

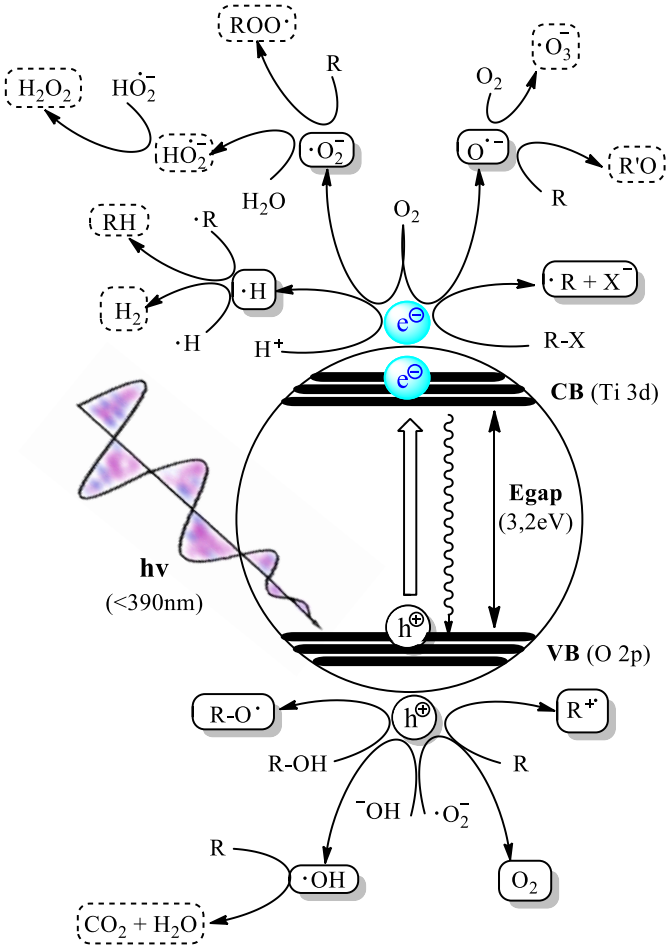

Figure 1 – Photocatalytic mechanism for anatase TiO_2 photocatalyst.

Many electron-donor species, like water, alcohols or hydroxyl anion, can be directly oxidized by photo-generated h^+. Likewise, electron acceptor species, like proton, molecular oxygen or halogenated compounds, can be directly reduced by photo-excited e^-.[5]

The crucial primary radical is •OH, since it is the most active and non-selective initiator of photocatalytic oxidations of organic pollutants. For example, hydroxyl radical easily reacts with alcohols and aromatics forming alkoxide radicals and hydroxylated products, respectively (*Equations 11-12*). [14,15]

11) $$ROH + \cdot OH \rightarrow RO\cdot + H_2O$$

12) $$C_6H_6 + \cdot OH \rightarrow C_6H_5OH + H\cdot$$

Equations 11-12

According to the huge role of hydroxyl radical, semiconductors like TiO_2, WO_3 and ZnO are known as oxidative photocatalysts, since they have in common a valence band potential (E_{VB}) more positive than the reaction oxidation potential (E_{ox}) and, hence, they can catalyse the direct photo-oxidation to ·OH radical. It is important to note that surface-bond hydroxyl groups or -OH moiety of adsorbed compounds have an $E_{ox} \sim +1.6\ V_{NHE}$, while free species like OH^- or H_2O have more positive oxidation potential ($E_{ox} \sim +2.7\ V_{NHE}$), meaning that also the formed hydroxyl radicals will have different oxidative performances.[16] The hydroxyl radicals coming from free species, also known as diffuse hydroxyl radical ($\cdot OH_{free}$), are one of the strongest oxidizing agents, while the adsorbed hydroxyl radicals ($\cdot OH_{ads}$) are less powerful but important as well.

The other crucial primary radical specie is the superoxide radical anion $O_2^{-\bullet}$. In order to catalyse the reduction of molecular oxygen, the conduction band potential (E_{CB}) of the photocatalyst should be more negative than the reaction reduction potential ($E_{red} \sim -0.33\ V_{NHE}$). Superoxide radical is weaker than ·OH; however, it is crucial in the formation of ROS like hydroperoxyl radical and hydrogen peroxide. Moreover, for photocatalysts not able to produce hydroxyl radicals, superoxide radical anion represents the dominant primary radical specie.[17]

The formation of ROS species is fundamental also in the microorganism disinfection. As suggested by Deng, the bactericidal activity of heterogeneous photocatalysis could be roughly summarized in the attack of the cellular membranes of bacteria, enhancing so the permeability of the membrane.[18] The intracellular lipidic membrane peroxidation is usually confirmed by the increased presence of malondialdehyde (MDA), commonly used as a marker of oxidative stress caused by free radicals. At this point, three main mechanisms of degradation are possible (*Figure 2*).

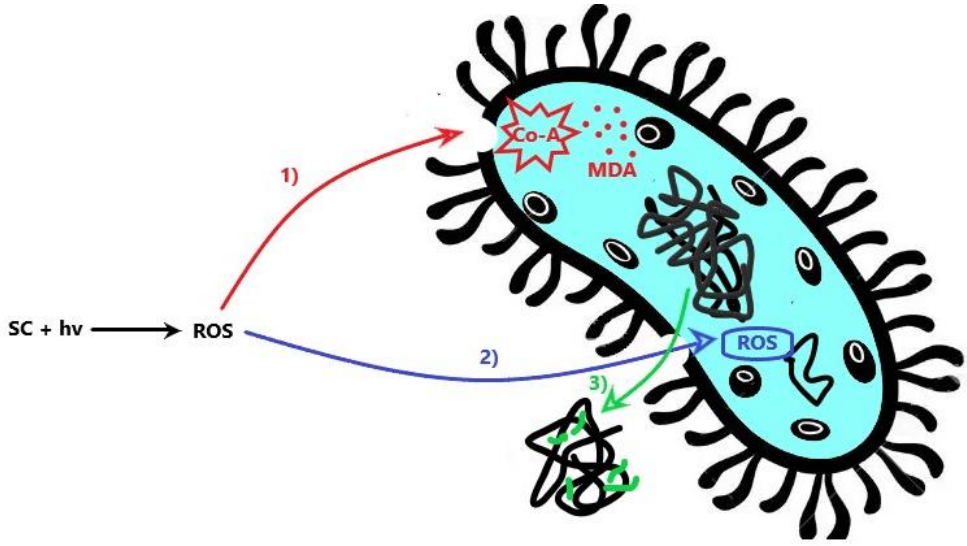

Figure 2 – Degradation mechanism for the ROS-mediated antibacterial activity.

In *Route 1*, ROS attack results in the damage of coenzyme A present on the cell membrane, leading to the reduction of cellular respiration activity and, eventually, in cell death. In this sense, an interesting interpretation could be that coenzyme A in bacterial cells is photochemically oxidized into the dimer form, which inhibited the respiration. In *Route 2*, the increased permeability of cell membrane causes the penetration of ROS inside the bacterium cytoplasm, to give further oxidation reactions with macromolecular components like DNA, RNA or proteins, damaging so internal constituent. Conversely, in *Route 3*, the breaking of cell membrane and cell wall ensures the leakage of internal constituents and, hence, the cell death.

1.1.3. Titanium dioxide (TiO_2) and other photocatalysts

Most of the photocatalysts are semiconductors composed by chalcogenides of transition, post-transition and f-block metals, hence made of an electronegative chalcogen and a metal.

The most used and important is titanium dioxide (TiO_2) because it is cheap, abundant, low toxic, chemical stable and high photoreactive. It is a n-type semiconductor and exists in 3 main crystalline phases (anatase, rutile, brookite). In photocatalytic application, anatase is commonly recognized as the most photoactive, even though it has a quite large band gap (~ 3.2 eV; necessity of UV-A light to promote photo-excitation).

In the last years, a wide number of pristine and modified TiO_2 have been prepared and even commercialized. The comparison of photocatalytic activity and the evaluation of visible light activity of modified TiO_2 photocatalysts is a theme of great debates. In this sense, the work of Ryu and Choi is exemplifying.[19] They conducted the comparison of the photocatalytic performances of 8

commercial variants of titanium dioxide across 19 substrates and they stressed out that "one photocatalyst does not fit all", hence, the necessity to target a specific application to build-up a photocatalyst system more functional as possible. From these results, they stressed out the impossibility to reflect all of the critical factors influencing photocatalysis in a single test assay, suggesting a multivariate statistical analysis as a possible solution to provide a glimpse into the real performance of a photocatalyst.[20]

Besides titania, many other photocatalysts have been used over the years. In *Table 1*, a list of common photocatalysts is given, together with their band gap structure.[21]

Table 1 – Photocatalysts and their band gap structure.

Photo-catalyst	SC type	Crystal structure	Band gap structure/eV			Required λ
			CB	VB	Band gap	
TiO_2	n-type	Anatase	- 0.5	+ 2.7	3.2	387.5 = UV-A
ZnO	n-type		- 0.3	+ 2.9	3.2	387.5 = UV-A
WO_3	n-type		+ 0.2	+ 2.8	2.6	477 = Vis (blue)
CdS	n-type		- 0.9	+ 1.5	2.4	516.5 = Vis (green)
Fe_2O_3	n-type	α-hematite	+ 0.3	+ 2.5	2.2	563.5 = Vis (green)
ZnS	n-type		- 1	+ 2.6	3.6	344.5 = UV-A
SnO_2	n-type		+ 0.5	+ 4	3.5	354 = UV-A
CeO_2	n-type		- 0.6	+ 2.2	2.8	443 = Vis (indigo)
In_2O_3	n-type		+ 0.6	+ 2.1	2.7	459 = Vis (blue)
CuO	p-type		- 1.2	+ 0.8	2	620 = Vis (orange)
Bi_2O_3	p-type	α- Bi_2O_3	+ 0.2	+ 2.9	2.7	459 = Vis (blue)

From *Table 1*, an interesting point is that many photocatalysts possess narrow band gap and, hence, they can be photo-excited by visible light. Anyhow, they commonly possess VB and CB potentials at not optimal positions. For instance, WO_3 and α-Fe_2O_3 have a CB potential more positive than the potential of O_2 reduction and, hence, they are not able to catalyse the single electron reduction of molecular oxygen to superoxide radical anion.[22]

Other interesting observations could arise from the comparison of band gap structures. In this sense, it is evident that TiO_2 and ZnO are quite similar; however, an important drawback of ZnO is the photo-corrosion, since the excitation in aqueous medium induces the weakening of zinc-oxygen bonds, resulting in the formation of O_2 and soluble Zn^{2+}.[23]

The light-induced corrosion is a problem noticed also for cadmium sulfide (CdS).[26] Anyhow, CdS could offer a number of interesting benefits due to its optimal band gap structure, that is enough

narrow to enable the activation with visible light and, at the same time, it ensures the adequate redox potential for a large number of photocatalytic reactions, like photo-splitting of water and the reduction of CO_2.

Another promising photocatalyst is CuO because is one of the photocatalysts with the most red-shifted absorption of light, reaching the orange wavelength region of visible light. Moreover, it is a p-type semiconductor and, when mixed with a n-type semiconductor, p-n junctions are formed in the photocatalyst composite, improving charge separation and photocatalytic efficiency.[24]

Moving to lanthanide chalcogenides, CeO_2 is probably the most important because, besides being cheap, low toxic and stable, the strong reducibility of Ce^{4+} has an important role in photo-degradation. Moreover, it possesses a unique fluorite-type structure, characterized by a large deviation in stoichiometric and a high amount of oxygen vacancies.[12] In this context, oxygen vacancies and Ce^{3+} showed synergistic effect in photo-degradation processes: the reduction of Ce^{4+} acts as e^- trap, preventing so the charge recombination; instead, oxygen vacancies can form colour centres, that are considered the main responsible for the visible light absorption of ceria.

In conclusion, semiconductor photocatalysis is really promising and numerous photocatalysts are available. Anyhow, in literature, a general agreement on important deficiencies affecting the photocatalytic activity of a single and pristine photocatalyst is largely present. Most significative problems are:

- High rate of charges carrier recombination: limitation of photocatalyst performance.
- Large band gap of semiconductors: in many cases, necessity to use UV light.
- Non optimal band gap structure: impossibility to catalyse some redox reactions.
- Complexity of photo-processes: together with photocatalysis, other processes (like fluorescence, phosphorescence, photoconductivity, phototropy, photolysis, …) can simultaneously happen in the system, reducing the rate of photo-oxidation of pollutants.

1.1.4. Methods to enhance photocatalytic activity

Over the years, many approaches have been proposed to improve the photo-activity and the visible light absorption of photocatalysts. In general, an improved photo-efficiency is gained when it is possible to spatially separate photo-generated charges (reducing so the probability of recombination), while an efficient absorption of visible light is linked to the narrowing of the semiconductor band gap. For the latter, the introduction of intra-band gap energy levels can be useful to obtain the photo-excitation with solar light or with low energetic light sources.

As starting point, it is important to highlight that the crystal structure of the semiconductor strongly affects the electronic structure and the charge properties. As already said, different crystalline phases have different band gap structures: for titania, the band gap of anatase ~ 3.2 eV, rutile ~ 3 eV, brookite ~ 3.4 eV. Moreover, also crystal defects are influent. For instance, lattice vacancies in the semiconductor, such as oxygen vacancies, are commonly recognized to be involved in the formation of colour centres and, hence, in the absorption of visible light. [25]

However, crystal defects can lead to negative photo-processes, like radiative and non-radiative recombination, and higher crystallinity may help to reduce crystal defects, with a general improvement of photo-efficiency. Moreover, also the particles size plays an important role, since the shorter the diameter, the higher the surface area and the adsorption sites for target molecules. Equally significant is the shortening of the diffusion pathway of charges gained by the reduced size of the photocatalyst, leading to a significant reduction of charges recombination.

Besides these initial considerations, the most important ways to improve the photocatalytic activity of a semiconductor are:

A. metal and non-metal ion doping;
B. noble metal surface deposition;
C. semiconductor composites.

A. <u>Metal and non-metal ion doping:</u>

A significant way to improve the performance of a photocatalyst is the ion doping. The scope of doping is to introduce foreign elements in the host matrix, without giving rise a new crystallographic phase. In this way, impurities energy levels are introduced in the system: when the new levels are intra-band gap, then they can narrow the band gap of the pristine semiconductor and promote the photo-excitation with visible light.[26] According to the amount of dopant, new energetic levels can be temporary localized electronic states (low amount of dopant) or permanent extrinsic dopant band (by doping at sufficient level). To be effective, these imported states should have both low probability for back electronic decay and negligible activity as recombination centres.[27]

Cations usually employed are transition metals (Co, Fe, Cu, …) or rare-earth elements (La, Ce, Eu). They insert d- or f- orbital energy levels close to the CB of the pristine semiconductor, where electrons can be excited by less energetic photons. Besides that, the substitution of host ion (e.g., Ti^{4+} of titania) with dopant causes the formation of crystal defects: the more the difference in ionic radii, the more crystal defects are created. These defects can be recombination centres, but also colour centres. Another consequence is the increase of charge separation caused by the redox capability of

the dopant, that may play as h^+ or e^- acceptor, leaving so the counter-charge "free" in the semiconductor.

In this sense, an interesting example is the doping of TiO_2 with cerium cations.[28] The reduction of h^+/e^- recombination was confirmed through photoluminescence spectroscopy, demonstrating the lower intense photoluminescence (so lower recombination) of Ce-doped TiO_2 than pristine one. Additionally, another study has proved the red-shifted absorption of Ce-doped TiO_2 than pure titania, pure ceria and the equimolar mix of them.[29]

When the redox capability of the dopant is too high, negative effects can arise. For instance, the rapid and switchable states of Fe dopant (Fe^{2+} and Fe^{3+}) in the doping of TiO_2 was indicated as a source of problems, since it may lead to shorter charge lifetime, drastically reducing the efficiency. Anyhow, it was proven the greater photocatalytic performance of Fe^{3+}-doped TiO_2 than the pristine one in the photo-degradation of organic pollutants, providing also evidences of the visible light absorption due to the introduction of the 3d orbital above the VB of TiO_2.[30]

Moving to the non-metal ion doping, it is largely used and the main dopants are N, C, S, P, B, Si and halogen anions. In a similar way to the metal, the non-metal doping is characterized by the introduction of intra-band gap p-orbital; and the substitution of chalcogen anion with dopant anion or vacancy creation, with formation of colour centres.[4] In *Figure 3*, it is proposed the band gap structure of the N- and S-doped titania, respectively.

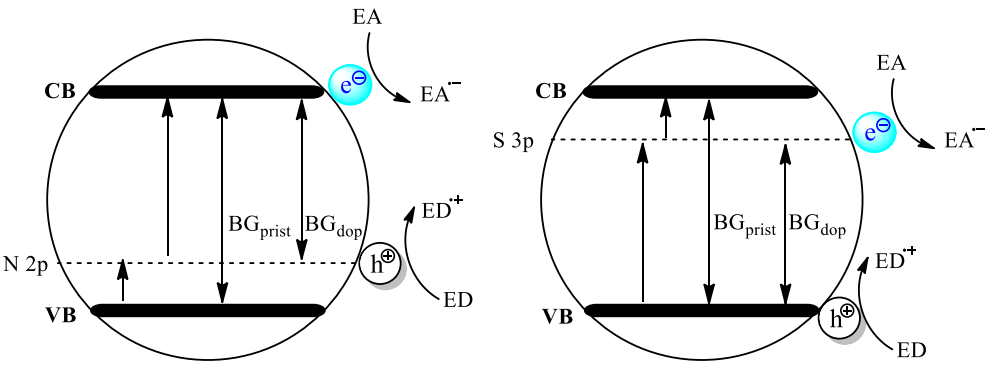

Figure 3 – Band gap structure of N-doped (left) and S-doped (right) TiO_2.

With S-doping, a new electronic level is inserted below the CB, while with N-doping above the VB. This implies a less powerful reductive and oxidative potential in the S- and N-doping, respectively, as expected by the position of new energetic levels. It is newsworthy to note that this problem is not limited to non-metal doping but to the technique itself, since the formation of intra-band gap level is the fundamental outcome of doping. Hence, the doping technique can be limited by lower redox potentials.[25]

Moreover, examples of mixed doping are even reported in literature. In 2017, Chen and Liu prepared Ce/N-doped TiO_2 over diatomite and they effectively used it for the degradation of oxytetracycline.[31] In this catalytic system, diatomite was the site of adsorption, while the co-doping resulted in the insertion of a N 2p orbital over the VB and a Ce 4d state below the CB, narrowing the band gap and allowing a greater visible light absorption.

B. Noble metal surface deposition:

Other relevant ways to increase the photo-efficiency are the noble metal surface deposition and the formation of semiconductor composites. Their action mechanisms are quite similar and, in both cases, the formation of a heterojunction causes a built-in electric field and the change in electronic distribution, resulting in the enhancement of charges mobility and separation. In this way, metallic Pt, Au, Ag, Ru and Pd are commonly used in the surface decoration of a semiconductor. At the semiconductor surface, the contact with noble metal results in the formation of a junction (e.g., Schottky junction). The latter is involved in the capture of e^- from the CB of the semiconductor to the noble metal. Hence, the deposited metal acts as electron reservoir, while h^+ are confined in the semiconductor: the main consequence is the spatial separation of charges and, so, the suppression of recombination.[25]

C. Semiconductor composites:

In semiconductor composites, the heterojunctions are formed by the mixing of two or more photocatalysts or crystalline phases, leading to multi-component and multi-phases composites, respectively. Since the unique nanoscale interaction and the band alignment created by the heterojunction, the vectorial transfer of charges happens. Basically, due to energetic reasons, excited electrons tend to move to lower energetic electronic states, while generated lacunes to higher levels. With the formation of heterojunctions, interfacial transfers between the bands of different components or phases are possible.[32] Depending on the band positions of semiconductors, 3 types of heterojunctions can be formed (*Figure 4*).

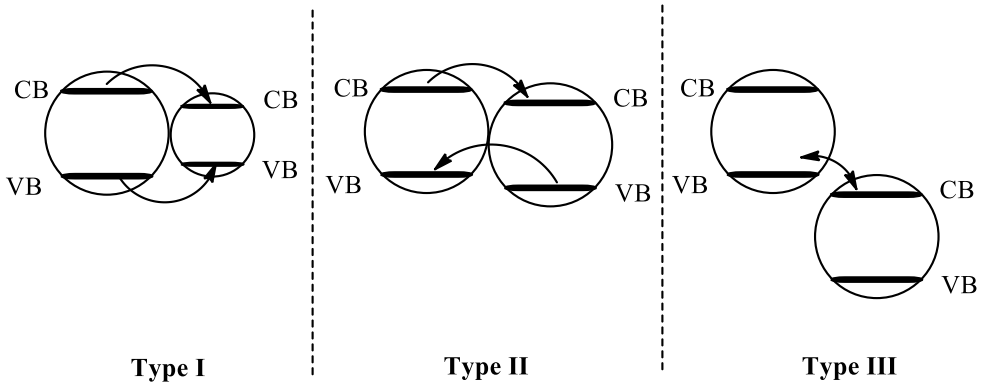

Figure 4 – Heterojunction formation in photocatalyst composites.

The best heterojunction is type II because it results in the spatial separation of charges, improving so the photo-efficiency. The worst one is type I, where charges are accumulated in only one semiconductor. This is the case of WO_3/TiO_2 system, where all photo-generated charge carriers are transferred to WO_3. Finally, in type III heterojunctions, the band positions are even further set off than type II semiconductors and the charge separation can be achieved when electrons of one semiconductor recombinase with holes of the other photocatalyst.

Nice examples of type II heterojunction are CdS/TiO_2 and SnO_2/TiO_2. Indeed, in both cases, an effective charge separation is obtained by their band alignments. In the first case, the main feature is the visible light activity of the photocatalyst composite, due to the narrow band gap of CdS. Moreover, the possibility to prepare CdS quantum dots can be used to tune the electronic properties by playing with size.[33] Moving to the second case, UV-activation is required due to the large band gap of the involved semiconductors. However, thanks to the optimal band positions, a stronger oxidation potential is obtained by the SnO_2/TiO_2 system, meaning that a larger number of photo-oxidation reactions are promoted by this photocatalyst composite.[34]

Another promising photocatalyst composite is CeO_2/TiO_2. In this sense, a nice application of this system, obtained by a simple sol-gel synthesis without any surfactant, is the visible light photo-degradation of tetracycline. Besides the interesting photocatalytic activity, the authors noticed that the presence of CeO_2 helped to control the anatase crystallinity, limiting the rutile phase.[35]

Finally, a very interesting example of multiphase composite is the mix of anatase and rutile titania nanoparticles, commercially known as P-25 (~ 80:20 of anatase and rutile, respectively). Compared to pure anatase or rutile, P-25 ensures greater photocatalytic performances due to synergistic effects and to the formation of a heterojunction between the two crystalline phases.

1.1.5. Common preparation methods

A multitude of structures and systems can be prepared to achieve the best photocatalytic performance. According to the larger surface area and the shorter diffusion paths, nanometric dimensions are commonly preferred, even if micrometric photocatalysts have proven adequate photocatalytic activity as well.

Different shapes of longitudinal nanostructures are possible, like nanoparticles, nanowires, nanotubes, nanorods and even more complex structures. For instance, Deng and coworkers have proposed the synthesis of hallow spheres of CeO_2 through an interesting template sol-gel synthesis over PSAA (PolyStyreneAcrylicAcid, with superficial -COO^- groups), followed by calcination.[36] The increased photo-activity of hallow spheres was gained by internal reflection of excitation light and the consequent enhancement of photo-absorption by the semiconductor.

For the purpose of this thesis, the attention will be focused on the main methods for the preparation of NanoParticles (NPs) of pristine or modified photocatalysts. Preparation methods can be divided in solid-phase, liquid-phase and gas-phase methods.

In solid-phase methods, raw materials are mixed and ground with a certain stoichiometric ratio and, eventually, calcinated at high temperatures.[21] In this context, a good example is the formation of CeO_2/g-C_3N_4 nanocomposite via ball milling method. The study emphasized the role of the ball milling for the enhancement of the interface interaction of semiconductors and the formation of heterojunctions in the system, with consequent improvement of photocatalytic activity.[37] In general, solid-phase methods are commonly used in the preparation of photocatalyst composite because they do not require any solvent and the apparatus is generally cheap and simple. The most important drawback is the possible formation of hard agglomerate of nanoparticles. Indeed, the agglomeration predisposes the nanoparticles to a potential loss of nano-geometry and surface composition, negatively affecting the photocatalytic performance.

Liquid-phase (or wet chemical) methods are the most frequent for the production of pristine and modified NPs, especially at laboratory scale. Among them, the sol-gel method is probably the most popular for the synthesis of TiO_2-based nanoparticles.[38] A general scheme of sol-gel synthesis, together with the possible nanostructures this method can provide, is proposed in *Scheme 1*.

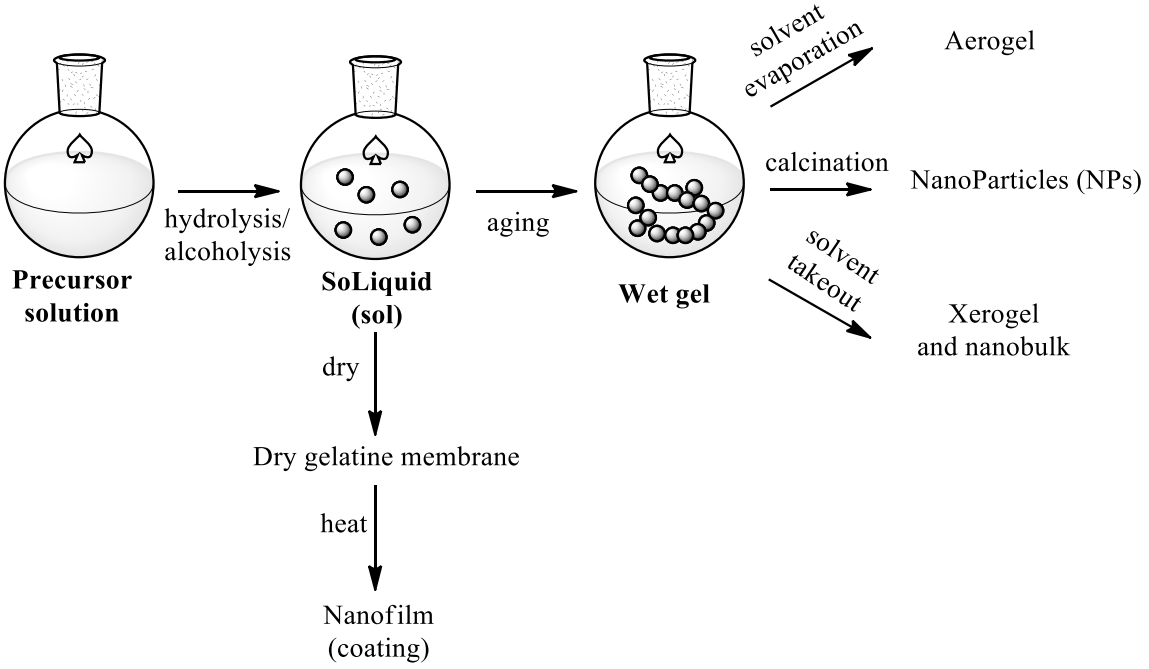

Scheme 1 – Sol-gel synthesis and its application for the development of many nanostructures.

Firstly, precursors of photocatalyst (soluble metal salts) are dissolved in the solvent, forming the precursor solution. At this step, the addition of small amount of metal or non-metal dopant in the precursor solution will result in the doping of the semiconductor. In any case, hydrolysis or alcoholysis of precursor leads to the formation of the colloidal solution (sol); then, through hydrolysis and condensation reaction, the aging of the sol results in the gel. In the last step, a heat treatment provides high pure nanoparticles with size uniformity. Therefore, a facile control of the reaction is possible by governing specific parameters like solution pH, solution concentration, dopant concentration (if present), reaction temperature and reaction time. Moreover, the method is quite simple and cheap. However, the use of solvent and metal alkoxides is quite hampering for industrial applications.

The ease of doping in sol-gel methods is one of the reasons of its wide application. For example, the cerium doping of TiO_2 is commonly performed by the preparation of two precursor solutions: the Ti (IV) solution, made of a titanium salt (e.g., titanium tetrabutoxide or tetraisopropoxide) dissolved in water or ethanol; and the dopant solution, composed by the dopant salt (usually, cerium (III) nitrate) in (acidic) water or ethanol. After that, the dopant solution is slowly added to the other one, under a vigorous stirring. The dopant concentration will affect the photocatalyst outcome: low amounts could result in the formation of localized dopant states with low lifetime; oppositely, excessive quantities of the dopant may produce a large amount of corresponding oxide (in this case, CeO_2 after calcination) at the TiO_2 surface and, hence, multi-phase photocatalyst composite rather than doped

titania. After the Ce-Ti sol formation, a period of aging provides the gel and, after solvent removal and calcination, the $Ce^{3+/4+}$-doped TiO_2 nanoparticles.[39]

An approach similar to sol-gel is the precipitation method. In this case, after the mixing of components, a precipitant is added in the solvent, gaining a precursor precipitate. After that, a thermal treatment is performed, obtaining photocatalyst nanoparticles.[40]

Conversely, in the hydrothermal method, inorganic or organic compounds are mixed in an aqueous solution at high temperatures (100-350°C) and high pressures. The resulting substances are filtered, washed and dried to gain ultrafine particles of high purity. The hydrothermal method is also employed in the preparation of films, made at liquid state without any post-treatment.

A simpler way to obtain a film is the liquid deposition method. In this case, the substrate is immersed in an appropriate reaction solution and, after a post-treatment at relatively low temperature (according to the used solvent), a dense and uniform film is deposited onto the surface; however, compared to hydrothermal films, these coatings have less adhesion to the substrate.

Finally, gas-state methods have in common the use of a gas to promote a physical transformation or a chemical reaction. Many times, a gas carrier is used to carry a substance in the gas state, where the reaction happens. In this regard, the chemical vapor deposition is generally used to form thin films (e.g., nitrides, carbides, metals, …) by the chemical reaction of 2 or more gases, while, in physical vapor deposition, a hard coating is formed by the vaporization and deposition of a substance over a substrate through techniques like vacuum deposition, sputtering or ion plating. Therefore, it is clear that an advanced and expensive apparatus is required for gas-state methods.[21]

1.2. Photocatalysis in innovative materials: the key role of the integration

In many industrial sectors, nanotechnologies have opened the way to achieve materials innovation, achieving novel functionalities and improved characteristics, such as higher durability, fire resistance, thermal stability, self-cleaning and photocatalytic properties. In this context, the development of engineered nanoparticles, which, by convention, mean objects having at least one dimension within the nanometer range (1-100 nm), has become a tremendous important topic.

Therefore, a relevant point to figure out relies on how to exploit the powerful photoactivity of semiconductor nanoparticles to develop innovative materials. The integration of the photocatalyst is an appealing challenge, promoting particular topics like photocatalytic cement-based coatings, concrete nanotechnology, renewable photocatalysis in concrete, nano-inclusions applied in cement-matrices, photocatalytic glass and many others.[41]

When a new photocatalyst is developed, the integration step is often not considered and the performance is frequently analysed through tests based on the direct contact of photocatalyst and target pollutant, such as by mixing the semiconductor powder directly in the aqueous solution containing the pollutant. With these conditions, the photoactivity is generally maximized because both the photoexcitation and the formation of radicals and ROS are favoured by the constant interaction between involved species. Anyhow, this model represents an ideal situation and it is quite far from a real case, especially if you consider functionalized solid materials.

Taking into account the most important progress in photocatalytic innovative materials, a significant resonance had come from TiO_2-based construction and building materials. Construction materials are clearly significant because they are directly exposed to people and the environment, affecting the indoor and outdoor environment in a strong way. Therefore, the application of heterogeneous photocatalysis to building materials could influence significantly the life quality of a community, providing an efficient, durable and eco-sustainable reduction of indoor and outdoor pollution, with interesting application also as antimicrobial materials.

In order to achieve a functional and durable photoactivity, TiO_2 should retain its photocatalytic performance after the integration, but, at the same time, it should be strongly anchored to the material. Indeed, the leaching of the photocatalyst from the functionalized material to the pollutant solution and/or in air should be avoided both to increase the efficiency over time and to reduce the release of free and potentially hazardous nanoparticles.

Another crucial point is the necessity to ensure the direct interaction of the semiconductor with the exciting light to generate radicals. Considering both the penetration strength of photons inside a material and the necessity to generate ROS from the interaction of excited photocatalyst with adsorbed molecules, such as H_2O or O_2, the superficial enrichment of functionalized material with photocatalyst is mandatory.

A final consideration has to be set on ROS-mediated processes, remembering that the photocatalytic-promoted degradation is strong, but also non-specific. The non-specificity of ROS reactions can play a double game, because the degradation processes can affect both target compounds but also host matrices or binders. Relevant consequences could be the lowering of the durability of the photocatalytic treatment and, even more alarming, the generation of potentially hazardous by-products from the photo-oxidation of the organic host matrix.

From these aspects, it is evident that the integration step is crucial to develop an innovative material with photocatalytic activity and the step is really short from an innovative material to a possible “problem-making” material. Integration approaches could be divided in the inclusion of TiO_2 in any of the forms of building materials by using NPs as a component of cement, concrete or mortar

or in the immobilization of titania onto the external surfaces of other materials, such as onto construction tiles, by the application of photocatalytic coatings.

In the following subchapters, the main progress in photocatalytic materials will be explored, with focuses on the integration approaches and on the durability of common photocatalytic treatments.

1.2.1. Inclusion of photocatalyst in building materials

Besides the low costs, the stability and the high photocatalytic activity, TiO_2 is commonly preferred in building materials because the good compatibility with traditional construction materials. In recent years, several advanced approaches have been developed to integrate nanometric titania inside construction materials, such as concrete, mortar, pavements, paints, etc., aiming to produce TiO_2-based building materials like tiles, coated glasses, films and tent material. For example, coating a layer of cement with a photocatalytic film has been demonstrated to decrease pollution levels in confined indoor environments. It must be noted that traditional air purification technologies are less efficient and economically less competitive for the treatment of low concentrations of pollutants present in indoor air streams.[42]

The inclusion technique can either be by mixing or dispersing the photocatalyst into the matrix of the building material. The mixing process can be categorized as either synchronous or ad-mixing, depending on the stage at which the mixing of TiO_2 is performed. The worst aspect of mixing processes is the agglomeration of particles, since the small sizes and the high surface energy of TiO_2, as well as the Brownian motion of the nanoparticles, can cause agglomeration, reducing so the photoactivity but also the mechanical strength of the material.[43]

Alternatively, dispersion techniques can be a better approach to fix agglomeration problems. For example, the bead or ball milling techniques have been attempted to disperse NPs. They are low cost and environment-friendly approaches, with high efficiency, controllability and large-scale applicability in industries. Anyhow the difficulty of handling the process with slurries having high solid fractions is a serious problem.[44]

A different and more efficient way to disperse sub-micro sized particles is the ultrasonic irradiation. The agglomeration of particles can be prevented by the shock waves generated from ultrasonic irradiation and collapsing cavitations; however, ultrasonic irradiation is an expensive and energy-intensive technique.[45]

Another way to circumvent aggregation problems relies on the use of water-reducing admixtures, like treatments with plasticizers, superplasticizers and surfactant. This approach is based on the modulation of the surface potential in order to prevent the agglomeration of semiconductor NPs.

Despite the inclusion techniques, the preparation of cement-based photocatalytic materials, namely "white cement" resulted in the booming of the TiO_2-inclusive concrete over the years. White cement has been effectively used for NOx removal, especially for outdoor applications, showing a greater efficiency in pollutants removal compared to concrete made of normal "grey" cement. This aspect could result in a decrease in many environmental problems, like acidification, ecotoxicity, eutrophication, human health degradation factors and smog formation.[46]

Among the numerous publications on TiO_2-inclusive concrete, some interesting studies are herein reported. The first one is focused on the NOx removal capacity of photocatalytic blocks of concrete, where different TiO_2 additives (TiO_2 as reference catalyst, and two doped titania, Fe-TiO_2, and V-TiO_2) were included.[47] The authors investigated the photocatalytic NOx abatement varying the composition of the concrete and they found that higher amount of $CaCO_3$ was a positive factor, suggesting its probable reaction with the final product of NOx photo-degradation, namely nitric acid. Moreover, the additional role of visible light photo-degradation was proven by the increase in NOx removal percentages of the mortars with the doped additives (Fe-TiO_2 was the most effective).

Another remarkable work, published in 2017, compared the nitrogen monoxide (NO) removal capacity of TiO_2-inclusive cementitious materials between wet and dry conditions.[48] The authors stressed out that the wetting condition plays a critical role in achieving a reasonable NO removal rate because the photocatalyst requires the presence of water to generate ROS. Anyhow, an excessive humidity can may raise an absorption competition with pollutant molecules, with negative consequences to the photocatalytic performance.

A different example is provided by the TiO_2-inclusive self-compacting glass mortar, where recycled broken glass pieces from a local glass beverage bottle were used as the aggregate and mixed with TiO_2 for evaluating photocatalytic NOx degradation.[49] While HNO_3 is the generally expected final photocatalytic NOx degradation product from cementitious materials, in this case it was reported the major formation of NO_2^- in place of NO_3^- as products of NOx photo-degradation. This means that nitrous acid (HONO) rather than nitric acid (HNO_3) may be largely formed, due to the larger presence of NO_2^- in the atmosphere, causing so the generation of even more hazardous secondary pollutants.

1.2.2. Photocatalytic coatings

Photocatalytic coatings are designed to confer an effective immobilization of the photocatalyst onto the surface of the material. An interesting feature is the possibility to retain the aesthetic characteristics, both for concrete, stones and other porous or non-porous building materials. Commonly, the coating can be made through two different approaches.

a) Photocatalytic paint

Titanium dioxide is largely used as a pigment to obtain white coloration and, in paint applications, the most used TiO_2 is the micrometric rutile, since its white brightness. A paint is generally composed of different components, such as binders, fillers, pigments, solvents, diluents, dispersing, stabilizer, thickeners and antifoam. Each components plays an important role. For example, the polymeric binder brings the adhesion to the substrate and the chemical resistance, while fillers reduce costs and enhance the physical properties. Moreover, it is quite common to use nanoparticles (e.g., SiO_2 NPs) in commercial paints because they positively affect the mechanical properties, the UV resistance and the rheological properties of paints.[50]

Due to the high dispersibility of TiO_2 in water, waterborne paint is commonly used. A conventional waterborne paint is prepared in two steps. In the first one, the so-called mill base is formed in a water dispersion by the mixing of the pigment, fillers, stabilizer, thickeners and auxiliary solvent; in the second step, the mill base is blended with the binder, a polymer latex, obtaining the waterborne paint.

Over the years, many attempts have been involved to develop a photocatalytic paint using nanometric anatase in the paint formulation. In a similar way to micrometric rutile pigment, the aim is to incorporate NPs in a (commercial) polymer host matrix. Once the photocatalytic paint is formed, it can be applied just by dipping the material surface inside the paint or by painting (for example a wall) with a brush. After that, a period of drying is generally required.

In this context, an interesting example is the preparation of an anatase TiO_2 dispersion in ethylene glycol, applied onto porous and non-porous materials, namely Noto stone and Carrara marble surfaces.[51] The authors stated the formation of a photocatalytic coating onto these surfaces through photo-degradation tests of organic pollutants in air; moreover, they highlighted both the aesthetic compatibility and the improved capillary absorption coefficient after the treatment.

Another interesting example is reported by Kim *et al.* in 2021 and it is based on the use of hydrophilic/hydrophobic silane-grafted TiO_2 NPs in the formulation of new photocatalytic paint for VOC (Volatile Organic Compounds) remediation.[52] The modified NPs were used as a component (from 10 to 20% wt.) of standard paint formulations, made of a binder (commercially available acrylic latex; 45 wt.% concentration in water) and fillers ($CaCO_3$ powder). An extensive comparison of the photocatalytic degradation of NOx pollutants for parent titania, modified anatase titania and paints, containing parent or modified anatase and coated onto a ceramic plate (dried at room temperature for 24 h). A simple scheme of the modification of anatase TiO_2 and the action way of modified NPs inside the waterborne paint is reported in *Figure 5*.

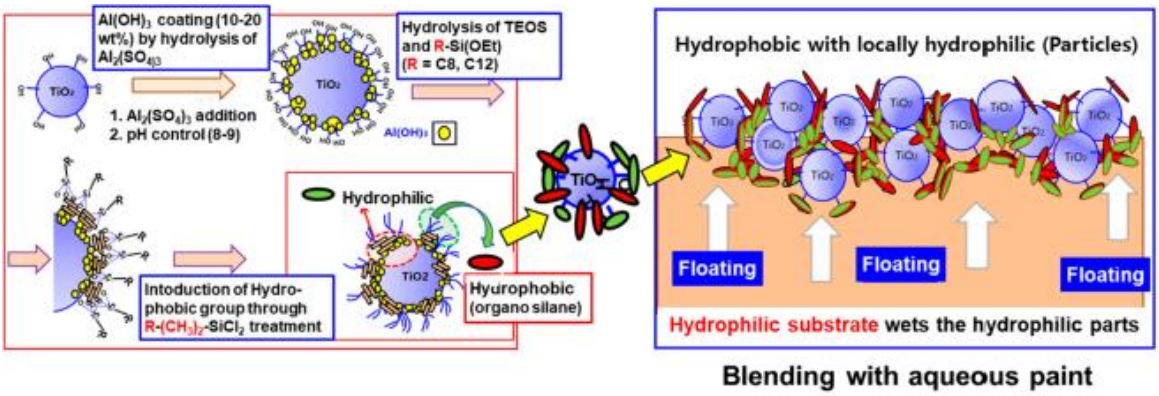

Figure 5 – On the left: modification of anatase titania with $Al(OH)_3$ and hydrophilic and hydrophobic silanes; on the right: incorporation of modified NPs in the paint and the floating of NPs toward the solid-air interphase.

The modification of the parent anatase titania was performed with $Al(OH)_3$ and a number of silanes. Aluminium oxide is frequently used as an inorganic coating for TiO_2 because it can increase the amount of -OH groups present on the surface of NPs. Additionally, the use of silane coupling agents is a common and versatile technique to modify TiO_2 and other metal oxide NPs, providing both the formation a covalent Ti-O-Si bond between the silane and NP and the modification of the surface energy of the photocatalyst.

Aiming to maximize the degree of exposure to the surface while maintaining the strong bonding strength with the paint, the authors suggested the necessity to keep the hydrophilic and hydrophobic regions at an appropriate ratio on the surface of titania. In this way, the uniform dispersion in photocatalytic paint and the strong bonding with the prevailing organic matrix have been simultaneously achieved.

Finally, they demonstrated the higher photocatalytic activity of pristine titania rather than the modified one, when used as powder. However, they also observed a stronger photo-activity of the photocatalytic paint containing modified titania than the parent one. Finally, they proven the UV stability of photocatalytic paint with modified TiO_2 through accelerated aging tests with a UV lamp.

b) Photocatalytic spray coating

Using suitable formulations, the direct application of NPs onto the material surface through spray techniques could present several advantages, such as the preservation of the aesthetic appearance of the treated surface and the formation of a uniform covering surface. For this reason, one of the most promising applications is for the cultural heritage conservation and an important material case study is surely stone, because it is widely used since ancient times and it is the material of many of historical constructions, sculptures, and monuments. Long-time exposure to weathering conditions and

atmospheric pollution can cause significant changes in the visual appearance of their surface. Typically, the surface of the stone is subjected to deterioration over time due to various sources, including the interaction with polluting gases and fine particulates, that may result in the alteration of the visual appearance, with phenomenon like blackening of architectural surfaces, besides the loss of the original structural features of the material. Moreover, biotic factors, such as the growth of microorganisms and biofilm formation, can cause the degradation of stone surfaces.[53]

Some interesting studies have been focused on the development of functional coatings based on TiO_2 NPs in the process of protecting monuments and artworks of historical and architectural nature.[54] Photocatalytic coatings provided the prevention of the bio-deterioration, the reduction of the formation of black crusts and salts, and hydrophobic properties to the surface. The last aspect resulted in the reduction of the penetration of water into the pores and the percolation, all this coupled with the retain of the aesthetic appearance.

A promising example of spray coating approach has been the photocatalytic coating formation on Lecce stone surfaces, using TiO_2 nanorods.[62] In this work, nanorods have been synthesized through a "hot-injection" method, based on the aqueous base-catalysed hydrolysis of titanium tetraisopropoxide in presence of oleic acid (used as coordinating and capping agent, to prevent aggregation or suspended matters), at quite high temperatures (80-100°C) under nitrogen overpressure. The rod shape was chosen because it allows a surface chemistry suitable for the dispersibility and processability in the non-polar organic solvent. Nanorods were dispersed in n-heptane or chloroform and, then, the spray coating, through a nitrogen cylinder connected to a gas nebulizer, allowed the immobilization of nanorods onto Lecce stones surface. The main outcomes were the formation of a coating with photocatalytic activity, demonstrated by the photo-degradation of methyl red, and able to reduce the pore sizes of the stone, with a relevant lowering of water and particulate penetrability.

1.2.3. Effects and durability of photocatalytic treatments

Besides the numerous benefits of integrating photocatalyst in innovative materials, there are a number of controversial reports on the mechanical effects, the potential release of hazardous substance and the durability of photocatalytic treatments.

For example, concerning the durability and mechanical effects of added TiO_2 into building materials, it has been reported that TiO_2 is chemically inert in the process of cement hydration; however, other studies suggested that nanoparticles can provide crystal nuclei, with the consequent promotion of cement hydration and, hence, causing an increase in the compressive strength of

photocatalytic mortars. Additionally, it has been reported that plausible reasons for the decline in photocatalytic performance and service life of photocatalytic building materials can be linked to the high brittleness and internal cracks, generated by the agglomeration of nanoparticles and an inadequate photocatalyst inclusion.[42]

Moving to photocatalytic coatings, many concerns and controversial efficacy have been described by many researches. A first point of discussion relies in the formation of the coating itself because it may behave as a barrier, impeding and limiting the rate at which both the light activates the photocatalyst and the adsorption of reactants.[55] Furthermore, the photocatalyst can cause the oxidation of organic coatings, limiting so the coating reliability and causing the possible release of nanoparticles or volatile organic pollutants in the air.

In this context, many toxicity studies have been devoted to properly assess the impact of different types of NPs, and their surrounding matrix, on human health. The best way to prevent inhalation and ingestion of NPs, but also to avoid dermal contamination, is to protect workers and consumers with an appropriate equipment or to reduce the release of NPs in the environment. For the latter aspect, the possible release from photocatalytic paints is a serious problem, especially after ageing (climatic, thermal and, mainly, UV) or when exposed to different media (pH and different organic matters).[56]

In parallel, studies on the degradation of the organic binder in photocatalytic paints have demonstrated controversial (often tremendously alarming) results. A number of studies have demonstrated that, rather than the VOCs elimination, the emission of new volatile compounds can occur during the irradiation of photocatalytic paints. In this context, Gunschera *et al.* have identified the emissions of many VOCs (formaldehyde, acetaldehyde furfural, acetophenone and n-butylbutyrate, among the largest) in the case of photocatalytic tiles.[57]

Another controversial issue is the potential formation of hazardous by-products, such as nitrous acid (HONO) from the degradation of NOx, that is potentially more harmful than primary reactants (NO and NO_2). In this context, the indoor air release of nitrous acid from photocatalytic paints, used in indoor applications, has been already described by Gandolfo *et al.* in 2015.[58] From all these features, it is clear that the photocatalytic effect initiated by UV-light could degrade the organic matrix of the coating and increase the release of NPs in the environment.

With this view, the work of Truffier-Boutry *et al.* is newsworthy.[59] In this study, two types of paints were investigated. In a first moment, two different "slurries" were prepared, both containing about 70% (w/w) of water and differing on the type of TiO_2 used (inactive micrometric or active nanometric). After that, the two slurries were added to the "basic paint", in turn formed by an acrylic-based binder, $CaCO_3$, water and other additives. Final paints reached 2.5-5% of TiO_2 and they were applied on plastic substrates (black plastic-vinylchloride/acetate copolymer).

The photocatalytic property was measured by EPR (Electron Paramagnetic Resonance) under solar simulator. Moreover, a Proton Transfer Reaction-Time of Flight-Mass Spectrometer (PTR-TOF-MS) was connected to a sealed reactor during the injection of a VOC (xylene) on painted surfaces, in order to online monitor both the degradation of a chosen pollutant (xylene) both the release of new VOCs during UV irradiation.

In this way, the authors showed that the tested photocatalytic paint can effectively remove xylene, in a greater way than the one made with micrometric titania. However, at the same time, the applied paint was subjected to the release of new hazardous organic compounds in the air. Upon irradiation, formaldehyde, methanol, acetaldehyde and formic acid were released by the paint, due to the photo-degradation of the organic matrix of the paint. In addition, SEM and XPS analyses highlighted an accumulation of TiO_2 NPs at the surface of the paint after UV ageing, caused by the decomposition of the organic matrix. In comparison, the non-aged surface possessed an enrichment of organic matter at the coating-air interface. The accumulation of NPs after UV ageing was linked to a higher probability of NPs release in the air, especially if a friction (e.g., abrasion) is applied to the coating. The authors dis not assess a direct relationship between the VOCs emission and the nanoparticles release, although they stressed out that both phenomena were caused by the photocatalytic degradation of the organic matrix under UV light irradiation. A simplified illustration of the emission of new VOCs and the release of NPs in the air is proposed in *Figure 6*.

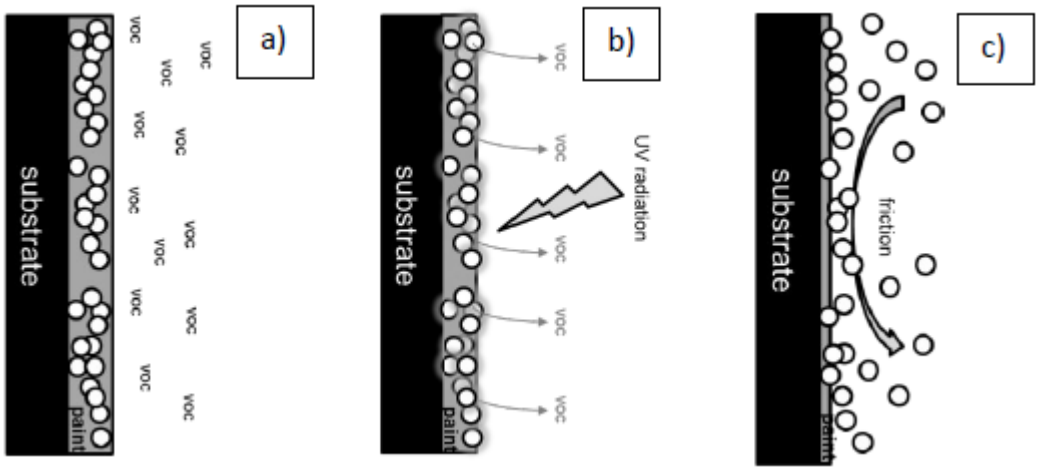

Figure 6 – a) Adsorption of VOC on the photocatalytic coating; b) photo-degradation of the polymer binder of the coating, with release of new VOCs; c) release of free NPs from the worn coating, caused by friction, scratch or other types of contacts.

From the results of their study, they stated a "safer-by-design" approach for the formulation of photocatalytic paints, by the settling of a list of crucial points (*Table 2*).

Table 2 – "Safer-by-design" principles.

"Safer-by-design" photocatalytic coating	
1) Creation of a "smooth" barrier onto NPs surface	To balance photocatalytic activity and coating lifetime.
2) Control the dispersion state of NPs in organic binder	To avoid excessive NPs agglomeration.
3) Localization of NPs on bigger particles	To improve affinity between NPs and polymer binder and to prevent the release of NPs.
4) Use of more resistant organic binders	To increase the coating lifetime.

A crucial aspect for safer photocatalytic paints is to balance an effective photocatalytic activity with an appreciable lifetime of the treatment. In this view, the application of polymeric coatings onto TiO_2 NPs can act as a "smooth" barrier to the photocatalytic process, so that the polymer binder remains intact for longer time, while the coated film exhibits an appreciable photo-degradation.[60] Moreover, a relevant influence is played by the degree of dispersibility of NPs in the surrounding organic matrix, avoiding agglomeration and maintaining an optimum photocatalytic efficiency of the paints. Additionally, the localization of TiO_2 NPs on bigger particles (e.g., by polymer grafting) was recognized to effectively prevent the release of NPs and to improve the affinity between inorganic (TiO_2) and organic (polymer binder) components. Finally, more resistant binders should be tested to reinforce the organic matrix and to ensure UV and thermal resistance.

A promising example of "safer-by-design" approach is the one proposed by Bonnefond *et al.* in 2016.[61] In order to minimize the degradation of the organic matrix, they tested a fluorinated host polymer, since fluoropolymers like polyvinylidene fluoride (PVDF) are not likely to be degraded by UV or oxidative ageing due to the presence of strong C-F bonds.[62] More in detail, they prepared a core-shell latex through seeded semi-batch emulsion polymerization, using commercial PVDF-*co*-HPF (polyvinylidene fluoride-co-hexafluoropropene) core-shell seeds with high molecular weight and copolymerizing a mixture of methylmethacrylate, butylacrylate and methacrylic acid (MMA, BA, MAA; ratio = 49.5 : 49.5 : 1 wt%) on the shell of the fluoropolymer, in order to produce a film forming latex. After mixing overnight, stable blends with good film-forming properties were prepared.

With this formulation, an extensive SEM-EDX analysis on the photocatalytic film, casted on glass, showed the large aggregation of NPs at the film-substrate interface, while Ti was mostly absent at the air-film interface. The aggregation could be explained by the lack of compatibility of TiO_2 with the organic latex. Anyhow, the UV ageing tests revealed the larger degradation of pure acrylic latex

rather than the fluorinated one, for which a small part of organic matrix (linked to the acrylic part, necessary to have a coating) was degraded during the UV and oxidative ageing.

1.3. Integration of (nano)particles in polymer-matrix composite

Among possible targets to achieve material innovation, composite materials are a highly promising case of study. Composites materials are made of two of more distinct phases and, in these systems, one or more discontinuous phases are surrounded by a continuous phase, usually called the matrix (*Figure 7*).

Figure 7 – Composite materials.

Discontinuous phases are commonly fillers or fibers. They are more resistant and rigid than the matrix and they are selected to achieve advanced mechanical performances, while the matrix ensures both the shape and the physical-chemical endurance of the product. From a mechanical point of view, the matrix should transfer the stress, applied on the composite material, to the more resistant discontinuous phase; moreover, the matrix should match an adequate stability, endurance, processability and incorporation of reinforcements.

Therefore, the coupling of more properties, coming from the distinct constituent, is the main reason of the strong interest to composite materials. General classifications could be based on the type of matrix and discontinuous phase involved. The choice of the matrix is mainly based on the type of application the composite material is involved. According to the type of the matrix, composite materials are divided in ceramic-matrix (based on aluminium oxide Al_2O_3, or silica SiO_2), metal-matrix (based on metals like Mg, Al, Ti or Cu) and polymer-matrix composite.

Similarly, the choice of the discontinuous phase is largely dependent on the type of application, since it is possible to design a large number of materials, from light-weighting to very dense composites. In this way, a possible distinction could be in fibers-reinforced composite (by using natural or synthetic fibers), particles-reinforced composite (by using sands, carbonates or powder-like fillers), structural-reinforced composite (like laminates or sandwich-panels) and many others.

Over the years, the interest on polymer-matrix composites is continuously increased because this matrix offers a series of benefits, like the low costs, the high processability and the ease preparation. Besides the outstanding performances of polymers, they are quite ease to process and to modify, both in the shape and in the components, allowing the preparation of matrices made *ad hoc* for the specific advanced application.

Anyhow, the preparation of a polymer-matrix composite through the simple formation of a binary mixtures of polymer and filler can have poor mechanical properties because of the lack of interaction between the two components, which results in weak interfaces. These interfaces are often the source of failure in composites, especially if there are present small-molecule chemical species (such as water, that can cause the delamination of the resulting composite).

In the following subchapters, the attention will be stressed on two main themes. The first one relies on the ways to couple particles and nanoparticles with the polymer matrix, since metal oxides (like TiO_2) are not meant to be highly dispersed in organic mixtures. Possible negative consequences could be the excessive agglomeration and the formation of separated phases, rather than dispersed particles inside the matrix.

The second point will consider the superficial migration of integrated particles inside the polymer matrix. The achievement of the surface enrichment through the migration of a component toward the surface of the advanced material can be a highly promising way to gain surface functionalization, without using post-production and superficial treatments. This feature is strongly appreciable and it could be a valid alternative for photocatalytic coating, since it should minimize intrinsic problems of this treatment, such as the release of NPs, the loss of efficiency over time and the low durability.

1.3.1. Organosilane coupling agents

The term organosilane (or just silane) coupling agent generally refers to Si-containing chemicals capable of forming covalent linkages between dissimilar materials, such as between organic polymers and inorganic fillers in reinforced polymer-matrix composites. The great increase of compatibility, derived by the presence of small amounts of coupling agent at the interface, is effective in many applications, ranging from paints and coating to dental materials and contact lenses, passing through adhesives and sealants.[63]

The general formula for a silane coupling agent typically shows the two classes of functionality: the organofunctional substituent and the hydrolysable group (*Figure 8*). Silanes with three hydrolysable groups are the more common for the surface modification of reinforcements because

they tend to deposit as a polymeric film, effecting a total coverage of the surface of the substrate and maximizing the introduction of organic functionality.

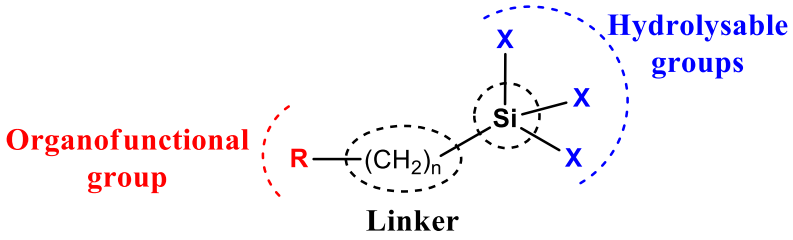

Figure 8 – Organosilane coupling agent.

The hydrolysable group (X group in *Figure 8*) is commonly alkoxy, acyloxy or halogen, meant to react with the inorganic substrate. Instead, the R group is a non-hydrolysable organic group that may impart desired characteristics, generally by its coupling with organics. Finally, also the linker between the organic functionality and the silicon atom is important to control the effectiveness and properties of a coupled system is determined. Its typical length is three C atoms, a consequence of the fact that the propyl group is synthetically accessible and it has good thermal stability. Anyhow, in specific applications, a shorter (e.g., in sensors and fluorescent materials) or a longer (e.g., in phase-transfer catalysis and liquid chromatography) length could be desirable.[64]

The coupling effect of silanes as adhesion promoter between inorganic and polymeric phases in schematized in *Scheme 2*.

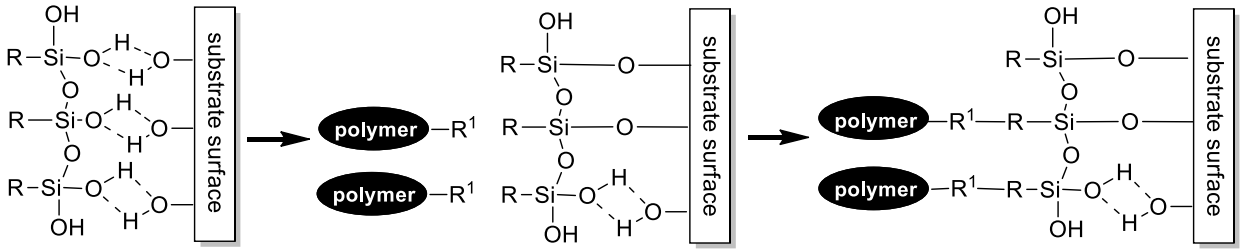

Scheme 2 – Coupling of a polymer with an inorganic material by the use of an organosilane.

In a first moment, the hydrolysis-promoted silanization reaction results in the modification of the surface substrate. Water could be added or it could come from other sources, like the atmosphere or present on the surface of the substrate.

After hydrolysis, a reactive silanol (Si-OH) group is formed. Usually, only one Si-OH group interacts with the substrate surface *via* hydrogen bond interaction; the other two silanol groups are present either in condensed or free form. In this sense, the degree of condensation to polysiloxane is largely determined by the amount of available water.

Finally, the covalent linkage with the substrate is effectively obtained after a period of drying or curing. The formation of covalent bonds to the surface proceeds with a certain amount of reversibility. As water is removed (by heating up to 120°C or at lower temperature under reduced pressure, for several hours) bonds may form, break, and reform to relieve internal stress.[65]

The efficiency of the silanization reaction largely depend on the type of the substrate and the most important factors are the concentration and the type of surface hydroxyl groups, the hydrolytic stability of the generated bonds and the physical dimensions of the substate. Good substrates are siliceous materials (like quartz, fumed silica, glass or colloidal silica), alumino-silicates, tin and metal oxides, such as TiO_2, SnO and Cr_2O_3. Instead, examples of substrates having poor compatibility with organosilanes are carbonates, marble, graphite and carbon black.[66]

The modification of the substate surface through silanization reaction results in a list of consequences, like the alteration of the wetting and adhesion characteristics, the possibility to create a covalent bond between organic and inorganic materials, the opportunity to perform chemical transformations at the heterogeneous interface and many others. In particular, the wettability of a substate from a liquid is associated to the critical surface tension of the solid (γ_c) and the surface tension of the liquid (γ_{lv}). In *Table 3*, there are listed many surface tensions of solids and liquids.

Table 3 – Surface tension of many liquid and solid materials.

Solid material	Surface tension (γ_c/mN m^{-1})	Liquid	Surface tension (γ_{lv}/ mN m^{-1})
Heptadecafluorodecyltrichlorosilane	12	n-Heptane	20
Poly(tetrafluoroethylene)	18.5	Methanol	22
Methyltrimethoxysilane	22.5	2,2,2-Trifluoroethyl Methacrylate	22.5
Methacryloxypropyltrimethoxysilane	25	Acetone	23
Paraffin wax	25.5	n-Decane	24
Ethyltrimethoxysilane	27	Cyclohexane	25
Propyltrimethoxysilane	28.5	Methacrylic acid	26
Glass, soda-lime (wet)	30	Chloroform	26.5
Poly(propylene)	31	Acetic acid	27
Trifluoropropyltrimethoxysilane	33.5	Dichloromethane	27.5
Poly(ethylene)	33	Toluene	28
Poly(styrene)	34	Methylmethacrylate	28
Cyanoethyltrimethoxysilane	34	Benzene	28
Aminopropyltriethoxysilane	35	Trichloroethylene	28.5
Poly(methylmethacrylate)	39	Nitromethane	36
Poly(vinylchloride)	39	Nitrobenzene	43
Mercaptopropyltrimethoxysilane	41	Ethylene glycol	48
Iron (dry)	46	Formamide	57
Glass, soda-lime (dry)	47	Water	72.5
Fumed silica	78	Hydrogen peroxide	74
Titanium dioxide (anatase)	91	Glycerol	76
Ferric oxide	107	Mercury	474.5

Assuming water as reference liquid and knowing that a liquid can wet a surface if $\gamma_{lv} < \gamma_c$, it is possible to predict the hydrophilic/hydrophobic behaviour of a substrate. Hydrophilic behaviour, associated with low contact angles and high wettability by water, is generally observed when $\gamma_c > 45$ mN/m. Instead, a hydrophobic surface is usually observed when $\gamma_c < 35$ mN/m. At first, the decrease in critical surface tension is associated with hydrophobic and oleophilic attitude, with large water contact angle together with the increased wetting by hydrocarbon oils. However, below 20 mN/m, superhydrophobic surfaces, resistant both by the wetting of water (hydrophobic) and hydrocarbon oils (oleophobic), are obtained.[67]

From *Table 3*, it is clear that surface treatment with organosilanes leads to a strong decrease of surface tension. In this way, the silanization reaction can ensure an effective modification of the surface of solid materials, generally switching from a hydrophilic to a hydrophobic (or even

superhydrophobic, such as with F-containing silanes) behaviour, improving so the wettability by organic solvents, hydrocarbons and monomers.[68]

Besides that, another fundamental point is the role of the organic functionality to promote chemical reaction at the interface, since this group remains available for covalent reaction or physical interaction with other phases. As usual, the choice largely depends on the application. For example, octadecyl, cyanopropyl and branched tricocyl silanes provide bonded phases for liquid chromatography; similarly, the treating of TLC (Thin-Layer Chromatography) plates with dodecyltrichlorosilane is used for reverse phase thin-layer chromatography.

For the purpose of this thesis, the attention will be focused on silanes used as coupling agents in polymer-matrix composites. In order to obtain a covalent bond with the organic phase, the organic functionality of the silane can react by a post-reaction with a finished polymer (grafting-to approach) or through copolymerization with the monomer (grafting-from approach). The first route is preferred with thermoplastic polymers, while, with thermosets, the copolymerization approach is clearly favoured. Generally, thermoplastics provide a greater challenge in promoting adhesion because silanes have to react with a pre-formed polymer rather than precursors, which not only limits the coupling but it causes problems in rheology during composite formulation and it could affect the thermal properties of composite. For this reason, the discussion will mainly consider the copolymerization approach.

Structures of many commercially available organosilanes are reported in *Figure 9*.

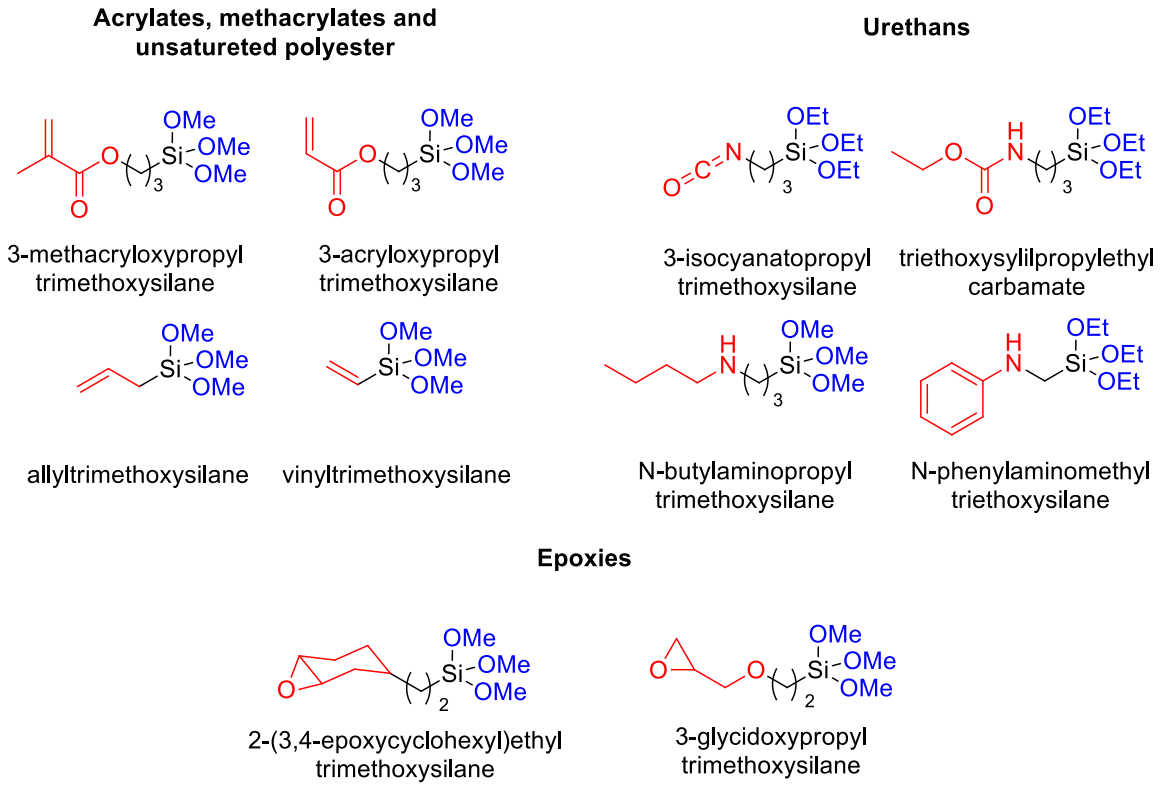

Figure 9 – Common silane-based coupling agents.

Silanes can be used to pretreat the filler or it can be blended with the monomer resin. For matrices that undergo to free-radical polymerization (such as acrylates, methacrylates and unsaturated polyesters), methacryloxy and acryloxy silanes are preferred, while vinylsilane or allylsilane generally mismatch the reactionary parameters of most unsaturated polyesters and they are preferably used in direct high-pressure copolymerization with ethylene, propylene and dienes.

Thermoset polyurethane can be effectively coupled with two types of silanes. Isocyanate-functionalized silanes are used to directly treat the filler or blended with the diisocyanate prior to cure. On the other hand, amine and alkanolamine functional silanes are mixed with the polyol. After the mixing of monomers, isocyanate silanes will couple with the polyol, while the amine and alkanolamine silanes with diisocyanate, forming urea and urethane linkages, respectively.

Moving to epoxy resins, epoxycyclohexyl and glycidoxy functional silanes are used to pretreat the filler or blended with the monomer, like glycidylbisphenol-A ether. Amine functional silanes can likewise be used to pretreat the filler or to be blended with the hardener portion.

At this point, some examples of silanization reactions are proposed. The attention will be prevalently focused on a specific silane coupling agent, γ-methacryloxypropyltrimethoxysilane (MAPTMS; see structure in *Figure 9*).

The first remarkable work is the study of the interactions of MAPTMS with fumed silica and PMMA in silica/PMMA composites.[69] The purpose of this work was to evaluate the differences in

silanization of SiO_2 when two different mechanism are approached. The first one (hydrolyzation mechanism) was studied in aqueous ethanol (95%) or in acetone, stirring the mixture for 2 hours at room temperature and, in some cases, using an amine catalyst (triethylamine). The second one (direct-condensation mechanism) was performed in anhydrous toluene with the amine catalyst and pre-dried silica (vacuum drying at 110°C for 4 hours), stirring at 60°C for 8 hours. After reaction, silica was separated by centrifugation, washed with fresh solvent and, finally, dried (overnight, at 25°C under vacuum and, additionally, at 110°C per 2 hours).

From studying the process outcome at each step, it was determined that, after vacuum drying at 25°C, two types of adsorbed silane were found: a firmly adsorbed and a loosely adsorbed silane. The loosely adsorbed silane could desorb and be incorporated into the polymer matrix through copolymerization with the monomer, resulting in crosslinking of the matrix. When the silanated silica was dried at 110°C for 2 h, the loosely adsorbed silane was removed and the amount of firmly adsorbed silane increased. Finally, methyl methacrylate was polymerized with the silanated fumed silica (5% wt/wt) to form composites. There was a positive correlation between the amount of firmly adsorbed silane and the amount of PMMA attachment. The highest efficiency was found with low concentrated silane solutions (1%) rather than more concentrated solutions (5%), because a monolayer was obtained. Finally, the use of anhydrous toluene as solvent did not show any advantages over the use of aqueous ethanol and acetone in terms of silane adsorption and PMMA attachment, as like as the use of amine catalyst in hydrolyzation conditions.

Another citable work is the surface modification of TiO_2 NPs with MAPTMS to form PBA (polybutylacrylate) matrix nanocomposite.[70] In order to improve the effect of surface modification, TiO_2 was pre-dispersed in ethanol via ultrasonic irradiation; after that, different amounts of silane were added in the dispersion, keeping a stirring for 2 hours and then heating to reflux condition for 4 hours, always in dry nitrogen atmosphere. The increase in dispersibility was evaluated via sedimentation rate, while FT-IR (Fourier Transform Infrared Spectroscopy) and TGA (thermogravimetric analysis) were performed to check the successful grafting of silane onto TiO_2 nanoparticles. Finally, both neat PBA film and TiO_2/ PBA film and composite were prepared and characterised, demonstrating a good compatibility after silanization of nanoparticles.

In a similar work, the modification of TiO_2 NPs with MAPTMS was carried out in ethanol solvent at 50°C and using ammonia as catalyst. The coupling of many techniques, like IR, TGA (ThermoGravimetric Analysis), TEM (Transmission Electron Microscopy), SEM (Scanning Electron Microscopy), DLS (Dynamic Light Scattering), UV-spectroscopy and XRD (X-Ray Diffraction), proved the grafting of silane onto TiO_2, with the consequent hydrophobic behaviour and the lower agglomeration of NPs.[71]

A final interesting example encloses the effects of organic surface treatment by MAPTMS on the photostability of rutile TiO_2 pre-coated with Al_2O_3, to be used in sunscreen formulations.[72] Firstly, a TiO_2 dispersion was obtained with a ball-milling technique; after that, the modification was carried in a round bottom flask, using a o-xylene solution and different concentration of silane. The functionalized powder was obtained after solvent washes, centrifugation and drying. From this work, it has been found that MAPTMS surface modification of titania is effective in reducing the photocatalytic activity by the reduction of surface -OH groups. In the extreme case, 72% of the photocatalytic activity was reduced compared to that of the non-modified TiO_2.

1.3.2. Migration of additives in polymer matrices

Polymer materials and migration phenomena is a theme of many studies and debates. Among them, concerns on food-contact plastics for the presence of possible migrants (such as polymer additives like plasticisers or UV stabilizer, oligomers, residual monomer and other small molecules) have settled an important monitoring of migrant release from plastics to foods and drinks.

Anyhow, the programmed migration of functionalized additives has long been recognized as a potential solution for functionalizing polymer surfaces, proving to be a low-cost and reliable method alternative to classic coatings. The premise is that, if a surface-tendent addictive is blended in small amount within a melt or in a solution of host polymer, physical processes (such as diffusion or spontaneous surface segregation) might be used to transport the additive to the surface of host polymer during normal polymer processing.[73]

Migration of additives in polymers is known to follow physical diffusion laws. Generally, migrants pass through voids and other gaps between the host polymer chains. How quickly and to what extent migration will occur is determined by the properties of host polymer and migrant.[74]

Considering the host polymer matrix, the migration ability of hosted small chemicals largely depends on the number and dimension of intramolecular voids. Basically, this aspect is largely linked to the density, crystallinity, molecular weight, degree of branching, degree of cross-linking and, especially, the glass transition temperature (Tg) of the polymer. In this sense, Tg is fundamental because it influences the mobility of polymer chains and the glassy/rubbery state of the host polymer.[75] Below Tg, chains have low mobility and the polymer is rigid and stiff, so the probability to find a large hole is limited. Instead, above the Tg, the polymer is flexible and larger voids are present in the plastic, drastically increasing the mobility of small molecules. Therefore, in general, the lower the Tg of the host polymer, the higher the migration rates of additives. Concerning the density, crystallinity and degrees of branching or cross-linking, these properties clearly influence the

distribution of chains inside the polymer materials and, hence, the possibility of migration. In general, a low dense and high amorphous polymer, with high degree of branching and cross-linking, is more likable to be involved in migration and release of additives. Finally, for the molecular weight (Mw) of host polymer, its influence on the migration is quite prominent, especially in relation to the molecular weight of the additive. In other words, the migration is more probable when the host matrix has a greater Mw than the additive; anyhow, after a certain level of host polymer Mw, undesirable effects can emerge.[76]

Moving to the organic additive, species with low surface energy tends to spontaneously migrate to the polymer-air interphase and lowest surface energies are reached by F-containing material and fluoropolymers. These materials have been effectively used to create low-energy surfaces *via* surface segregation, just by blending low amounts of fluorinated additives inside the host polymer.[77] This last aspect is commercially important because low levels of additive can prevent potential processing problems and it keeps the cost of the end product low. Additionally, fluoropolymers present a number of interesting and peculiar properties, provided mainly by the unique features of F atom. Fluorine is a good and non-bulk H-substituent and it allows the replacement of C-H bond with strong C-F bond.[78] This aspect can result in many interesting features, like high thermal, chemical, aging, and weather resistance, inertness to hydrocarbons, acids, and alkalis, low dielectric constants, low flammability and low refractive index.[79]

Among fluoropolymers, fluorinated (meth)acrylate polymers are very interesting because they couple the characteristics of (meth)acrylates (e.g., good adhesion to substrates) and those of fluoropolymers (low surface energy). Moreover, (meth)acrylates having fluorinated side chains have proven to be compatible with many common (meth)acrylate monomers and polymer segments through copolymerization. This aspect is crucial to further utilize unique advantages conferred by F-groups while maintaining the product more economical and processable.[80]

Researchers have studied the influence of fluorine concentration on surface segregation and they have found that additives with higher F content tend to migrate to the polymer/air interphase with a faster rate; moreover, they are more likely to remain at the surface.[81] For example, it is well known that the poly(perfluoroalkyl acrylate)s (PFAAs) and poly(perfluoroalkyl methacrylate)s (PFAMAs) with long fluorocarbon side chains results in excellent surface properties, since they generally exhibit ultra-low surface energies (8–10 mN/m). However, their poor solubility and miscibility in organic solvents, coupled with low adhesion to the substate, limits the production use. In addition, the use of long-chain perfluoroalkyl acids and their precursors is regulated by a very restrictive global regulation, in order to decrease the environmental risk derived by the use of these fluoropolymers, strongly associated to bioaccumulation phenomena in wildlife. For example, it has been reported that

chemicals such as perfluorooctanoic acid and perfluorooctane sulfonate are highly toxic, very resistant to biochemical degradation and inclined to bioaccumulate.[82]

For these reasons, nowadays, the modification of surfaces is mostly based on short-fluorinated side chains chemicals and other non-fluorinated chemicals because they can provide additional benefits, like good solubility in organic solvents, high optical transmittance and less eco-impacting. In this sense, a noticeable work based on the use of a monomer with only one fluorocarbon ($–CF_3$), namely 2,2,2-trifluoroethylmethacrylate (TFEMA), together with MMA, in order to produce copolymers with improved surface and optical properties, is herein reported.[83] The copolymerization was attained with various monomer ratios through radical polymerization (THF solution; 60 °C for 18 h; nitrogen atmosphere, AIBN (1 wt % to monomer) as initiator). After that, the polymer products were rinsed using methanol and dried under vacuum at 65 °C. The surface and optical properties of pure PMMA, pure PTFEMA and copolymers of MMA and TFEMA were studied preparing a film onto silicon wafers and glass plates through a spin-casting technique. On the basis of obtained results, the authors stated that the surface and optical properties of the PMMA can be successfully controlled by incorporating the TFEMA unit. PTFEMA-PMMA films exhibited a linearly controlled surface energies (27.2–39.5 mN/m) as the function of TFEMA content. Moreover, they found higher light transmittance values with increasing level of fluorine content in both region of UV-Vis and NIR (300-2000 nm).

Alternatively, the blending of low surface energy PFAA and PFAMA materials with short fluorinated side chain (i.e., $–CF_3$, $–CF_2CF_3$, $–(CF_3)_2$, $–CF_2CF_2CF_3$) in PMMA can result in similar modifications, imparting advanced surface properties to common polymers. In this sense, a remarkable study on the surface energies of blends of PMMA with different polyfluoromethacrylates made of short side chain monomers (2,2,2-trifluoroethyl methacrylate (TFEMA), 1,1,1,3,3,3-hexafluoroisopropylmethacrylate (HFIPMA), 2,2,3,3,3-pentafluoropropyl methacrylate (PFPMA) and 2,2,3,3,4,4,4-heptafluorobutyl methacrylate (HFBMA)) is herein reported.[84] The surface energies of blend films, made by spin casting a α,α,α-trifluorotoluene solutions onto cleaned silicon wafers, was largely examined. The authors observed that the PTFEMA/PMMA blends resulted in laterally phase-separated structure, whereas the blends with fluoropolymers having longer side chains (PPFPMA, PHFIPMA, and PHFBMA) were vertically separated, in the form of a top PFMMA layer and bottom PMMA layer, regardless of the blend ratio. Due to these different phase structures, the surface energy of the PTFEMA/PMMA blend varied proportionally with the blend ratio (from 17.6 to 26 mN/m), whereas the others remained at very low levels (10.2–12.6 mN/m) even when the blends contained 90 wt.% of PMMA.

Beside the difference in surface energy, other factors affecting the migration can be addressable to only entropic free energy contributions. In other words, when the surface energy of additive and host polymer is quite similar, the migration can be attained playing with two types of entropic contributions. The first contribution is called purely entropic effect and it derives from the fact that higher molecular weight species experience greater entropic for residing near a phase interface, while for low molecular weight additives this contribution is less prominent.[85] The second factor is linked to the great mobility of chain ends, enhancing the molecular configurational freedom near interfaces and, hence, favour surface enrichment. In this sense, the number of chain ends increases with smaller molecular weight, hence they are more favoured to move to the interface.[86]

In this sense, an interesting example is the investigation of the role of the molecular weight of the additive in the surface migration of a copolymer additive (PS-b-PMMA) having a surface tension similar to the host polymer (PS).[87] In this work, it was observed that the selective enrichment of the air/polymer interface with the additive resulted only when the molecular weight of host PS was substantially higher than the one of the additive; in the opposite case, blends surface was found to be depleted of the copolymer.

1.3.3. Sedimentation/flotation of integrated particles in polymer matrices

The integration of functionalized particles to achieve a surface enrichment with specific inorganic materials has been found as a prominent way to develop advanced composite materials. In polymer-matrix composite, particles are integrated prior the polymerization/curing of the system, and they have to be mixed with viscous polymer melts or syrups to get a homogeneous dispersion.

As already discussed, a relevant problem is the instauration of multiple interfaces between integrated particles and organic medium, causing phenomena like agglomeration of inorganic particles and phase separation. Even if compatibility problems can be fixed, such as by the use of coupling agent or plasticizers, another important effect is still playing in the system.

Inorganic fillers inside a viscous media generally experience a falling, since their density is normally higher than the one of the surrounding media, and the normal consequence is the tendency of particles to sediment inside the viscous organic medium. In order to achieve a standardized composite material, it is important to predict the behaviour of integrated particles and their velocity of falling. For this purpose, the tendency of sinking or floating largely depends on the densities of solid particles and viscous liquid involved; instead, the velocity of falling/floating can be obtained from the Stokes's law.[88] The basement of this law relies on the fact that a particle inside a viscous fluid experience upward and downward forces. The sinking is clearly caused by the gravitational

force; while upward forces are caused by the viscosity and the buoyancy. The buoyant upward force is exerted by the fluid in opposition of the weight of immersed object and its magnitude, as explained by Archimede's principle, is equivalent to the weight of displaced liquid and, so, it is strongly dependent on the density of involved liquid and solid. Moreover, the viscosity of the medium exerts an upward frictional force (F_d). In this sense, Stokes' law is the empirical law that assess the frictional force exerted on spherical objects in a viscous fluid having laminar flow (*Equation 13*):

$$F_d = 6\pi\mu R v \quad (13)$$

Equation 13

R = radius of the sphere (m); μ = dynamic viscosity (kg/m·s), v = flow velocity of the sphere (m/s)

If a particle only experiences its own weight while falling in a viscous fluid, then a terminal velocity is reached when the sum of the frictional and the buoyant forces on the particle exactly balances the gravitational force. In other words, there is no more acceleration in the system when upwards and downwards forces are balanced, so it is reached the maximum velocity for the falling sphere. In this way, it is possible to reduce the balance of forces as the matching of the upward frictional force (F_d) and the downward excess force (F_e), coming from the difference of gravitational force and buoyant force (both caused by the action of gravity). Since F_e can be expressed as (*Equation 14*):

$$F_e = \frac{4}{3}(\rho_p - \rho_f) g \pi R^3 \quad (14)$$

Equation 14

R = radius of the sphere (m); g = gravitational field strength (m/s²); ρ_p = density of the particle (kg/m³); ρ_f = density of the fluid (kg/m³).

hence, balancing the two forces and resolving respect to v, it is possible to calculate the terminal velocity (m/s) attainable by a sphere as it falls through a fluid (*Equation 15*):

$$v = \frac{2}{9} \frac{\rho_p - \rho_f}{\mu} g R^2 \quad (15)$$

Equation 15

When $\rho_p > \rho_f$ = vertically downward movement (sinking); when $\rho_p < \rho_f$ = vertically upward movement (flotation).

From this equation, it is clear that the velocity of falling is proportional to the square of the radius of the sphere and inversely proportional to the dynamic viscosity of the organic medium. Therefore, the dimension of the filler largely affects the velocity of falling and, in general, the larger the radius, the faster the sedimentation of the filler; while, for the viscosity effect, the higher the viscosity of the medium, the lower the velocity of falling.

In this way, it is expected that particles of nanometric dimension are minimal affected by sedimentation/floating processes and they are more likely to have really low movements when

immersed in a liquid. That is actually not true, because it is known that nanoparticles are widely subjected to random motions, called Brownian motion. Anyhow, this motion plays oppositely to the gravitational force, hence the sedimentation is not a concrete possibility for nanoparticles and, instead, a formation of a colloidal system is generally obtained, as in the case of colloidal silica, used as thixotropic agent in many applications.

As a consequence of the low tendency of nanoparticles to migrate toward surfaces, a number of attempts have been involved to solve this problem. Among them, the use of coupling agents like silanes is a common solution to decrease the level of aggregation of nanoparticles, leading an increased dispersibility in the organic medium and, hence, to a more homogeneous dispersion of nanoparticles inside the polymer-matrix composite. Anyhow, this method does not allow a surface enrichment of integrated particles.

In order to improve the surface functionalization with inorganic nanoparticles, the coupling of silanes and fluoropolymers, able to self-segregate to interphases, could be a possible solution. Only a few papers have studied the migration of fluoropolymers toward the air/solid interface in organic-inorganic hybrid nanocomposite, even if a gradient distribution of the F atom along the cross section of the matrix has been reported using this approach.[89] For instance, a citable work could be the development of inorganic–organic hybrid latex containing fluorine as binders for aqueous coating.[90] In this experiment, the hybrid latex was prepared in a multistage emulsion polymerization of (meth)acrylates and fluorinated (meth)acrylates in the presence of nano-SiO_2 particles and silane (γ-methacryloxypropyltriisopropoxysilane (MAPTIPS)). The effects of fluoride and alkoxysilane on the morphologies of composite particles were observed and it was found that fluoroacrylates may encapsulate on the core of silica by controlling reaction conditions. Results of XPS showed that the content of fluorine in the outmost surface was high, due to the fluorinated side chains enrichment by their orientation toward the surface. Moreover, it was showed that the phase separation between organic and inorganic for modified SiO_2 was lightened, while it was so apparent for raw SiO_2, causing a lower presence of fluorine at the surface in the lack of MAPTIPS.

Another remarkable work is the fluorine modification conducted on TiO_2 to enhance the anti-icing property through the fabrication of a very hydrophobic surface.[91] The aim of the work was to couple the high reflective action of ultra-white titania together with the superhydrophobic activity of fluoropolymer through the grafting of the latter onto the surface of the former. To achieve that, TiO_2 was firstly modified with MAPTMS silane, in order to introduce C=C bonds. Then, dodecafluoroheptyl methacrylate (DFHMA) monomers were successfully grafted on the TiO_2 via a grafting-from approach, leading to a grafted fluoropolymer through the copolymerization of C=C bond, pre-introduced by silanization reaction. The polymerization was conducted in toluene, allowing

firstly the complete dispersion of titania through strirring and, then, adding a different amount of radical initiator (azobisisobutyronitrile (AIBN), pre-dissolved and added dropwise for a time of 3 hours), setting the temperature at 75°C and using a nitrogen atmosphere. After the complete addition of AIBN, the free-radical polymerization was kept for 4 hours more. At the end, the dispersed TiO_2 particles were centrifuged, washed, and dried (80 °C for 6 h). The chemical components of the TiO_2 particles were investigated by XPS: for fluorine-modified TiO_2, the fluorine content reached a peak value of 7.3%, while the water contact angle enhanced to a maximum value of 146°, indicating a very hydrophobic surface. Finally, the anti-icing property was demonstrated through the decrease of the crystallization temperature of a water droplet for F-modified TiO_2 (-19.4°C; 10.3°C lower than unmodified TiO_2), moreover, it was observed a freezing delay time of 25 min (test at T = -10 °C).

A final nice work was conducted to study the migration and surface enrichment of fluorinated TiO_2 nanocomposites, added as additives inside the matrix of materials used as propellants (nitrocellulose and nitroglycerine).[92] The emulsion polymerization was conducted using pre-silanized TiO_2 (silane = MAPTMS) dispersed in water, added into a beaker containing the emulsifier and DFHMA (dodecafluoroheptyl methacrylate) monomer. Some KPS (potassium persulfate, used as initiator) was introduced when the temperature was at 75°C, keeping the polymerization process for 2 h. Finally, the emulsion was cooled to room temperature and added dropwise into ethanol. The fluorinated TiO_2 nanocomposites were obtained by washing, filtering and drying in a vacuum oven at 40°C overnight. In this case, fluoropolymer-modified titania was used because its great potential as additive. Indeed, the initial burning gas generation rate and the wear of erosion of gas to bare surface can be depressed through the surface enrichment of fluorinated additive; instead, TiO_2 NPs have proven to greatly reduce the erosion of propellant materials. Thereby, the surface migration and enrichment technology were attended to provide a good way to tailoring the surface properties of the material by the less use of additives.

1.4. Results and discussions

The importance of developing smart and eco-friendly technologies to fight both pollutants and pathogenic microorganism have made Advanced Oxidation Processes (AOPs) really attractive, since they can afford the best balance between efficiency of degradation and (eco)sustainability. Among them, the use of semiconductor photocatalysts, like TiO_2 nanoparticles, is particularly interesting because these species can achieve the formation of powerful oxidizing species just by their light-excitation. In this context, charge carriers are formed and involved in a complex series of redox

reactions, resulting in the generation of Reactive Oxygen Species (ROS), in turn responsible for the complete degradation through mineralization of pollutants in aqueous and gas phases.

Over the years, many attempts have been involved to find a suitable way to apply photocatalysts in many materials, like building materials, historical monuments or polymer materials. Considering micrometric TiO_2 and its application as white pigment in a wide range of materials, one of the most popular approaches is to "mimic" the same process for nanometric titania, developing so photocatalytic paints and coatings just by dispersing TiO_2 in a system made by a solvent (often water) and an organic binder, necessary to ensure the adhesion to the material.

Anyhow, many concerns and controversial efficacy have been described. A first point of discussion is the formation of the coating itself, that could act as a barrier to the exciting light and to the adsorption of reactants. Furthermore, the photocatalyst can cause the oxidation of organic coatings, limiting so the coating reliability and causing the possible release of nanoparticles or volatile organic pollutants in the air.

In this context, the formulation of photocatalytic paints and coatings should follow a "safer-by-design" approach, established to limit the possible side-effects of these treatments. A crucial aspect is to balance an effective photocatalytic activity with an appreciable lifetime of the treatment. Moreover, a relevant influence is played by the degree of dispersibility of NPs in the surrounding organic matrix. Additionally, the localization of TiO_2 NPs on bigger particles (e.g., by polymer grafting) was recognized to effectively prevent the release of NPs and to improve the affinity between inorganic (TiO_2) and organic (polymer binder) components. Finally, more resistant binders should be used to ensure UV and thermal resistance.

From these considerations, the "safer-by-design" incorporation of TiO_2 nanoparticles (NPs) in polymer materials is the topic of the proposed work. The produced prototypes are both PMMA/TiO_2 composites and PMMA/SiO_2/TiO_2 composites. For the latter, they were formulated in order to be used in industrial applications, such as in composite kitchen sinks or in other interior design furniture (like shower trays, bathroom sinks, whirlpools or others).

The investigation started from the modification of commercially available and synthesized titania NPs through the silanization reaction, in order to form a polysiloxane coating having a functional chain (in particular, a methacrylate group) onto the surface of TiO_2. The tested samples were both pristine anatase titania, activable with UV-A light, and samples activable with visible light (e.g., Ce-doped TiO_2). The non-modified NPs were analysed through SEM-EDX, XRD and FT-IR analyses, while the chemical characterization of modified samples were based on FT-IR, TGA and SEM-EDX analyses.

Successively, the modified TiO_2 was dispersed in specific methacrylate monomers, having different side chains, and used to develop a photocatalytic pre-polymer through a partial polymerization approach. In other words, a thermal-controlled polymerization via free radicals was studied in order to ensure a strong covalent bond between NPs and organic matrix, the localization of the photocatalyst in strong bigger particles and the possibility to migrate toward surfaces. The obtained product is a viscous liquid, where TiO_2 is dispersed: in this sense, the analyses performed were the viscosity and the dry and ash residues determinations.

Finally, a wide number of PMMA/TiO_2 composites and PMMA/SiO_2/TiO_2 composites were produced, using a formulation that include the use of the photocatalytic pre-polymer as minor component (from 0.45% to 0.9% of TiO_2 in the final prototype). The surface and the section of these surfaces were analysed through SEM-EDX analysis and their superficial photocatalytic activity were evaluated through the degradation of two type of pollutants: the ones present in aqueous phase (test performed following the ISO standard 10678:2010) and in gaseous phase, selecting NOx as pollutant targets.

1.4.1. Synthesis and modification of TiO_2 NPs

The use of the coupling agent γ-methacryloxypropyltrimethoxysilane (MAPTMS) was investigated in order to create a hydrophobic polymer coating onto a large number of titania samples. This modification can achieve both a good dispersibility in organic media, the formation of a "smooth" barrier onto NPs and the introduction of the methacrylic function, covalently bonded to the photocatalyst. These features are crucial for the successive steps.

Considering that common TiO_2-based photocatalysts are activable only with the use of UV light, in a first moment it was studied the synthesis of cerium-doped TiO_2 NPs, since it could accomplish a visible light activation through the formation of colour centers and/or the instauration of intra-bandgap levels in the semiconductor. Likewise, it is important to highlight that CeO_2 nanoparticles can significantly mitigate reactive oxygen species.[93] The CeO2 NPs have a favourable comparison on human health, where, like all chemical compounds, it is possible to have adverse effect, as well as beneficial biological effects.[94]

- **Synthesis of Ce-doped TiO_2 NPs**

The work was based on the sol-gel synthesis of Ce-doped TiO_2 NPs.[95] The used approach is schematized in *Scheme 3*, while the used apparatus in *Figure 10*.

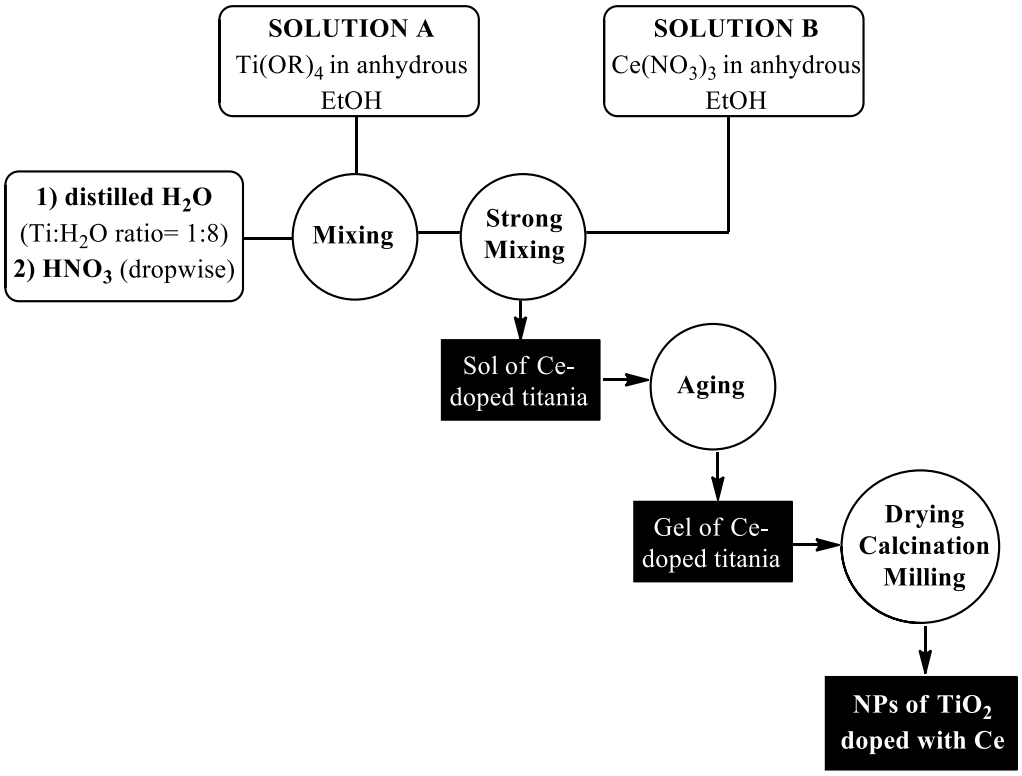

Scheme 3 – Synthesis of Ce-doped TiO_2 NPs.

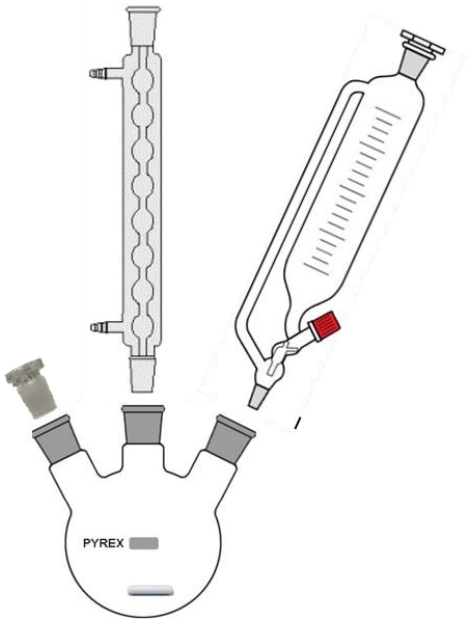

Figure 10 – Experimental layout for the synthesis of TiO_2 NPs.

Solution A is the source of Ti (IV), while solution B is the source of doping, in particular metallic cerium cations. Firstly, the titanium tetralkoxide was dissolved in anhydrous ethanol, in order to ensure a complete dissolution while avoiding the start of alkoxide hydrolysis, that was promoted only when distilled water is added in the system. To further promote the formation of TiO_2, an acid source (HNO_3) was added dropwise after a certain time. After that, the solution B was slowly added in the

system under a continuous stirring. At the end of the addition, the stirring rate was raised in order to have a vigorous agitation for at least 1 hour. In this way, the sol was obtained. After that, the system was led to aging until the gel formation. At this point, the solvent was firstly removed and, then, the obtained solid was dried in oven, calcinated at high temperature and finely grounded, obtaining light-yellow nanoparticles. The pictures of sol, gel and final NPs are reported in *Figure 11*.

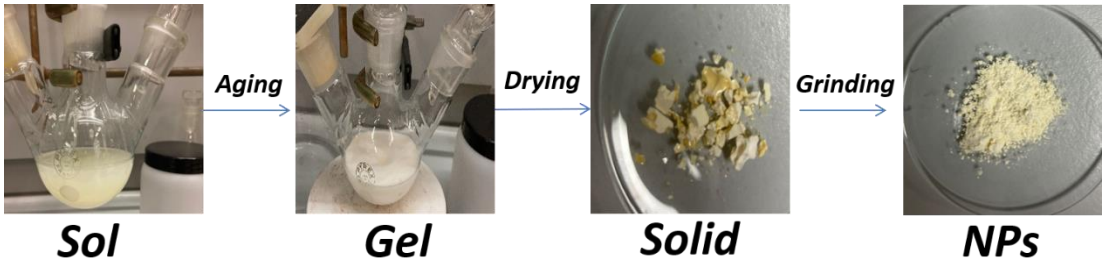

Figure 11 – Pictures of sol, gel and nanoparticles of Ce-doped TiO_2.

In order to evaluate an appropriate Ti source, two tetralkoxide were tested: titanium tetrabutoxide (compound **1**) and titanium tetraisopropoxide (compound **2**). A number of trials have been performed with these precursors, as shown in *Table 4*. In all the tests, it was used the same dopant precursor ($Ce(NO_3)_3 \cdot 6H_2O$, compound **3**) and the doping concentration was constant (percent mass ratio of Ce/TiO_2 = 0.4%).

Table 4 – Tests conducted for the synthesis of Ce-doped TiO_2 NPs.

Entry	Ti (IV) precursor	Aging time (h)	Yield (%)	Comments
1	$Ti(OBu)_4$ (**1**)	12	/	Gel partially formed
2	$Ti(OBu)_4$ (**1**)	48	70%	Gel partially formed
3	$Ti(OBu)_4$ (**1**)	72	80%	Gel partially formed
4	$Ti(O^iPr)_4$ (**2**)	12	80%	Gel partially formed
5	$Ti(O^iPr)_4$ (**2**)	48	87%	Gel fully formed
6	$Ti(O^iPr)_4$ (**2**)	72	85%	Gel fully formed

In particular, it was evaluated the aging time required to form the gel and its complete formation was obtained only in *Entries 5* and *6*, where precursor **2** was used and at least 48h of aging was performed. Considering the lower time, the best result was obtained in *Entry 5*: for this reason, the following characterization will enclose principally the Ce-doped NPs obtained from these experimental conditions and will be considered as compound **4**.

Chemical characterization

The synthesized NPs were analysed through XRD and SEM-EDS analysis. With the XRD analysis, a number of titania samples were compared, including the synthesized Ce-doped TiO_2 (compound **4**), a synthesized pure sample (compound **5**, obtained with the same sol-gel method and conditions of compound **4** but without the dopant source) and a commercial sample (P-25 Degussa from Evonik supplier, compound **6**). In *Figure 12*, the XRD signals are shown.

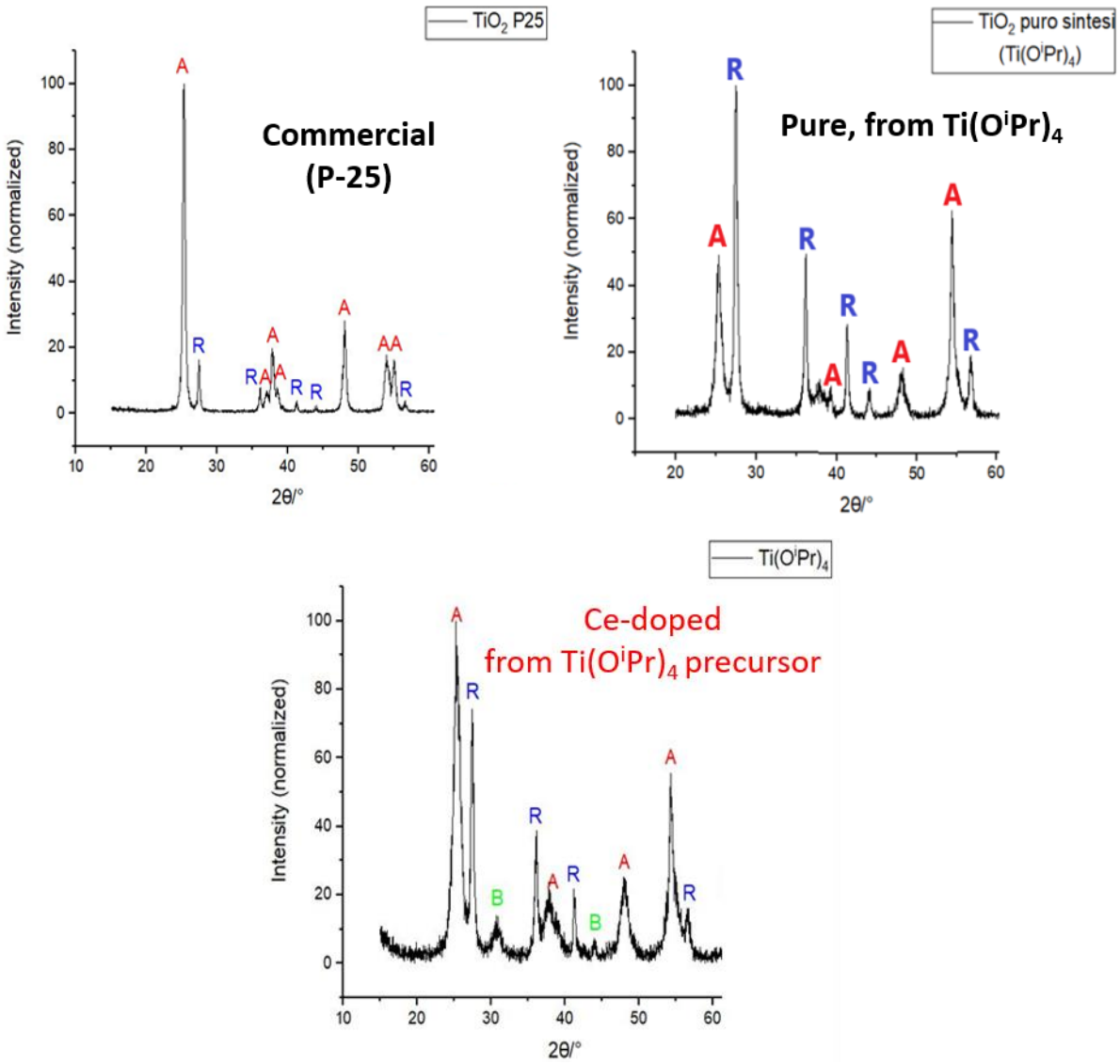

Figure 12 – XRD diffractograms of TiO_2 samples: top left: commercial (pristine), sample **6**; top right: synthesized (pristine), sample **5**; bottom: synthesized (doped), sample **4**. A = anathase phase; R = rutile phase; B = brookite phase.

The result of this analysis is reported in *Table 5*.

Table 5 – Results of XRD analysis.

Sample Name	% anatase phase	% rutile Phase	% brookite phase	Anatese lattice parameters	
				a	c
Crystalline anatase (literature)	100%	/	/	3.784	9.511
P-25 (commercial, 6)	83.2%	16.8%	/	3.788	9.513
Pure TiO_2 (synthesized, 5)	64.5%	35.5%	/	3.783	9.485
Ce-TiO_2 (synthesized, 4)	42.7%	27.9%	29.4%	3.790	9.478

A first topic of discussion is the lower presence of the anatase phase in the synthesized samples, and the doped one has the lowest concentration (43% in **4**, 65% in **5**, more than 80% in **6**). Besides the signals of anatase and rutile phases, in the doped sample **4** is present a third phase, that was recognized as the brookite polymorph of titania, while any detectable presence of cerium crystalline structure (e.g., CeO_2) was detected. This is consistent with the doping way of functionalization, based on low amount of dopant to ensure a crystalline modification but, at the same time, to avoid the formation of new phases relative to the dopant specie. Anyhow, the large formation of the brookite phase is still surprising and it seems to be largely influenced by the presence of the Ce ions, since the sample synthesized without dopant only have rutile and anatase phases. A possible interpretation is the probable interference of Ce(III) ions during the formation of the crystalline phase of TiO_2, that preferentially lead to the formation of the brookite phase.

Another relevant point is the lattice parameters of the anatase phase, since it is known in literature that there is a dependence of lattice parameters on the crystallite dimensions: in particular, lower sizes are related with higher *a* parameter and lower *c* parameter.[96] Considering that doping processes commonly result in the formation of anatase crystallites of lower dimensions respects to pure ones, so it is possible to indirectly check the doping of the anatase structure by comparing the *a* and *c* parameters with the ones of pure samples. In accordance with the literature, the XRD analysis confirmed that the doped sample **4** has the lowest *c* parameter and the highest *a* parameter.

In *Figure 13*, there is shown the SEM morphological investigation made on NPs. The images are taken at similar magnification (450K and 630K) and using the same EHT and WD (2 kV and 1.9 mm, respectively).

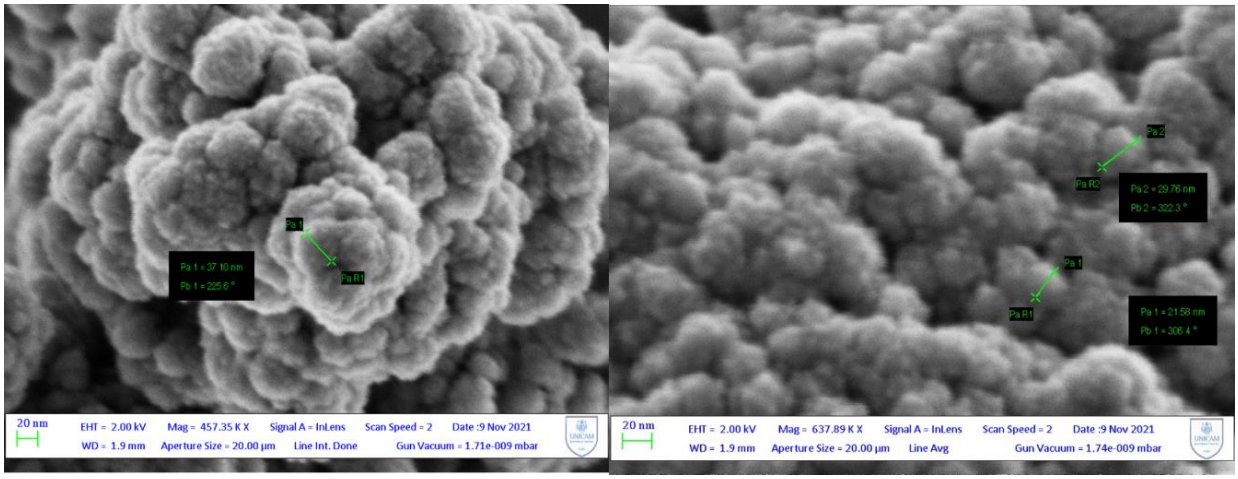

Figure 13 – SEM images of pristine TiO_2 (synthesized, sample **5**) and Ce-doped TiO_2 (synthesized, sample **4**).

From these images, it is clear that NPs are agglomerated in larger structures. Anyhow, it was possible to partially determine the size of the single nanoparticle, confirming the lower dimensions of doped TiO_2 respect to the pure one (20-30 nm vs 35-45 nm). Additionally, the EDS spectrum of doped sample **4**, together with the semi-quantitative X-ray elemental microanalysis, are reported in *Figure 14*. Even in this case, it was not possible to detect an appreciable presence of Ce in the NPs.

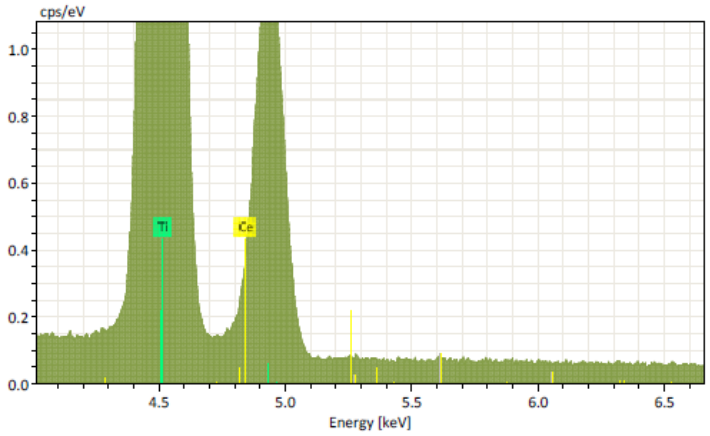

Element	At. No.	Netto	Mass [%]	Mass Norm. [%]	Atom [%]	abs. error [%] (1 sigma)	rel. error [%] (1 sigma)
Nitrogen	7	15565	2.87	2.86	5.99	0.36	12.47
Oxygen	8	55645	28.78	28.64	52.51	3.15	10.93
Silicon	14	3881	0.23	0.23	0.24	0.03	14.81
Titanium	22	597194	67.15	66.82	40.95	1.96	2.91
Cerium	58	8290	1.45	1.45	0.30	0.07	4.58
		Sum	**100.49**	**100.00**	**100.00**		

Figure 14 – EDS spectrum and elemental microanalysis for Ce-doped TiO_2 (synthesized, sample **4**).

- **Silanization reaction**

The mechanism of silanization reaction with MAPTMS (compound **7**) can be schematized as in *Scheme 4.*

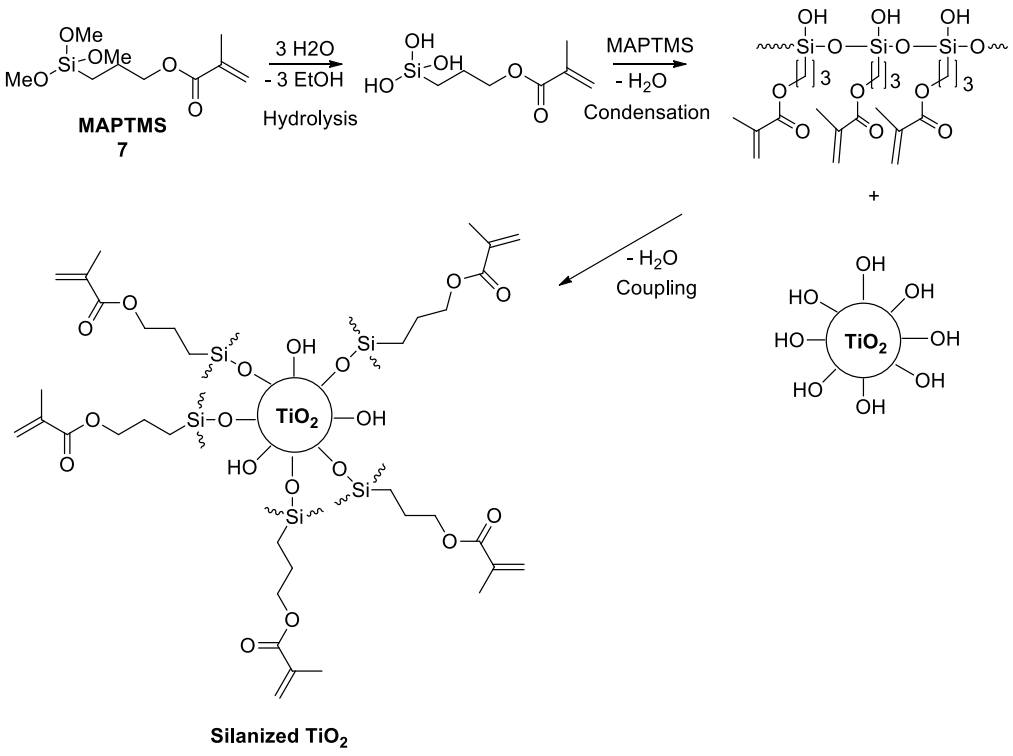

Scheme 4 – Mechanism for the silanization reaction of TiO_2 NPs with MAPTMS.

Basically, NPs were dispersed in EtOH (96%), using an ultrasound vibration for a prolonged time (30 minutes at least). After that, the coupling agent **7** was added and the silane were mixed for 2 hours with the NPs, in order to ensure an initial hydrolysis of methoxy groups and an interaction between silane and substrate. At this moment, the interactions are H-bonds between silanol groups and surface -OH group of titania. In order to promote a covalent bonding, high temperatures are required, since the elimination of water from the system can result in a greater coupling between silane and TiO_2. In this way, the solution was centrifugated and the solvent physically removed; then, the wet slurry was uniformly distributed (to increase as more as possible the superficial area) placed to drying in an oven at 110°C for 4 hours or more. At the end, the solid was milled, obtaining the modified NPs.

In order to check the hydrophobic nature of modified NPs and the increased dispersibility in organic solvents, a number of tests were performed. As example, it was tested the tendency of dispersion for non-modified and modified TiO_2 in different liquid phases. For this purpose, a mixture 1:1 of water and methylmethacrylate (MMA, **8**) was prepared. After the addition and an initial

mixing, it was clear the tendency of the bare titania to prefer the aqueous layer, while the silane-modified sample was completely dispersed in MMA (*Figure 15*).

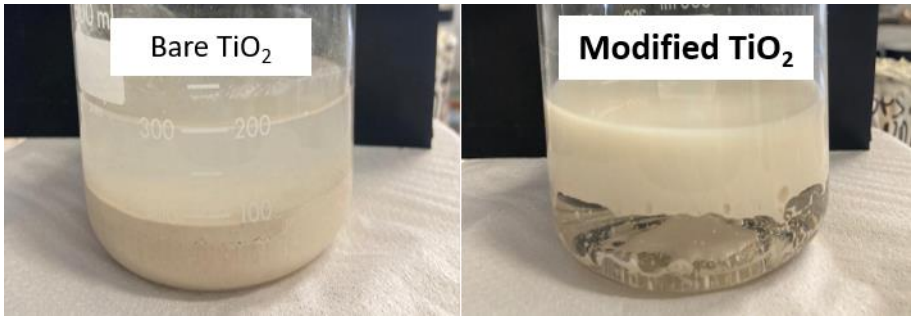

Figure 15 – Pictures of 1:1 mixture of water and MMA with bare (left) and modified (right) TiO_2 NPs.

Another interesting experiment was the estimation of the water contact angle. In few words, a small quantity of bare or modified TiO_2 was uniformly distributed and a drop of water was placed onto them. The pictures taken from this experiment are reported in *Figure 16*.

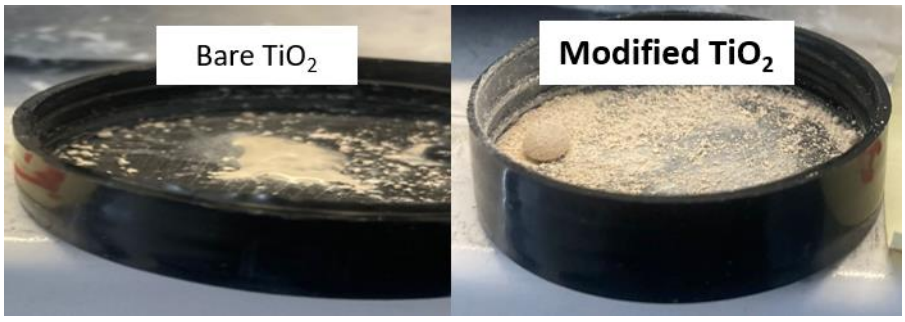

Figure 16 – Hydrophilic and hydrophobic behaviour of bare (left) and modified (right) TiO_2 NPs.

From *Figure 16*, it is clear the hydrophobic behaviour of modified titania, since the water droplet maintains its spherical form. Conversely, the hydrophilic nature of unmodified TiO_2 is evident and the complete wetting was observed after few moments.

Chemical characterization

The modified NPs were analysed through FT-IR, TGA and SEM-EDS analyses. Many trials have been conducted before setting the final parameters for the silanization reaction. For instance, it was performed the reaction using increasing amount of silane **7** (5%, 10%, 20%, 50% and 100%, weight percentage respect to the mass of TiO_2). In order to check eventual differences, FT-IR and TGA analyses were performed. In *Figure 17*, it is reported the IR spectra of pure (top left) and modified TiO_2 using 5% (top right) and 50% (bottom) of MAPTMS.

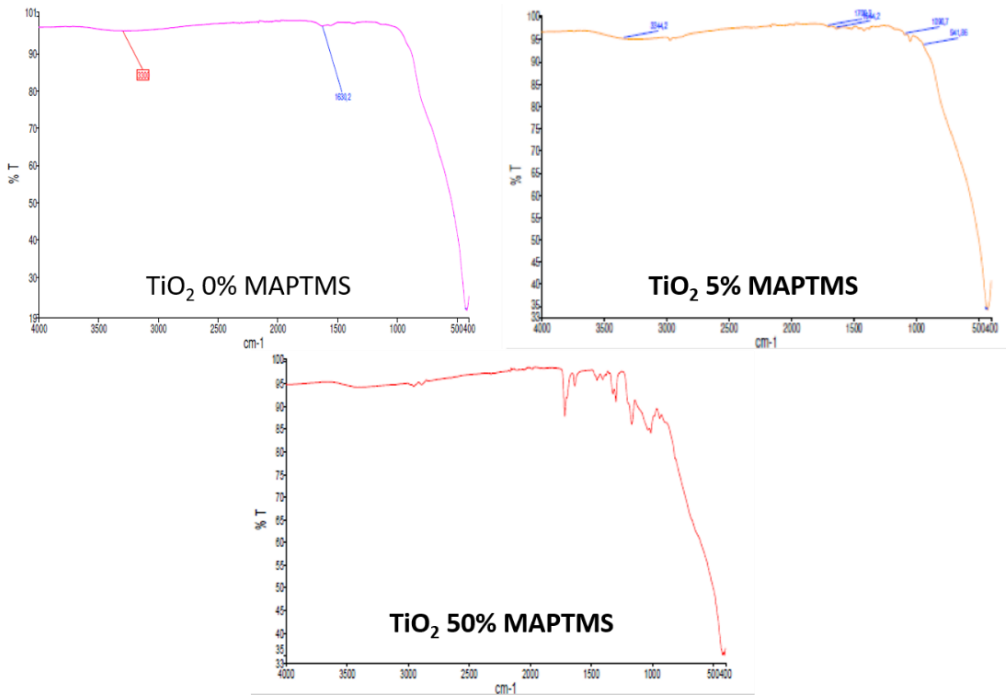

Figure 17 – FTIR spectra of TiO_2 samples: top left: bare titania (sample **6**); top right: titania modified with 5% of silane; bottom: titania modified with 50% of silane.

The signals relative to the methacrylate function of compound **7**, in particular 1710 cm^{-1} (stretching of C=O) and 1640 cm^{-1} (C=C vibration), are present in both the modified samples and they have intensity proportional to the amount of silane used. Moreover, the signals at 1090 cm^{-1} and 940 cm^{-1} were assigned to the stretching of Si-O-Si and Si-O-Ti bonds.

Moreover, the TGA analysis enabled the determination of the polymer amount present on the treated samples. In *Figure 18*, the graphs obtained with different amount of silane (5, 50 and 100%), while the results are resumed in *Table 6*.

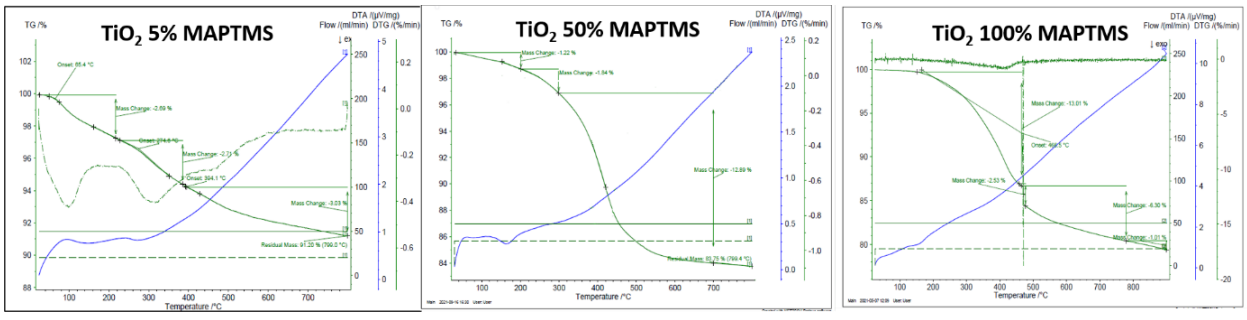

Figure 18 – TGA thermograms of treated titania: left: titania modified with 5% of silane; middle: titania modified with 50% of silane; right: titania modified with 100% of silane.

Table 6 – Results of TGA analysis.

Amount of 7	Weight loss in ΔT 50-100°C	Weight loss in ΔT 200-300°C	Weight loss in ΔT 400-800°C	Total weight loss
0	2.7 %	0.5%	0	3.2%
5%	2.7%	2.7%	3%	8.4%
10%	2.3%	2.2%	6.2%	11.7%
20%	1.9%	2.1%	11.3%	15.3%
50%	1.3%	2.1%	19.4%	22.8%
100%	1.2%	1.8%	23.3%	26.3%

From the literature, it is possible to divide the thermal degradation of silanized inorganics in three thermal events: the evaporation of water (from 50 to 100°C), a second water evaporation, caused by the condensation of superficial -OH groups (200-300°C) and the degradation of the polysiloxane (>350°C).[91] In the tested samples, the first and second events are more prominent when low amount of compound **7** was used. For the third event, the percentage of degradation increase proportionally until 50%, while any important difference was noted respect to the experiment with 100% of silane.

Considering the obtained results, the best prove was considered the one performed with 50% of coupling agent **7**. In this way, the optimized silanization reaction was performed to a large number of TiO_2 samples (*Table 7*).

Table 7 – TiO_2 samples treated with the silanization reaction.

Compound	TiO_2 Type	Description
6	UV-active, commercial	Mix of anatase and rutile
9	UV-active, commercial	Pure anatase
4	Vis-active, synthesized	Ce-doped
10	Vis-active, commercial	Doped
11	Vis-active, commercial	Mix of two catalysts

The SEM-EDX analysis of silanized TiO_2 (sample **11-sil.**) is reported in *Figures 19* and *20*.

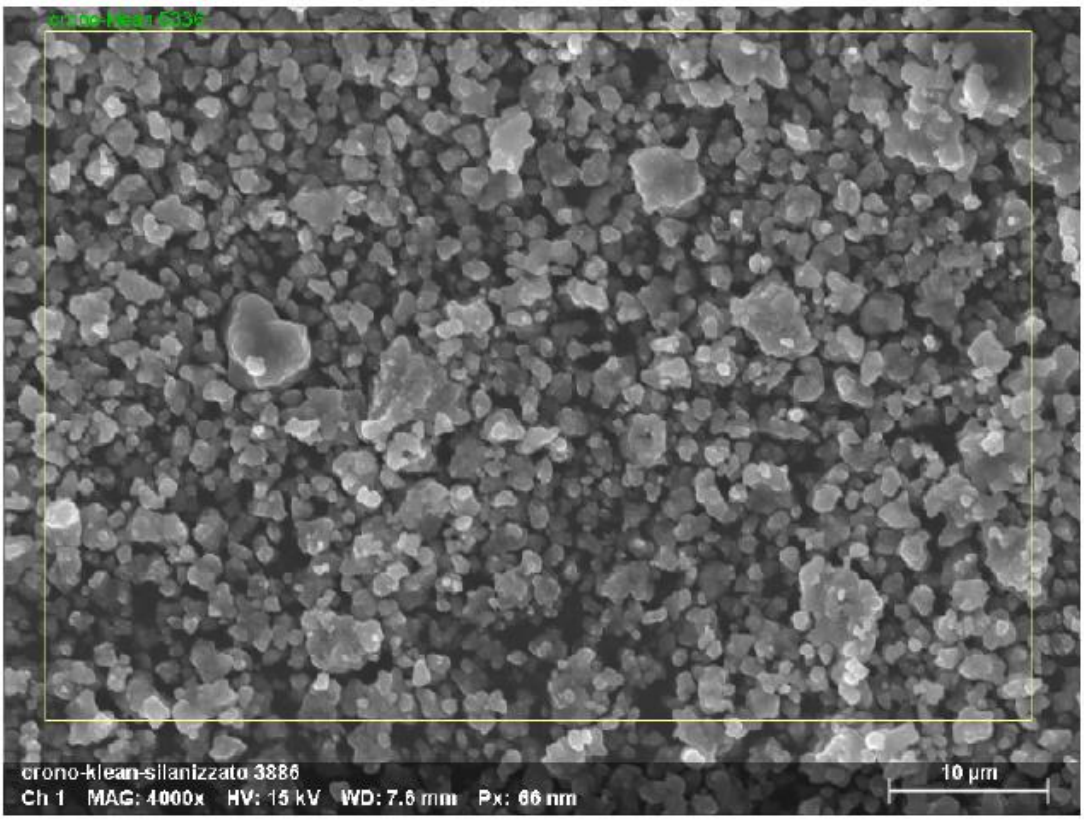

Figure 19 – SEM images of silane-modified TiO_2 NPs (sample **11-sil.**).

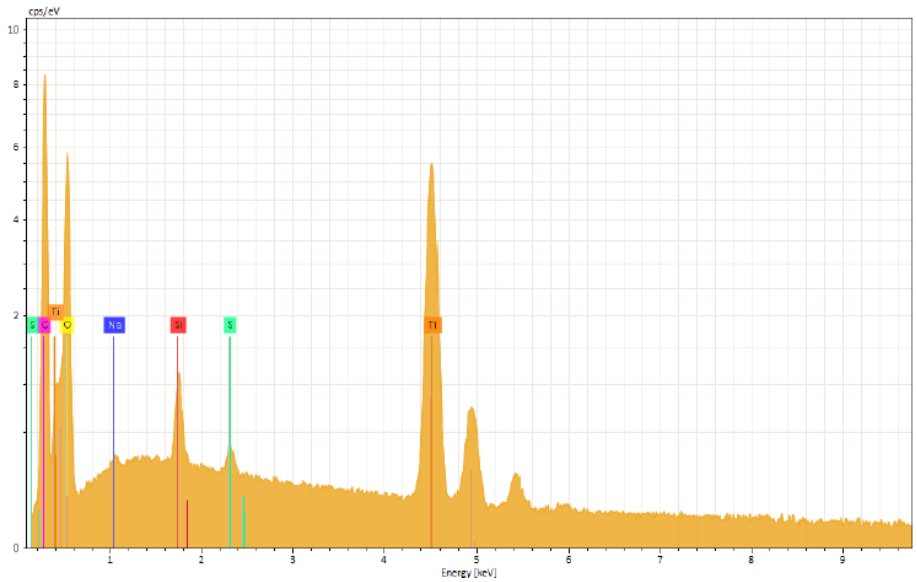

crono-klean 5336 silanizzato

Element	At. No.	Netto	Mass [%]	Mass Norm. [%]	Atom [%]	abs. error [%] (1 sigma)	rel. error [%] (1 sigma)
Carbon	6	43621	34.82	29.38	43.51	4.15	11.92
Oxygen	8	33344	47.90	40.41	44.92	5.84	12.19
Sodium	11	505	0.13	0.11	0.09	0.01	9.06
Silicon	14	7231	1.12	0.95	0.60	0.05	4.47
Sulfur	16	1792	0.34	0.28	0.16	0.02	4.62
Titanium	22	76506	34.23	28.88	10.73	1.00	2.91
		Sum	118.54	100.00	100.00		

Figure 20 – EDS spectrum and elemental microanalysis for silane-modified TiO_2 NPs (sample **11-sil.**).

The large amount of carbon (C) is consistent with the silanization process; moreover, the NPs after the treatment showed a similar morphology to non-modified ones.

1.4.2. Preparation of photocatalytic pre-polymer

After the silanization, the modified titania was used to prepare a photocatalytic pre-polymer. Briefly, NPs were dispersed in different methacrylate monomers. An ultrasound irradiation was ensured to finely disperse TiO_2 and, then, the dispersion was placed to react through a partial polymerization, with a controlled ramp of temperatures.

For this purpose, a thermal-activable radical initiator was used in the initiation phase, from which a methacrylate radical is formed. The latter is then involved in the propagation reactions and it can react both with a free monomer or with the methacrylate function covalently bonded to titania. The final result is a viscous liquid, made by unreacted methacrylate and the dissolved polymer, in turn formed by pure polymethacrylate and by a functionalized polymethacrylate, having the photo-activable portion. The process is schematized in *Scheme 5*.

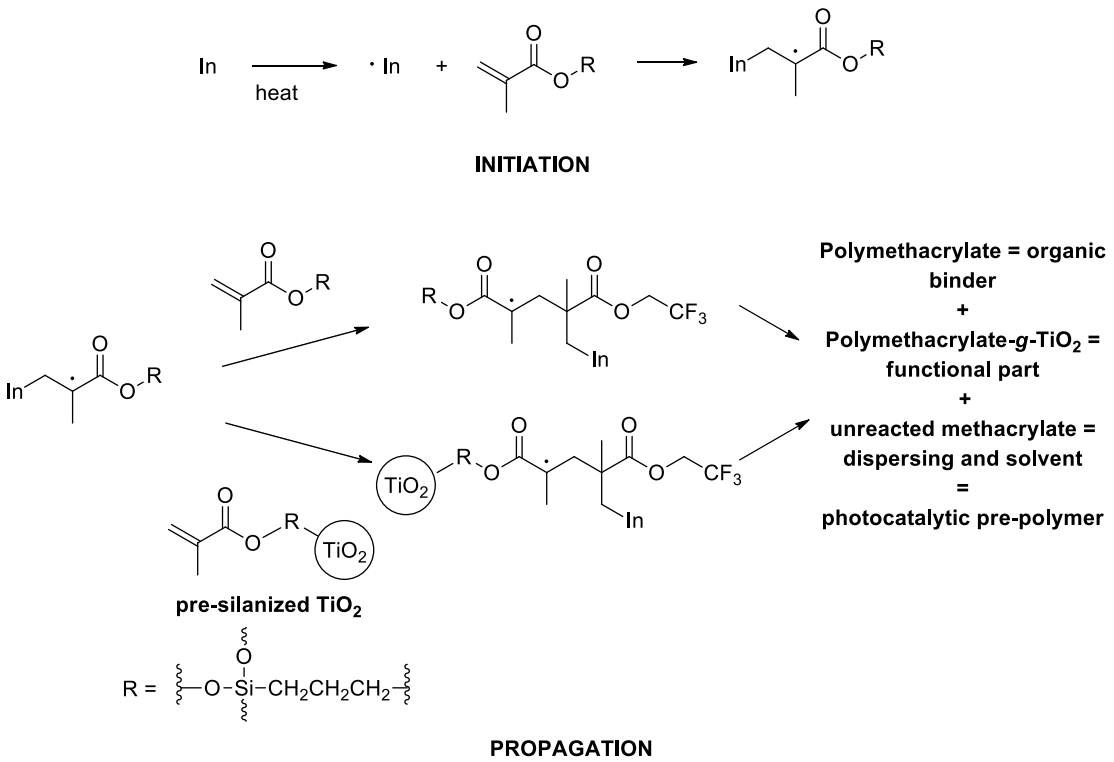

Scheme 5 – Initiation and propagation reactions in the thermal-activated radical polymerization of methacrylate monomers in presence of MAPTMS-modified TiO_2 NPs.

The pictures of pre-polymers obtained during this work are reported in *Figure 21*.

Figure 21 – Pictures of photocatalytic pre-polymers, made by different TiO_2 samples. On the left: pre-polymer made with UV-activable TiO_2 sample **6**; on the right: made with Vis-activable TiO_2 sample **11**).

The different coloration of pre-polymers derives from the type of titania used. In any case, the process was studied by varying many parameters in the system. Herein, the discussion will enclose all the tests performed to obtain a standard pre-polymer, while the efficiency of this product will be described in the next chapter, since a significant goal of the entire work was the development of prototypes made of reinforced composite material having a surface with photocatalytic activity.

The partial polymerization was performed using only three components:

i) Methacrylate monomer:
   - Methylmethacrylate (MMA, **8**);
   - 2,2,2-Trifluoroethylmethacrylate (TFEMA, **12**);
   - Isobornyl methacrylate (IBOMA, **13**).

ii) TiO_2 NPs: samples **4**, **6**, **9**, **10**, **11;** tested both pristine or silane-modified.

iii) Radical initiator:
   - Azobisisobutyronitrile (AIBN, **14**);
   - Bis(4-*tert*-butylcyclohexyl)-peroxydicarbonate (BCHPC, **15**).

Hence, different methacrylate monomers were tested: MMA is probably the most popular acrylate monomer and it was tested as reference compound. Concerning IBOMA **13**, it is a bio-derived (camphor) methacrylate having a hindered side chain group.[95] Finally, TFEMA **8** was used because it has a short fluoroalkyl, so it can create a fluoropolymer having stable C-F bonds and a certain tendency to the surface migration.

Concerning the photocatalytic component, it was tested both pure and modified TiO_2 NPs. Moreover, many tests were concentrated on finding the best quantity of dispersed NPs in the methacrylate. In this way, the partial polymerization was tested using 1%, 5%, 10%, 20%, 30% and 40% of TiO_2 (wt %).

Finally, two radical initiators were tested. They have similar half-life behaviour they were selected because suitable for the process.[98] Anyhow, it was noted that pre-polymers made with

compound **14** tend to completely polymerize in few weeks, even if it stored at low temperatures. Oppositely, the pre-polymers prepared with compound **15** were stable even after 6 months.

The lab equipment, shown in *Figure 22*, was based on a three-neck round-bottom flask, equipped with a condenser, an immersion thermal probe and a pipe of N_2 to directly feed the inert gas and replace O_2, that could interfere in the radical process. A magnetic stirrer was used to ensure a continue mixing of the dispersion in the process. It is important to note that, during the process, the viscosity of the system tend to dramatically increase, so a proper choice of the mixer system is mandatory to achieve a successful process.

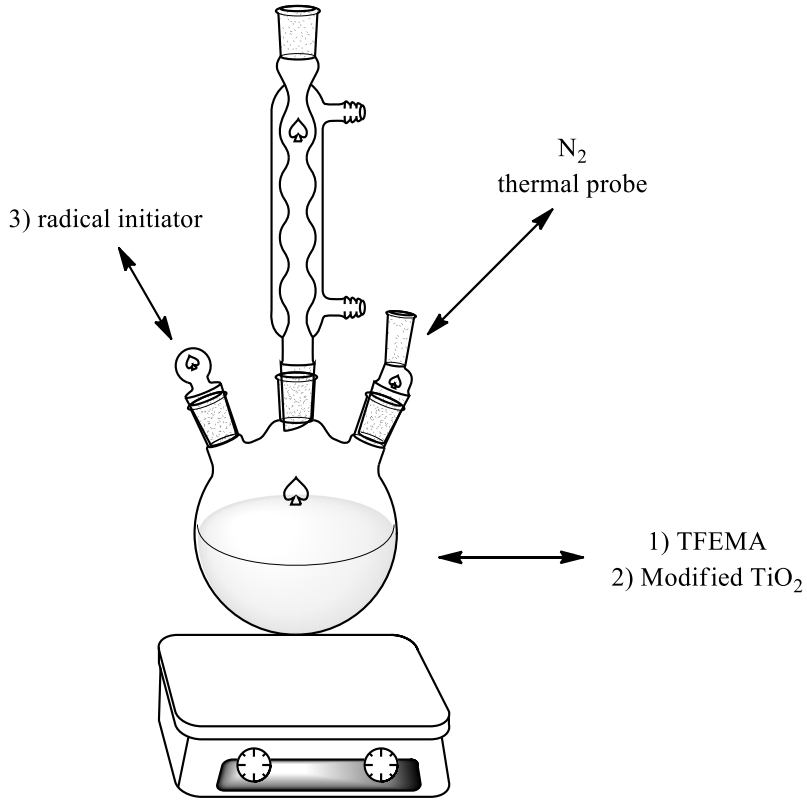

Figure 22 – Laboratory equipment for the production of the photocatalytic pre-polymer.

For this reason, in the semi-industrial apparatus (*Figure 23*), a propeller was connected to a vertical electrical stirrer, in order to ensure a greater and controlled mixing, fundamental to the effective acquisition or dispersion of heat during the process.

Figure 23 – Semi-industrial equipment for the production of the photocatalytic pre-polymer.

The heating and cooling of the reactor was regulated by a thermo-cryostat, an instrument connected to an immersive thermal probe and capable to set the programmed temperature in the system by varying the temperature of the external water jacket. The regulation of the temperature in the system is the crucial point of the entire process, since the exothermicity of the polymerization reaction acts as a self-acceleration for the entire process, leading to an out-of-control reaction and, hence, to problems in terms of safety and reactor integrity. Additionally, these polymerizations result in the formation of a solid PMMA rather than a viscous liquid (pre-polymer).

Another source of complications was noticed when modified NPs were used. Many experiments clearly indicated the impossibility to produce a pre-polymer with titania treated with an inappropriate silanization reaction, since the formation of an insoluble solid was always noticed in these cases. The probable explanation is the release of free silane molecules during the process, that can act as cross-linker agents, with the consequent formation of insoluble polymers. When the silanization was performed ensuring the covalently-bonded modification, this problem was not noticed and a large number of photocatalytic pre-polymers were easily prepared.

Finally, it was noted some critical issues in mixing when the partial polymerization was performed using more than 20% of titania, due to the high presence of NPs and the increasing viscosity, caused by the partial polymerization.

The viscosity and the dry (130°C) residue determinations were used to determine the efficiency of polymerization, since, for the same quantity of dispersed NPs, these parameters were strongly dependant on the polymerization outcome. In *Table 8*, their mean values are resumed according to the amount of TiO_2 and the type of methacrylate used in the pre-polymer.

Table 8 – Pre-polymers produced.

Pre-polymer type	Amount of TiO_2 (% wt)	Methacrylate	Viscosity (cP, at 20°C)	Dry residue (%)
I	1% (silanized)	TFEMA (**12**)	2,000-3,000	8-10%
II	5% (silanized)	TFEMA (**12**)	5,000-8,000	15-18%
III	10% (silanized)	TFEMA (**12**)	10,000-13,000	25-29%
IV	20% (silanized)	TFEMA (**12**)	30,000-55,000	36-42%
IV-B	20% (pristine)	TFEMA (**12**)	/	36-42%
V	20% (silanized)	MMA (**8**)	25,000-30,000	40-41%
VI	20% (silanized)	IBOMA (**13**)	/	49-51%
VII	30% (silanized)	TFEMA (**12**)	150,000-250,000	46-50%
VII-B	30% (pristine)	TFEMA (**12**)	/	46-50%
VIII	30% (silanized)	MMA (**8**)	/	45-47%
IX	40% (silanized)	TFEMA (**12**)	/	51-56%

For the determination of viscosity, a sufficient volume of pre-polymer was required and, so, it was possible to determine only with the semi-industrial preparations. The main trend is the increase of viscosity together with the increase of titania, such as for the dry residue. Anyhow, for the latter, any significant difference was noted among the trials at 30 and 40% of TiO_2 (pre-polymers **VIII** and **IX**).

Finally, it was performed a precipitation process, using a non-solvent (e.g., n-hexane) in order to collect the solid part present in the pre-polymer.[99] The extracted polymer and the liquid part for pre-polymer **IV** are shown in *Figure 24*.

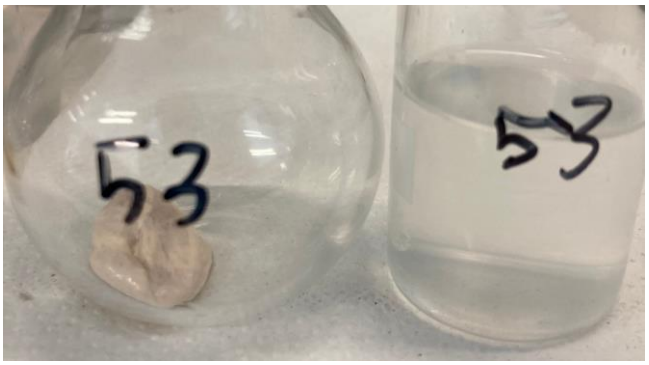

Figure 24 – Polymer extraction with non-solvent from photocatalytic pre-polymer **IV**.

Additionally, the extracted polymer was dissolved in a solvent (e.g., dichloromethane) and, after a period of mixing, the re-precipitation with non-solvent was performed (*Figure 25*).

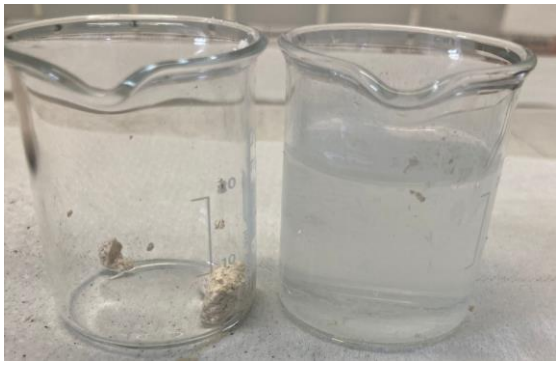

Figure 25 – Polymer extraction after precipitation-dissolution-reprecipitation from photocatalytic pre-polymer **IV**.

In both cases, it is evident that the extracted polymer has the coloration of the titania, indicating that the TiO_2 remain embedded in the polymer matrix, even after the polymer is dissolved in a solvent. Additionally, the ash residue (600°C) of extracted polymer (both after precipitation and after precipitation-dissolution-reprecipitation) was determined, as shown in *Table 9*.

Table 9 – Ash residue after precipitation and precipitation-dissolution-reprecipitation of pre-polymer **IV**.

Amount of TiO_2 (% wt)	Methacrylate	Ash residue (%)
10%	TFEMA (**8**)	19-20%
20%	TFEMA (**8**)	39-40%
20%, after dissolution and re-precipitation	TFEMA (**8**)	44-45%

1.4.3. Prototypes and determination of photocatalytic activity

In this section, it is described the preparation of PMMA/TiO_2 and PMMA/SiO_2/TiO_2 composite materials, in order to evaluate the superficial photocatalytic activity of these prototypes. For this purpose, the test method was the determination of the photocatalytic activity of surfaces in an aqueous medium by the degradation of Methylene Blue (MB), following the ISO standard 10678:2010.[100] The experimental layout is reported in *Figure 26*.

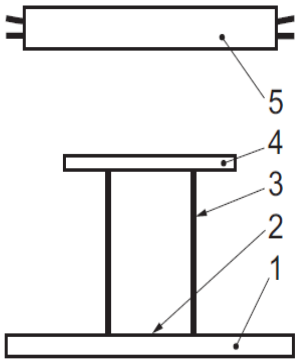

Key
1 sample
2 testing area, point where light intensity is measured
3 testing cylinder
4 glass pane (5.3)
5 UV-radiation light source (5.4)

Figure 26 – Schematic diagram of the measuring device for the degradation of MB using a test cylinder.

Briefly, the test is based in a light-off and in a light-on experiments, lasting 3 hours each. In the light-on experiment, a BLB (blacklight blue) lamp was used, while the light-off test was conducted in the dark. In both cases, the MB solution fills the test cylinder, in turn glued onto the surface of the material. The scope is to evaluate the difference in the absorbance of the MB solution, measuring the absorbance of the solution at regular intervals of time (20 minutes).

In accordance to the Lamber-Beer law, the absorbance of the MB solution is directly proportional to the concentration. Hence, by the construction of a calibration line (*Figure 27*), it is possible to determine the concentration (in ppm) of the solution during the test.

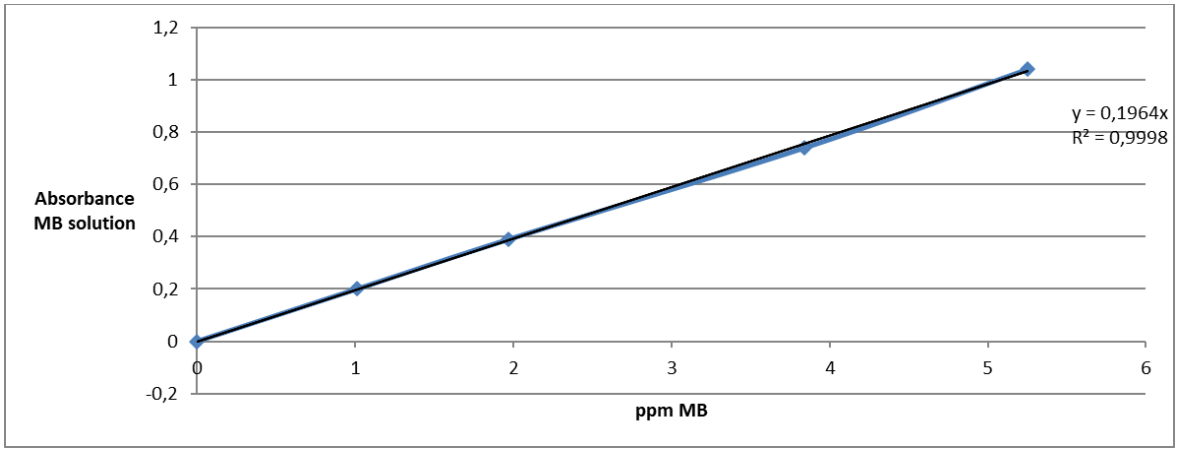

Figure 27 – Calibration line and equation for the determination of the concentration of MB during the degradation test.

In conclusion, by this test, it is possible to calculate both the percentage of degradation of MB and the photocatalytic parameters P_{MB} (specific photoactivity) and ξ_{MB} (photonic efficiency). For P_{MB} and ξ_{MB}, it is necessary to determine the specific degradation rate in the light-off and light-on experiments (R_{dark} and R_{irr}, respectively) by applying the following equations (*Equations 16-17*):

16) $$R_{dark} = \frac{\Delta A_{\lambda,dark} \cdot V}{\Delta t \cdot \varepsilon \cdot d \cdot A}$$ 17) $$R_{irr} = \frac{\Delta A_{\lambda,irr} \cdot V}{\Delta t \cdot \varepsilon \cdot d \cdot A}$$

Equations 16-17

where:

ΔA_λ = absorbance difference among two consecutive measures;

V = volume of MB solution (3,5 x 10^{-5} m^3);

Δt = time difference among two consecutive measures (0.33 h);

ε = molar extinction coefficient of MB in water at the concentration of 10µM (7402,8 m^2/mol at c = 10 µmol/L and λ = 664 nm);

d = optical path distance (0.01 m);

A = irradiated area (0.001256 m^2).

R_{dark} and R_{irr} are expressed in mol/(m^2·h).

In this way, the specific photoactivity is calculated as (*Equation 18*):

18) $$P_{MB} = R_{irr} - R_{dark}$$

Equation 18

while the photonic efficiency as (*Equation 19*):

19) $$\xi_{MB} = \frac{P_{MB}}{E_p}$$

Equation 19

where the photonic intensity of UV radiation (E_p) is calculated, based upon a constant UV-radiation intensity E, using *Equation 20*:

20) $$E_p = \lambda_{max} \cdot E \cdot 30{,}074 = 0.11$$

Equation 20

where:

λ_{max} = peak wavelength of UV-radiation (λ = 365 nm);

E = UV radiation intensity, measured with an UV-radiometer (10 W/m^2).

- **Photocatalytic activity of PMMA/TiO_2 composites**

Photocatalytic pre-polymer, prepared in the previous step, were mixed with an acrylic syrup and the resulting dispersion was used to prepare a large number of PMMA/TiO_2 composites. For acrylic

syrup, it is intended a viscous liquid made by dissolved PMMA in MMA. Therefore, it is quite similar to the photocatalytic pre-polymer and it misses only of the photocatalytic component. At this point, it is important to highlight that photocatalytic pre-polymer was used as a minor component of the composite, so it is meant that low quantities of titania have to be directly incorporated in the polymer matrix and not applied as a superficial coating.

Prototypes were obtained by free-radical polymerization, dissolving a radical initiator in the system and pouring the resulting dispersion in a mold, in turn made by a PVC gasket comprised by two metallic plates. After the complete filling, the molds were immersed in a hot-water bath, ensuring the polymerization to PMMA/TiO_2 composites.

In order to check the photocatalytic activity of the surfaces of obtained prototypes, the degradation of MB was evaluated. For this purpose, also different prototypes, made through alternative approaches, were used as references and the discussion will enclose the photoactivity results obtained by different approaches (*Table 10*).

Table 10 – Tested approaches for the development of PMMA/TiO_2 composite materials.

Approach type	Description
Case study approach	Mixing of pre-polymers **I-IX** with acrylic syrup
Alternative approach A	Mixing of pristine TiO_2 with acrylic syrup
Alternative approach B	Mixing of silane-modified TiO_2 with acrylic syrup
Alternative approach C	Mixing of photocatalytic paint, made of titania **6** in a commercial organic binder, with acrylic syrup

PMMA/TiO_2 materials are shown in *Figure 28*. In these initial prototypes, the discussion is limited to the titania sample **6** (for the type of TiO_2, *Table 7*).

Figure 28 – PMMA/TiO_2 prototypes made with the case study approach (left), alternative approach B (right) and alternative approach C (middle).

Results of the MB degradation tests with PMMA/TiO_2 prototypes are listed in *Table 11*. For the type of pre-polymers, the reference is *Table 8*; for the alternative approaches, you can refer to *Table 9*.

Table 11 – Results of MB degradation using different approaches.

Approach type	% TiO_2 in composite	MB degradation	P_{MB} (mol/(m^2h))	ξ_{MB}
Case study – pre-polymer I	0.9%	15.5%	1.71 x 10^{-5}	0.015%
Case study – pre-polymer II	0.9%	16.3%	1.90 x 10^{-5}	0.017%
Case study – pre-polymer III	0.45%	10.2%	1.14 x 10^{-5}	0.010%
	0.9%	19.7%	2.28 x 10^{-5}	0.021%
Case study – pre-polymer IV	0.45%	10.9%	1.14 x 10^{-5}	0.010%
	0.9%	23.6%	2.97 x 10^{-5}	0.027%
Case study – pre-polymer IV-B	1.5%	11.7%	1.32 x 10^{-5}	0.013%
	2.5%	18.7%	2.16 x 10^{-5}	0.019%
Case study – pre-polymer V	1.5%	10.3%	1.14 x 10^{-5}	0.010%
	2.5%	19.4%	2.28 x 10^{-5}	0.021%
Case study – pre-polymer VI	1.5%	6.7%	8.56 x 10^{-6}	0.008%
	2.5%	16.7%	1.90 x 10^{-5}	0.017%
Case study – pre-polymer VII	0.45%	12.3%	1.71 x 10^{-5}	0.015%
	0.9%	20.6%	2.28 x 10^{-5}	0.021%
Alternative A	1.5%	4.5%	6.84 x 10^{-6}	0.006%
	2.5%	8.1%	1.14 x 10^{-5}	0.010%
Alternative B	1.5%	6.7%	8.56 x 10^{-6}	0.008%
	2.5%	9.3%	1.43 x 10^{-5}	0.013%
Alternative C	1.5%	7.9%	1.14 x 10^{-5}	0.010%
	2.5%	14.6%	1.71 x 10^{-5}	0.015%

In order to settle the photocatalytic activity for the surfaces of tested materials, cut-off values were imposed. In particular, tests with $\xi_{MB} < 0.005\%$ were considered negative and the corresponding prototypes as photo-unreactive. Instead, tests with photonic efficiency comprising the range $0.005 \leq \xi_{MB} < 0.010\%$ were listed as partially positive and the prototype was considered to have an ambiguous photocatalytic activity. Only tests with $\xi_{MB} > 0.010\%$ were considered fully positive and the surface of these materials as effectively photo-reactive.

With this view, in *Table 11*, there are listed all the tests having from sufficient to important photocatalytic activities for the various approaches. It is important to specify that the quantity of TiO_2 used in the prototypes are expresses as the percentage ratio of the mass (in g) of titania and the total mass of PMMA/TiO_2 composite.

Only the prototypes made with the photocatalytic pre-polymers **I**, **II**, **III**, **IV**, **VII** can ensure a good photo-activity with the lowest concentration of TiO_2. In these cases, it was generally required a quantity of 0.45% to have a sufficient photocatalytic activity, while optimal results were obtained with only 0.9% of titania.

On the other hand, when TFEMA was replied with MMA (pre-polymer **V**) or IBOMA (pre-polymer **VI**), or when unmodified TiO_2 was used to prepare the pre-polymer (**IV-B**), important photocatalytic results were obtained only by raising the amount of TiO_2 (up to 2.5%). The same requirement was noticed when alternative approaches B and C were used, while, when bare TiO_2 NPs were just mixed with the acrylic syrup (alternative approach A), any significant photo-activity was noticed, even at high concentrations.

Focusing on the prototypes made with photocatalytic pre-polymers, it was considered an additional benefit the possibility to use it in low quantities. In other words, the prototypes having a pre-polymer content lower than 5% were highly appreciable. Hence, the best results were obtained when photocatalytic pre-polymers **IV** and **VII** were used, since they ensured an important photocatalytic activity, by using low concentrations of photocatalyst and low quantities of photocatalytic pre-polymer. For instance, it was required 2.5% and 5% of pre-polymer **IV** (0.45 and 0.9% of TiO_2 in the final composite) to have sufficient and optimal photo-activity, respectively. For pre-polymer **III**, 5 to 10% of pre-polymer was required, while the percentage for pre-polymer **I** and **II** was even higher.

From this initial screening, it was chosen to continue the investigation with photocatalytic pre-polymer **III**, **IV** and **VII**. The focus was placed on widening the approach toward many samples of titania, hence pre-polymers made with different TiO_2 NPs were prepared. From the initial results, it was chosen to produce prototypes having a percentage of TiO_2 = 0.45-0.9 %. From the determination of the photocatalytic activity of these prototypes, value of $\xi_{MB} > 0.010\%$ were always achieved, demonstrating the applicability of the process for different titania photocatalysts. In *Figure 29*, the chart of the MB absorbance toward the time for the prototype made with the pre-polymer **III**, having 0.9% of titania **4** (Ce-doped TiO_2), while, in *Table 12*, the photocatalytic parameters calculated from this test.

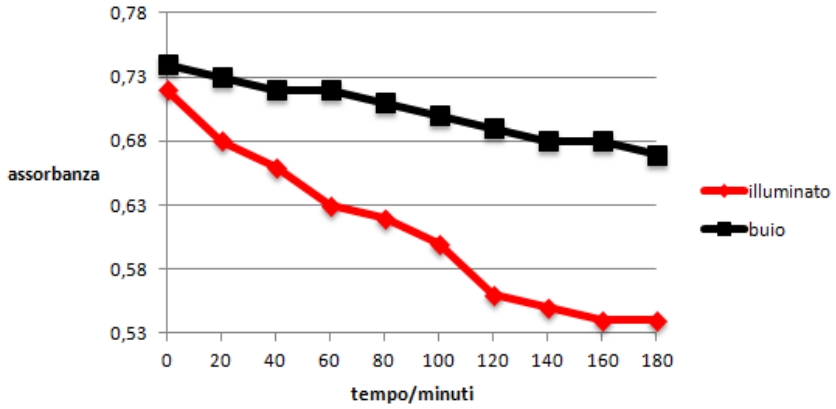

Figure 29 – Progress of the MB absorbance during the light-on (red line) and light-off (black line) experiments.

Table 12 – Results of MB degradation for prototype made with pre-polymer **III** and having 0.9% of TiO_2 **4**.

MB degradation	P_{MB} (mol/(m²h))	ξ_{MB}
16.6%	1.71×10^{-5}	0.015%

The MB degradation test confirmed the photocatalytic activity of PMMA materials, functionalized with titania **4** with an approach based on the silanization and subsequent formation of a photocatalytic pre-polymer. Anyhow, since the low availability of **4**, it was used only in PMMA/TiO_2 composites, while the other samples were tested also in the production of PMMA/SiO_2/TiO_2 prototypes.

- **Photocatalytic activity of PMMA/SiO_2/TiO_2 composites**

After having evaluated the method effectiveness in a simpler case, the attention was shifted to the development of highly-filled PMMA composites with photocatalytic surfaces. Even in this case, the main objective was to use the photocatalytic pre-polymer as minor component of the prototype. Hence, the acrylic syrup was firstly mixed with the filler (silica particles) and, then, a low amount of photocatalytic pre-polymer was dispersed in the system. The manufacture of prototypes involved the same molding process exposed in the previous section; anyhow, in this case, even semi-industrial and industrial prototypes were produced, as shown in *Figure 30*.

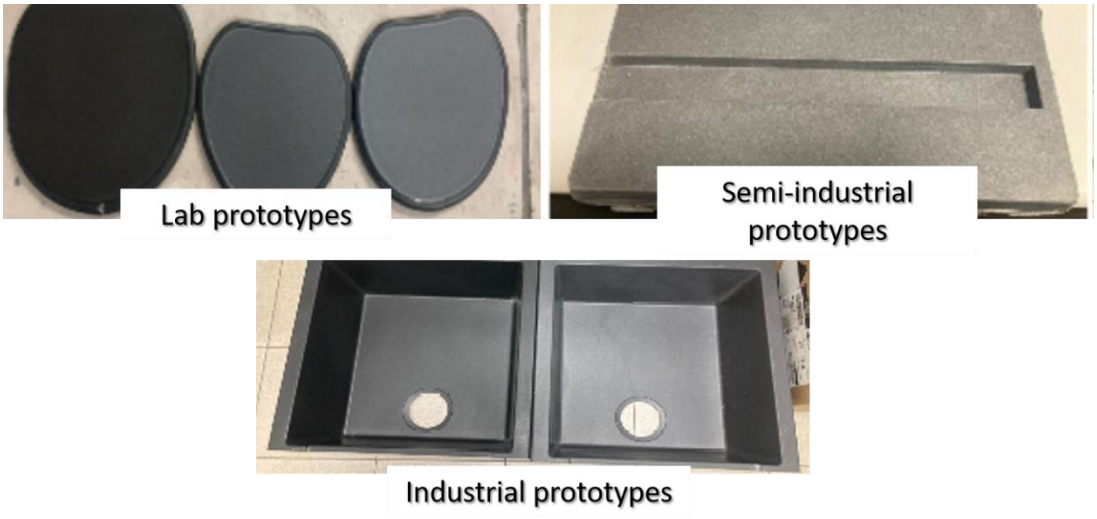

Figure 30 – PMMA/SiO_2/TiO_2 prototypes made with photocatalytic pre-polymers.

After the production of prototypes, the photocatalytic activity was measured. For the type of TiO_2, you can refer to *Table 7*; for the type of pre-polymers, the reference is *Table 8*. Moreover, the quantity of TiO_2 used in the prototypes are expresses as the percentage ratio of the mass (in g) of titania and the total mass of PMMA/SiO_2/TiO_2 composite. The cut-off values imposed for the determination of photocatalytic activity were: $\xi_{MB} < 0.005\%$ = negative test; $0.005 \leq \xi_{MB} < 0.010\%$ = partially positive; $\xi_{MB} > 0.010\%$ = fully positive.

In a first moment, the pre-polymers **III**, **IV** and **VII**, having the titania **11**, were used to test the method effectiveness. From these results, a really interesting photocatalytic activity was measured. Therefore, it was chosen to perform an extensive screening on the photocatalytic performances of different TiO_2 samples. The obtained results are resumed in *Table 13*.

Table 13 – Results of MB degradation for PMMA/SiO_2/TiO_2 prototypes.

Pre-polymer type	TiO_2 sample	% TiO_2 in composite	MB degradation	P_{MB} (mol/(m^2h))	ξ_{MB}
pre-polymer III	**11**	0.45%	5.4%	8.56×10^{-6}	0.008%
		0.9%	13%	1.83×10^{-5}	0.016%
pre-polymer IV	**6**	0.45%	7.8%	9.51×10^{-6}	0.009%
		0.9%	23.3%	2.47×10^{-5}	0.022%
pre-polymer IV	**9**	0.45%	2.6%	5.70×10^{-6}	0.005%
		0.9%	5.2%	8.56×10^{-6}	0.008%
pre-polymer IV	**10**	0.45%	13.9%	1.71×10^{-5}	0.015%
		0.9%	25.7%	3.42×10^{-5}	0.031%
pre-polymer IV	**11**	0.45%	11.8%	1.14×10^{-5}	0.010%
		0.9%	28.5%	3.23×10^{-5}	0.029%
Case study – pre-polymer VII	**11**	0.45%	12.3%	1.71×10^{-5}	0.015%
		0.9%	18.6%	2.28×10^{-5}	0.020%

From these results, significant photoactivities were obtained with all samples. The only exception is when compound **9** was used. The possible explanation could be an ineffective modification during the silanization. Anyhow, the results obtained with samples **10** and **11** were highly stimulating, since they involved the incorporation of Vis-activable photocatalysts.

For this reason, it was tested the photocatalytic activity of prototypes, made by the pre-polymer **IV** and having TiO_2 sample **10 (**in a percentage of 0.45 and 0.9%), toward a different pollutant: nitrogen oxides. The NOx degradation was measured using a UV-A and a visible (blue LED) light excitation and the experiment was conducted in an external laboratory (CE.RI.COL laboratory). Charts of NOx concentration over time with different light sources are depicted in *Figure 31*.

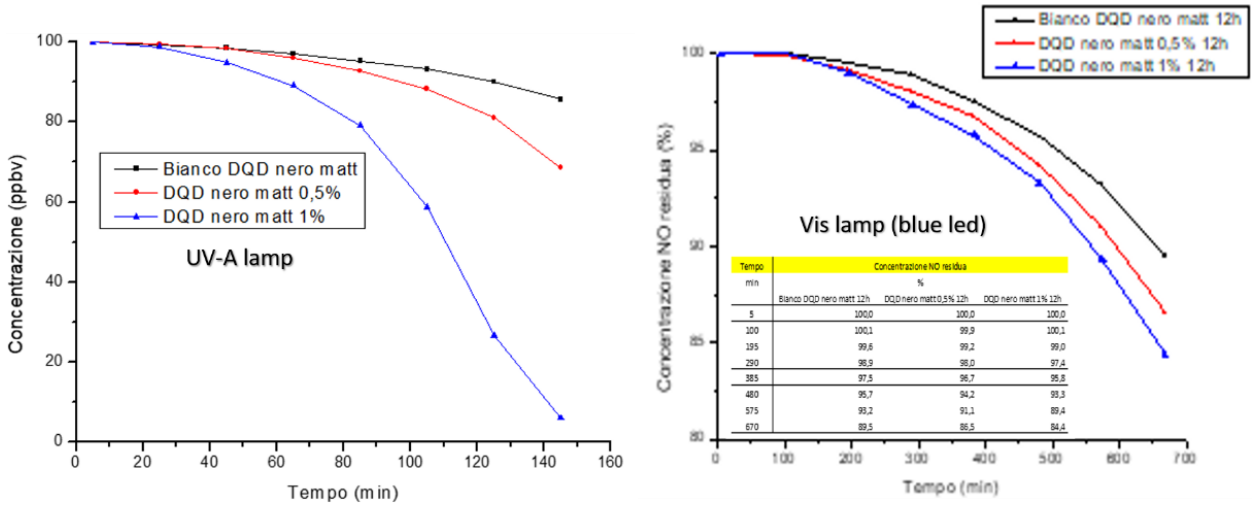

Tempo min	Concentrazione NO residua %		
	Bianco DQD nero matt 12h	DQD nero matt 0,5% 12h	DQD nero matt 1% 12h
5	100,0	100,0	100,0
100	100,1	99,9	100,1
195	99,6	99,2	99,0
290	98,9	98,0	97,4
385	97,5	96,7	95,8
480	95,7	94,2	93,3
575	93,2	91,1	89,4
670	89,5	86,5	84,4

Figure 31 – Charts of NOx degradation over time with UV-A (left) and visible light (right) illumination. Black line: light-off experiment; red line: light-on experiment, with prototype having 0.45% of TiO_2 sample **10**; blue line: light-on experiment, with prototype having 0.9% of TiO_2 sample **10**

With the UV-A irradiation, a significant decrease of pollutant concentration was noted respect to the blank experiment, especially when 0.9% of TiO_2 was present in the composite. Anyhow, the photodegradation performance was heavily lower with the visible light lamp and only a minimal degradation was measured in that cases.

Chemical characterization

The surfaces of prototypes made with the pre-polymer **IV,** having TiO_2 sample **11** in a percentage of 0.45 and 0.9% were analysed through SEM-EDS analysis. In both cases, light spots of micrometric dimensions were observed (*Figures 32* and *33*). The SEM images have similar magnification (1.43 K vs 1.12 K) and same EHT (15 kV) and WD (8 mm).

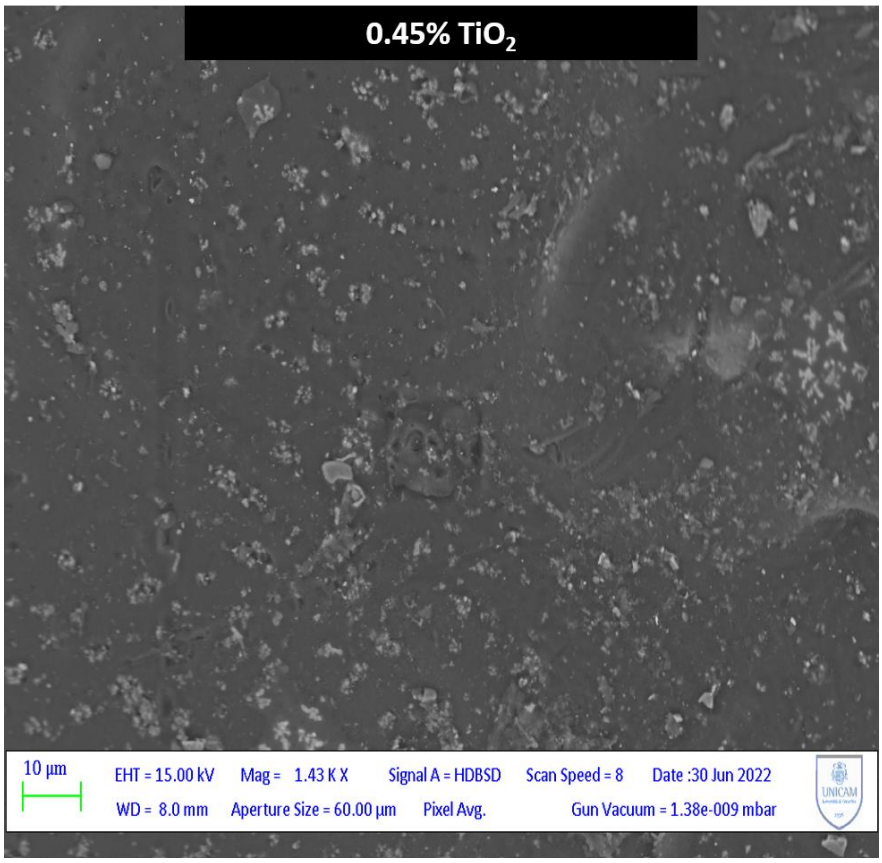

Figure 32 – SEM image of the surface of PMMA/SiO_2/TiO_2 composite, made with pre-polymer **IV** and having TiO_2 **11** (0.45%)

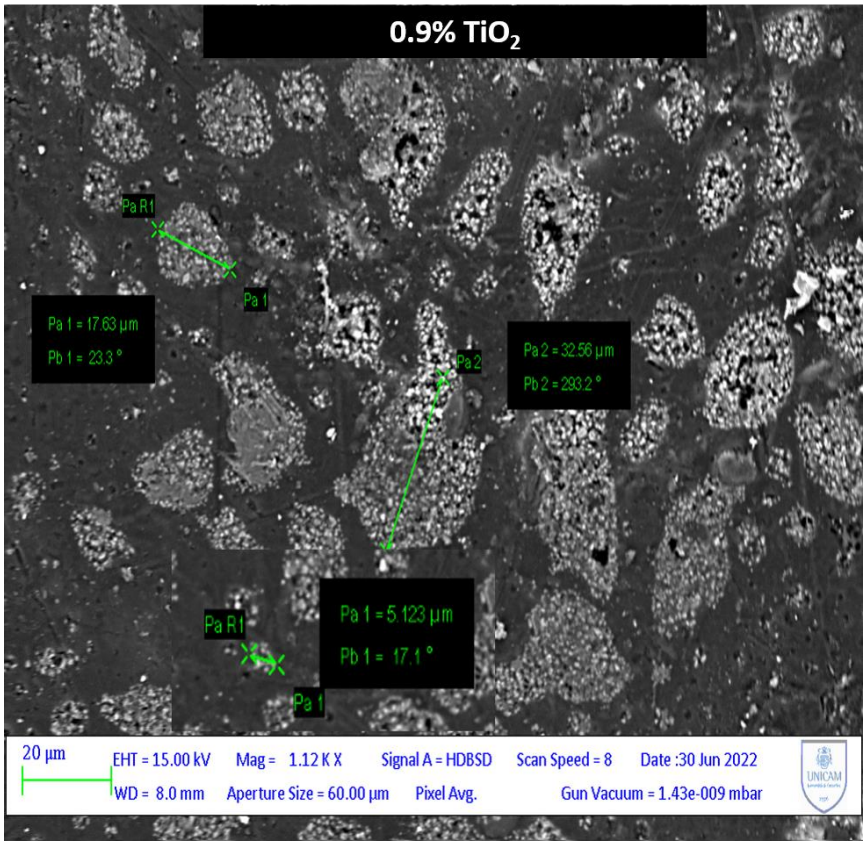

Figure 33 – SEM image of the surface of PMMA/SiO_2/TiO_2 composite, made with pre-polymer **IV** and having TiO_2 **11** (0.9%)

Additionally, the EDS microanalysis of the surface and the section of prototypes was performed. In *Figure 34*, the SEM picture of the white spots found on the surface of these materials, while in *Figure 35*, the elements found by EDS analysis and their quantification.

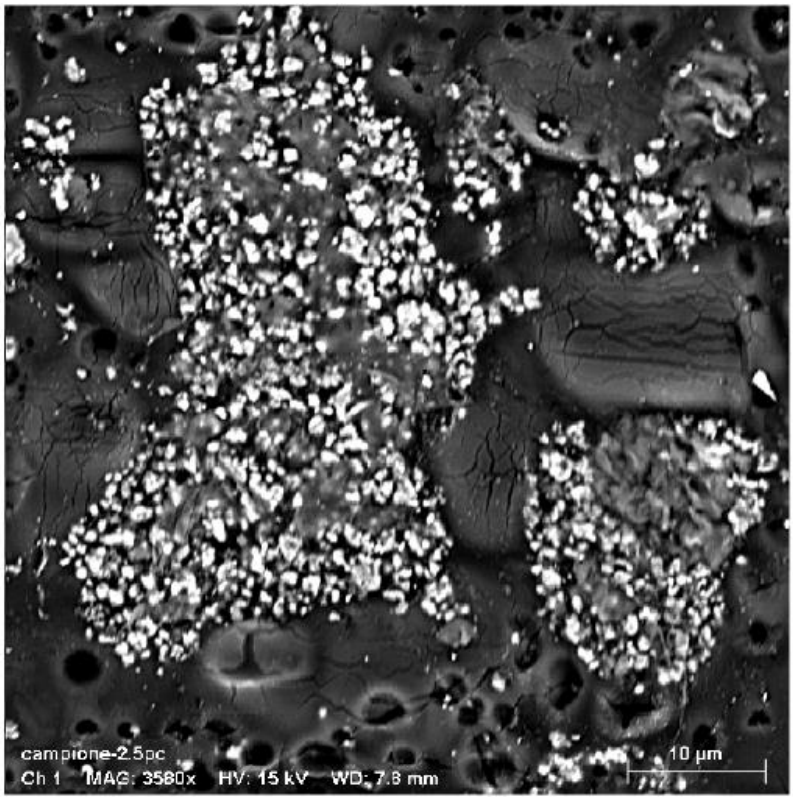

Figure 34 – SEM image of the white spot onto the surface of PMMA/SiO_2/TiO_2 composite.

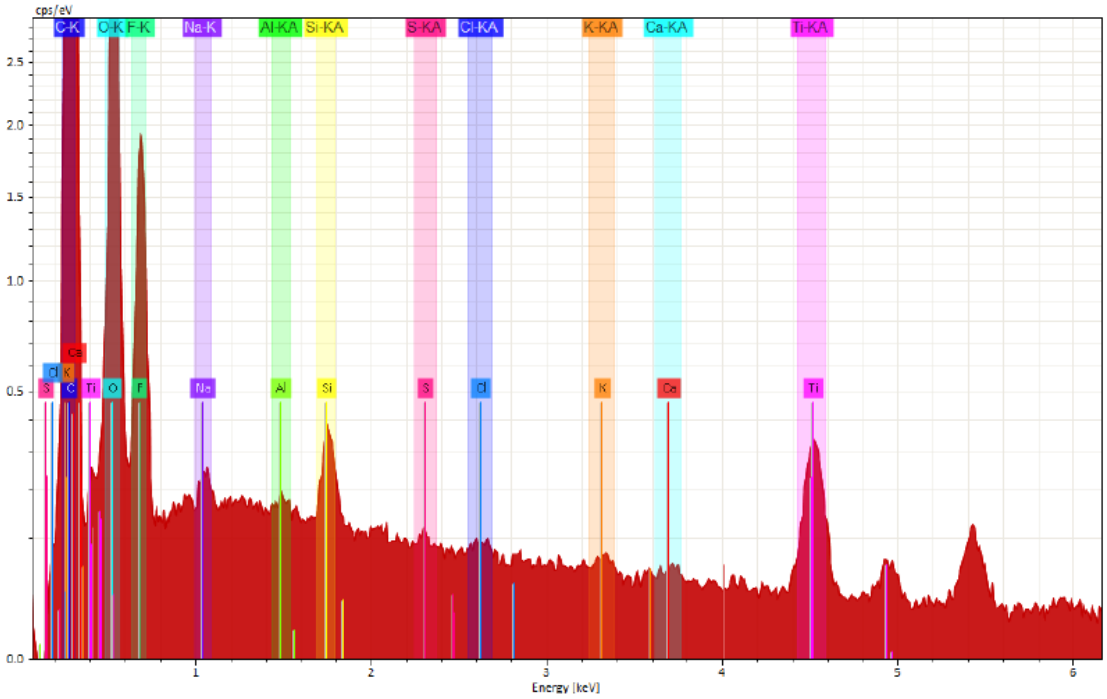

Map

Element	At. No.	Line s.	Netto	Mass [%]	Mass Norm. [%]	Atom [%]	abs. error [%] (1 sigma)	abs. error [%] (2 sigma)
Carbon	6	K-Serie	76184	55.68	55.68	64.60	6.38	12.75
Oxygen	8	K-Serie	25435	29.84	29.84	25.99	3.73	7.47
Fluorine	9	K-Serie	10957	11.52	11.52	8.45	1.59	3.18
Sodium	11	K-Serie	539	0.08	0.08	0.05	0.01	0.02
Aluminium	13	K-Serie	315	0.04	0.04	0.02	0.00	0.01
Silicon	14	K-Serie	2044	0.26	0.26	0.13	0.01	0.03
Sulfur	16	K-Serie	117	0.02	0.02	0.01	0.00	0.00
Chlorine	17	K-Serie	278	0.05	0.05	0.02	0.00	0.01
Potassium	19	K-Serie	287	0.08	0.08	0.03	0.01	0.01
Calcium	20	K-Serie	176	0.06	0.06	0.02	0.01	0.01
Titanium	22	K-Serie	4418	2.36	2.36	0.69	0.08	0.16
			Sum	100.00	100.00	100.00		

Figure 35 – EDS spectrum and elemental microanalysis of the surface of PMMA/SiO_2/TiO_2 composite.

In *Figure 36*, the SEM image of the section of prototypes. Also in this case, the EDS spectrum and the elemental analysis are reported (*Figure 37*).

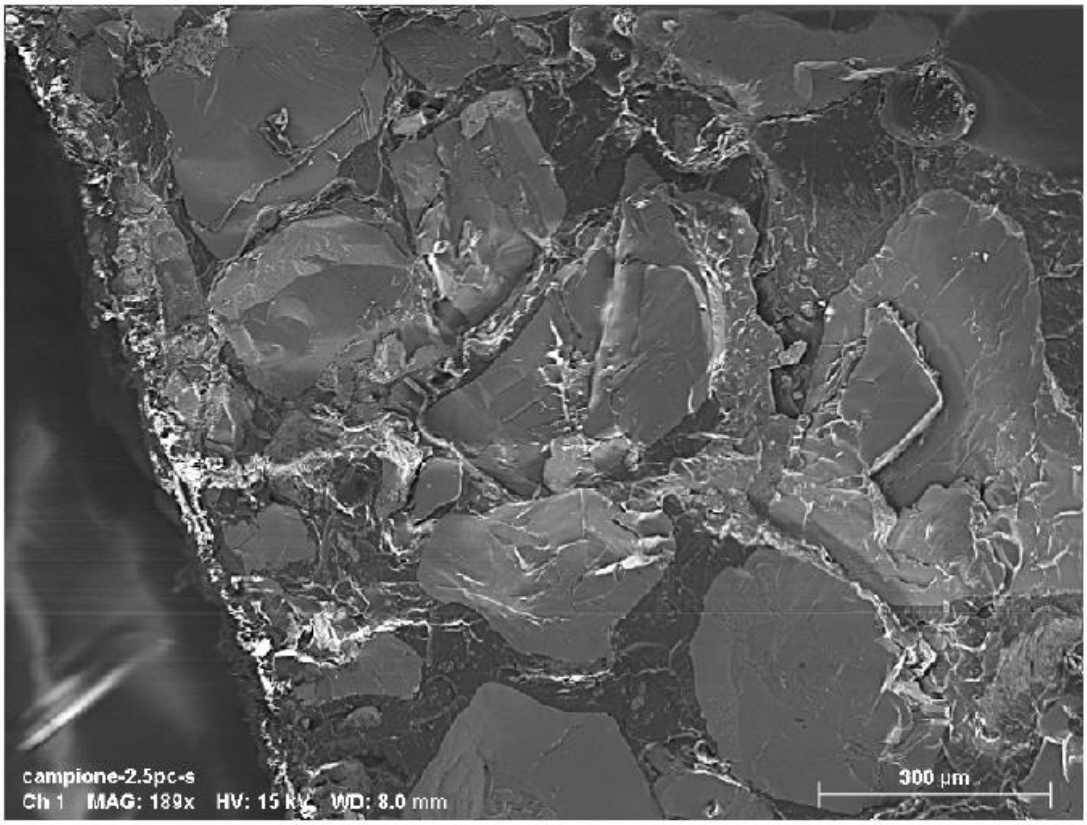

Figure 36 – SEM image of the section of PMMA/SiO_2/TiO_2 composite.

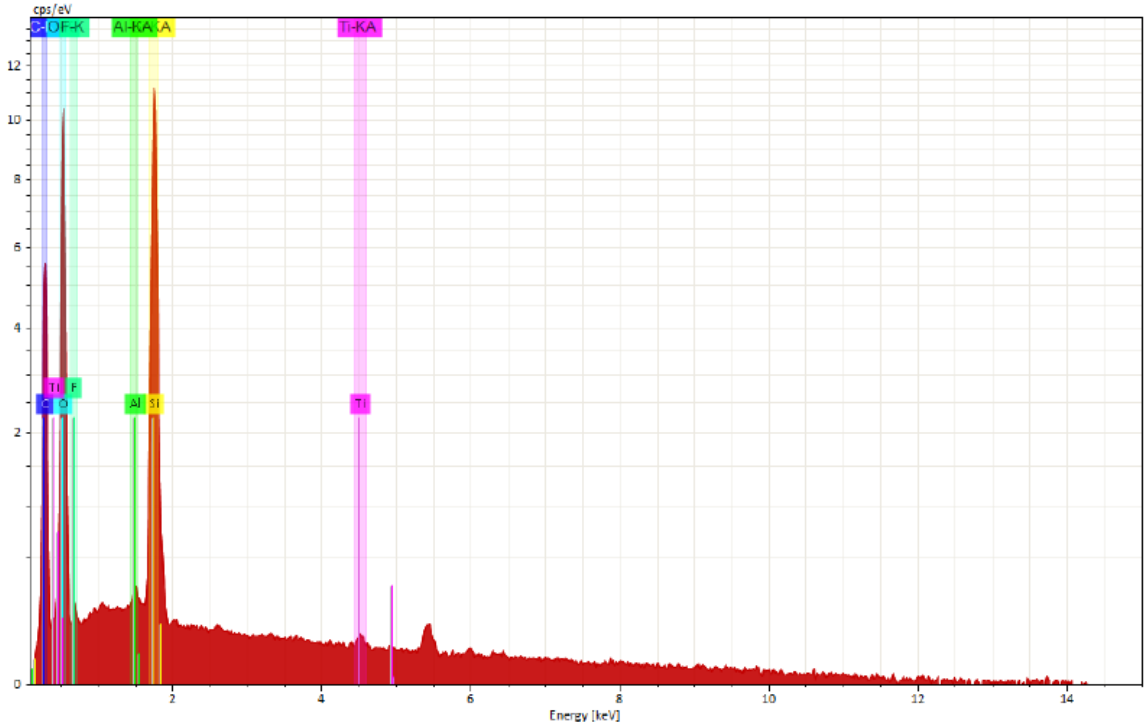

Map

Element	At. No.	Line s.	Netto	Mass [%]	Mass Norm. [%]	Atom [%]	abs. error [%] (1 sigma)	abs. error [%] (2 sigma)
Carbon	6	K-Serie	36584	51.67	36.13	45.95	6.25	12.50
Oxygen	8	K-Serie	74931	67.11	46.93	44.80	7.69	15.38
Fluorine	9	K-Serie	401	0.46	0.32	0.26	0.14	0.27
Sodium	11	K-Serie	187	0.05	0.03	0.02	0.01	0.01
Aluminium	13	K-Serie	749	0.14	0.10	0.06	0.01	0.02
Silicon	14	K-Serie	118872	23.16	16.20	8.81	0.96	1.93
Chlorine	17	K-Serie	259	0.07	0.05	0.02	0.01	0.01
Titanium	22	K-Serie	567	0.34	0.24	0.08	0.02	0.04
			Sum	142.99	100.00	100.00		

Figure 37 – EDS spectrum and elemental microanalysis of the section of PMMA/SiO_2/TiO_2 composite.

From the SEM-EDX analysis, it emerges a strong presence of titanium (Ti) and fluoro (F) elements at the surface (normalized mass of 2.36% and 11.52%, respectively), while these elements are deficient in the section (normalized mass of 0.24% and 0.32%, respectively).

Therefore, a concrete functionalization with Ti and F atoms of the surfaces was confirmed by SEM-EDS analysis. Coupling this result with the effective photo-degradation of MB and NOx, in this work it was performed a suitable functionalization of the surface of polymer-matrix composites through the use of a photocatalytic pre-polymer as a minor component, obtaining a manufacture with superficial photocatalytic activity, good mechanical properties and adequate aesthetic appeal.

1.5. Experimental protocols

1.5.1. Materials and methods

All the solvents and reagents for the synthesis and the silanization of TiO_2 nanoparticles were of analytical grade and purchased from Merck. Titania samples, methacrylate monomers and radical initiators were purchased by the Delta srl company. For the analysis, solid samples were dried at 50 °C under vacuum for 24 hours. All the chemicals were used without any pre-treatment.

Synthesis of Ce-doped TiO_2 NPs 4

In a three-neck flask, 0.0625 mol of $Ti(OR)_4$ were dissolved in 50 mL of anhydrous ethanol. After a certain time, 10 mL of distilled water were slowly added and, then, 3 mL of HNO_3 dropwise, forming the solution A. Meanwhile, the solution B was prepared by dissolving 0.14 mmol of $Ce(NO_3)_3 \cdot 6H_2O$ in 1 mL of ethanol. After the complete addition of the acid, the solution B was added dropwise in the solution A and, after that, a vigorous stirring was ensured (for 1 hour, at least) forming the sol. The sol passed to gel after a period of aging at room temperature for 48-72 hours. Hence, the solvent was removed by vacuum distillation and the solid was calcinated at high temperature (600°C) in a muffle. Finally, the grounding ensured the formation of a fine powder of Ce-doped titania nanoparticles.

Silanization of TiO_2 NPs

In a beaker, 23.5 g of TiO_2 nanoparticles were dispersed in 500 mL of EtOH (96%). An ultrasound irradiation was performed for 20 minutes or more, then was ensured the mixing of the dispersion with a magnetic stirred. At this point, MAPTMS silane was slowly added (from 5 to 100%, weight percentage respect to the mass of titania); after the complete addition, the dispersion was stirred for 2 hours or more. At the end, the dispersion was centrifugated and the solvent was easily removed (and recovered, by distillation), while the slurry, deposited at the bottom after the centrifugation, was placed to dry in an oven at 110°C for 4 hours or more and, then, finely grounded to powder.

Preparation of photocatalytic pre-polymers

In a three-neck flask, a defined amount of modified TiO_2 NPs was dispersed in a methacrylate monomer. An ultrasound irradiation was performed for 20 minutes or more, then it was ensured the mixing of the dispersion with a magnetic stirrer. At this point, the dispersion is heated to a certain temperature, so the radical initiator was added. After a period of polymerization, the dispersion is progressively cooled down to room temperature, obtaining a viscous liquid.

Preparation of PMMA/TiO_2 composites

In a plastic can, an adequate amount of pre-polymer was mixed with an acrylic syrup. The latter is a viscous liquid made by dissolved PMMA (20%, % wt) in MMA. The mass of TiO_2 is calculated according to the quantity of titania used in the specific photocatalytic pre-polymer: the lower the % of TiO_2 in the pre-polymer, the higher the amount of pre-polymer required. For the manufacture of prototypes, a radical initiator was firstly dissolved in the system. After that, the dispersion was poured in a metallic mold and, then, immersed in a hot-water bath. After a certain time, the mold was opened, obtaining the prototype.

Preparation of PMMA/SiO_2/TiO_2 composites

In a plastic can, an adequate amount of pre-polymer was mixed with an acrylic syrup and silica particles. The mass of TiO_2 is calculated according to the quantity of titania used in the specific photocatalytic pre-polymer. For the manufacture of prototypes, a radical initiator was firstly dissolved in the system. After that, the dispersion was poured in a metallic mold and, then, immersed in a hot-water bath. After a certain time, the mold was opened, obtaining the prototype.

Photocatalytic activity of surfaces by the degradation of Methylene Blue

The test was performed in accordance to the ISO standard 10678:2010. The measuring device was the test cylinder (diameter of 4 cm), glued onto a material sizing 5x5 cm and filled with 35 mL of MB solution (4 ppm). The temperature during the test was 20-21°C. The lamp used was the Philips TL-D 18W BLB lamp and the irradiance was set at 10 W/m^2 (measured with the UV-AB radiometer IM-213 RS Pro). The absorbance of MB solution was measured with the UV-Vis spectrophotometer Ci7600 X-Rite.

X-Ray Diffraction (XRD)

X-ray Diffraction measurements were performed by scanning drop-coated films of TiO_2 NPs in a wide range of Bragg angle 2θ at a rate of 2 min^{-1}. A Philips PW 1830 instrument was used, and it was operated at a voltage of 40 kV with a current of 30 mA using monochromatic Cu Kα radiation (λ = 1.5405 Å). The diffracted intensities were recorded in the 2θ range of 10°–80°To elucidate the crystalline structure, the resulting images were compared with the Joint Committee on Powder Diffraction Standards (JCPDS) library.

Scanning Electron Microscope - Energy-Dispersive X-ray Spectroscopy (SEM-EDS)

Samples were deposited on aluminum stabs using self-adhesive carbon conductive tabs and they were sputtered with chromium (5 nm) by Quorum QT150 (Quorum, Laughton, UK). The analysis was carried out in a Field Emission Scanning Electron Microscopy (FE-SEM, Sigma Family, Zeiss, Oberkochen, Germany) operated at 15 KV, equipped with the energy-dispersive X-ray spectroscopy (EDX, Quantax, EDS, Bruker).

Fourier-Transform Infrared Spectroscopy (FTIR-ATR)

FTIR spectra were recorded with a Perkin-Elmer FT-IR spectrometer Spectrum Two UATR, equipped with ZnSe crystal. The measurements were performed in a 400-4000 cm^{-1} range at a 2 cm^{-1} resolution, 4 scans and processed by a Perkin-Elmer data manager (Spectrum).

Thermogravimetric analysis analysis (TGA)

TGA analysis was carried out using a Perkin-Elmer STA 6000 thermal analyzer, equipped with Al_2O_3 crucibles. 10 mg of modified TiO_2 NPs were heated from room temperature to 900 °C, under air atmosphere with a heating rate of 10 °C/min.

Centrifugation of TiO_2 dispersions

The centrifugation of the ethanolic dispersion of TiO_2 and silane was performed with the NEYA 8 instrument, setting a cycle of 3000 rpm for 30 minutes.

Viscosity determination

The viscosity was measured with the rotational viscosimeter Brookfield Amatel model DV1. Before the analysis, the sample is thermoset at 20°C, then the viscosity is measured at different shears (2,4, 10, 20 rpm; using different spindles for different range of viscosity).

Dry residue determination

The dry residue was measured with the thermo-balance Sartorius model MA 160-A. The drying was conducted at 130°C with semi-automatic conclusion (the test is concluded when the balance reveals a weight loss lower than 2 mg in 24 seconds).

1.5.2. Characterization

Ce-doped TiO_2 NPs 4

XRD (%) anatase: 42.7; rutile: 27.9; brookite: 29.4.

Silanized TiO_2 NPs

For samples treated with 50% of MAPTMS. *TGA* (%): water evaporation: 3.4%; polymer content: 19.4%; inorganic residue: 77.2%. *FTIR* (neat, cm^{-1}): 1710, 1640, 1090, 940.

1.6. Conclusions

The development of a "Safer-by-Design" (SbD) approach to use photocatalysts in materials is a fundamental point. The concept of SbD for nanomaterials aims to the reduction of hazardous side-effects, in particular the release of nanoparticles to the environment.

For this purpose, it was studied the incorporation of TiO_2 nanoparticles in polymer materials through the intermediate formation of a photocatalytic pre-polymer. This step was crucial to effectively bind TiO_2 to a fluoropolymer, achieving so the embedment of NPs in a strong macromolecule, that have also a prominent tendency to migrate toward interphases via surface segregation. Equally important was the silanization of TiO_2 NPs, since it effectively promoted the presence of a methacrylic function onto the nanoparticles.

Moreover, another point to highlight is the nature of the photocatalytic pre-polymers: it is a viscous liquid, with coloration from white to pale brown, and it can be easily used as additive (in low quantity) in the formulation of polymer-matrix composites, like highly filled PMMA/SiO_2 composites.

For this purpose, a large number of PMMA/TiO_2 and PMMA/SiO_2/TiO_2 composites were produced. The discussion principally enclosed on the prototypes made at laboratory level; anyhow, even semi-industrial and industrial prototypes were manufactured. These products were made with different approaches and using different type of TiO_2 samples, including visible light activable ones, like Ce-doped TiO_2 nanoparticles.

In order to determine the photocatalytic activity of the surface of these materials, the degradation of MB was tested, in accordance to ISO 10678:2010. The study on PMMA/TiO_2 prototypes enabled to check the method effectiveness, that was confirmed also with PMMA/SiO_2/TiO_2 composites. In this sense, it was observed sufficient photo-activity when 0.45% of TiO_2 was present in the prototype,

while greater results were achieved with 0.9%. Moreover, both UV-A and Vis activable samples proved to be positively integrated in this kind of materials.

In accordance to the pre-polymer viscosity and to the low quantity of product required to produce proto-active composite, the best pre-polymer formulations were **IV** and **VII**, while the most promising TiO_2 samples were **10** and **11**.

For the prototypes made with sample **10**, the degradation toward NOx pollutants was evaluated. A strong photocatalytic activity was observed only when an UV-A irradiation was used, while a little activity was noticed with a visible light lamp.

In conclusion, during this work, many PMMA/TiO_2 and PMMA/SiO_2/TiO_2 prototypes were produced. In these materials, TiO_2 was incorporated in a way that ensure both a surface enrichment and a safe functionalization, achieving so the development of an innovative material having superficial photocatalytic activity.

Bibliography

[1] a) Landrigan, P. J.; Fuller, R.; Acosta, N. J. R.; Adeyi, O.; Arnold, R.; Basu, N.; Baldé, A. B.; Bertollini, R.; Bose-O'Reilly, S.; Boufford, J. I.; *et al. Lancet* **2018**, *391*, 462–512; b) Bianchi, C. L.; Cerrato, G.; Pirola, C.; Galli, F.; Capucci, V. *Environ. Sci. Pollut. Res.* **2019**, *doi.org/10.1007/s11356-019-05218-7*.

[2] Meng, F. S.; Wang, Y. Y.; Zhang, L. S.; Cheng, P. X.; Xue, H.; Meng, D. B. *Water Air Soil Pollut.* **2016**, *227*, 6.

[3] Elgohary, E. A.; Mohamed, Y. M. A.; El Nazer, H. A.; Baaloudj, O.; Alyami, M. S. S.; El Jery, A.; Assadi, A. A.; Amrane, A. *Catalysts*, **2021**, *11*, 1498.

[4] Zhu, D.; Zhou, D. *Env. Nanotech., Monit. & Manag.* **2019**, *12*, 100255.

[5] Teoh, W. Y.; Scott, J. A.; Amal, R. *J. Phys. Chem. Lett.* **2012**, *3*, 629−639.

[6] Fujishima, A.; Honda, K. *Nature* **1972**, *238*, 37−38.

[7] Kawai, T.; Sakata, T. *Nature* **1980**, *286*, 474−476.

[8] Frank, S. N.; Bard, A. J. *J. Am. Chem. Soc.* **1975**, *97*, 7427–7433.

[9] Carey, J. H.; Lawrence, J.; Tosine, H. M. *Bull. Environ. Contam. Toxicol.***1976**, *16*(*6*), 697-701.

[10] Matsunaga, T.; Tomoda, R.; Nakajima, T.; Wake, H. *FEMS Microbiol. Lett.* **1985**, *29*, 211–214.

[11] Byrne, C.; Subramanian, G.; Pillai, S. C. *J. Environ. Chem. Eng.* **2018**, *6*, 3531–3555.

[12] Fauzi, A. A.; Jalil, A. A.; Hassan, N. S.; Aziz, F. F. A.; Azami, M. S.; Hussain, I.; Saravanan, R.; Vo, D. V. N. *Chemosphere* **2022**, 286, 131651.

[13] Kisch, H. *Angew. Chem. Int. Ed.* **2012**, *51*, 2.

[14] Turchi, C. S.; Ollis, D. F. *J. Catal.* **1990**, *122*, 178−192.

[15] Park, H.; Choi, W. *Catal. Today* **2005**, *101*, 291−297.

[16] Tojo, S.; Tachikawa, T.; Fujitsuka, M.; Majima, T. *Chem. Phys. Lett.* **2004**, *384*, 312−316.

[17] Gerischer, H.; Heller, A. *J. Phys. Chem.* **1997**, *95*, 5261−5267.

[18] Deng, Y.; Li, Z.; Tang, R.; Ouyang, K.; Liao, C.; Fang, Y.; Ding, C.; Yang, L.; Su; L., Gong, D. *Environ. Sci.: Nano*, **2020**, *DOI: 10.1039/C9EN01318K*.

[19] Ryu, J.; Choi, W. *Application. Environ. Sci. Technol.* **2008**, *42*, 294−300.

[20] Prieto-Mahaney, O. O.; Murakami, N.; Abe, R.; Ohtani, B. *Chem. Lett.* **2009**, *38*, 238−239.

[21] Zhang, F.; Wang, X.; Liu, H.; Liu, C.; Wan, J.; Long, Y.; Cai, Z. *Appl. Sci.* **2019**, *9*, 2489.

[22] Gerischer, H. *J. Electrochem. Soc.* **1966**, *113*, 1174−1182.

[23] Abe, R.; Takami, H.; Murakami, N.; Ohtani, B. *J. Am. Chem. Soc.* **2008**, *130*, 7780−7781.

[24] Jongh, P. E. D.; Vanmaekelbergh, D.; Kelly, J. J. *Chem. Commun.* **1999**, *12*, 1069–1070.

[25] Marschall, R. *Adv. Funct. Mater.* **2014**, *24*, 2421–2440.

[26] Li, X. Z.; Li, F. B. *Environ. Sci. Technol.* **2001**, *11*, 2381–2387.

[27] Tennakone, K; Bandara, J. *Energy Mater. Sol. Cells* **2000**, *60*, 361−365.

[28] Kumaravel, V.; Rhatigan, S.; Mathew, S.; Bartlett, J.; Nolan, M.; Hinder, S. J.; Sharma, P. K.; Singh, A.; Byrne, J. A.; Harrison, J.; Pillai, S. C. *Phys. Chem. C* **2019**, *123*, 21083−21096.

[29] Giamello, E.; Paganini, M. C.; Gionco, C.; Agnoli, S.; Reeder, A. E. *J. Mater. Chem. A*, **2013**, *DOI: 10.1039/C3TA12018J*.

[30] Tong, T.; Zhang, J.; Tian, B.; Chen, F.; He, D. *J. Hazard Mater.* **2008**, *155 (3)*, 572–579.

[31] Chen, Y.; Liu, K. *J. Hazard. Mater.* **2017**, *324*, 139–150.

[32] Karacsonyi, E.; Baia, L.; Dombi, A.; Danciu, V.; Mogyorosi, K.; Pop, L. C.; Kovacs, G.; Cosoveanu, V.; Vulpoi, A.; Simon, S.; Pap, Z. *Catal. Today* **2013**, *208*, 19.

[33] Serpone, N.; Borgarello, E.; Grätzel, M. *J. Chem. Soc., Chem. Commun.* **1984**, 342.

[34] Bedja, I.; Kamat, P.V. *J. Phys. Chem.* **1995**, *99*, 9182.

[35] Pudukudy, M.; Jia, Q.; Yuan, J.; Megala, S.; Rajendran, R.; Shan, S. *Mater. Sci. Semicond. Process.* **2020**, *108*, 104891.

[36] Deng, W.; Chen, D.; Chen, L. *Ceram. Int.* **2015**, 41, 11570–11575.

[37] Wei, X.; Wang, X.; Gao, B.; Zou, W.; Dong, L. *ACS Omega* **2020**, *5*, 5748–5755.

[38] Navio, J.; Marchena, F.; Macias, M.; Sanchez-Soto, P.; Pichat, P. *J. Mater. Sci.* **1992**, *27*, 2463–2467.

[39] Fu, X.; Liang, X. *Appl. Mech. and Mat.* **2013**, *320*, 220-225.

[40] El-Shazly, A. N.; Rashad, M. M.; Abdel-Aal, E. A.; Ibrahim, I. A.; El-Shahat, M. F.; Shalan, A. E. *J. Environ. Chem. Eng.* **2016**, *4*, 3177–3184.

[41] Silvestre, J.; Silvestre, N.; de Brito, J. *Eur. J. Environ. Civ. Eng.* **2016**, *20*, 455–485.

[42] Gopalan, A.-I; Lee, J.-C; Saianand, G.; Lee, K.-P.; Sonar, P.; Dharmarajan, R.; Hou, Y. I.; Ann, K. Y.; Kannan, V.; Kim, W.-J. *Nanomater.* **2020**, *10*, 1854.

[43] a) Poon, C. S.; Cheung, E. *Constr. Build. Mater.* **2007**, *21*, 1746–1753; b) TioCem®—High Tech Cement for the Reduction of Air Pollutants. 2008. Available online: https://www.yumpu.com/en/document/view/22223710/tiocem-heidelbergcement (accessed on 03 November 2023).

[44] He, R.; Huang, X.; Zhang, J.; Geng, Y.; Guo, H. *Materials* **2019**, *12*, 2182.

[45] Kusters, K. A.; Pratsinis, S. E.; Thoma, S. G.; Smith, D. M. *Powder Technol.* **1994**, *80*, 253–263.

[46] Lowke, D.; Gehlen, C. *Cem. Concr. Res.* **2017**, *95*, 195–204.

[47] Pérez-Nicolás, M.; Navarro-Blasco, I.; Fernández, J. M.; Alvarez, J. I. *Constr. Build. Mater.* **2017**, *149*, 257–271.

[48] Seo, D.; Yun, T. S. *Build. Environ.* **2017**, *112*, 233–240.

[49] Chen, J.; Poon, C.-S. *J. Environ. Manag.* **2009**, *90*, 3436–3442.

[50] Malaki, M.; Hashemzadeh, Y.; Karevan, M. *Progr. in Org. Coat.* **2016**, *101*, 477-485.

[51] Gherardi, F.; Colombo, A.; D'Arienzo, M.; Di Credico, B.; Goidanich, S.; Morazzoni, F.; Simonutti, R.; Toniolo, L. *Microchem. J.* **2016**, *126*, 54–62.

[52] Kim, J.-H.; Hossain, S. M.; Kang, H.-J.; Park, H.; Tijing, L.; Park, G. W.; Suzuki, N.; Fujishima, A.; Jun, Y.-S.; Shon, H. K.; *et al. Catalysts* **2021**, *11*, 193.

[53] Munafò, P.; Goffredo, G. B.; Quagliarini, E. *Constr. Build. Mater.* **2015**, *84*, 201–218.

[54] Petronella, F.; Pagliarulo, A.; Striccoli, M.; Calia, A.; Lettieri, M.; Colangiuli, D.; Curri, M. L.; Comparelli, R. *Crystals* **2017**, *7*, 30

[55] Velazquez-Palenzuela, A.; Dam-Johansen, K.; Christensen, J.M. *Prog. Org. Coat.* **2020**, *147*, 105856.

[56] Hanus, M.J.; Harris, A.T. *Progr. in Mater. S.* **2013**, *58*, 1056-1102.

[57] Gunschera, J.; Andersen, J.R.; Schulz, N.; Salthammer, T. *Chemosph.* **2009**, *75*, 476-482.

[58] Gandolfo, A.; Bartolomei, V.; Gomez Alvarez, E.; Tlili, S.; Gligorowski, S.; Kleffmann, J.; Wortham, H. *Appl. Catal. B: Env.* **2015**, *166-167*, 84-90.

[59] Truffier-Boutry, D.; Fiorentino, B.; Bartolomei, V.; Soulas, R.; Sicardy, O.; Benayad, A.; Damlencourt, J.; Gebel, G.; Pepin-Donat, B.; Lombard, C.; Gandolfo, A.; Wortham, H.; Brochard, G.; Audemard, A.; Porcar, L.; Gligorovski, S. *Environ. Sci.: Nano* **2017**, *DOI: 10.1039/C7EN00467B.*

[60] Baudys, M.; Krysa, J.; Zlamal, M.; Mills, A. *Chem. Eng. J.* **2015**, *261*, 83-87.

[61] Bonnefond, A.; Gonzalez, E.; Asua, J. M.; Leiza, J. R.; Ieva, E.; Brinati, G.; Carella, S.; Marrani, A.; Veneroni, A., Kiwi, J.; Pulgarin, C.; Rtimi, S. *Cryst.* **2016**, *6*, doi:10.3390/cryst6100136.

[62] a) Lin, S. C.; Argasisnski, K. Fluoropolymer Alloys. In *Fluoropolymers 2*; Hougham, G.; b) Patrick, E. C.; Johns, K.; Davidson, T. E.; Kluwer Academic Publisher: New York, NY, USA, **1999**; pp 121-136.

[63] Liu, G.; Xiangli, F.; Wei, W.; Liu, S.; Jin, W. *Chem. Eng. J.* **2011**, *174*, 495-503.

[64] Leyden, D. E. *Silanes, Surfaces and Interfaces.* New York: Gordon & Breach, **1985**.

[65] Plueddemann, E. P. *Silane Coupling Agents.* New York: Plenum Press, **1982**.

[66] Kang, T.; Jang, I.; Oh, S. G. *Colloids Surf. A: Physicochem. Eng. Asp.* **2016**, *501*, 24-31.

[67] Yang, H.C.; Hou, J.; Chen, V.; Xu, Z.K. *J. Mater. Chem. A* **2016**, *4*, 9716 - 9729.

[68] Bach, L. G.; Islam, M. R.; Kim, J. T-; Seo, S.-Y.; Lim, K. T. *Appl. Surf. S.* **2012**, *258*, 2959–2966.

[69] Liu, Q.; Ding, J.; Chambers, D. E.; Debnath, S.; Wunder, S. L.; Baran, G. R. *J. Biomed. Mater. Res.* **2001**, *3*, 384-393.

[70] Xiang, B.; Jiang, G.; Zhang, J. *Plast., Rub. and Comp.* **2015**, *44 (4)*, 148-154.

[71] Nguyen, T.-C.; Nguyen, T.-D.; Vu, D.-T. Dinh, D.-P.; Nguyen, A.-H.; Ly, T.-N.-L.; Dao, P.-H.; Nguyen, T.-L.; Bach, L.-G.; Tha, H. *J. of Chem.* **2020**, *https://doi.org/10.1155/2020/1381407.*

[72] Siddiquey, I. A.; Ukaji, E.; Furusawa, T.; Sato, M.; Suzuki, N. *Mat. Chem. and Phys.* **2007**, *105*, 162–168.

[73] Chan, C. M. *Polymer surface modification and characterization*. New York: Henser, **1994**.

[74] Hedenqvist, M.; Angelstock, A.; Edsberg, L.; Larsson, P. T.; Gedde, U. W. *Polym.* **1996**, *37*, 2887-2902.

[75] Bridson, J. A. *Plastic Materials*. Oxford: Butterworth Heinemann, **1995**.

[76] Lee, H.-J.; Archer, L. A. Macromol. **2001**, *34*, 45-72.

[77] Park, I. J.; Lee, S.; Choi, C. K. *J. Appl. Polym. Sci.* **1994**, *54*, 1449-1454.

[78] Yao, W.; Li, Y.; Huang, X. *Polym.* **2014**, *55-14*, 6197-6211.

[79] Ameduri, B. *Chem. Rev.* **2009**, *109*, 6632–6686.

[80] Guo, T.-Y.; Tang, D.; Song, M.; Zhang, B. *J. Polym. Sci. Pol. Chem.* **2007**, *45*, 5067–5075.

[81] Su, Z.; Wu, D.; Hsu, S. L.; McCarthy, T. J. *Macromol.* **1997**, *30*, 840-845.

[82] Sun, Y.; Zhao, X.; Liu, R.; Chen, G.; Zhou, X. *Prog. Org. Coat.* **2018**, *123*, 306–313.

[83] Heo, H. J.; Han, D. J., Sohn, E.-H. *J. of Fluor. Chem.* **2019**, *219*, 92–97.

[84] Sohn, E.-H.; Ha, J.-W.; Lee, S.-B.; Park, I.J. *Langmuir* **2016**, *32*, 9748–9756.

[85] Jones, R.; Richards, R. W. *Polymers at surfaces and interfaces*. New York: Cambridge University Press, **1999**.

[86] Jaldbert, C.; Koberstein, J. T.; Yilgor, I.; Gallagher, P.; Krukonis, V. *Macromol.* **1993**, *26*, 3069.

[87] Lee, H.; Archer, L. A. *Polym.* **2002**, *43*, 2721-2728.

[88] Bird, R. B.; Stewart, W. E.; Lightfoot, E. N. *Transport Phenomena* John Wiley & Sons, **2001**, ISBN 0-471-41077-2.

[89] Glaris, P.; Coulon, J. F.; Dorget, M.; Poncin-Epaillard, F. *Compos. Part B Eng.* **2015**, *73*, 10.

[90] Qu, A.; Wen, X.; Pi, P.; Cheng, J.; Yang, Z. *Coll. and Surf. A: Physicochem. Eng. Aspects* **2009**, *345*, 18–25.

[91] Qi, Y.; Chen, S.; Zhang, *J. Appl. Surf. Sci.* **2019**, doi:10.1016/j.apsusc.2019.01.073.

[92] Sun, N.; Tian, C.; Xiao Z. *Propel., Explos., Pyrotech.* **2016**, *41*, 5, 798-805.

[93] Caimei, F.; Peng, X.; Yanping, S. *J. of Rare Earths* **2006**, *24*, 309-313.

[94] Bronziotis, A. A.; Giarra, A.; Libralato, G.; Pagano, G.; Guida, M.; Trifuoggi, M. *Front. Environ. Sci.* **2022**, *10*, 948041.

[95] Abdelnohre, S.; Khafaga, A. F.; Noreldin, A. E.; Arif, M.; Chamdhry, M. I.; Losacco, C.; Abdeen, A.; Abdel-Daim, M. M. *Sci. Total Envirom*. **2019**, *672*, 1021-1032.

[96] Matěj, Z.; Matějová, L.; Kužel, R. *Powd. Diffr.* **2013**, *28*, S161-S183.

[97] Zhang, Y.; Li, Y.; Thakur, V. K.; Wang, L.; Gu, J.; Gao, Z.; Fan, B.; Wu, Q.; Kessler, M. R. *RSC Adv.* **2018**, *8*, 13780.

[98] Tran, A. D.; Koch, T.; Liska, R.; Knaack, P. *Monatshefte fuer Chemie/Chemical Monthly* **2021**, 152, 10.1007/s00706-020-02726-y.

[99] Godiya, C. B.; Gabrielli, S.; Materazzi, S.; Pianesi, M. S.; Stefanini, N.; Marcantoni, E. *J. of Envir. Manag.* **2019**, *231*, 1012–1020.

[100] ISO 10678: 2010, *'Fine ceramics, advanced technical ceramics – determination of photocatalytic activity of surfaces in an aqueous medium by degradation of methylene blue'*, ISO, Geneva, **2010**.

Chapter 2: Innovative monomers for the design of materials with disinfectant activity

2.1. Antimicrobial compounds

Antimicrobial compounds have a vibrant history. Even though the lack of knowledge and technologies respect to modern medicine and other related scientific branches, the acute observation of natural processes and a raw and intuitive experimental approach from brilliant individuals have been the basis of a primitive use of antimicrobial compounds to treat diseases and sickness.

These treatments were mainly based on the use of moldy or fermented natural compounds. For example, ancient Chinese populations were used to treat boils or to fight foot infections by applying moldy soybeans coated onto sandal. Similarly, ancient Egyptians and Greeks, were used to treat infections by applying particular molds or by using the mix of many plants, a tradition still important and handed down by Medieval monks and herbalists up to the present day. Modern technologies have proven the efficacy of many of these plants and molds, demonstrating the release of natural products and antibiotics able to kill bacteria and to prevent the spread of infections.[1]

Another type of antimicrobial activity, based on the use of metals, was similarly discovered since the anticity. The employment of silver bowls to maintain water and other beverages pure for long periods was a common practice in ancient civilizations, such as the Greeks, as reported by Herodotus, or the Romans who kept wine in silver containers to avoid moldering. The empiric knowledge that such practice could prevent festering and decomposition probably led to the custom of using silverware and cutlery by the wealthy throughout time. In the era of explorations and the conquest of new territories, such as the American "Wild West", settlers and pioneers adopted a similar habit to avoid spoilage, by inserting silver tableware or coins into their water or milk barrels.[2] The use of metallic compounds in modern pharmacology and in disinfection treatments is still one of the most important ways to achieve antimicrobial activity. In this sense, the use of metallic SCs for the degradation of pollutants and microorganism is described in *Chapter 1*.

The most important discovery in the field of antimicrobial substances was the identification of the antibiotic activity of a specific fungus, penicillin. In this sense, Alexander Fleming, in 1925, observed and reported the outstanding activity of *Penicillium* colonies in the prevention of the proliferation of *Staphylococcus aureus* germs on an agar plate.[3] Inhibitory species was then identified and purified, making it possible to produce penicillin-made antibiotic drugs (*Figure 1*).

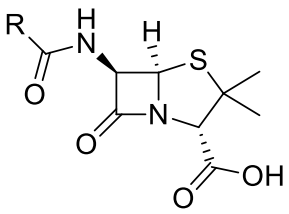

R = $-CH_2CH=CHCH_2CH_3$ [2-pentenylpenicillin (penicillin F)]
$-CH_2C_6H_5$ [benzylpenicillin (penicillin G)]
$-CH_2OC_6H_5$ [penicillin V]
$-CH_2-S-CH_2-CH=CH_2$ [penicillin O]

Figure 1 – Chemical structure of penicillin.

After the outstanding results of Fleming, the studies and the production of antimicrobial agents are in an exponential and continuous growth and development. In order to furnish an adequate overall vision, in *Chapter 2.1.1* the attention will be focused on the classification of antimicrobial compounds, defining so the application fields of these compounds.

2.1.1. Classification of antimicrobial/disinfectant compounds

Compounds with antimicrobial activity are agents involved in the inhibition of microorganisms' proliferation, mitigating so the microbial growth and the possibility of infection. Hence, the term "antimicrobial" includes a wide spectrum of substances acting in contrast to an even wider spectrum of microorganisms, generally enclosing pathogenic bacteria, viruses, fungi, parasites and protozoa. According to the specific target, antimicrobial agents can be divided in distinct classes, as schematized in *Figure 2*.

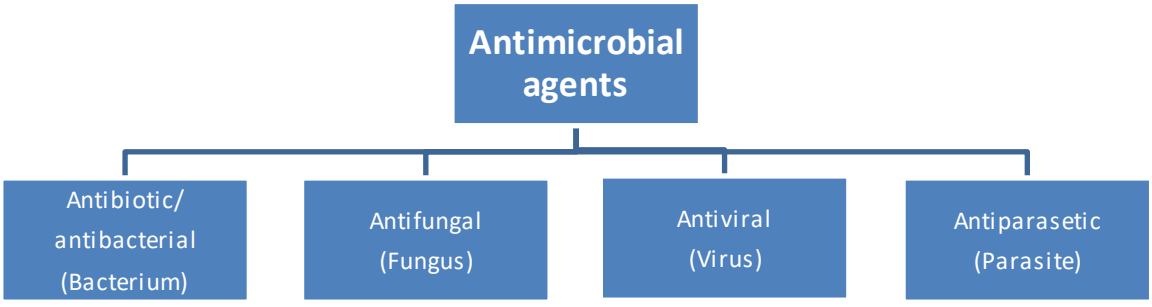

Figure 2 – Antimicrobial agents and different sub-classes.

It should be noted that antibiotics and antibacterial agents are substances capable to fight bacterial infections. The distinction commonly relies on the origin of these agents: the former indicates chemical substances *produced* by live microorganisms, such as bacteria, molds and fungi, while

antibacterial is generally referred to synthetical chemicals. Regardless the terminology, the activity of these compounds occurs through various mechanisms, such as disrupting bacterial cell walls, interfering with essential metabolic processes, arresting bacterial growth, or causing cell death. According to its way of mechanism, an antibacterial agent can have a bacteriostatic action, stopping the bacterial proliferation, and/or a bactericidal action, causing the bacteria death, such as by its irreversibly binding to the cell membrane of bacteria. To be effective as drugs, antibiotics should possess selective toxicity, solely affecting the metabolism and replication of bacteria.[4]

Moving to antivirals, they are specialized antimicrobial agents developed to prevent viral infections by inhibiting viral replication and propagation. They are essential in managing viral illnesses (including influenza, HIV/AIDS, hepatitis) and they have recently gained more relevance due to the coronavirus pandemic.[5]

Finally, antifungals are specifically formulated and engineered to prevent and treat fungal infections, which can affect humans and essential activities such as agricultural industry. These agents are employed in the medical field for conditions such as candidiasis and ringworm, as well as in agriculture, to protect plants from fungal diseases. An example of this class of molecules is rhodamine-based molecules, a class of heterocyclic organic compounds having a thiazolidinedione moiety (*Figure 3*).[6]

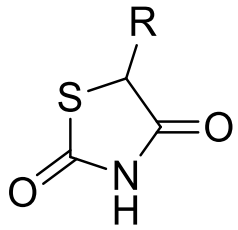

Figure 3 – Chemical structure of thiazolidinediones.

Nonetheless, the widespread and often indiscriminate use of antimicrobial agents has raised concerns about the development of antimicrobial resistance, a phenomenon leading to the evolution of microorganisms' mechanisms to survive at the effects of antibiotics or other antimicrobial agents. In this sense, antibiotic resistance represents a challenging global health crisis, since the abuse of antibiotics, coupled with the natural adaptability of bacteria, has led to drug-resistant species.[7] The consequences of antibiotic resistance are extensive, impacting patient outcomes, increasing healthcare costs, and representing serious pressure on public health. An analysis of data from the US Centres for Disease Control and Prevention has reported that yearly in the United States, at least two million people are infected with antibiotic-resistant bacteria, and at least 23 000 persons die from them annually. In addition, data from the World Health Organisation and the British report "*Review*

on Antimicrobial Resistance" suggest that by the year 2050, millions of people could die from infections for which there will be no effective treatments, with one death occurring every three seconds.[8]

To deal with antibiotic resistance, it is first necessary to reduce unnecessary antibiotic prescriptions. Furthermore, investments in research and development of new antibiotics and alternative treatments are critical to keep an advantage on the evolving resistance mechanisms. Furthermore, international collaboration is vital in controlling the spread of resistant bacteria across borders, as antibiotic-resistant infections can spread rapidly. This phenomenon poses a significant challenge for the global scientific system, which is increasingly driven towards research and development of new antimicrobial strategies.

From these considerations, it emerges that one of the smarter ways to prevent and control eventual pandemic situations is to selectively use antimicrobial agents with a low resistance potential and restrict those with a high resistance potential. In this way, an appreciable approach is the chemical disinfection.[9] This kind of approach is essential for eliminating or reducing harmful microorganisms in various settings, from healthcare facilities to public spaces, ensuring cleanliness and preventing the spread of infectious diseases. Meanwhile, the mechanism of these compounds is generally less specific than antibiotic one, which results in a lower antimicrobial power but also in a lower resistance development by pathogens. Anyhow, their non-specific action should not result in side-effects to human health. In summary, a chemical disinfectant requires more than just having a microbicide activity to be widely used and it should be non-toxic, odourless, not harmful to the disinfected material, with detergent activity and penetration capacity. Furthermore, a disinfectant should be simple to use and affordable.

In general, disinfectants are organic and inorganic substances that can initiate complicated chemical reactions to harm microbial cells or viruses, such as protein denaturation, membrane modification, dissolving of membrane lipids, and oxidation of functional groups on enzymes with consequent enzymatic inactivation.[10] In this way, for chemical disinfectant is intended an agent used to decontaminate tissue, things, or sites due to their capability to kill pathogenic bacteria in different environments. When these molecules are involved also in the eradication of spores, they are defined as sterilisers, while an antiseptics agent is the one used to prevent severe sepsis and systemic infections when applied to living tissues, such as skin or mucous membranes.

In a similar way to antibiotics, it is crucial to remember that disinfectants include many chemical agents that can be combined or used alone in a wide range of products, each of which has a different activity level against microbes. For this reason, a specific disinfectant agent must be chosen according to: i) the nature of the material to be treated, ii) types of target microorganisms, and iii) environmental

conditions. Moreover, numerous factors, such as formulation, presence of an organic load, operating temperature, synergistic effects, and dilution might affect the antimicrobial efficacy of the final product.[11]

The most used disinfectants are the chlorine-based agents, like chlorine dioxide and trichloroisocyanuric acid, and the cationic detergents, especially quaternary ammonium compounds such as didecyldimethylammonium chloride, and benzalkonium chloride (*Figure 4*).

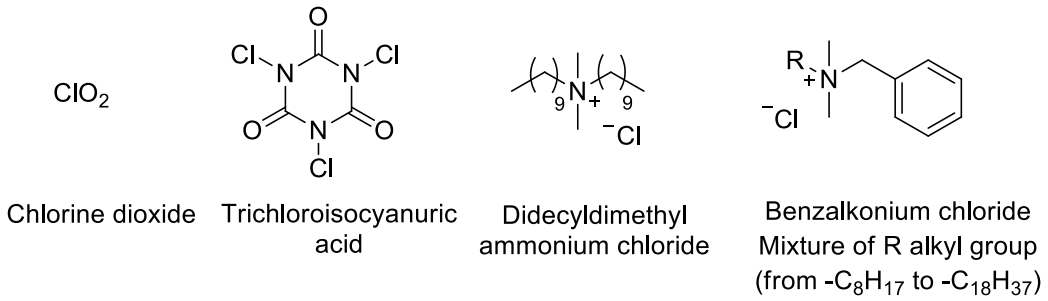

Figure 4 – Chemical structure of common disinfectants.

Chlorine-based disinfectants are commonly used in the treatment of water. In this sense, Cl_2O is a common reagent in the chlorination of potable water, while trichloroisocyanuric acid is preferred as disinfectant for the sanitation of swimming pools and spas. Moreover, their strong bleaching activity is largely exploited in many industrial sectors. Moving to cationic detergents, they are becoming a popular choice as disinfectant because they couple a remarkable degree of microbicidal activity with a high detergent action.[12] Among them, quaternary ammonium salts are largely used because they have demonstrated a powerful microbicidal actions, often working together to have a synergistic effect. Quaternary ammonium compounds will be extensively described in *Chapter 2.2*.

2.1.2. Polymers with antimicrobial/disinfectant activity

As seen in previous sections, many types of biocidal agents have been developed to combat microorganisms, including antibiotics, disinfectants and antiseptics. However, after the application, these compounds have a short-term antimicrobial action and, when applied onto material surfaces, these sites are contaminated again once re-exposed to microorganisms. In addition, the prolonged and often reckless use of many disinfectants is toxic and has caused severe environmental damage.

In this challenging context, Antimicrobial Polymers (APs) have gained increasing importance. APs can be used as an alternative to the currently overused antibiotics, since synthetic antimicrobial polymers frequently exhibit a good antimicrobial activity together with low microbial resistance

rates.[13] Therefore, APs are widely used to produce antimicrobial surfaces and they are emerging as an appealing opportunity in a wide range of sectors, from food packaging to medical and hospital equipment.

Antimicrobial polymers could be divided in two main groups:

a) Polymers Biocides

Polymer biocides are a class of polymers with intrinsic antimicrobial activity. Two important examples of natural biocidal polymers are chitosan and ε-polylysine: the first one is a cationic polysaccharide of animal origin obtained by deacetylation of chitin; the second one is a homo-polypeptide of the lysine amino acid produced by bacterial fermentation (*Streptomyces albulus*).[14] Structure of cationic chitosan and ε-polylysine are reported in *Figure 5*.

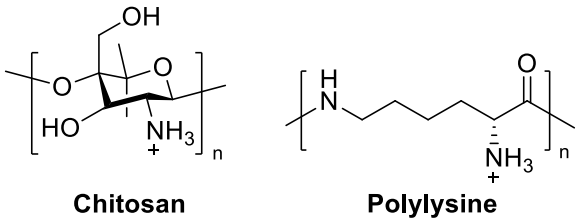

Figure 5 – Chemical structure of chitosan and polylysine.

Moving to synthetic biocidal polymers, the most popular are polypeptides, synthesized from amino acids and linked together by peptide bonds, or commercially-available polymers functionalized with an active group, such as through grafting approaches. For the latter, an intriguing and easy option is to develop cationic monomers, such as by the covalently bonding a quaternary ammonium salt to a monomer or a pre-formed polymer.

In this way, multifunctional Poly(Vinyl Amine)s (PVAms) are an interesting example of antimicrobial polymers, developed by miming natural antimicrobial peptides. Recently, Chattopadhyay *et al.* have proposed a simple and robust one-pot method for the synthesis of antimicrobial PVAms bearing azetidinium groups in water.[15] The procedure utilizes two functional couplers: a β-aminoalcohol having a reactive cationic azetidium group, and a β-chloroalcohol bearing an azetidium group as well. These couplers were subsequentially used to modify a poly(vinyl amine) by post-polymerization processes (*Scheme 1*).

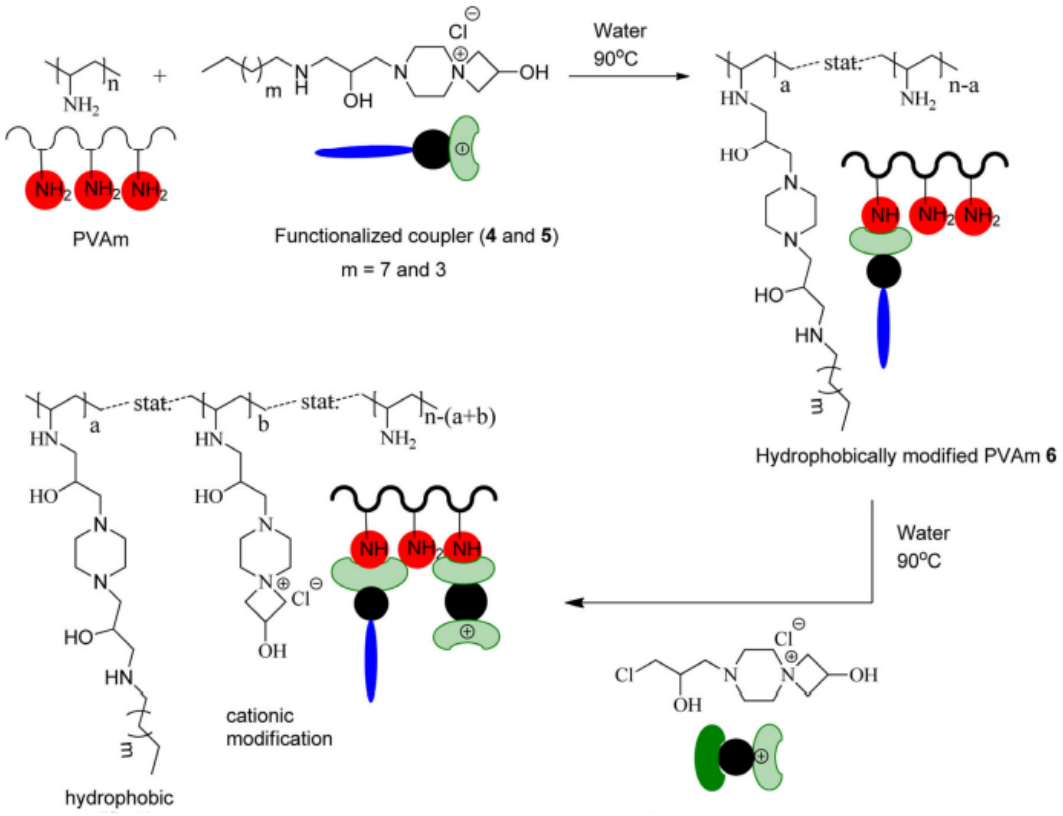

Scheme 1 – Multifunctional PVAms, used as antimicrobial polymers.

The resulting polymer was hence functionalized by the insertion of the hydrophobic section in the first time; then, in a second moment, it was performed a cationic modification to ensure a synergetic antimicrobial action. The structure-activity relations of these antimicrobial polymers were analysed, suggesting the ability of these materials to differentiate between microorganisms and mammalian cells such as blood cells. The antimicrobial PVAms may produce coating cellulose-based materials, such as onto cotton. The antimicrobial efficacy of this coated surface was studied against bacteria like *Escherichia coli*. The antibacterial effectiveness was investigated by exposing the *E. coli* to the polymer, and it was detected that, compared to cotton that has not been treated, cotton with PVAms surface showed 99.9% bacterial growth suppression.

A different class of biocidal polymers are the Self-IMmolative Polymers (SIMPs), a type of macromolecules that spontaneously undergo depolymerization into smaller molecules when activated by specific external conditions. One example is silyl-protected ether group of poly(benzyl ether)s with pendant allyl side chains.[16] Through photoinitiated thiol-ene radical addition and using cysteamine, they are converted into polycations. After that, when exposed to fluoride ions, the intact polycations spontaneously depolymerize into their respective monomers with excellent sensitivity and selectivity (*Scheme 2*).

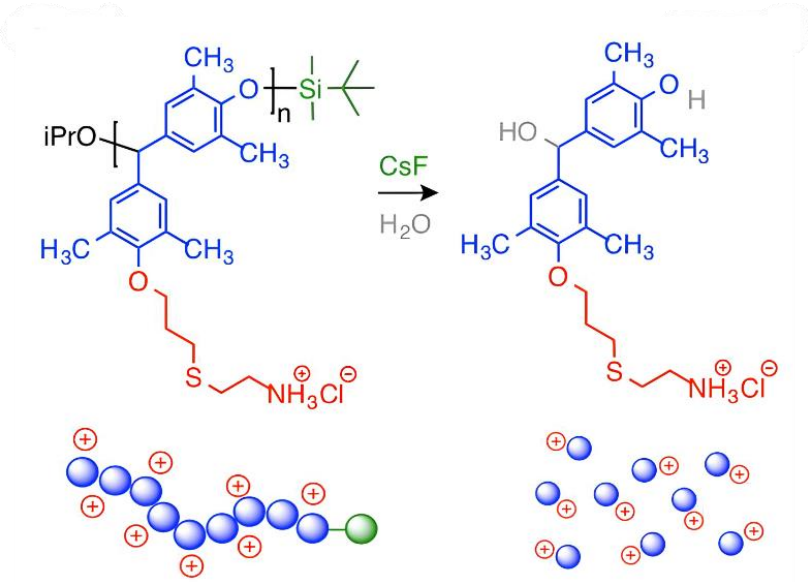

Scheme 2 – Mechanism of action of a poly(benzyl ether) SIMP.

The antibacterial effectiveness was maintained after induced depolymerization, but the haemolytic toxicity was greatly diminished. The number average molecular weight Mn and polydispersity index of a self-immolative polymer is an essential determining factor of the depolymerization kinetic. Changing molecular weight may represent a strategy to tune the aqueous solubility of polycations. These molecules were tested, and they showed significant activities against a wide range of bacteria, such as *H. Coli*, *S. aureus* and *B. subtilis*.

b) Antimicrobial coating

Antimicrobial coatings are a class of materials applied to various surfaces to inhibit the microbial growth and/or to ensure an effective elimination of microorganisms. These coatings act as a protection tool, actively preventing the proliferation and spread of microorganisms on a variety of surfaces by incorporating sophisticated antimicrobial agents into different materials including plastics, metals, and ceramics. This technology is finding application in diverse sectors, from healthcare and consumer electronics to food processing and public infrastructure, fundamentally improving the way we approach hygiene and disease prevention.

In this context, antimicrobial polymers are widespread in coating applications. Numerous remarkable examples are based on the coating of surfaces with a polymer layer having metallic antimicrobial agents, such as silver, copper or titania nanoparticles. Likewise, the covalent bonding of organic quaternary ammonium salts (QASs) to polymeric matrices is an effective method to gain an antimicrobial polymeric coating.[17] For the latter, the large variety of suitable polymer matrices, combined with a wide choice of available cations, allows an endless list of options that can fit with specific fields of use for any material of interest. An interesting example is the functionalization of

polyisoprene oligomers, that is a portion still reactive, especially at their chain ends. Oligomers can be modified to insert polymerizable biocidal active groups; after that, a polymeric film, meant to incorporate the functionalized oligomer, could be obtained (e.g., by radical photopolymerization).

There are different procedures to apply antimicrobial coating, like the spraying onto the surfaces, the dipping of materials into a solution of antimicrobial polymers and the incorporation during the manufacturing process. The spraying and the dipping approaches ensures the formation of an external polymeric layer. If the introduction of the antimicrobial agent is designed to ensure a covalent bond to the polymeric coating, so these approaches could result in an effective and safe functionalization of materials surface. Anyhow, the durability of these coating is generally limited and they lack of efficiency over prolonged time. On the other hand, the incorporation of antimicrobial agent during the manufacturing processes of a polymeric material should be designed to ensure a covalent bond as well; moreover, it should provide a uniform distribution of active agent along the whole polymer structure, resulting so in a more durable activity and with a lower risk of release of undesirable substances in the surrounding environment.[18]

In conclusion, polymers having high and long-term biocidal efficacy should be designed to no-leaching the active moieties, and their applications can be expanded by designing and employing different polymeric structures. Nevertheless, there is still a high demand for developing antimicrobial materials aimed at multi-species pathogenic microbes including bacteria, fungi, protozoa, prions and viruses, etc. In particular, the non-enveloped viruses, which have no lipid bilayer envelope surrounding the capsid, are very stable and virulent, and difficult to control and/or destroy by conventional antimicrobial materials. Along with the promotion of antimicrobial properties, low cytotoxicity needs to be achieved for the applications where biocompatibility is a decisive factor.[19]

2.1.3. Action mechanism of antimicrobial polymer surfaces

The most important feature to be highlighted on antimicrobial polymer is the possibility to solve the issues of the use of conventional antimicrobial agents, since functionalized polymer have effectively proven to overcome the easily susceptibility to bacterial resistance of natural or low molecular weight antibacterial drugs. For this reason, one of the most important filed of application for synthetic antimicrobial polymers is in the production of antimicrobial surfaces. To have antimicrobial activity, a surface could act through repelling or killing mechanisms, as resumed in *Figure 6*.[20]

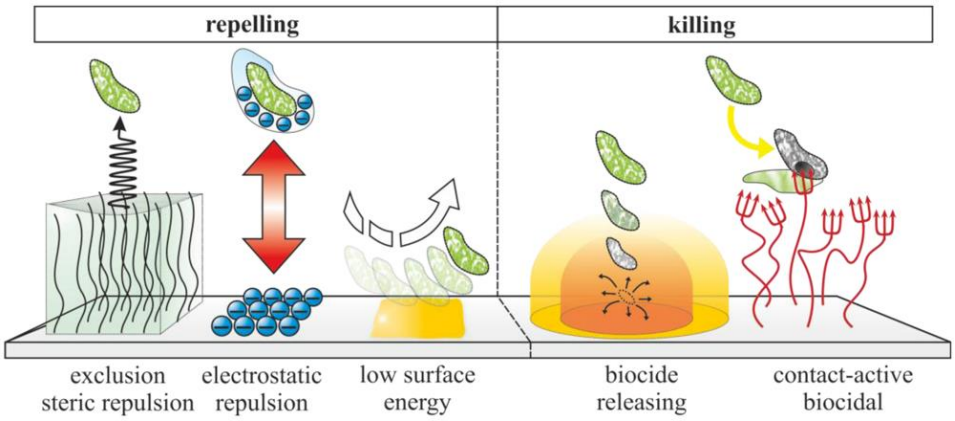

Figure 6 – Repelling and killing mechanisms in antimicrobial materials.

The first set of mechanisms is focused on the preparation of surfaces that avoid the adhesion of microbes on the surface. This activity can result by applying steric or physical repulsion techniques. Among the latter, it is possible to functionalize the surface with negatively charged surfaces, promoting the repulsion of negatively charged bacterial cell walls, or with low surface energy species, through the design of (super)hydrophobic surfaces with high angles of contact to aqueous suspensions of bacteria, limiting so the contact with the treated surface.

On the other hand, the killing mechanisms can be divided in release or contact killing. The former focuses on the diffusion and release of cytotoxic substances from the material surface. These cytotoxic compounds cause the death of microbes in the immediate surrounding areas. The latter mechanism generally involves amphiphilic polycations. These polymers can interact with the cell membrane v*ia* different mechanisms, such as cation exchange, causing the lysis-induced rupture of bacterial cell membranes.

For these reasons, cationic amphiphilic polymers are widely used as antimicrobials and disinfectants. Their antibacterial action has been reported to inhibit the bacterial growth in solutions and on surfaces. In this context, the polymer matrix and its structural properties play a fundamental role. Essentially, polymeric matrices should exhibit crucial properties, like non-toxicity, simple and affordable production, long-term stability and wide range of antibacterial efficacy, even after brief contact durations.[21] Polymers functionalized with QASs are one of the most important antimicrobial materials that go in this direction. Considering their chemical stability, non-volatility, low toxicity, extended lifespan, and selectivity, biocidal surfaces incorporating quaternary ammonium compounds have made it possible to solve the issues of the use of low molecular weight QASs alone.[22]

The antimicrobial activity of cationic polymers depends on three parameters: cation charge, hydrophilic/hydrophobic balance, and polymeric structure. In fact, the presence of cationic charges along the polymer chain has the feature of increasing the electrostatic interaction with bacterial cells. Some examples of suitable cations, in addition to quaternary ammonium group, are phosphonium,

sulfonium and metal ions such as Ag^+.[23] Choosing the appropriate cationic groups is a fundamental stage in the development of biocidal polymers, because they will determine the specific affinity of the polymer with the anionic components of bacterial membranes (*Figure 7*).[24]

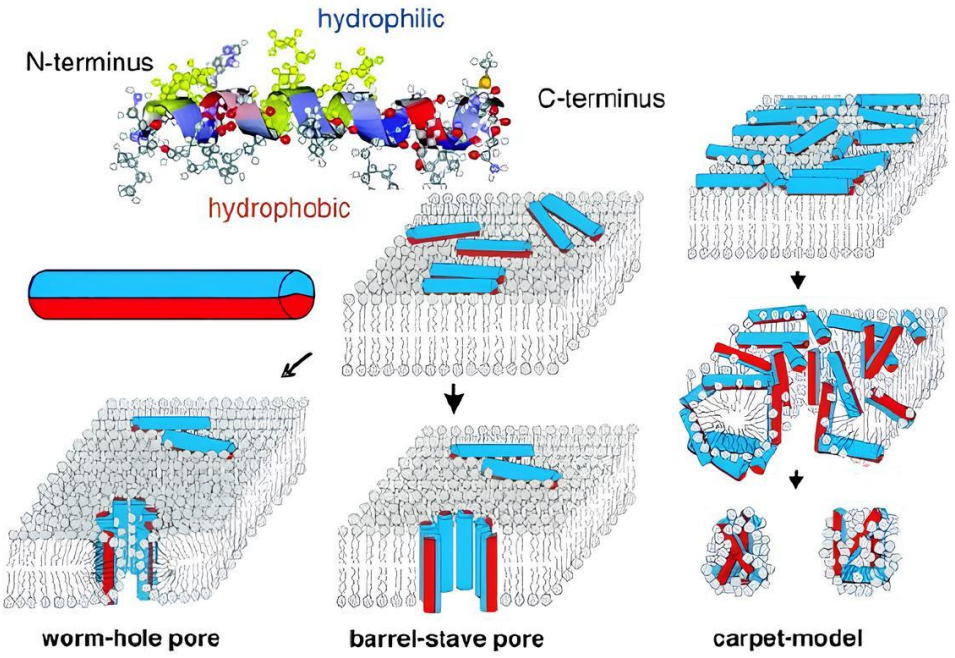

Figure 7 – Formation of pores and degradation of the cellular membrane of bacteria.

In addition to cationic groups, alkyl lateral chains play a crucial role in the activity and biocompatibility of biocidal polymers. This optimal balance between hydrophilic and hydrophobic components is known as the "amphiphilic balance". It is reasonable to draw the conclusion that it is essential to get a well-defined spatial relationship of the entire polymer to produce effective antimicrobial materials. Charged and non-polar moieties need to be locally balanced, for example, at the monomer level, and not just globally. Additionally, the connecting sections between the cationic groups play an important role in the resulting activity.[25] The achievement of this kind of specific control in the synthesis of antimicrobial polymers is the key point of interest for researches in this field.

2.2. Quaternary ammonium salts (QASs)

Quaternary Ammonium Salts (QASs) or Quaternary Ammonium Compounds (QACs) are a broad class of nitrogen salts. QASs are commonly listed as a subclass of the amine group, that is in turn an essential organic compound containing a nucleophilic nitrogen atom. The general structure of quaternary ammonium compounds reflects the complete substitution of N atom, leading to the

formation of a salt made of a positively charged molecular ion and a negative counterion, quite often a halide, as shown in *Figure 8*.

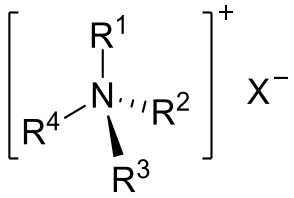

Figure 8 – Chemical structure of a general QAS.

The ionic nature of QAS is due to the nitrogen cation, that can be defined as the polar head, while the R substituents are the hydrophobic tails, generally made of alkyl, cycloalkyl, phenyl, benzyl or vinyl groups. Due to the difference in polarity between the polar head and the lipophilic tails, QASs are prominent surfactants, giving reasonably electrolytic solutions when dissolved in a solvent. In this sense, quaternary ammonium salts are generally very soluble in polar protic solvents like water and alcohol, but the solubility in these solvents reduces as the number of carbon atoms in the R groups rises to 14 or more.[26]

Considering the amphiphilic structure and the excellent surface chemistry of quaternary ammonium salts, the majority of applications are related to their strong affinity for surfaces. In this sense, QASs tend to adsorb on a wide range of surfaces, since most of the surfaces (including skin, mucosa and hair) are negatively charged and, hence, they tend to attract and adsorb positively charged compounds.[27]

Furthermore, QASs are good penetrants, natural wetting agents, built-in detergents, powerful surfactants and important antibacterial agents, making them highly desirable in applications like antimicrobial surfaces, sanitizers, disinfectants, detergents, antifouling and herbicides. Moreover, these compounds are extensively used in organic synthetic approaches and other interesting applications as reactive substrates, reagents, phase-transfer catalysts, ionic liquids and electrolytes.[28] They are also used in electrochemistry, for example, in the technique of cyclic voltammetry and as antistatic. The applicability and the main features affecting QASs activity are resumed in *Figure 9*.

Figure 9 – Overview of the main features and applications of QASs.

A final remarkable application of QAS is in the development of fracturing fluids, that are materials used to ensure a safe and complete sealing of oil and gas reservoirs through a coupling of low- or ultra-low-permeability with a stimulation measure. For this scope, synthetic polymer fracturing fluid has the characteristics of strong thickening ability, good gel breaking performance, good thermal stability and no residue.[29] Compared with other fracturing fluids, it has better temperature and salt tolerance, shear resistance, rheological property, sand carrying performance and other advantages, which has become the focus of many researches. Among synthetic fracturing fluids, synthetic polyacrylamides with long chain linear structure are widely popular; however, when used in low-permeability and ultra-low-permeability reservoirs, it has poor viscosity retention and poor temperature tolerance.

In view of the poor temperature tolerance of polyacrylamide fracturing fluid, an interesting work is the formation of a ternary hydrophobic associating polymer prepared by the free radical polymerization of acrylamide (AM), methacryloyloxyethyl trimethylammonium chloride (DMC) and a self-made double tailed hydrophobic monomer (PMB-16). Eventually, zirconium acetylacetonate was used as crosslinking agent.[30] The work is schematized in *Scheme 3*.

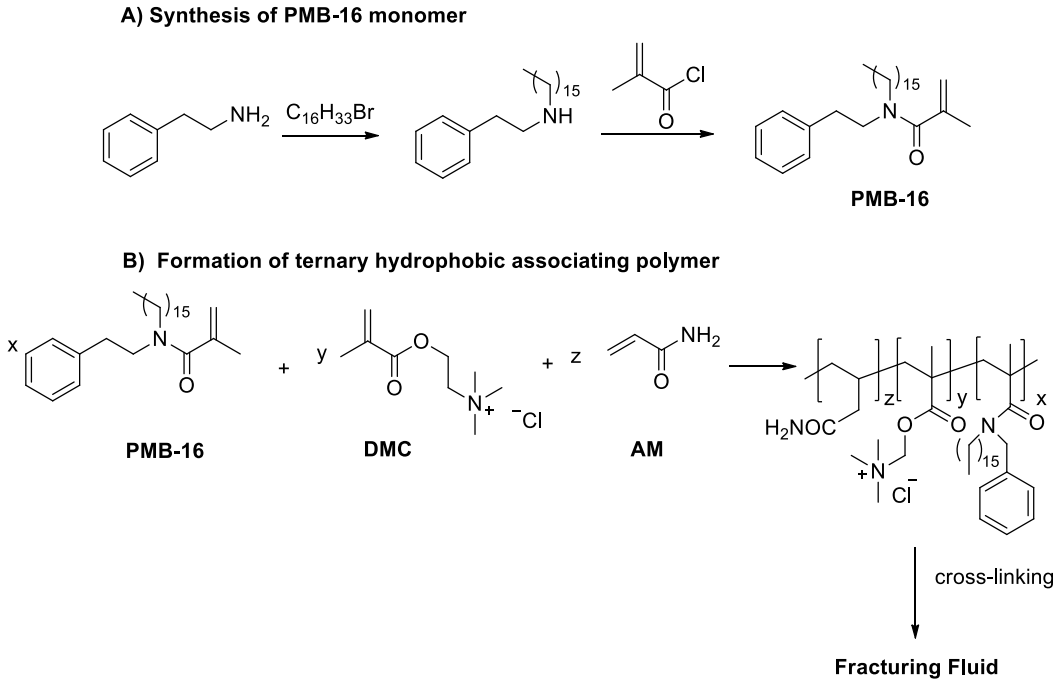

Scheme 3 – Synthesis of hydrophobic monomer (PMB-16) and its use in the preparation of fracturing liquids.

The double tailed hydrophobic monomer PMB-16 was synthesized by the reaction of phenylethylamine, 1-bromohexadecane and methacryloyl chloride, the ternary hydrophobic associating polymer was synthesized by free radical copolymerization of PMB-16 with acrylamide and methacryloyloxyethyl trimethylammonium chloride. From the results of performance evaluation, it emerged that aqueous solution of these ternary polymers had excellent temperature and salt resistance. Additionally, using zirconium acetylacetonate as crosslinker, the system presented good thickening, temperature resistance, shear stability and low residue content.

2.2.1. Synthesis and reactivity of QASs

Bimolecular nucleophilic substitution reaction (S_N2) between primary, secondary, or tertiary amines and an alkyl halide is the simplest method for producing QASs.[31] Anyhow, it is generally difficult to perform a mono-alkylation through this mechanism because the reaction products are more reactive than the starting material, hence a mixture of tertiary amine and quaternary ammonium salts is generally formed by the reaction of primary and secondary amines with alkyl halides, especially using an excess of the latter reactant. Furthermore, being a S_N2, the speed of the reaction can be affected by the nature of the solvent. Polar aprotic solvents, that lower the energy of the transition state, are the most suitable. Even the structure of halide and the leaving group have a strong influence on the rate of reaction, due to steric hindrance and coordination effects.

In order to obtain a functionalized QAS, an effective approach is to vary the chemical nature of the starting amine or halide, promoting so the functionalization by the preparation of adequate starting materials. In this way, primary, secondary, and tertiary amines can be made *via* a variety of techniques, including Gabriel synthesis, reductive amination, Hoffmann degradation, and reduction of nitro-compounds.[32] These techniques can be used to obtain amines with precise characteristics, ideal for the production of various ammonium salts, performing the quaternization reaction through the already discussed S_N2 reaction with adequate alkyl halide.

In *Scheme 4*, it is proposed a list of synthetic approaches to obtain a QAS from a functionalized primary amine. Anyhow, it is important to highlight that the selective mono-alkylation can be performed also onto primary and secondary amines, or by using substituted reaction partners (e.g., functionalized aldehydes or ketones in the reductive amination).

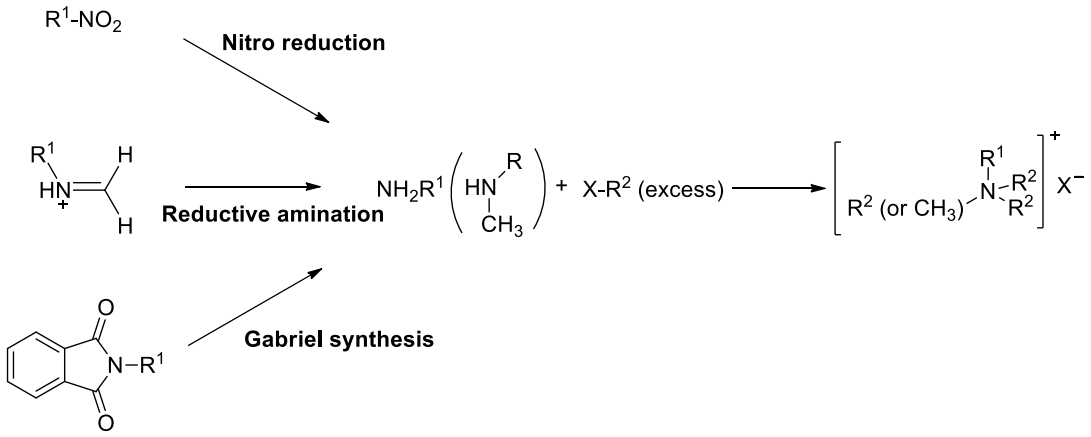

Scheme 4 – Synthetic strategies to obtain a functionalized amine (primary or secondary) and the successive quaternization.

The reactivity of quaternary ammonium salts depends mostly by the inductive effect of the nitrogen atom, which increases the acidity of the protons attached to the carbon atom in the alpha position.[33] Reactions of QASs can vary according to the used salt and the reaction conditions. Their reactivity makes them versatile compounds with applications in organic synthesis, water treatment, analytical chemistry, and various industrial processes. Generally, the reaction of quaternary ammonium cations can be divided in four different types: substitution, rearrangement, ion exchange and elimination (*Scheme 5*).[34]

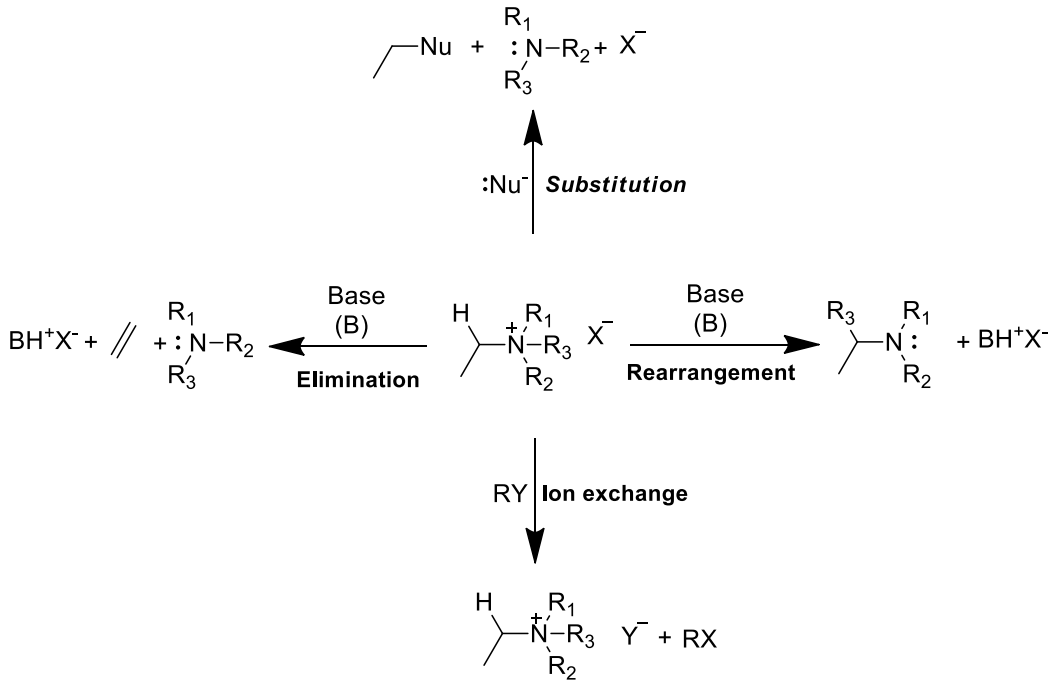

Scheme 5 – Common reactions involving QASs.

QASs are also used in organic synthesis, especially as reagents and catalysts. In particular, they are essential intermediates in the Hoffmann reaction, as shown in *Scheme 6*.

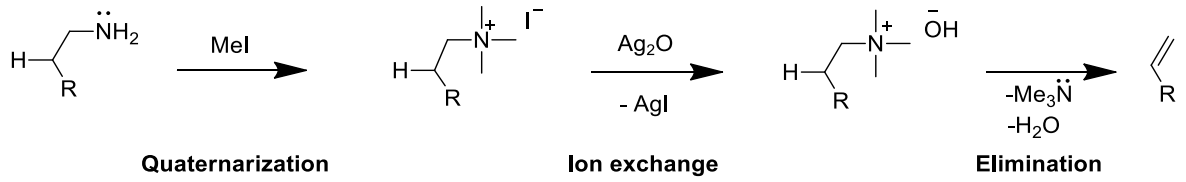

Scheme 6 – Hoffmann synthesis.

Another interesting example of a synthetic route involving a quaternary ammonium salt intermediate has been reported for the synthesis of a wide number of epoxyalkylamines (*Scheme 7*).[35]

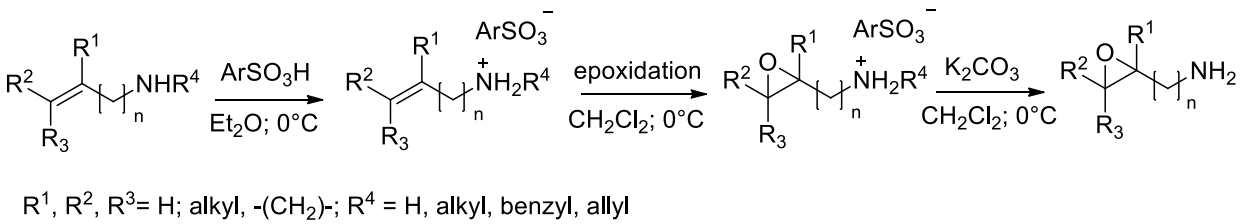

Scheme 7 – Synthesis of epoxyalkylamines.

Epoxyalkylamines are important building blocks in the synthesis of ethylene and ethylamine dipeptide isosteres, and other pharmacologically important compounds such as alkaloids, amino

sugars, or oxygenated amino acids. In this works, authors reported a facile and versatile method, where, in the first step, it is performed the quaternization of alkenylamines with stoichiometric amount of the corresponding arenesulfonic acid in ether solution, forming hygroscopic quaternary ammonium salts of alkenylamines. After that, it was induced the peroxidation of the alkene group and, finally, epoxyalkylamines were easily obtained by treating epoxyalkylammonium salts with solid potassium carbonate in methylene chloride or acetonitrile solution at 0°C.

Finally, thanks to their stability, low toxicity, and low cost, QASs are also used as phase transfer catalysts that facilitate the migration of a reagent from one phase to another and in the production of ionic liquids and DESs (Deep Eutectic Solvents).[36]

2.2.2. Antimicrobial properties of QASs

Focusing on the disinfectant activity of QASs, it is important to firstly asses a structure-activity relationship. In this sense, it is widely known that the nature of the salt is fundamental to ensure an effective mechanism of inhibition of microbial growth and/or microbicidal effect. In order to have disinfecting, germicidal, bactericidal, and fungicidal effects, one first point relies on the length of the hydrophobic tails, since important antimicrobial activity is often observed when at least one long aliphatic chain (in the range of C_8H_{17} - $C_{18}H_{37}$) is covalently bonded to the nitrogen atom.[37] Anyhow, it is important to remember that the use of long chains strongly affect the solubility of the resulting quaternary ammonium salt in protic polar solvents and, often, a balance between short and long alkyl substituents is fundamental to couple the antimicrobial effect of these compounds with an appreciable solubility in many solvents, very important in terms of applicability and processing.

Moreover, the presence of a cationic head is crucial for the interaction with target pathogen. In this way, the positively charged nitrogen is clearly more propense to interact with negatively charged cell membranes, such as Gram-positive bacteria, *via* electrostatic interactions.[38] After the interaction, the bactericidal action on Gram-positive bacteria is attributable to the QAS's ability to penetrate the semipermeable membranes of bacteria (such as for *Staphylococcus aureus*) due to the lipophilicity given by the long alkyl chain. Therefore, it is evident the coupled activity of the polar head and the long hydrophobic alkyl chain, resulting in an adequate interaction with the bacterial cell membrane and in a prominent antimicrobial activity, respectively.

In *Figure 10*, it is schematized the interaction approach with polar head and the most important ways of bacterial inactivation induced by QASs. [39]

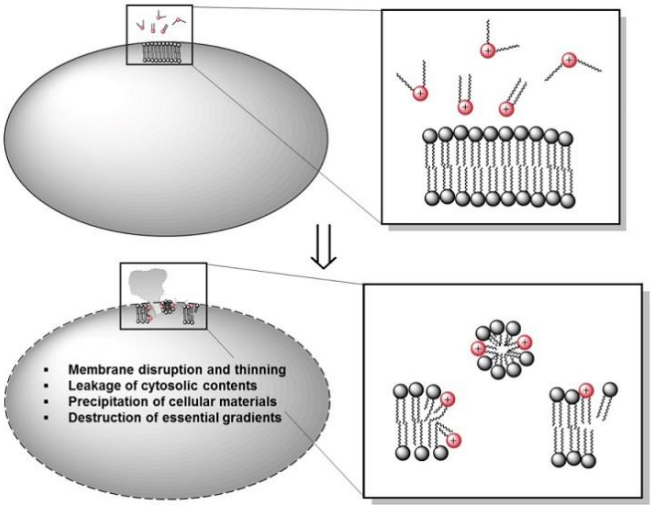

Figure 10 – Inactivation of bacteria induced by QASs.

After the interaction, microbials are eliminated directly by cell membrane disruption, reorganization, or pore formation. In this context, long alkyl chains can penetrate the cell membrane, causing irreversibly processes, such as the membrane thinning caused by the disruption of the double layer of amphiphilic macromolecules of membrane. This fact results in many consequences, among which the destruction of the essential gradients inside the cell, the precipitation of cellular materials and the leakage of cytosolic contents. Moreover, QASs are recognized to be involved in inactivation processes of energy-producing enzymes, in the denaturation of proteins and in the inactivation of microbial spores.

Another important feature to highlight relies on the large influence of QAS concentration for the properties provided by these salts. In this sense, it is proven the bacteriostatic activity at low concentrations, consequence of the electrochemical gradient alteration and, so, the alteration of the bacterial membrane functionality. At high concentrations, QASs have bactericidal action, which causes microbial cell lysis. The effectiveness generally increased under basic pH conditions.

Moving to viruses, it was proven the efficiency of inactivation of a long list of quaternary ammonium compounds against lipophilic viruses (e.g., *herpes simplex*, *vaccinia*, *influenza*, *adenoviruses*); however, it was demonstrated their inefficacy toward hydrophilic viruses.

Due to their antimicrobial, antiviral, antifungal and antialgae activities, QASs are frequently utilised in various important sectors, such in food processing facilities as sanitizers, as skin antiseptics, and for surface and linen disinfection; moreover, QASs are also used as antifouling agents to prevent microbial growth on specific surfaces.[40]

A final consideration has to be placed on the discovery of resistance mechanism for low molecular quaternary ammonium salts, since it was proven that some organisms have evolved a target site for QASs. It is unclear whether this resistance mechanism is innate in the bacterium or evolved

subsequently following a genetic change. The first resistance mechanisms to QAS were studied in *Staphylococcus* cultures and several genes within the bacterium were discovered that controlled resistance to these antimicrobials.[41]

A smart solution to avoid this problem is the incorporation of QASs in polymeric materials and it will be described in the *Chapter 2.2.3*.

2.2.3. QASs in antimicrobial/disinfectant polymers

Disinfectant materials functionalized with QASs have becoming more and more popular, since the possibility to ensure a durable antimicrobial surface. In this sense, the coating of QAS-functionalized polymers onto different substrates, such as wood, paper, metals, or glass, has allowed an efficient biocidal activity due to the mechanism of action that occurs by contact with microorganisms. Various biological contact tests revealed that the quaternary ammonium groups maintain biocide properties even after being introduced into the polymer matrix. Studies have also been done about the tertiary amino group, common precursor of the quaternary ammonium, because it would have a similar activity. However, tertiary amine oligomers were tested in the same conditions and it was compared to oligomers made of QASs, demonstrating the much stronger activity of the ammonium group as antibacterial agent.[42]

Besides the chemical stability, non-volatility, low toxicity and extended lifespan of disinfectant surfaces incorporating QAS, the development of QAS-functionalized polymer has proven to be beneficial to suppress the bacterial resistance, that is a critical point for many conventional antibacterial substances. The antimicrobial activity of these polymers depends on three parameters, namely: cation charge, hydrophilic/hydrophobic balance, and polymeric structure.

Biocidal polymers with QASs can be obtained using two synthesis strategies.[43] These techniques are commonly known as grafting techniques and they are basically divided in two types. The first one, the grafting-from approach, is based on the use of functional monomers and, in order to obtain a QAS-functionalized polymer, it is possible to polymerize the monomer having an amine precursor, performing then the quaternization to ammonium salts, or proceeding before with the QAS formation and then polymerization. Conversely, in the second technique, known as grafting-to approach, QASs are covalently bonded to pre-formed polymer matrices. However, despite the technique of grafting used to coat most antimicrobial surfaces, it is not always possible to obtain an effective product suitable for every application. For example, with the "grafting to" technique, it is possible to graft polymers with very complex architectures, but this grafting also causes an irregular distribution of the charge density and, therefore, a reduction of local antimicrobial activity. On the contrary, "grafting

from" approach allows greater control of the surface balance charge density. However, it is impossible to graft more complex polymer architectures that could improve the antibacterial activity of materials. In addition, in all cases, it is required that the introduction of quaternary ammonium groups should be preceded by quaternization to be permanently charged.

Grafting-from approaches are commonly performed starting from acrylic or methacrylic acid, achieving so polyacrylates with antibacterial activity. They are preferred both for the final properties of material (easy handling and modification of acrylates) and for the greater availability in finding the respective monomers. In this way, many QAS-functionalized polymers are obtained using as monomer 2-(dimethylamino)ethyl methacrylate (DMAEMA), which is commercially available and characterized by high structural versatility.

In this context, a nice example could be the study of Okeke *et al.*, reporting the synthesis of four different quaternary ammonium salts starting from DMAEMA, just by varying the alkyl halide.[44] The quaternization of DMAEMA and the subsequent polymerization of the methacrylate moiety are schematized in *Scheme 8*.

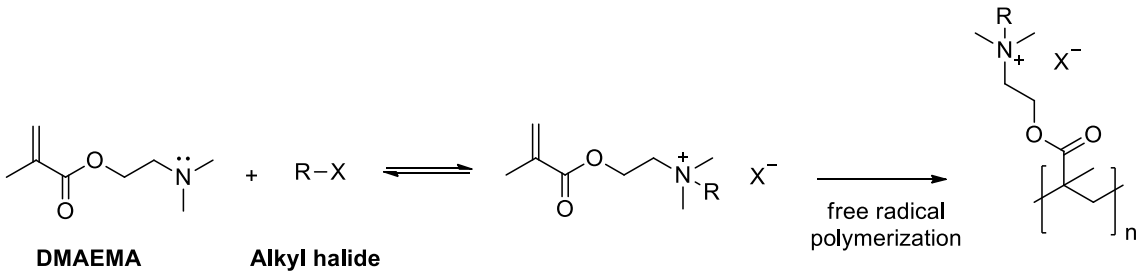

Scheme 8 – Synthesis of a QAS-functionalized methacrylate by the quaternization of DMAEMA and the successive polymerization.

The identic approach was used in the work of Guiqian *et al.*, where it is reported the synthesis of four new monomers from DMAEMA through the quaternization with benzyl chloride, butyl bromide, dodecyl bromide, and hexadecyl bromide.[45] The monomers then were polymerised to obtain the corresponding biocidal polymers, differing in alkyl chain length and counterion (Br or Cl). According to the length of alkyl chain introduced, the solubility of formed QAS greatly varied. In this way, authors performed the free-radical polymerization of DMAEMA-QAS monomers with short alkyl chain (coming from the reaction with benzyl chloride and butyl bromide) in aqueous solution, using ammonium persulfate (APS) as initiator and maintaining the polymerization solution at 50°C for six hours. Conversely, the polymerization of monomers having long alkyl chain was carried out in THF, in the presence of AIBN as initiator and heating the solution at 60°C for several hours.

Another interesting example is the one reported by Dizman *et al.* in 2006.[46] The work summary is reported in *Scheme 9*.

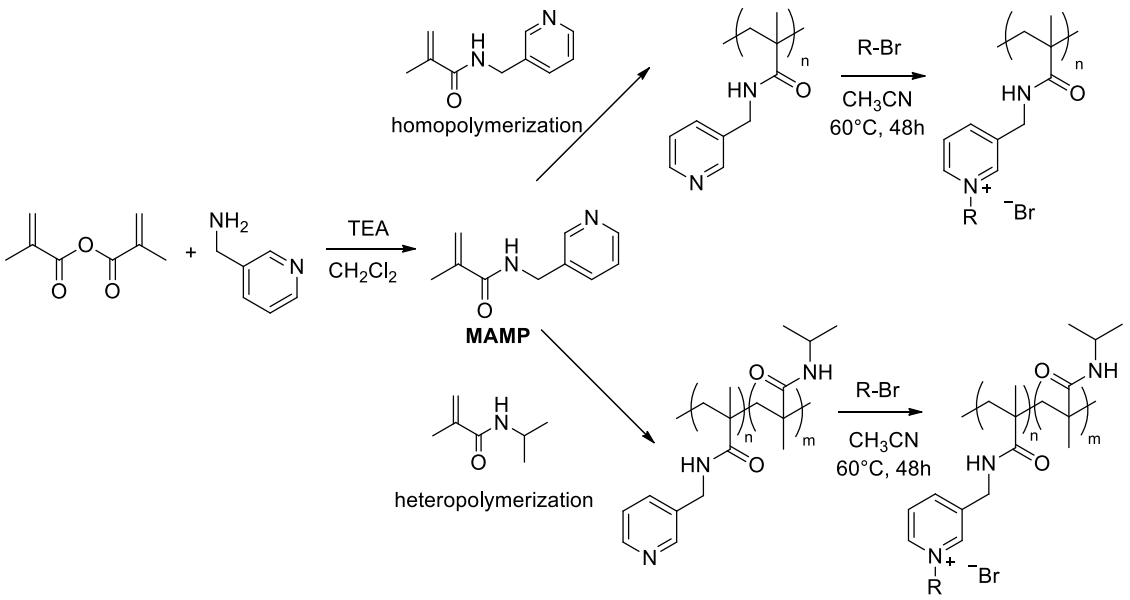

Scheme 9 – Synthesis of a methacrylamide monomer (MAMP), its use in polymer materials and the final quaternization.

In this study, authors proposed the synthesis of new methacrylamide monomer containing a pyridine moiety, namely 3-(methacrylamidomethyl)pyridine (MAMP), by reacting methacrylic anhydride and 3-(aminomethyl)pyridine, using triethylamine (TEA) as reaction catalyst and dichloromethane as solvent. The monomer was homopolymerized in 1,4-dioxane and copolymerized with N-isopropyl acrylamide in DMF at two different compositions using AIBN as an initiator. Finally, the pyridine groups of the homopolymer and copolymers were reacted with various bromoalkanes (in large excess, containing 12, 14, and 16 carbon alkyl chains) to obtain the polymers with pendant pyridinium groups. The copolymers with low MAMP content were water-soluble and showed temperature-responsive behaviour in aqueous solutions. The lower critical solution temperatures (LCSTs) of these polymers varied between the temperatures of 25 and 42 °C and the LCST of quaternized copolymers were higher than that of the neutral copolymer because they were more hydrophilic; anyhow, the LCST of the quaternized copolymers decreased with an increase in the alkyl chain length on the pyridinium group, reasonably with increasing hydrophobicity. The antibacterial activities of water-soluble copolymers were investigated against *Staphylococcus aureus* and *Escherichia coli* using the broth dilution and spread plate methods, whereas the water-insoluble polymers were tested for the antibacterial activity against the same types of bacteria using the shaking flask method. The quaternized water-soluble copolymers showed excellent antibacterial activities, whereas the neutral polymers and quaternized water-insoluble homopolymers and copolymers were not active.

Moving to grafting-to approaches, a citable study is the one of Sha *et al.*, where QASs were directly grafted to the alcohol-formaldehyde polyvinyl system (*Scheme 10*).[47] In particular, the epoxy group present in the salt reacts with the hydroxyl group of the polymer in a basic environment, leading to the epoxide ring's opening and the formation of a polymer containing QASs.

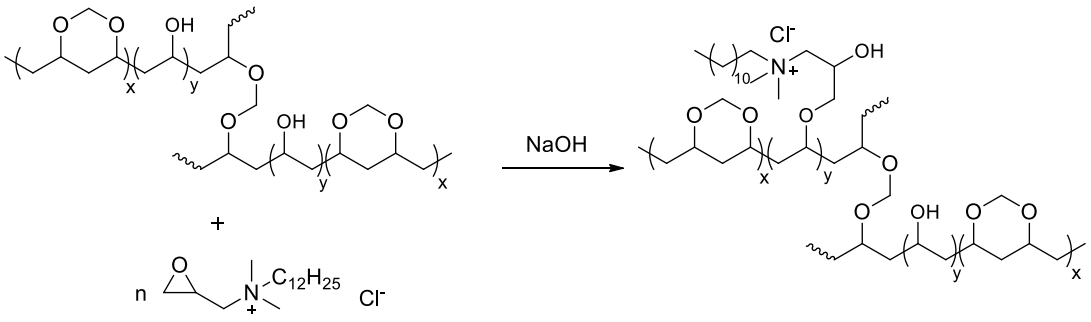

Scheme 10 – Synthesis of a QAS-functionalized polymer.

Finally, it is interesting to assess the role of the counterion in the antimicrobial performance of polymeric QAS. For instance, the replacement of Ca^{2+} and/or Mg^{2+} on cellular membranes by biocidal cations may occur during the sterilization process.[48] In addition, some interesting works have focused on tuning the antimicrobial activity of polycations by exchanging counter anions. In this context, an interesting study was proposed by the Chauhan's group.[49] They prepared two types of bioactive polymers, i.e., poly(4-vinyl-2-hydroxyethyl pyridinium) chloride and poly[1-vinyl-3-(2-sulfoethyl imidazolium betaine)] bromide and replaced the chloride and bromide counter anions with various anions via an anion exchange reaction, as shown in *Figure 11*.

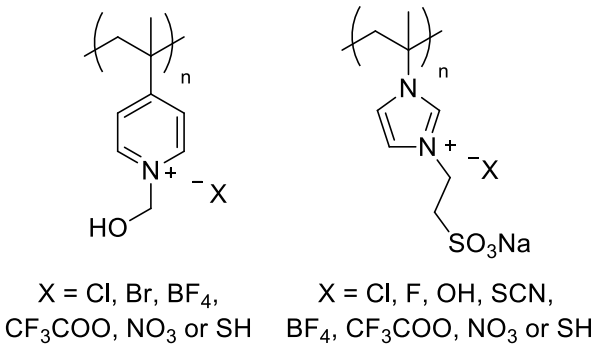

Figure 11 – Bioactive polymers with different counter-ion.

From this work, it was suggested that the structure of the counter anion has a profound effect on the efficiency and selectivity towards different microbes due to the discrepancy of polymer morphology and the solubility of polycations in water, resulting in various degrees of antimicrobial performance. More in detail, Cl^- of the original pyridinium polymer was exchanged with Br^-, OH^-, SH^-, NO_3^-,

BF_4^- and CF_3COO^- and their antimicrobial properties were studied against fungi (*A. niger* and *Mucor circenelliods* (*M. circenelliods*)) and bacteria (*Bacillus coagulans* (*B. coagulans*) *BTS-3*). In comparison, the polymer with OH^- as the counter anion presented the strongest antimicrobial activity with MIC values of 520 and 1040 ppm against *A. niger* and *M. circenelliods* fungi, respectively, and 65 ppm against *B. coagulans* bacterium. Similarly, the Br^- from the original polysulfobetaine polymer was replaced with Cl^-, F^-, OH^-, SH^-, SCN^-, NO_3^-, BF_4^- and CH_3COO^- and the antimicrobial activities of prepared polysulfobetaines were determined against three fungi and two bacteria. For different types of microorganism, polymers with different counter anions exhibited significant differences in term of antimicrobial activity. For Gram-positive bacteria, i.e., *B. coagulans*, the polysulfobetaine having OH^- counter-ion possessed the strongest activity. In contrast, for Gram-negative bacteria, i.e., *Pseudomonas aeruginosa* (*P. aeruginosa*), the most effective ones were the ones with F^- and NO_3^-. Regarding antifungal activity, SH^- and OH- counterion showed maximum activity against *M. circenelliods* and *Byssochlamys fulva* (*B. fulva*), respectively.

2.3. Polyurethanes and polyurethane-acrylates

PolyUrethanes (PUs) and Poly (Urethane-Acrylates) (PUAs) are polymers of great interest and with a wide-ranging application, such as automotive, thermal insulation, coatings, adhesives, construction, antimicrobial, biomedical and many others. Additionally, it is well known the biological action of PUs, based on the formation of urea linkages by the reaction of isocyanate end-groups with the amino groups found in human tissues. These linkages may help to promote adhesion by maintaining tissues together. Moreover, due to their antimicrobial, self-healing qualities, capacity for stimulating cellular ingrowth, and their possibility to be reshaped, polyurethane materials perform particularly well in skin adhesive applications, including several benefits, such as quicker application and no tissue trauma.[50]

The large applicability of PUs materials relies on the facile adaptation of properties just by varying the chemical composition, the molecular weight and the ratio of the soft-to-hard segments. In this context, the most important topics for improve the powerful properties and to further broad the applicability of PUs materials is to base their production on sustainable and/or renewable monomers, to use non-toxic catalyst and to impart new innovative properties on these materials. Furthermore, the polymerization through UV-curing technology has attracted a conspicuous attention due to the low energy consumption and the fast-curing conditions, resulting so in an environmentally friendly and in a suitable polymerization technique in the fields of drug delivery systems, coatings, and adhesives. Moreover, UV-curing technology has proven to ensure less VOC emissions, a crucial

aspect in this kind of applications.[51] Among UV-curable resins, poly(urethane-acrylates) have been drawing growing interest thanks to their unique properties as excellent abrasion and chemical resistance, adhesion to substrates, light stability, water resistance and weatherability, as well as mechanical properties which are highly desirable for industrial applications.[52]

In this way, the most important features regarding PUs and PUAs, with a strong focus on the functionalization of these materials with quaternary ammonium compounds, will be described in the following chapters.

2.3.1. Polyurethanes: synthesis and applications

The term "polyurethanes" refers to a unique class of polymeric materials with various chemical composition. In 1937, in Bayer laboratories, by studying the interaction of a polyester diol and a diisocyanate, it was synthesized and characterized for the first time a PU polymer.[53]

The main PU repetition unit is the urethane group obtained by the reaction between a diol (alcohol with two hydroxyl groups -OH) or polyol (alcohol with more than two hydroxylic groups), with a diisocyanate (a compound with two reactive groups -NCO) or polyisocyanate (a compound with more than two reactive groups -NCO) in the presence of a catalyst.[54]

The catalyst is used to speed up the reaction, typically by increasing the electrophilic nature of isocyanate through electron-withdrawing groups on the nitrogen or oxygen atom. Catalysts generally include tertiary amines and organometallic compounds; additionally, stabilizers can be added to improve the stability and durability of the synthesized polyurethane.

In *Scheme 11*, it is shown the general reaction of a diisocyanate and diol to obtain a PU.

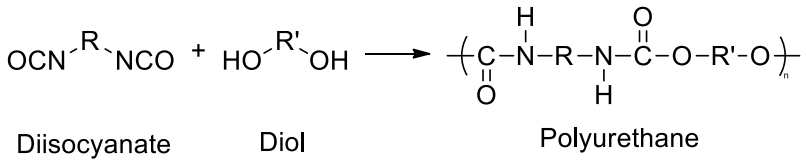

Scheme 11 – Synthesis of a PU.

The properties of a polyurethane material are strongly influenced by the nature of precursors and in the polymerization technique because they can lead, for example, to different branching degree or to a larger spacing between polymer chains (e.g., with monomers having sterically-hindered side chains). Conventional PU materials are based on aromatic diisocyanates such as toluene diisocyanate (TDI) and methylene diphenyl diisocyanate (MDI). However, these reagents are related with the release of toxic and carcinogenic aromatic diamines as a consequence of *in vivo* degradation.

Therefore, aliphatic and cycloaliphatic isocyanates, such as hexamethylene diisocyanate (HMDI) and isophorone diisocyanate (IPDI), are commonly preferred, especially in coating applications, where they are widely used to produce transparent and UV-resistant coatings.[55] The structure of most common diisocyanates is reported in *Figure 12*.

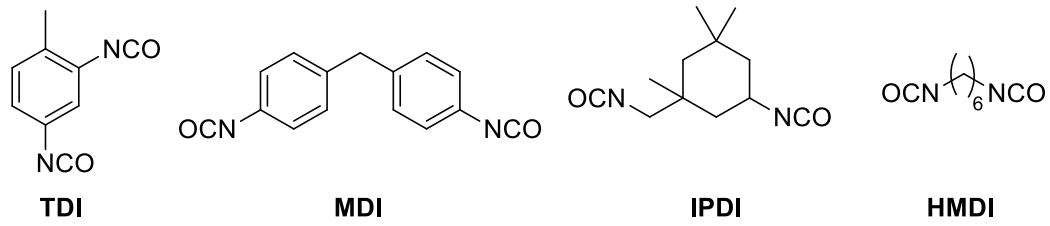

Figure 12 – Common diisocyanate monomers.

Moving to the second reagent, various diols and polyols can be used as starting materials including polyether polyols, polyester polyols, poly (tetramethylene ether) glycols, and others. Examples include polyethylene glycol (PEG), a non-toxic, inert, and non-volatile polymer, polycaprolactone (PCL), a biodegradable polyol produced by the ring-opening polymerization of ε-caprolactone and polypropylene glycol (PPG). Their structures are shown in *Figure 13*.

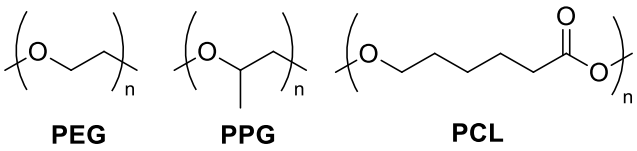

Figure 13 – Common diol monomers.

The large size of the polyurethane market is because of a wide range of products and, in this context, the polyol component plays a crucial role. Indeed, a low molecular weight polyol (with a few hundred units) is mostly used to create rigid PUs, whereas high molecular weight polyols (above ten thousand units) are used to create flexible PUs.[56] This outcome could be explained considering each involved reagent as a segment of the PU material: polyols could be defined as "soft segments", while the diisocyanate as "hard segment". Therefore, reducing the length of the soft segment by using a short polyol reasonably results in a hard polymer; on the opposite, a longer polyol can effectively play as a softener of the material. The segmental structure of a PU material is depicted in *Figure 14*.[57]

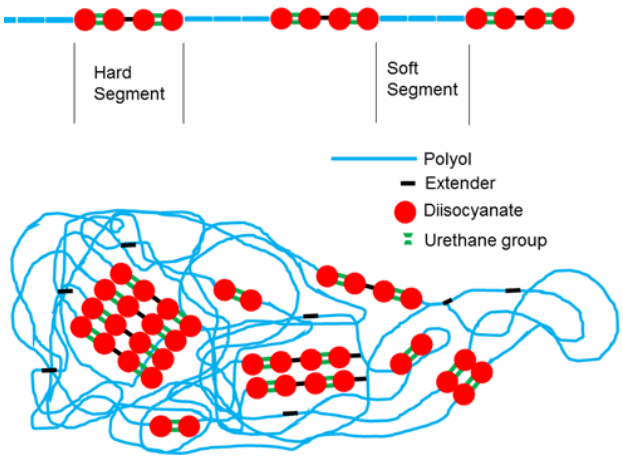

Figure 14 – Soft and hard segments in a PU material.

The presence of hard and soft segments is crucial to understand the characteristics of polyurethane materials. The formation of hydrogen bonds between O and H atoms of the urethane linkage can result in the formation of semi-crystalline regions formed by diisocyanate-derived portions, as suggested in *Figure 14* in the region where red circles (indicating the diisocyanate portion) are accumulated. Likewise, the long chains of soft regions tend to entangle, interacting each other and forming an amorphous region. Therefore, the phase separation between the hard and soft fragments and the hydrogen bonds formations, due to the generation of urethane linkages, are primarily responsible for the high variety of mechanical features that PUs can have.

Another important distinction of PUs materials is based on thermoplastic and thermosetting polyurethanes.[58] Basically, in accordance to the type of interaction between polymer chains, the use of difunctional monomers leads to linear and/or branched polymer chains, where H-bonds and apolar interactions are the main intermolecular interactions. Conversely, the formation of a cross-linked network, by choosing a poly-functional monomer or by using cross-linker agents, is the basis of thermosetting PUs. The choice of a thermoplastic or thermosetting PU largely relies on the specific application and on the desired properties: thermoplastics are melt-processable, with high flexibility and distinct tensile strength; while thermosetting PUs are not re-shapable but they can ensure greater mechanical properties and they can be designed to form thermosetting elastomers.

Furthermore, in order to reduce the strong dependence of PU industry to fossil-based materials, numerous researches have recently concentrated on polyols derived from organic and renewable sources like sorbitol, amino acids, furan derivatives, cellulose, lignin, vegetable oils and derivatives (*Figure 15*).[59] In fact, the use of sustainable materials avoids the depletion of limited resources, reducing greenhouse gas emissions and health related issues.

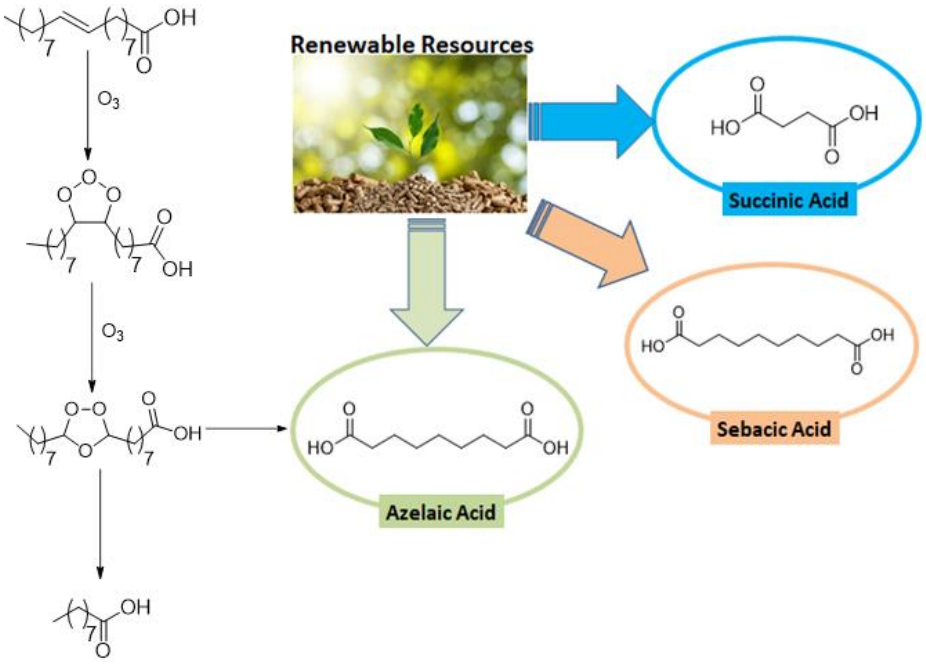

Figure 15 – Diols from renewable resources.

Similarly, there is a strong interest in finding valuable bio-based precursor for the synthesis of diisocyanates. Among them, biomass-derived lysine is largely used as a starting material to synthesize methyl or ethyl esters of lysine diisocyanate (LDI, *Figure 16*), in turn obtained from the reaction between a lysine ester and triphosgene (typical product yield of about 50%). LDI is used for the synthesis of bio-based PUA and, thanks to its asymmetric aliphatic structure, it leads to the formation of amorphous polyurethanes.

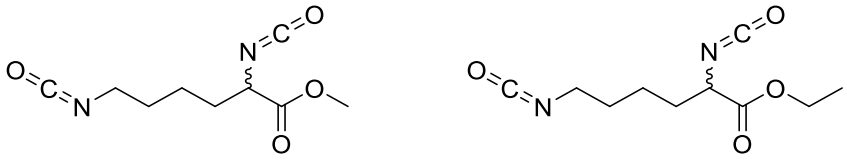

Figure 16 – Chemical structure of methyl and ethyl esters of LDI.

The most important sectors where PUs have found a great applicability are paints, surface coatings, adhesives, sealants, elastomers, insulators, elastic fibers, and foams.[60] For the latter, the production of PU foams commonly involves the use of blowing agents and/or gelling methods. Considering the blowing reaction, one of the possibilities is the formation of carbon dioxide, responsible of the foam formation, by the reaction of the isocyanate end group of PU with water, as shown in *Scheme 12*.

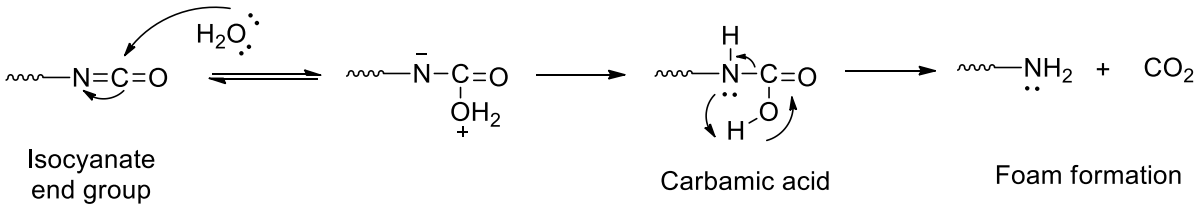

Scheme 12 – Mechanism of PU foams.

PU foams can be distinguished in two categories, rigid and flexible foams. The morphology and microstructure of the foam determine the differences between them and crucial factors are the degree of cross-linking during the polymerization reaction, the ratio of hard-soft segments in the polymer and the segmental movement of the urea groups. In this context, rigid PU foams are one of the most popular, versatile, and energy-saving insulation plastic materials. This kind of material offers numerous favourable characteristics, including low thermal conductivity, low density, stability, high strength-to-weight ratio, low moisture permeability, and low water absorption. Numerous commercial products, such as carpet underlays, furniture, bedding, automotive interior parts, packaging, biomedical uses, and nanocomposites, use polyurethane foams.[61]

2.3.2. Polyurethane ionomers and QAS-functionalized PUs

Ionomers are polymers containing ionic groups within the polymer chain. From a general point of view, PU ionomers are effectively obtained by the reaction of ionic diol and ionic diisocyanate. Therefore, the two starting monomers are the source of ionic moieties into the chains; anyhow, ionic reactants can also be added after PU formation performing a post-polymerization functionalization. According to the effective charge resulting by ionic moieties, PU ionomers can be classified in anionomers, cationomers and zwitterionomers. A general zwitterionic ionomer is depicted in *Figure 17*.[62]

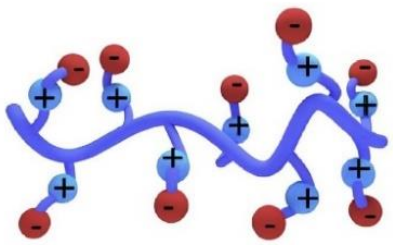

Figure 17 – General visualization of a zwitterionic ionomer.

When incorporated in the backbone of PU chain, ionic groups can effectively give them distinctive properties. For example, the presence of ionic groups could work as an internal emulsifier, leading to the possibility to produce waterborne polyurethane dispersion, made up of linear thermoplastic polyurethane chains dispersed in water. Typically, the first step in the production process of waterborne polyurethanes is the formation of an NCO-terminated prepolymer, which is quickly dissolved in a solvent, such as acetone. Then, the pre-polymer is generally placed to react with a chain extender (such as diamine), increasing so the molecular weight of the polymer. At the end, the solvent is eliminated, allowing the phase inversion and the formation of the polyurethane dispersion in water. The waterborne polyurethane dispersions can be used for coating flexible materials, especially in situations where high abrasion resistance is required. Examples of applications are coating of fabrics, leather, and paper.[63]

Moreover, PU ionomers are effectively used to produce disinfectant surfaces and biocidal polymers, especially when coupled with quaternary ammonium salts. A remarkable study on the synthesis of a QAS-functionalized polyurethane is the one reported by Wang *et al.*, based on the formation of a PU polymer having an amine group and the subsequent quaternization of amine-bearing polymer to QAS-functionalized PU (*Scheme 13*).[64]

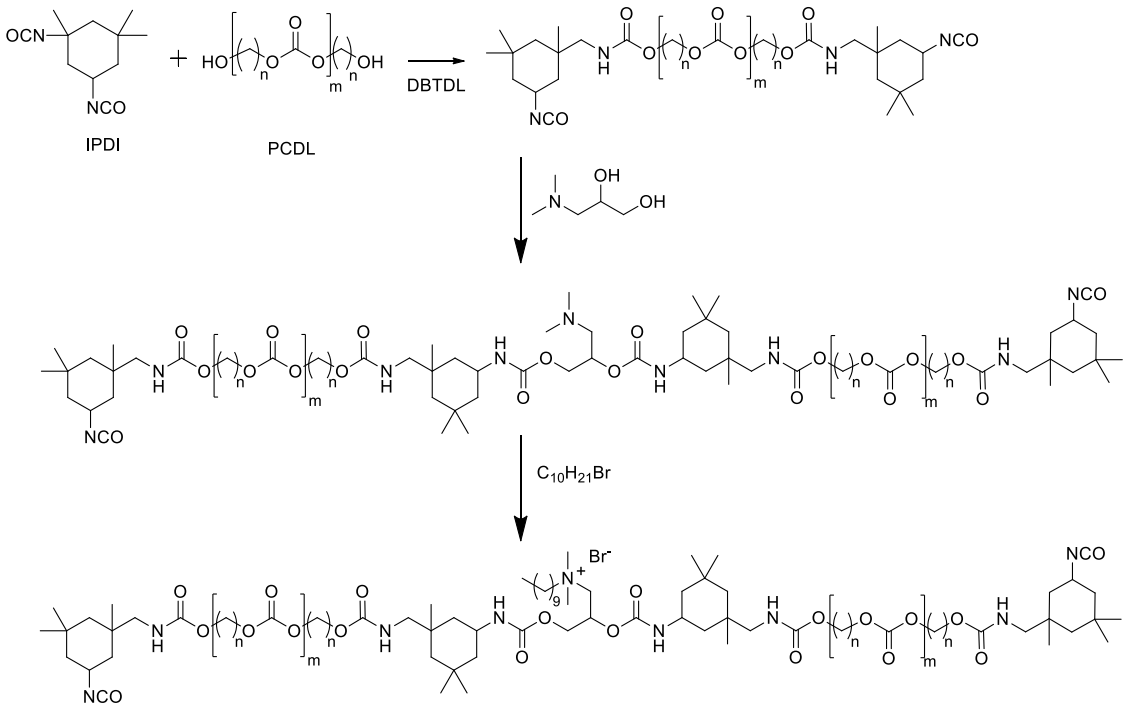

Scheme 13 – Synthesis of a QAS-functionalized PU by the use of N,N-dimethylisoserinol.

Firstly, authors prepared a prepolymer having NCO-terminal groups by the polymerization of isophorone diisocyanate and poly(carbonate diol) in presence of dibutyltin dilaurate (DBTDL) as

catalyst. Subsequently, 3-dimethylamino-1,2-propandiol was used to ensure both a chemically binding between two polyurethane chains and, more important, a site of functionalization. In this way, the final quaternization with 1-bromodecane resulted in the formation of a quaternary ammonium compound covalently bonded to the PU material and having a long alkyl group (-$C_{10}H_{21}$), crucial to provide strong antimicrobial activity.

As a further example, Park *et al.* reported the synthesis of a polyurethane with antimicrobial activity starting from 3-aminopropopan-1,2-diol, which was initially protected with a tert-butyloxycarbonyl (Boc) group and then reacted with MDI. In the second and last step of the reaction, deprotection with trifluoroacetic acid and quaternization with 1-bromodecane and iodomethane were performed, respectively (*Scheme 14*).[65]

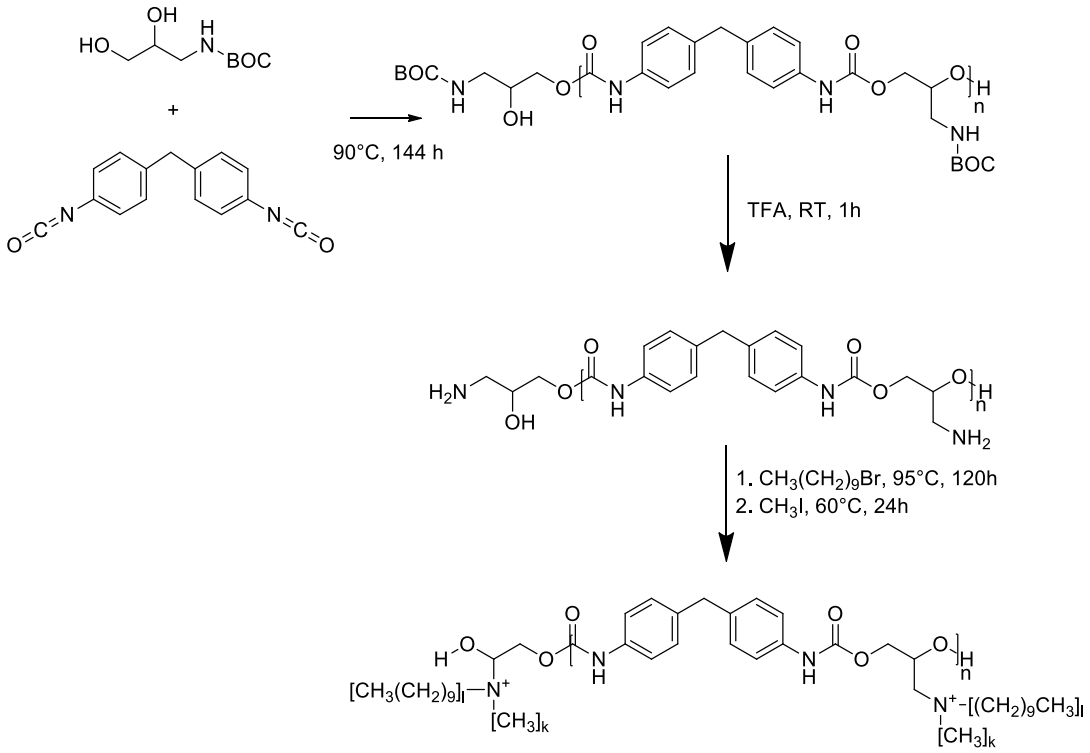

Scheme 14 – Synthesis of a QAS-functionalized PU by the use of N-protected isoserinol.

The quaternization of deprotected amine was effective to ensure a QAS function covalently bonded to the PU chain. In this sense, the stepwise addition of 1-bromodecane and iodomethane resulted in a mixture of quaternary ammonium salts, having a different number of long and short alkyl chains. Since short alkyl halides are more propense to react via S_N2 reaction, the quaternization was performed with 1-bromodecane as first reagent, keeping the reaction for long times (120 h) and heating the reaction mixture at 95°C; after that, the methylation with iodomethane ensured the complete quaternization of remaining amine groups.

Another interesting property of PU ionomers is the Shape Memory Effect (SME). In fact, these materials have proven to alter their shape when a temporary deformation force is applied and to return to their previous shape with an external stimulus, without changing their structural conformation (*Figure 18*).[66]

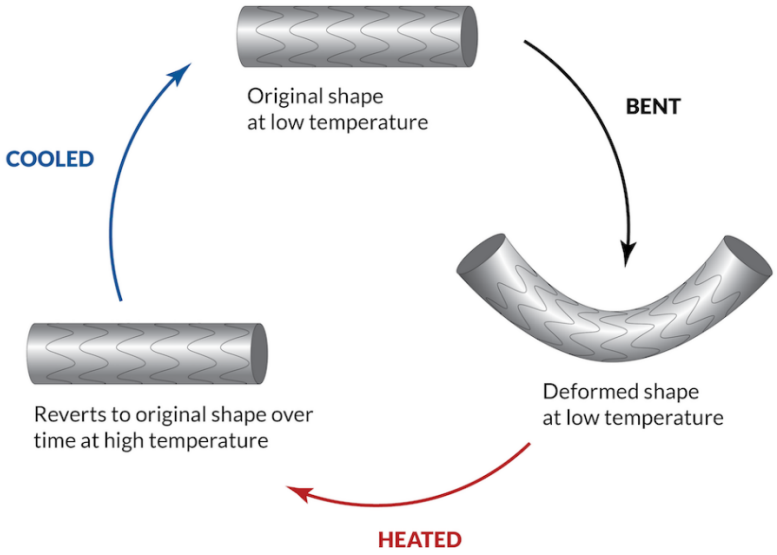

Figure 18 – Shape memory effect in PU ionomers.

Ionomers can alter the glass transition temperature of the soft segment and the crystallization of the hard segment, two elements that are crucial to the shape memory effect. Moreover, the coupling of SME and biocompatible PU materials properties makes them highly suitable for use in biomedical applications.[67]

2.3.3. Synthesis of polyurethane-acrylates

PUAs are commonly appreciated because they proved exceptional results in abrasion resistance, solvent resistance, water resistance, weatherability, flexibility, and hardness. Moreover, they can be design to ensure biocompatibility, strongly desirable for biomedical applications, such as soft tissue repair, dental repairs, and medicated plasters and tissue adhesives. Additionally, the ease polymerization of the methacrylate moiety through free-radical polymerization makes PUAs as one of the most suitable resins for coating applications, especially in UV-curing processes.[68]

PUA is generally obtained through three steps:

- Reaction of an excess of diisocyanate with polyol in the presence of a catalyst, resulting in the formation of urethane oligomer chains (or PU pre-polymer) with isocyanate end-groups.

- Reaction of isocyanate end-groups with an acrylic end-capping agent, commonly hydroxyl functional acrylic monomers, to obtain a urethane acrylate oligomer (UAO) with reactive unsaturation at the end of the polymer backbone.
- Radical polymerization by UV radiation of vinyl group of end-capped acrylates, in the presence of a photo-initiator system (e.g., benzophenone as type II photo-initiator and methyl diethanolamine as co-initiator), to obtain PUA

The sequence of these steps is schematized in *Scheme 15*.[69]

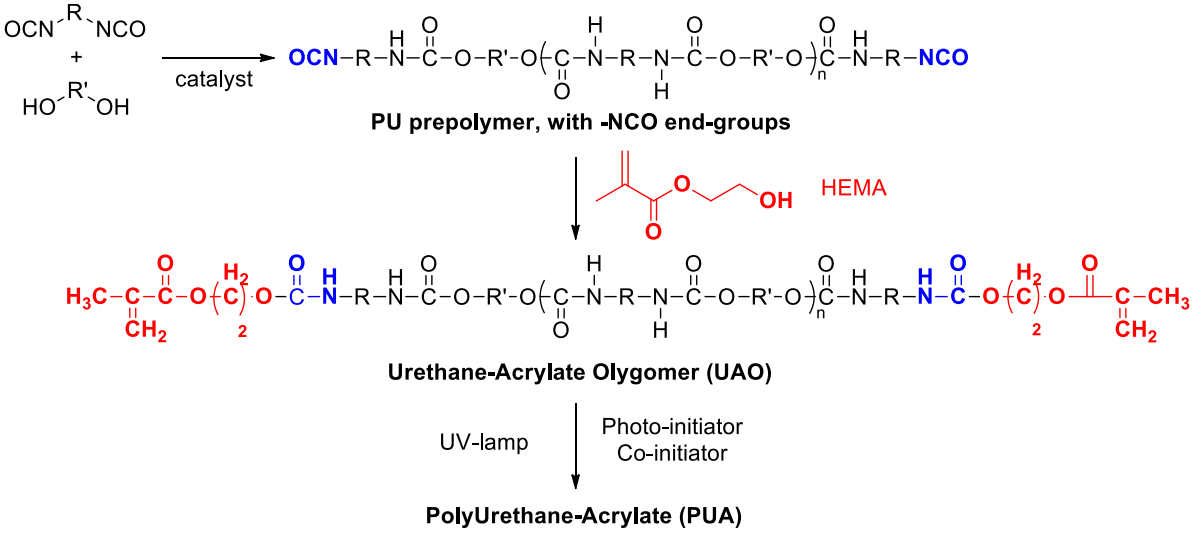

Scheme 15 – Synthesis of PUA.

In consistence with the proposed synthetic approach, the PU oligomer with -NCO end groups are obtained by standard PU polymerization. In order to obtain a more sustainable product, the use of aliphatic and cycloaliphatic diisocyanates, together with a polyol deriving from renewable sources, is strongly preferred. In this context, even the catalyst is highly important. The most employed catalysts during this synthesis are tin-based compounds, one of the most used is the dibutyltin dilaurate (DBTDL), but its homogenous nature means that complete removal of the catalyst from the polymer matrix is not feasible. Furthermore, many studies have been shown the potential toxicity of tin, and this aspect limits its use in the synthesis of polymers involved in biomedical application.[70]

Moving to the end-capping agent, 2-hydroxyethyl methacrylate (HEMA) is mostly preferred than 2-hydroxyethyl acrylate (HEA) due to numerous health risks the latter poses.[71] End-capping (meth)acrylates are also called reactive diluents as they control the viscosity, improve workability, surface finish, strength, chemical and scratch resistance, elongation, shrinkage and control the cross-link density. They present also good solvent power, low viscosity, low toxicity, high cure rate and

lower cost. Reactive diluents, therefore, help to improve the properties of PUA and in particular to reduce the high viscosity of the pre-polymer.

Finally, the UV-induced polymerization of multifunctional monomers or oligomers has increasingly drawn attention by researchers over the years. Due to its many advantages (e.g., instant drying, solvent-free formulations and reduction of energy consumption), it is used in a great variety of industrial applications. Under UV radiation, a three-dimensional polymer network is formed without the use of high temperatures and the final product shows excellent resistance to organic solvent, chemicals and heat.[72] Photoinitiated polymerization begins with the absorption of light by an initiator, leading to the formation of radical species able to start the polymerization.

Radical photoinitiators can be divided into different classes. The bond α-cleavage type (Norrish type I) is depicted in *Scheme 16*. Basically, the irradiation with UV light leads to a homolytic cleavage of the photoinitiator, with the consequent generation of two highly reactive radical species.[73]

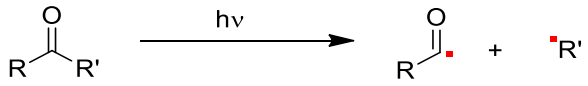

Scheme 16 – Bond α-cleavage in the formation of radical initiator.

The second class of photoinitiator is the hydrogen abstraction type (Norrish type II). In *Scheme 17*, it is depicted the generation of radicals in these initiators. In few words, the photolysis of aromatic ketones (such as benzophenone, 4-benzoylbenzoic acid, 4,4'-bis(dimethylamino)-benzophenone, 1,4-dibenzoylbenzene, anthraquinone and others) in the presence of a co-initiator (hydrogen donor species) drives to the formation of a ketyl radical and a hydrogen donor radical.

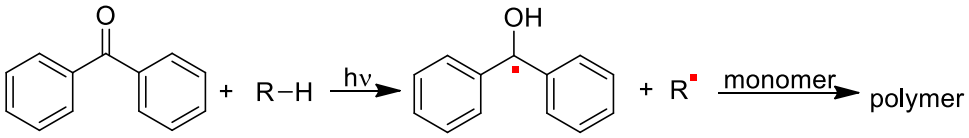

Scheme 17 – Hydrogen abstraction in the formation of radical initiator.

Ketyl radicals are relatively stable and they are usually not reactive towards vinyl monomers due to steric hindrance and unpaired electron delocalization. For this reason, several co-initiators (hydrogen donors) are generally added. They react rapidly with the electronically excited photoinitiator to produce a reactive radical that allows the start of the polymerization.[74]

With the aim to produce bio-based PUA with a sustainable catalyst, the research group of Marcantoni has developed a low-impact, sustainable and efficient procedure for the synthesis of bio-based PUA promoted by solid supported $CeCl_3 \cdot 7H_2O$–NaI/SiO_2 catalytic system (*Scheme 18*).[75]

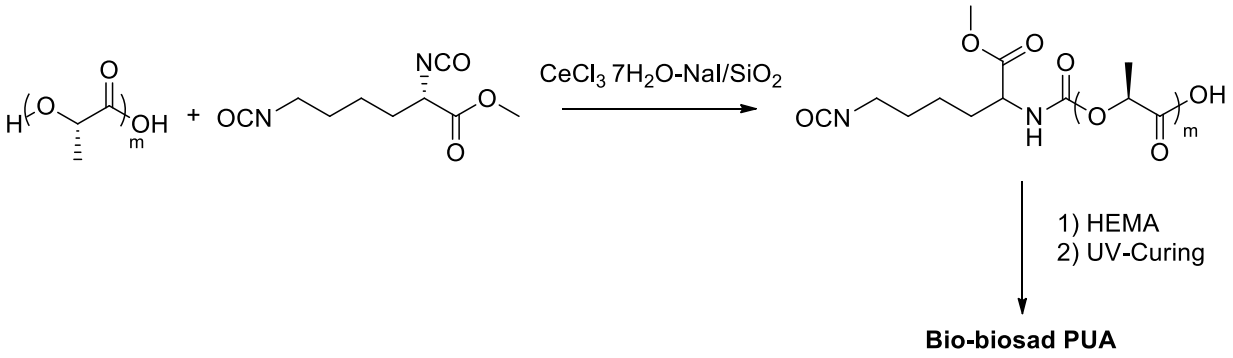

Scheme 18 – Synthesis of bio-based PUA.

The very soft reaction conditions did not result in the oligomers alteration with the subsequent formation of polyamide derivatives. Additionally, the eco-compatible and inexpensive solid-supported catalyst ensured a remarkable activity in the PUA synthesis and it was proven that $CeCl_3 \cdot 7H_2O$–NaI/SiO_2 catalytic system can be recycled for seven times without a decrease in activity, obtaining a pre-polymer with a molecular weight of 1.800 Da. Furthermore, it was used as monomers renewable poly(L-lactic acid) (PLLA) and L-lysine diisocyanate. With this design, the synthesized PUA encloses the bio-based economy principles, allowing so the generation of a PUA suitable for biomedical applications and drug delivery systems, especially due to the very low toxicity of monomers and catalyst. The bio-based PUA was finally compared in terms of chemical and thermal properties to ones coming from fossil-based materials, prepared with the same approach. In this way, DSC, TGA and SEM analyses have proved that bio- and fossil-based PUAs have similar chemical characteristics and behaviour.

2.4. Results and discussions

The spread of pathogenic infections and the proliferation of drug-resistant microorganisms is a topic of great concern and it represents a challenging global health crisis. To deal with that, an appreciable approach is to restrict as more as possible antimicrobial agents with high resistance, while agents having low resistance potential, reduced toxicity and ease applicability should be preferred for the daily cleaning and disinfections.

In this context, chemical disinfectants, such as quaternary ammonium salts (QASs), are popular agents to contrast harmful microorganisms in various settings, from healthcare facilities to public spaces, ensuring cleanliness and preventing the spread of infectious diseases. However, after the application, these compounds have a short-term antimicrobial action and, when applied onto material surfaces, these sites are contaminated again once re-exposed to microorganisms. In addition, the prolonged and often reckless use of many disinfectants is toxic and has caused severe environmental

damage. Finally, a number of microorganisms have shown an alarming resistance toward low molecular weight disinfectants.

An interesting solution is to incorporate disinfectant agents in polymer materials, developing so materials like antimicrobial polymers (APs) or disinfectant coatings. These approaches frequently ensure good antimicrobial activities together with low microbial resistance rates. QASs applied in disinfectant materials have becoming more and more popular. Besides the chemical stability, non-volatility, low toxicity and extended lifespan of disinfectant surfaces incorporating QAS, the development of QAS-functionalized polymer has proven to be beneficial to suppress the bacterial resistance, that is a critical point for many conventional antibacterial substances.

From these considerations, the work aimed to develop an approach to synthesize new ammonium salts and to apply them in innovative antimicrobial polymer coatings. The synthesized QASs derived from two sources: the commercially available 3-amino-1,2-propanediol (or isoserinol) and pent-4-en-1-amine (the latter, synthesized from 5-bromopent-1-ene). These compounds can fulfil both a facile derivatization of the ammine group to QAS and a potential linking with many polymer materials, since the presence of a diol and a C=C bond, respectively. The antimicrobial activity was tested and the obtained compounds were then used as building blocks for the synthesis of polyurethane acrylate films. For the latter, in the initial phase of the work, it has been conducted both an extensive optimization of the polymerization conditions of PUA and a screening on starting materials.

2.4.1. Synthesis of PUA

In order to optimize the polymerization conditions and to design a polyurethane-acrylate system through a safe and robust process, at the beginning the attention was focused on the selection of adequate starting materials and catalysts; after that, an efficient method to synthesized a PUA was effectively developed.

The discussion will enclose the three synthetic step necessary to produce PUAs:

- Synthesis of PU prepolymer with terminal -NCO groups
- Synthesis of UAO
- UV-curing to produce PUA

- **Synthesis of PU prepolymer with terminal -NCO groups**

In order to design a polymeric material with reduced or any toxicity issue, it is important to settle a list of considerations on the monomers used. Therefore, in this study, the general orientation was to

prefer cycloaliphatic rather than aromatic diisocyanates, because the latter are involved in the formation and the release of carcinogenic substances in degradation processes. In this way, an excess of isophorone diisocyanate (IPDI, **2**) was placed to react with polyethylene glycol (PEG 400, **1**), producing the PU prepolymer with isocyanate end groups, **3**. At this point, it is important to note that PEG 400 is known for its antifungal properties, a relevant fact in antimicrobial applications. Furthermore, in order to avoid toxicity issues, tin-based catalyst was replaced with a non-toxic Lewis acid, in particular indium (III) chloride (0.1% by weight). The reaction was carried out at 70°C for 15 minutes with a **2**:**1** ratio equal to 1.5:1 (*Scheme 19*).

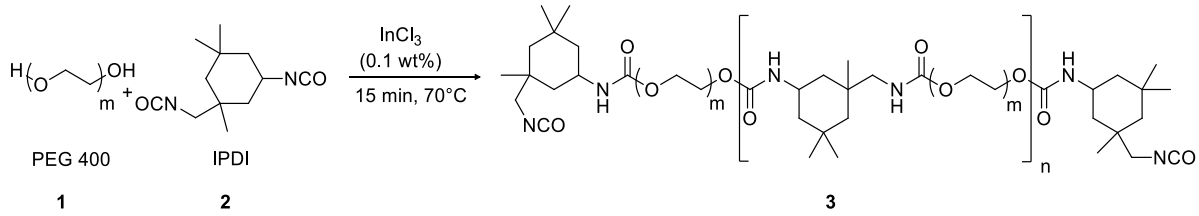

Scheme 19 – Synthesis of PU pre-polymer **3** with -NCO terminal groups.

Chemical characterization

The progress of the reaction was checked through FTIR analysis (Fourier Transform Infrared Spectroscopy). The spectrum of compound **3**, shown in Figure 19, presents the characteristic peaks of the isocyanate (-NCO stretching) and carbonyl moieties (-C=O stretching) of the urethane bond at 2254 cm^{-1} and 1715 cm^{-1}, respectively.

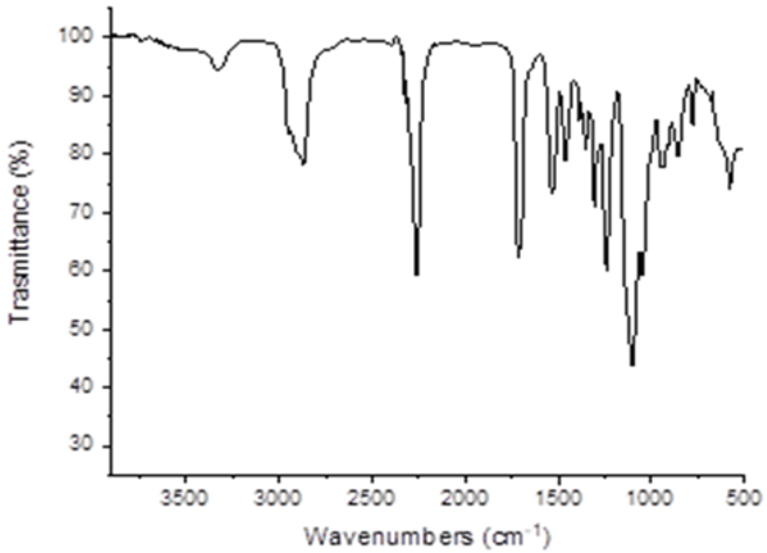

Figure 19 – FTIR spectrum of pre-polymer **3**.

^{1}H-NMR (*Figure 20*) and ^{13}C-NMR (*Figure 21*) were also performed for a complete chemical characterization. From the ^{13}C-NMR spectrum, peaks at 155.81 ppm and 122.00 ppm relative to the carbonyl group of the urethane bond and the primary -NCO group, respectively, are observed. Considering the lower reactivity of primary rather than secondary isocyanates, end-chain groups should be mainly constituted by primary -NCO groups, as confirmed by the NMR analysis.

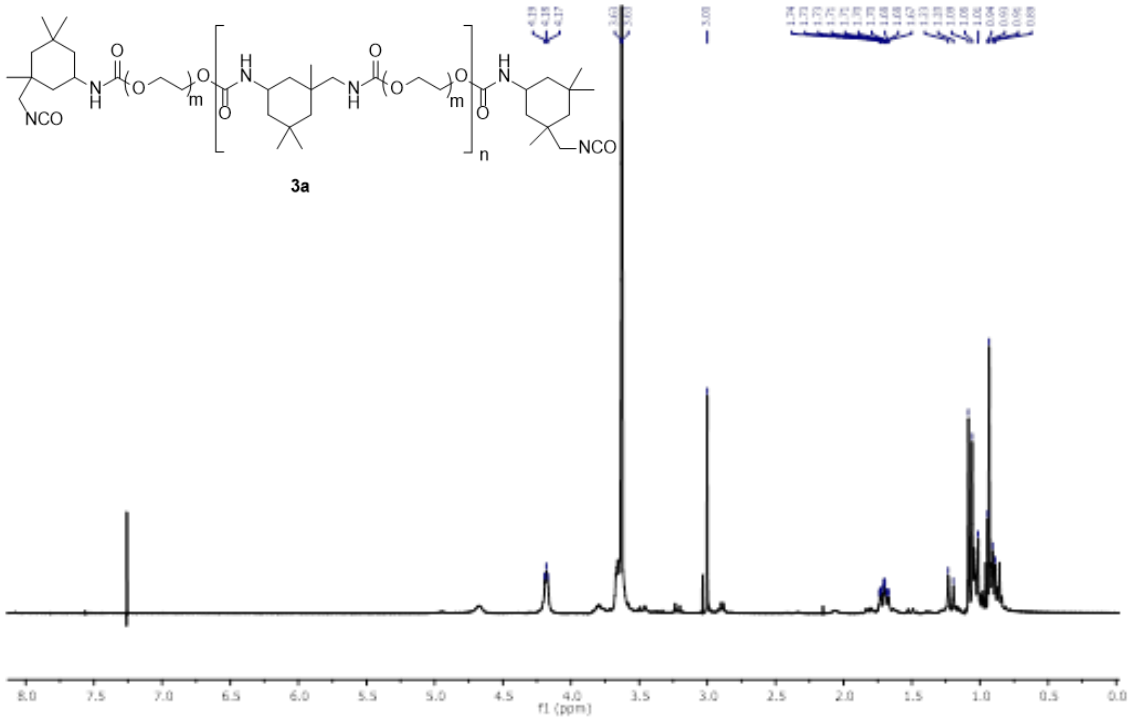

Figure 20 – ^{1}H-NMR spectrum of pre-polymer **3**.

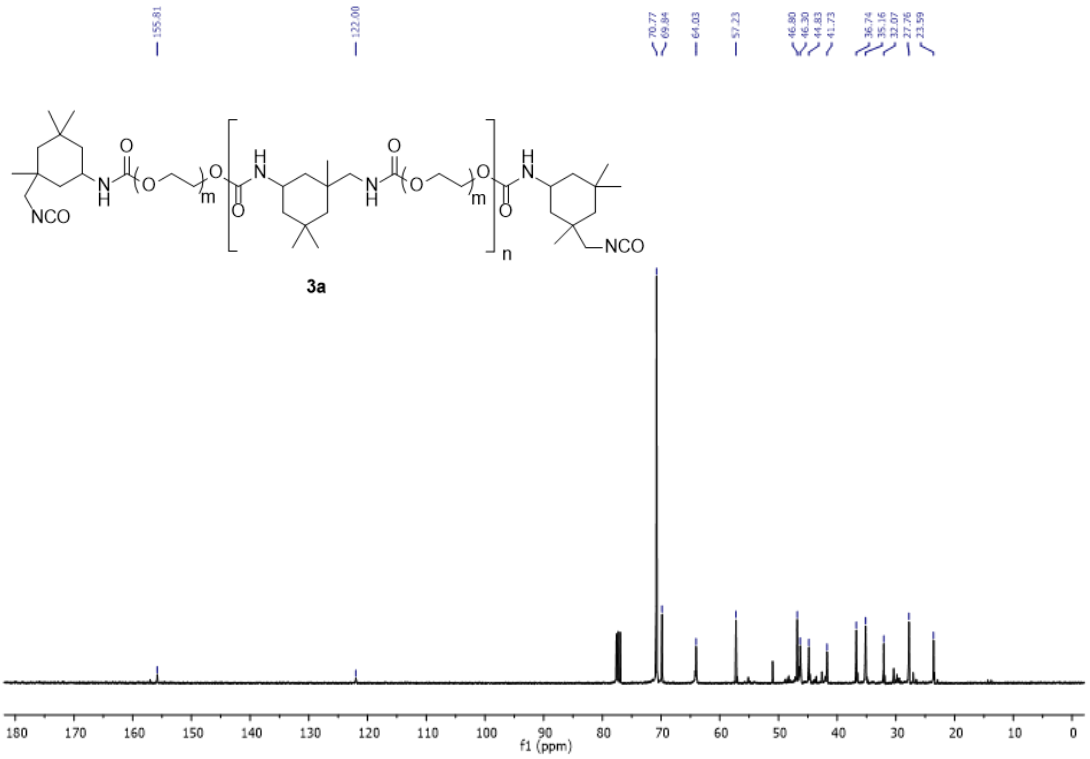

Figure 21 – ^{13}C-NMR spectrum of pre-polymer **3**.

Finally, the GPC analysis was used to check the conversion rate and the molecular weight of the formed PU pre-polymer. From this analysis, it was determined a conversion percentage of 97% and a weight average molecular weight for the synthesized prepolymer of 1,800 Da, as schematized in *Table 1*. The latter was determined by considering the ratio between the areas of peaks relative to the diisocyanate (*Figure 22*, peak b) and the prepolymer (*Figure 22*, peak a).

Table 1 – Results of GPC analysis on pre-polymer **3**.

Compound	M_n (g/mol)	M_w (g/mol)	Conv. (%)
3	1,200	1,800	97

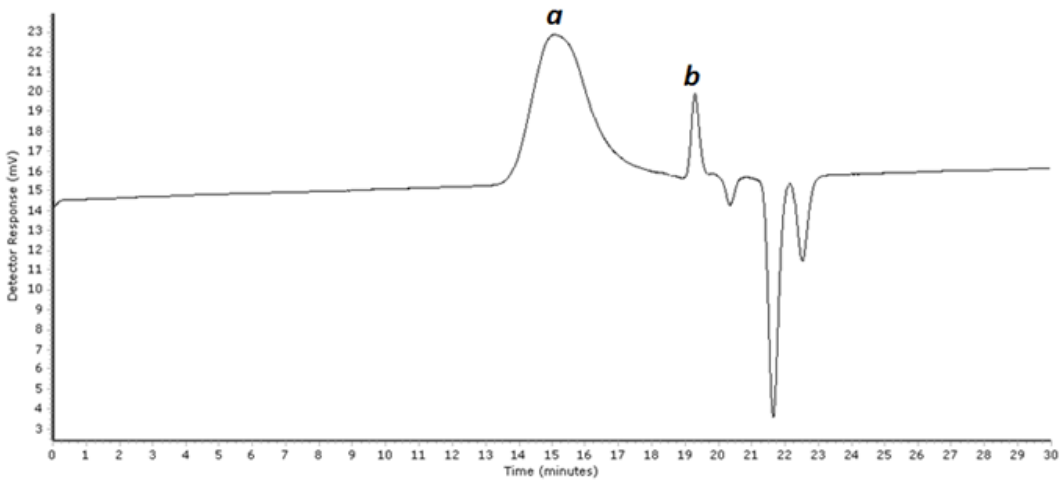

Figure 22 – GPC chromatogram of the reaction crude. Peak a = compound **3**; peak b = compound **2**.

In particular, we observed that the molecular weight plays a key role in the formation of compound **3a**. When the value is above 2,000 Da, the terminal -NCO groups are less available for further reaction with 2-hydroxyethyl methacrylate and the formation of the urethane acrylate oligomer was more difficult.

- **Synthesis of Urethane Acrylate Oligomer (UAO)**

In the second step, the prepolymer **3** was treated with 2-hydroxyethyl methacrylate (HEMA, **4**) to obtain the urethane acrylate oligomer **5**. The reaction was carried out at 50° C for 4 hours, as shown in Scheme 20. HEMA was preferred than the corresponding acrylate (2-hydroxyethyl acrylate (HEA)) due to numerous health risks the latter poses.

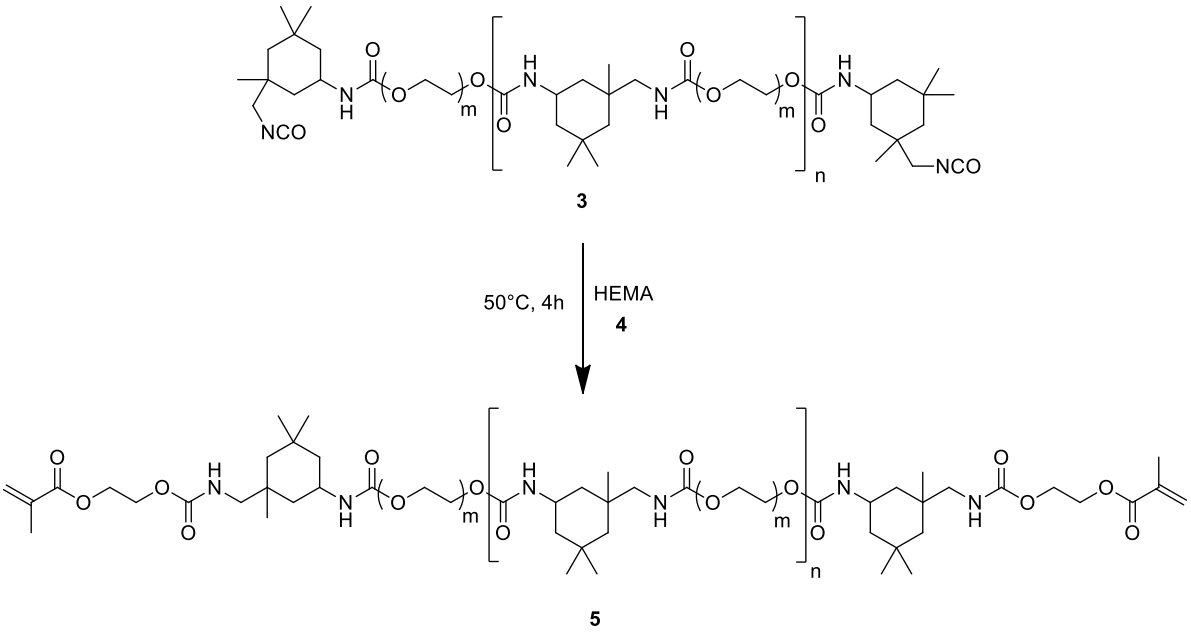

Scheme 20 – Synthesis of UAO **5**.

Chemical characterization

The reaction was monitored through FT-IR analysis until the complete disappearance of the peak at 2254 cm^{-1} relative to the isocyanate group and the increase in intensity of signals at 1643 cm^{-1} (-C=C- stretching) and 814 cm^{-1} (for -C=C- bending), characteristic of the carbon-carbon double bond (*Figure 23*).

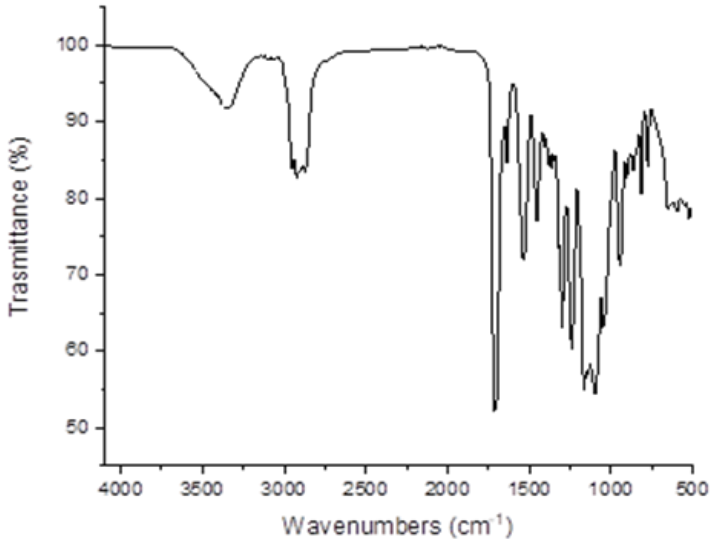

Figure 23 – FTIR spectrum of UAO **5**.

Even in this case, the GPC analysis was used in the determination of both the molecular weight of products (Mw = 1,900 Da) and the conversion percentage (84%, calculated from the ratio between

the peaks area of oligomer (*Figure 24*, peak a) and HEMA (*Figure 24*, peak b)). The result of GPC analysis is listed in *Table 2*.

Table 2 – Results of GPC analysis of UAO **5**.

Compound	M_n (g/mol)	M_w (g/mol)	Conv. (%)
5	1,400	1,900	84

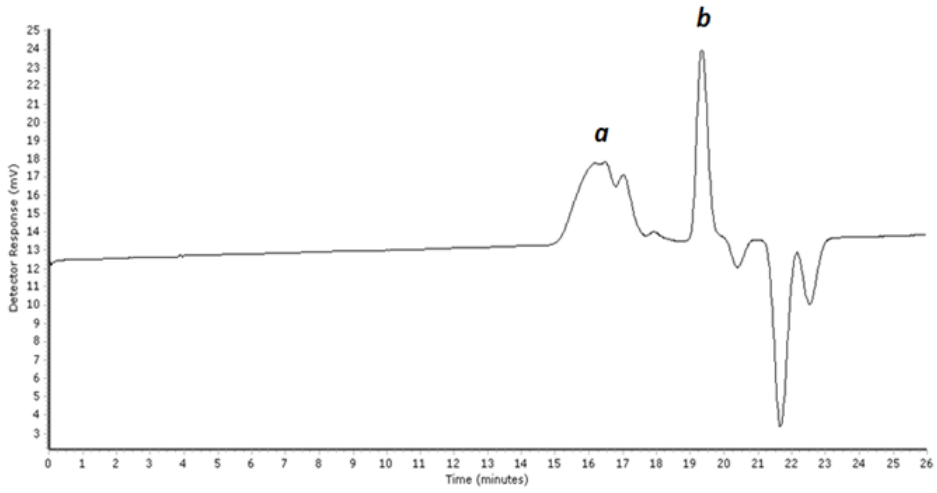

Figure 24 – GPC chromatogram of the reaction crude. Peak a = compound **5**; peak b = compound **4**.

From ^{1}H-NMR, the characteristic peaks of vinyl protons at 5.55 ppm and 6.21 ppm are observed, confirming the formation of the urethane acrylate oligomer (*Figure 25*).

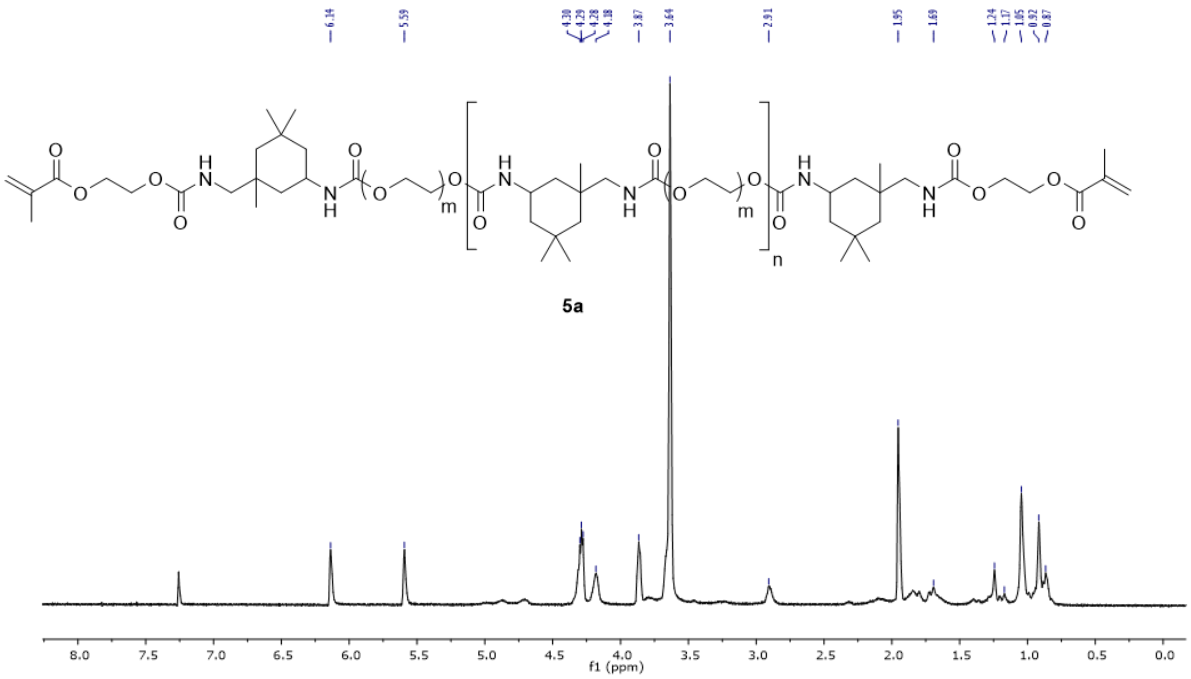

Figure 25 – ^{1}H-NMR spectrum of UAO **5**.

- **UV-curing to produce PUA**

The last stage was the UV-curing of compound **5** in the presence of a photoinitiator (benzophenone, **6**) and a co-initiator (methyldiethanolamine, **7**), forming the PUA 8 (*Scheme 21*). The polymerization through UV-curing technology was chosen because it has attracted a conspicuous attention as environmentally friendly and suitable polymerization technique, especially for coatings applications.

After the complete dissolution of the photo-initiator and co-initiator, the UAO solution was poured into a mould, and the residual solvent was evaporated in the oven overnight at 37° C. The radical polymerization was performed under a UV lamp for 15 minutes, obtaining the polymeric film (compound **8**), shown in *Figure 26*.

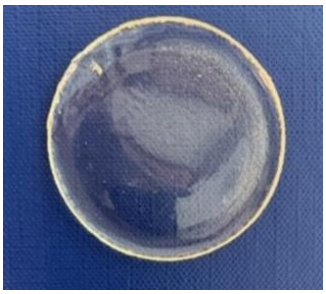

Figure 26 – Film of PUA **8**.

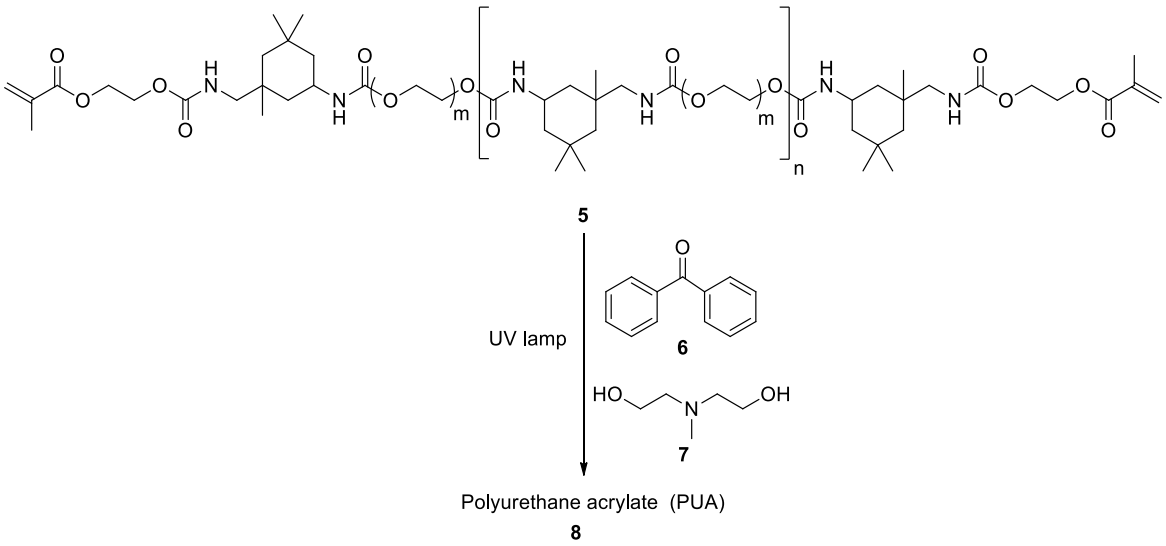

Scheme 21 – Synthesis of PUA **8**.

Chemical characterization

The polymeric film was characterized by FTIR and TGA analyses. From FTIR analysis (*Figure 27*), it was observed a decrease of signals related to the double bonds by increasing the exposure time under the UV lamp. This behaviour indicates that carbon-carbon doublw bonds are effectively reacting during the UV-curing, forming cross-linking reactions during the curing polymerization.

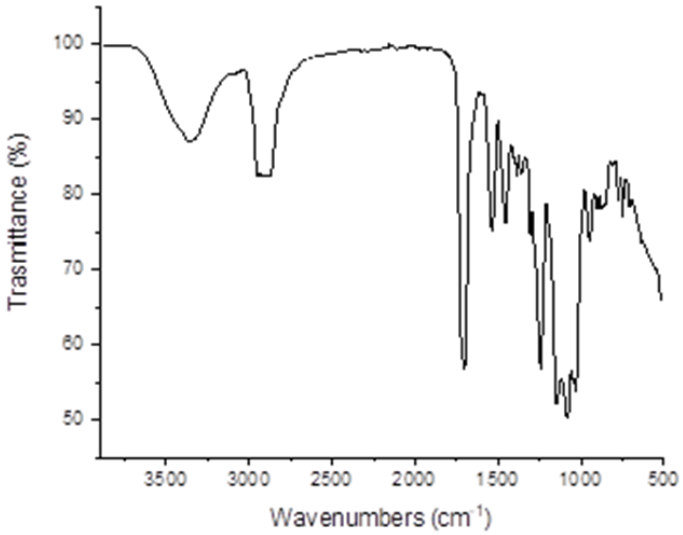

Figure 27 – FTIR spectrum of PUA **8**.

The TGA analysis (*Figure 28*) shows two weight losses. The first occurs in the temperature range between 300°C and 350°C and is caused by the thermal degradation of the hard segments. On the other hand, the second decomposition step between 400°C and 450°C is attributable to the degradation of the soft component present in the polymer.[76] It should be noted that, besides the

presence of urethane, ester or ether groups, in polyurethanes there are present also other chemical bonds, like allophanate and urea groups, deriving from reactions involving the isocyanate component. The thermal decomposition temperature of the latter groups lies in the range of 144°C – 260°C. The thermal stability of the groups present in PUs is in the order:

ester, ether >> urethane >> allophanate, urea.

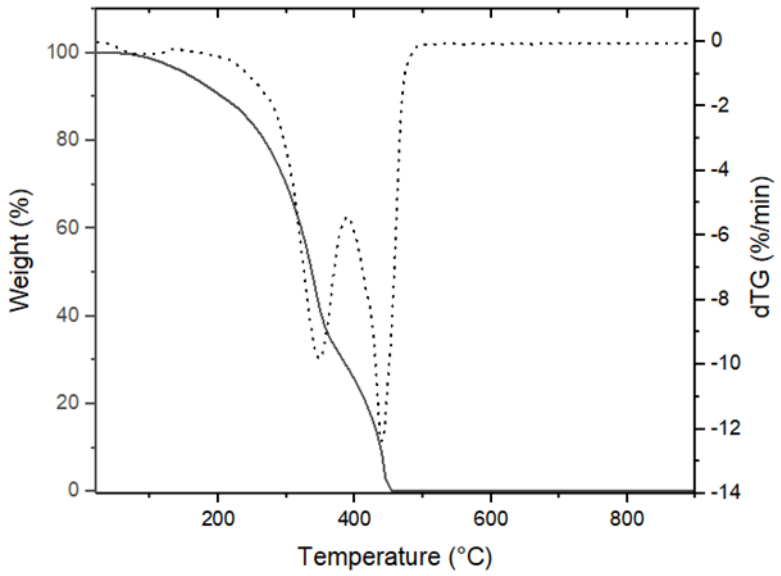

Figure 28 – TGA thermogram of PUA **8**.

2.4.2. Synthesis and incorporation of QAS in PUA materials

After the optimization of the PUA polymerization, the attention moved to the synthesis of disinfectant compounds, in particular quaternary ammonium salts, and to the possible ways to incorporate them in PU and PUA materials. In order to check the antimicrobial activity of synthesized QASs, it was measured the Minimal Inhibitory Concentration (MIC) toward a number of bacteria.

Several functionalization strategies with different target molecules were the object of the study. Basically, these strategies could be divided according to the parent amine: 3-amino-1,2-propanediol (Isoserinol) and pent-4-en-1-amine. Isoserinol is a bio-derived compound suitable in PU, polyesters and other polymer applications, since the presence of the diol. Concerning pent-4-en-1-amine, it could be a synthetic valuable compound in C=C polymerizations, or it could be further functionalized.

- **Functionalization strategies starting from Isoserinol**

Two approaches were studied to ensure a functionalized PU or PUA, covalently bonded with a QAS derived from isoserinol **9**. These approaches are shown in *Scheme 22*.

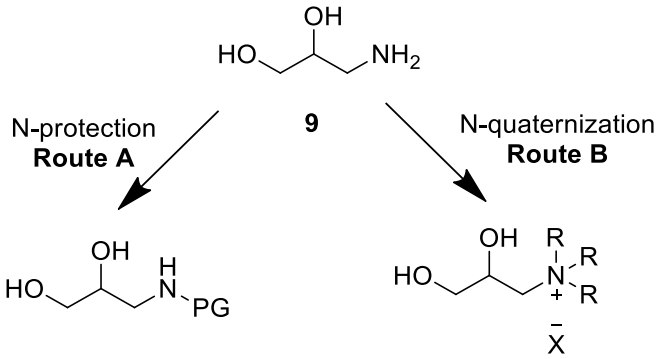

Scheme 22 – Tested approaches for the incorporation of QAS in polymers, starting from isoserinol **9**.

Following *Route A*, it was firstly performed the protection of the amine group, then the diol was incorporated in a PU system and, after the deprotection, it was performed a step-wise quaternization to QAS. In *Route B*, it was firstly performed the quaternization and the obtain QAS, having the diol moiety, was incorporated in a PUA material.

Route A

In the first study, the synthesis of the quaternary ammonium salt was performed after the bonding of the isoserinol **9** to the polymer chain. For this purpose, it was necessary to protect the amine function of the diol: hence, the first step of functionalization was the protection of the starting material with *tert*-butoxycarbonyl (Boc) group (*Scheme 23*).

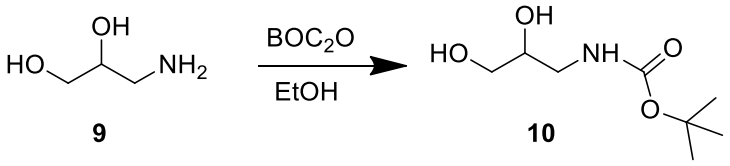

Scheme 23 – Protection of isoserinol **9** to compound **10**.

After the protection of the amine function, many attempts have been made in order to effectively bind the N-protected diol in polyurethane systems. Among them, it was studied the reaction of compound **10** with the PU pre-polymer **3**, aiming to obtain the functionalized oligomer **11** (*Scheme 24*).

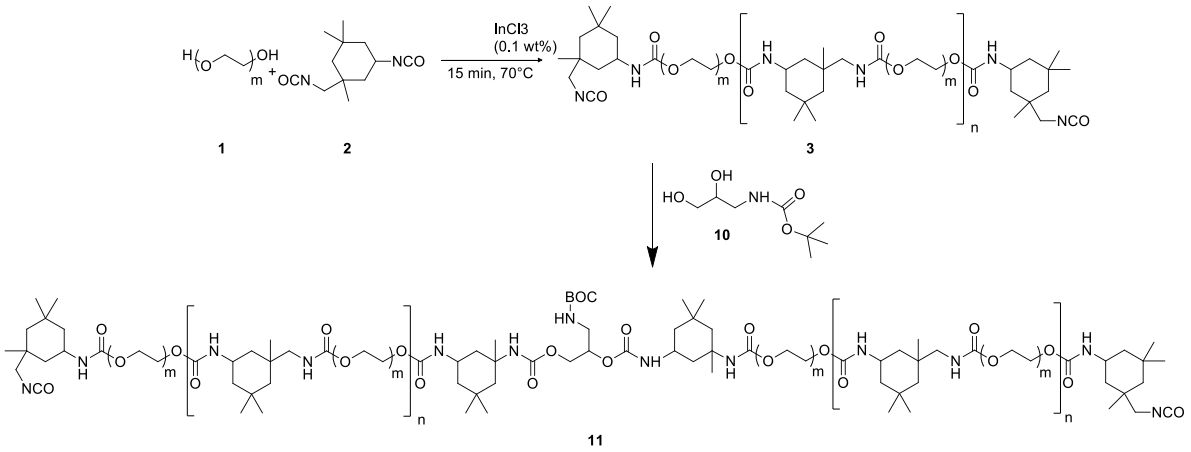

Scheme 24 – Synthesis of functionalized oligomer **11**, having N-Boc functionality.

To check the reaction, ^{1}H-NMR analysis of the reaction crude was performed (*Figure 29*). Anyhow, from the spectrum, it is possible to assess only the signals of the pre-polymer compound (**3**), while signals attributable to compounds **10** or **11** were not detected.

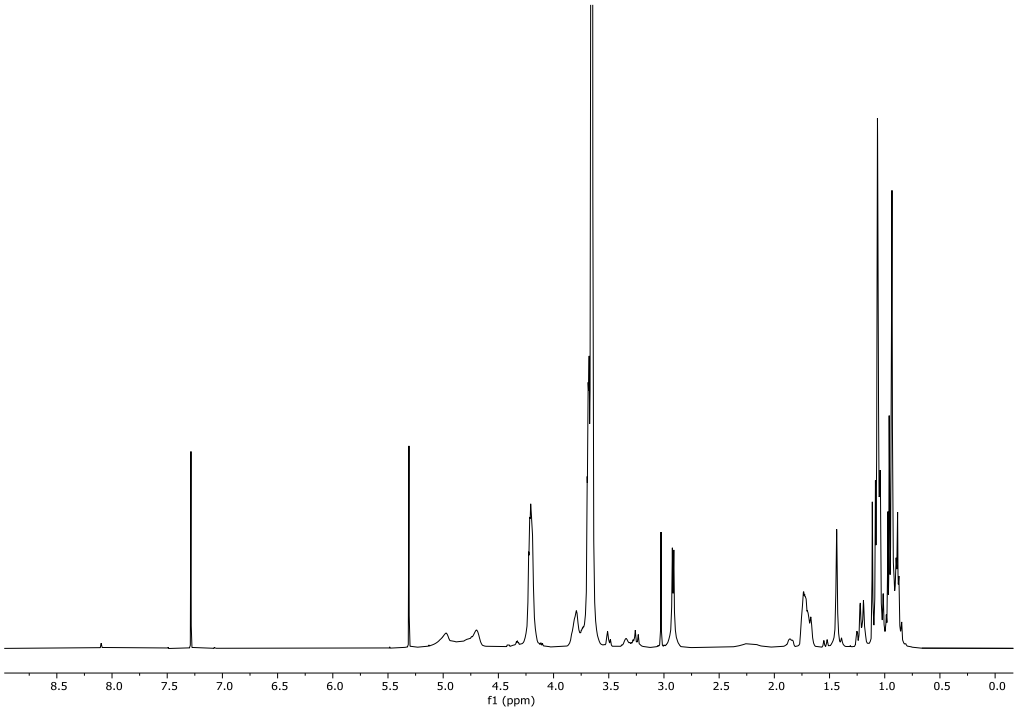

Figure 29 – ^{1}H-NMR of reaction crude, for the synthesis of compound **11**.

For this reason, the functionalization strategy was changed and the alternative way is schematized in *Scheme 25*. Basically, compound **10** can be used as a diol for the synthesis of PU having a side chain with N-protected functions. Hence, after the deprotection and quaternization, a QAS-functionalized polyurethane can be achieved.

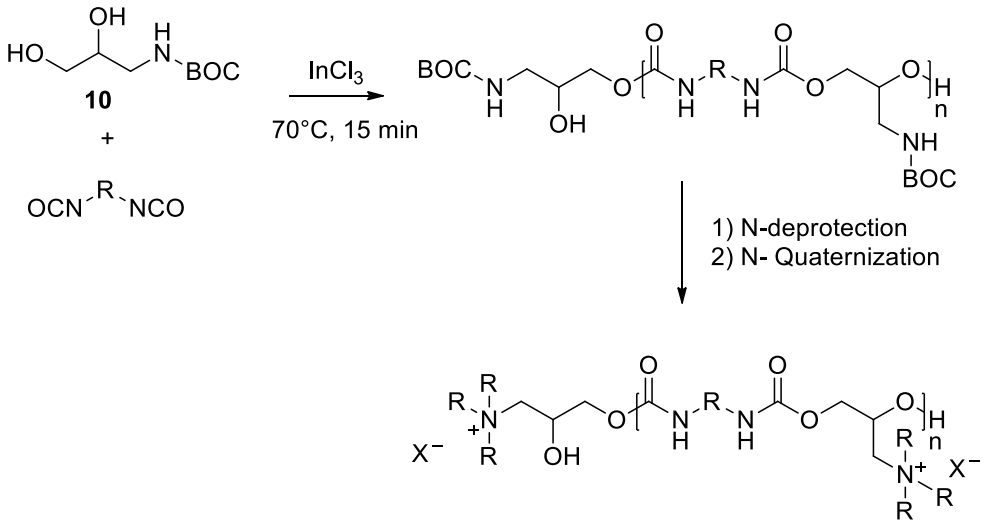

Scheme 25 – Alternative way to introduce compound **10** in PU material and the successive deprotection and quaternization to QAS.

To check this strategy, it was firstly studied the reaction of IPDI **2** or MDI **12** with the N-protected isoserinol **10**. The reaction was carried out at 70°C for 15 minutes using $InCl_3$ as catalyst, as shown in *Scheme 26*.

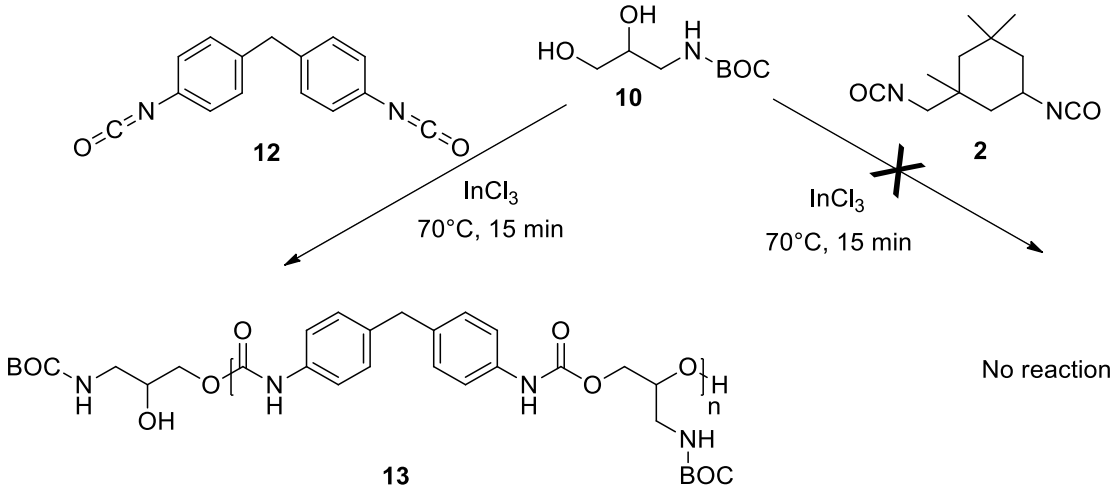

Scheme 26 – Reaction of compound **10** with IPDI **2** and MDI **12**.

From this step, it was clear that more reactive diisocyanates are more prone to react with compound **10**. Instead, using IPDI **2**, the reaction product was not observed and this result can be attributed to the lower reactivity of aliphatic rather than aromatic diisocyanates.

Chemical characterization

In *Figure 30*, it is reported the IR spectrum of the compound **13**. The reaction was considered concluded when the characteristic isocyanate peak at 2254 cm^{-1} disappeared.

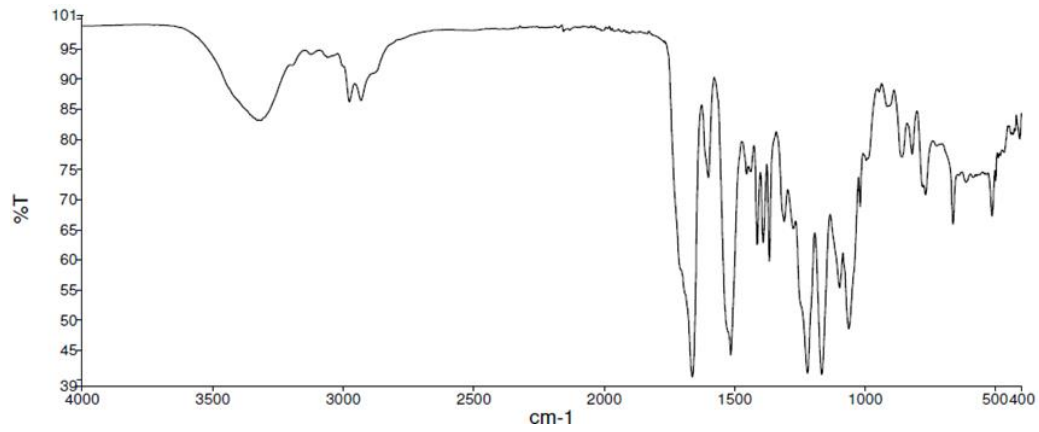

Figure 30 – FTIR spectrum of compound **13**.

The structure of compound **13** was confirmed also by ^{1}H-NMR, as shown in *Figure 31*.

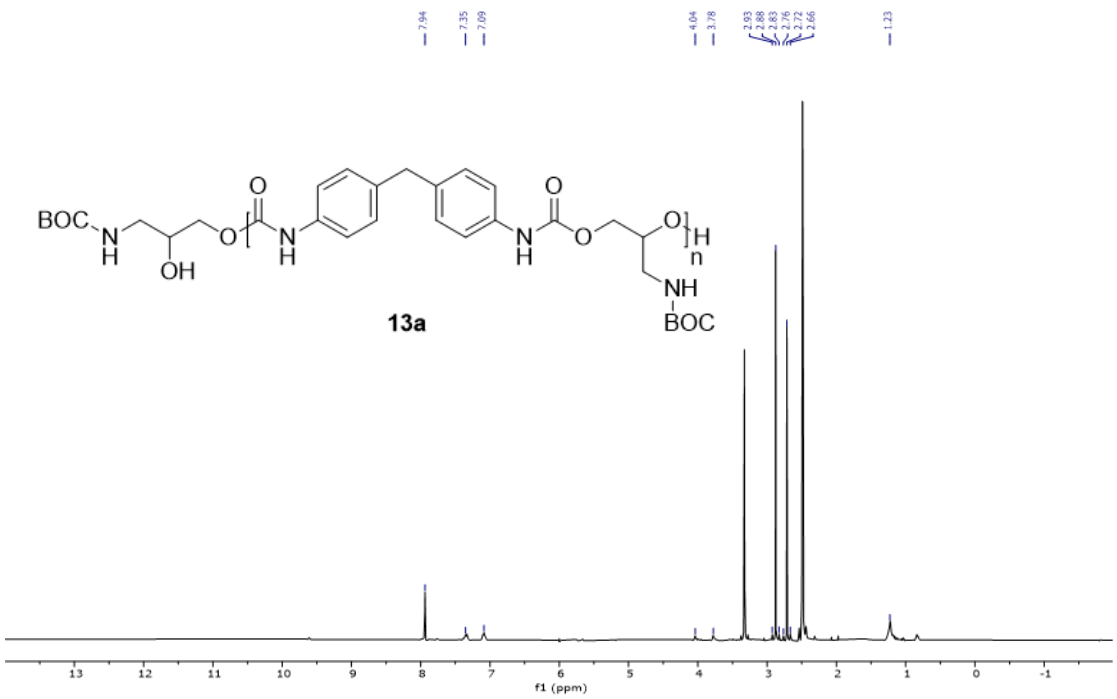

Figure 31 – ^{1}H-NMR spectrum of compound **13**.

The successive step was the deprotection of the amine group by the use of trifluoroacetic acid (TFA) at room temperature for one hour (*Scheme 27*).

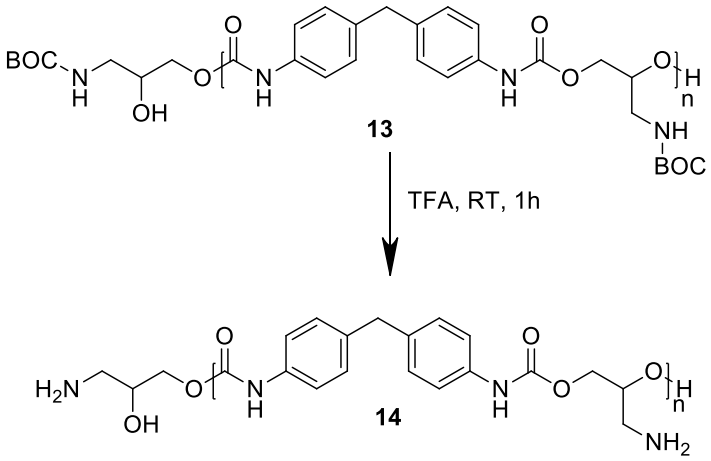

Scheme 27 – Deprotection of compound **13** to compound **14**.

Chemical characterization

The formation of compound **14** was confirmed by ^{1}H-NMR (*Figure 32*), where the peak at 1.3 ppm, characteristic of the methyl protons of the tert-butyl group, is no longer observed.

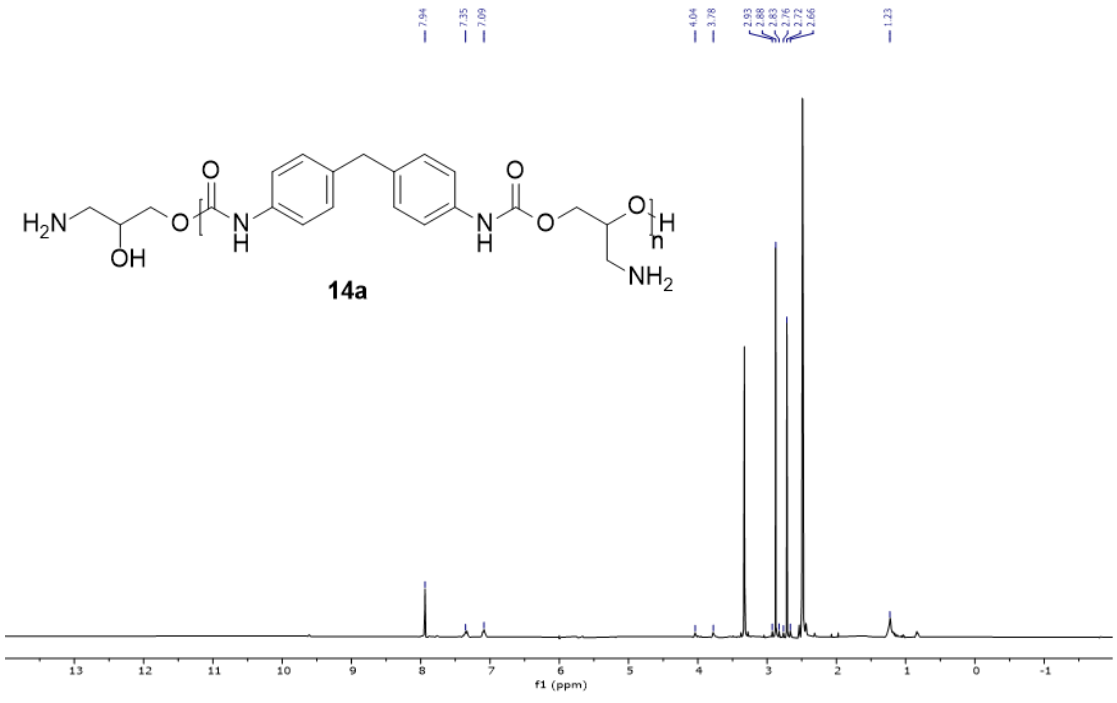

Figure 32 – FTIR spectrum of compound **14**.

Finally, the formation of the quaternary ammonium salt on the prepolymer was carried out by the stepwise reaction with a long alkyl halide (1-bromodecane (**15**) at 95°C overnight and, then, iodomethane (**16**) at 30°C overnight (*Scheme 28*).

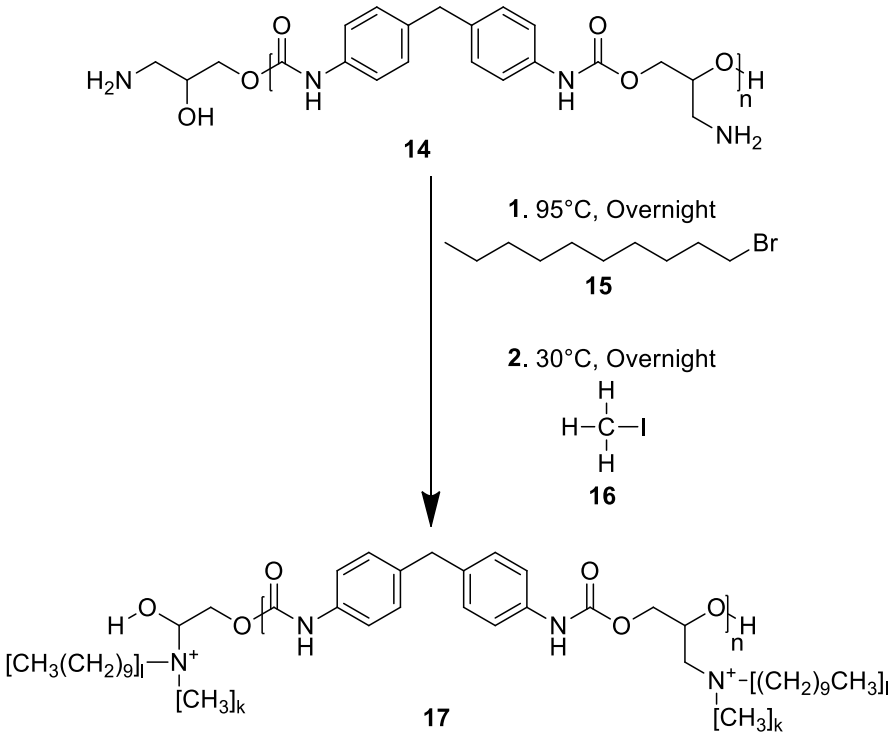

Scheme 28 – Stepwise quaternization of compound **14** to compound **17**.

Chemical characterization

Compound **17** was characterized through ^{1}H-NMR (*Figure 33*) and ^{13}C-NMR (*Figure 34*). However, it was not possible to determine the effective quaternization of the amine functions and a certain degree of uncertainty on the number of aliphatic chains bonded on the N atom is present.

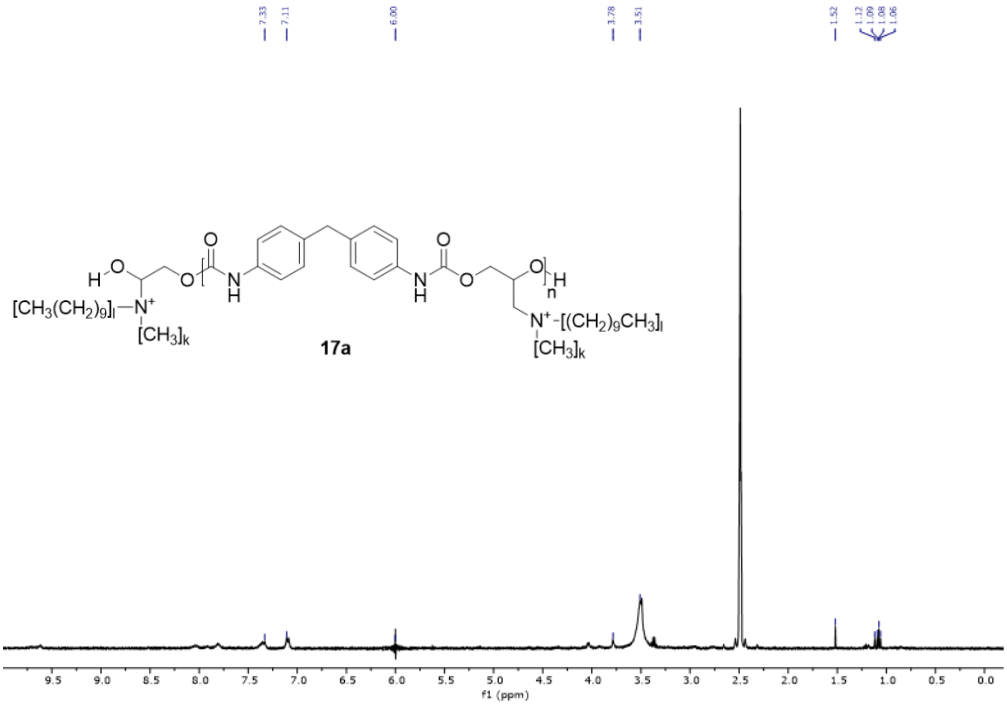

Figure 33 – ^{1}H-NMR spectrum of compound **17**.

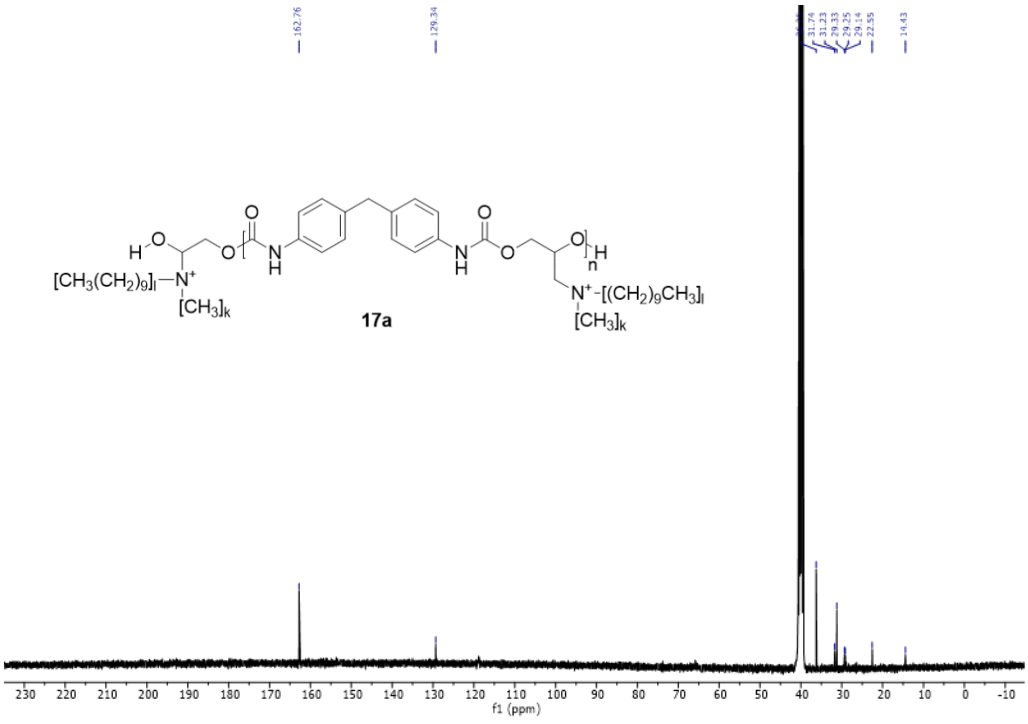

Figure 34 – ^{13}C-NMR spectrum of compound **17**.

Route B

The most important problem related with *Route A* was the impossibility to determine the effective quaternization of the PU pre-polymer. Aiming to overcome this problem, a further procedure was

studied to develop a PUA with antibacterial activity. The quaternary ammonium salt was first synthesized and then used as a building block in the preparation of the final polymer matrix, as depicted in *Scheme 29*.

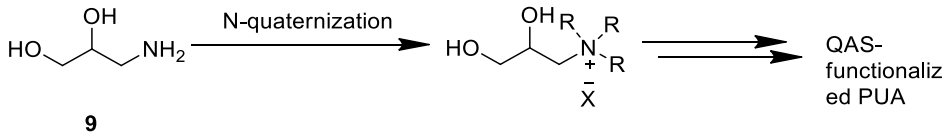

Scheme 29 – Synthetic approach in Route B.

This synthetic route involves the reaction of the 3-aminopropan-1,2-diol (**9**) with an excess of 1-bromodecane **15** (5 eq.) at 90 °C overnight to obtain compound **18**, which was subsequently reacted with an excess (3 eq.) of iodomethane **16** at 30 °C overnight to obtain the quaternary ammonium salt (**19**, *Scheme 30*), a white/pale yellow solid (*Figure 35*).

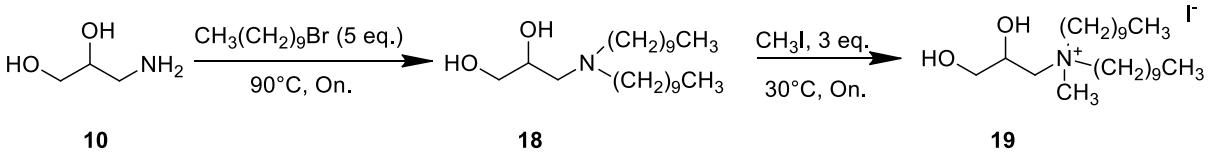

Scheme 30 – Stepwise quaternization of compound **9** to compound **19**.

Figure 35 – Synthesized QAS **19**.

Chemical characterization

Compound **19a** was characterized by FT-IR analysis (*Figure 36*), where peaks around 3300 cm^{-1}, 2950 cm^{-1} and 2850 cm^{-1}, characteristic of the stretching of -OH, $-CH_3$ and $-CH_2$ groups, respectively, were observed.

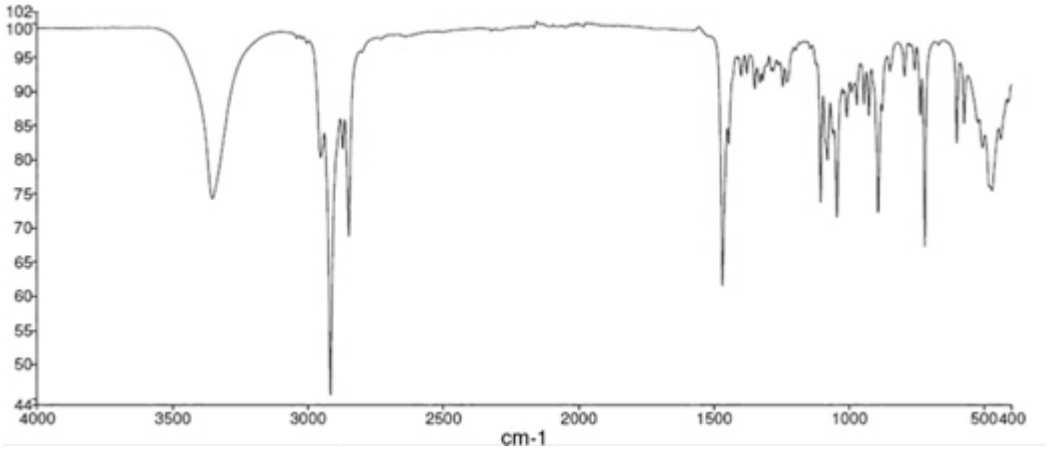

Figure 36 – FTIR spectrum of compound **19**.

The formation of compound **19** was also confirmed by the ^{1}H-NMR and ^{13}C-NMR analysis (*Figures 37* and *38*).

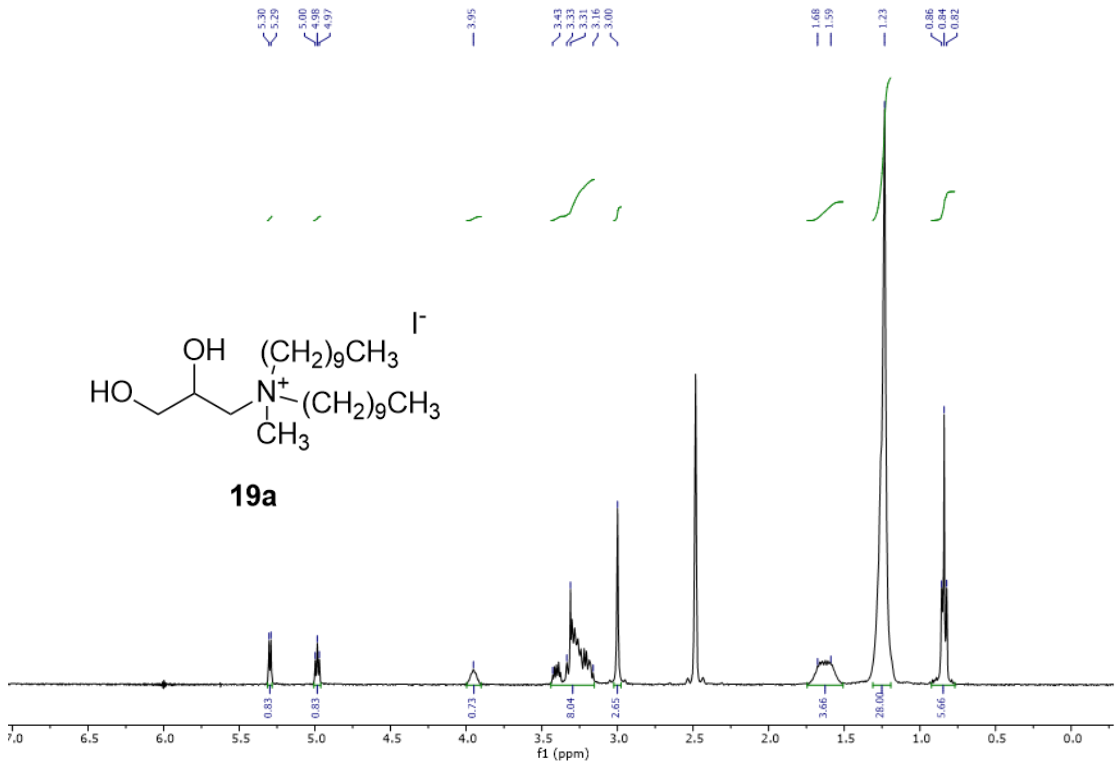

Figure 37 – ^{1}H-NMR spectrum of compound **19**.

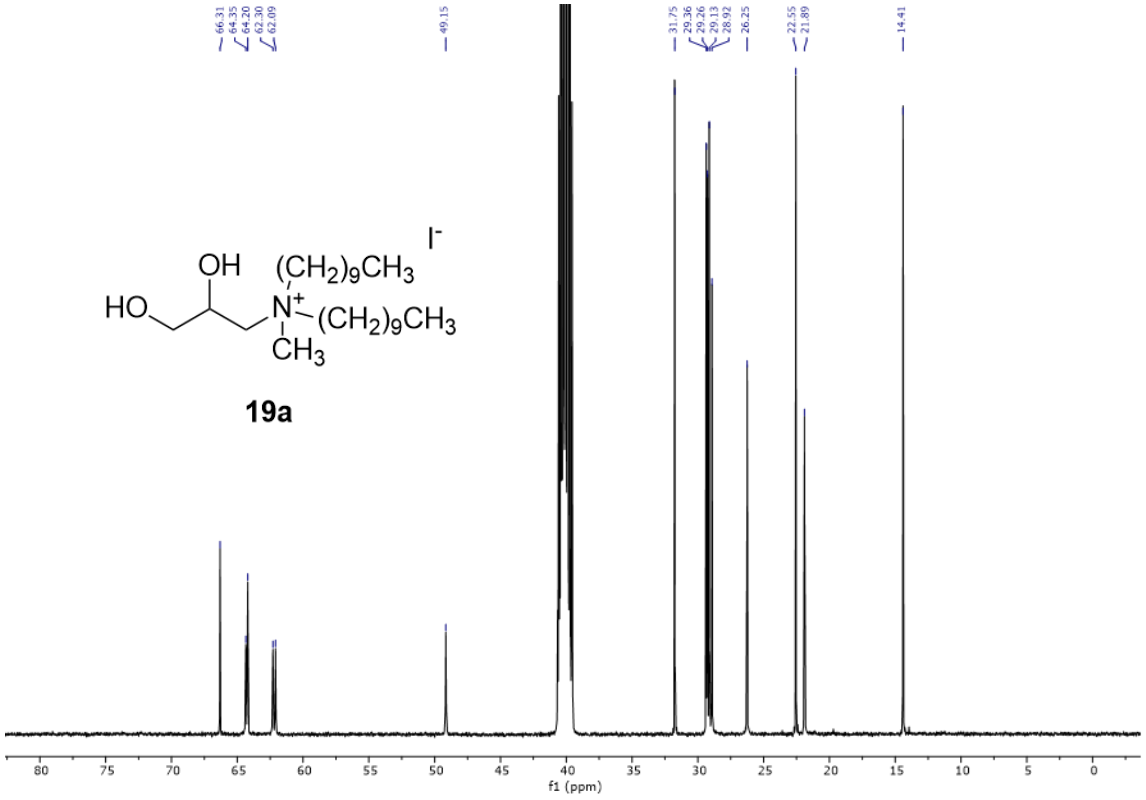

Figure 38 – ^{13}C-NMR spectrum of compound **19**.

After that, the ammonium salt was added to PEG 400 **1** in a small amount, followed by the addition of an excess of IPDI **2**. Subsequently, the obtained prepolymer was placed to react with HEMA **4**, and the synthesized UAO was subjected to the UV-curing process with the formation of QAS-functionalized PUA **21**. The entire process is schematized in *Scheme 31*.

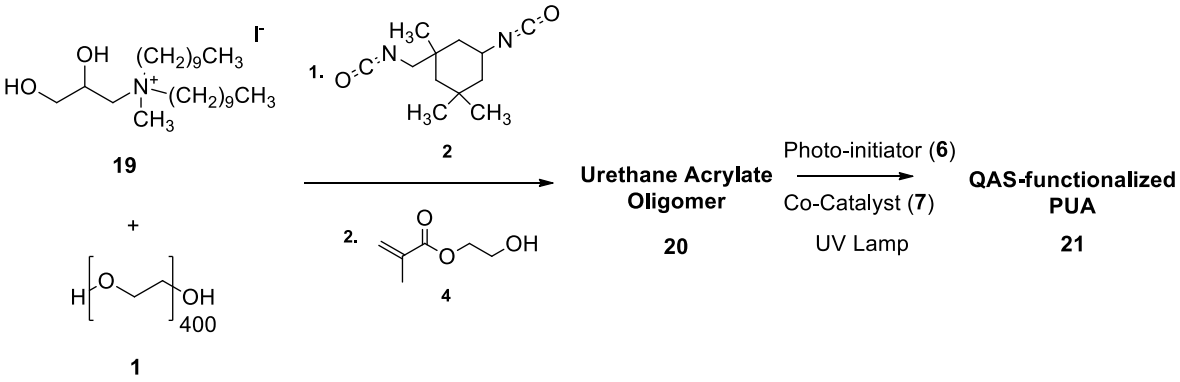

Scheme 31 – Stepwise quaternization of QAS-functionalized PUA **21**.

Chemical characterization

In *Figure 39*, it is shown the PUA film (on the left) and the QAS-functionalized PUA (on the right). It is quite evident the formation of opaque region in the functionalized film. Commonly, this

macroscopic outcome is linked with the formation of crystalline and semi-crystalline regions in the polymer system, that can be explained by the increased number of hard segments and by the presence of ionic species.

Anyhow, from the FT-IR analysis of compound **21**, reported in *Figure 40*, it was not possible to detect the signals of QAS incorporated in the PUA material because it was used in small percentages, and the spectrum does not show significant variations respect to the one of non-functionalized PUA.

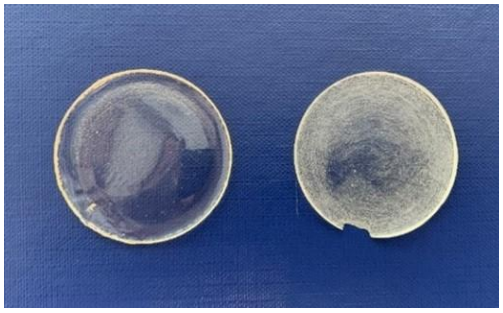

Figure 39 – PùUA film **8** (left) and QAS-functionalized PUA **21** (right).

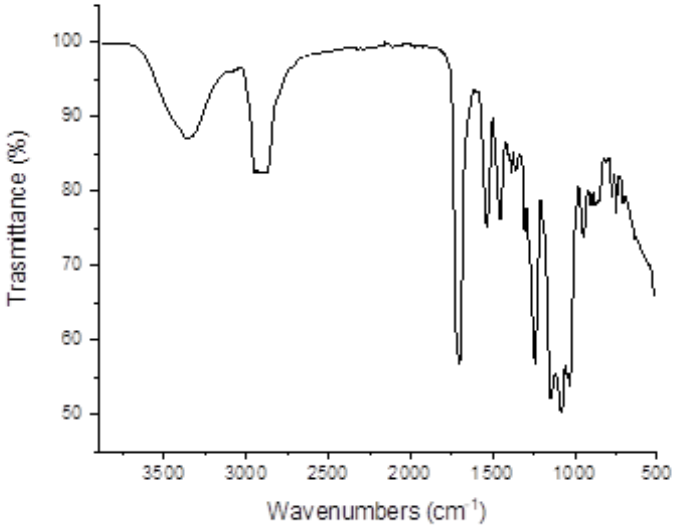

Figure 40 – FTIR spectrum of compound **21**.

Additionally, the TGA analysis (*Figure 41*) was used in order to check eventual differences respect to normal PUA. Also in this case, any significant differences were noted in thermal properties of PUA with and without QASs.

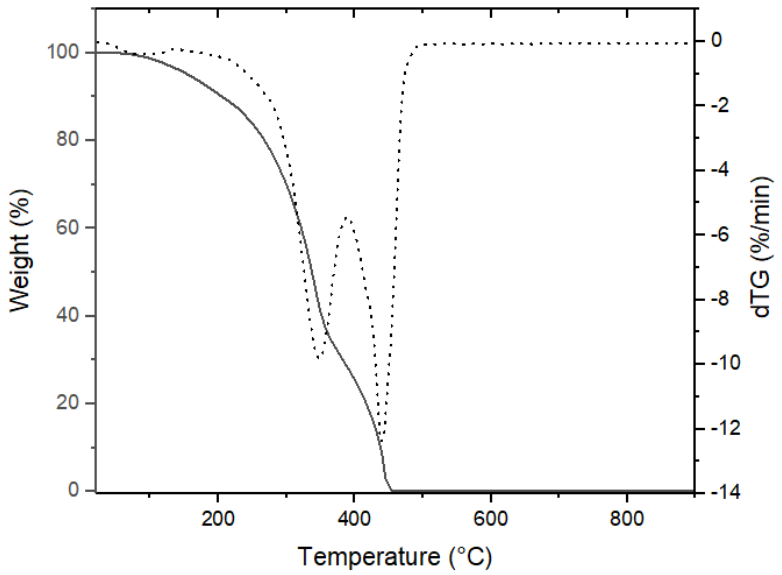

Figure 41 – TGA thermogram of compound **21**.

- **Functionalization strategies starting from pent-4-en-1-amine**

An alternative synthetic approach was based on the derivatization of 5-bromo-1-pentene (**22**) to pent-4-en-1-amine (**24**). After the quaternization, the final product (**26**) should be characterized by the presence of two aliphatic chains having ten carbon atoms, as in the case of compound **19** (*Scheme 32*).

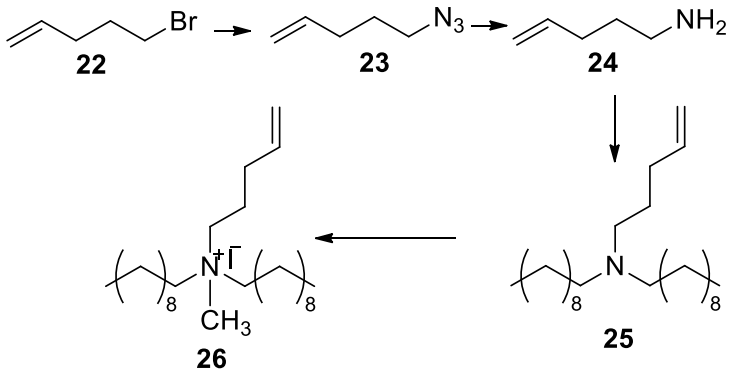

Scheme 32 – Synthetic approach to achieve compound **26** from **22**, via compound **24**.

The first step was the reaction of the starting material (**22**) with NaN_3 to give 5-azidopent-1-ene (**23**), as depicted in *Scheme 33*.

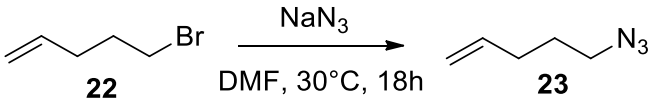

Scheme 33 – Synthesis of compound **23**.

The reaction was studied in different conditions, as schematized in *Table 3*. The optimized conditions (*Entry 2*; 60% yield) were obtained by performing the reaction found in a closed vial system at 30°C for 18 hours. Respect to the flask (*Entry 1*), the closed vial ensured a higher yield because the high volatility of the starting material; while lower yields have been obtained by longer reactions times (*Entries 3* and *4*), probably due to the formation of side product.

Table 3 – Optimization of reaction conditions for the synthesis of **23**.

Entry	System	Time (h)	Yield (%)
1	Flask	18	25
2	Closed vial	18	58
3	Closed vial	24	51
4	Closed vial	72	50

Chemical characterization

Signals from ^{1}H-NMR and ^{13}C-NMR spectra, reported in *Figure 42* and *Figure 43*, are consistent with the data reported in literature. In particular, the vinylic function was confirmed by the presence of signals at 5.80 and 5 ppm, related to vinyl hydrogens, and at 137 and 115 ppm, related to the two vinyl carbons.

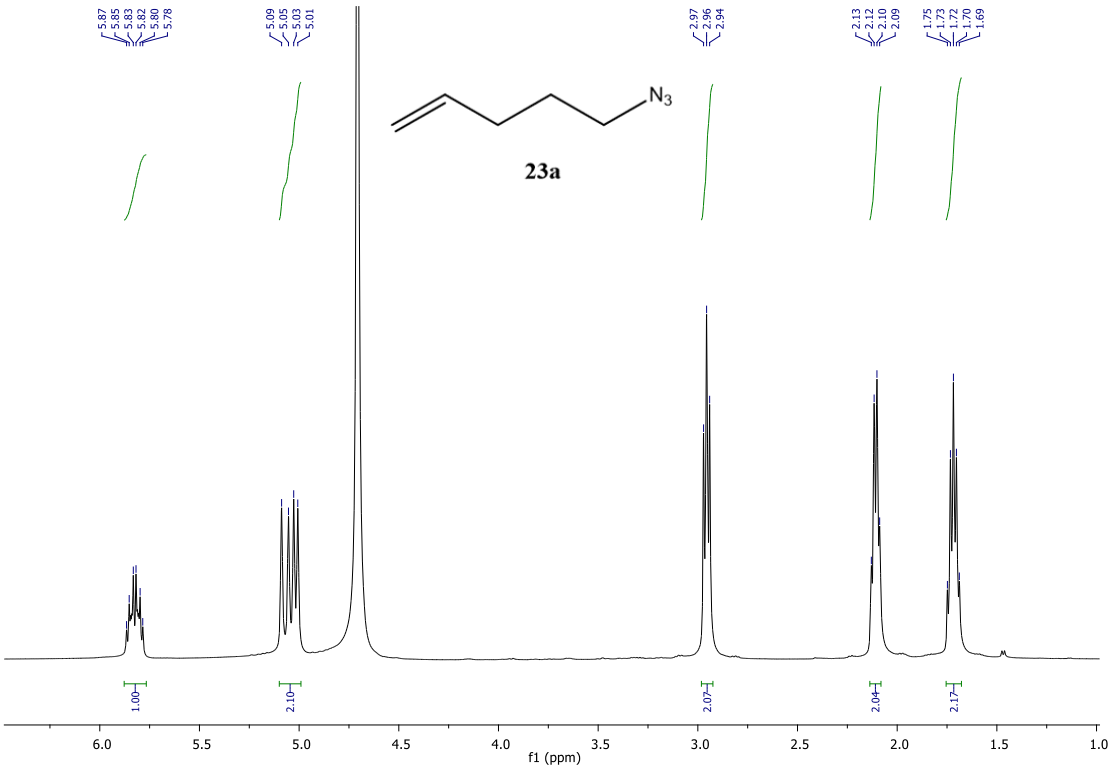

Figure 42 – ^{1}H-NMR spectrum of compound **23**.

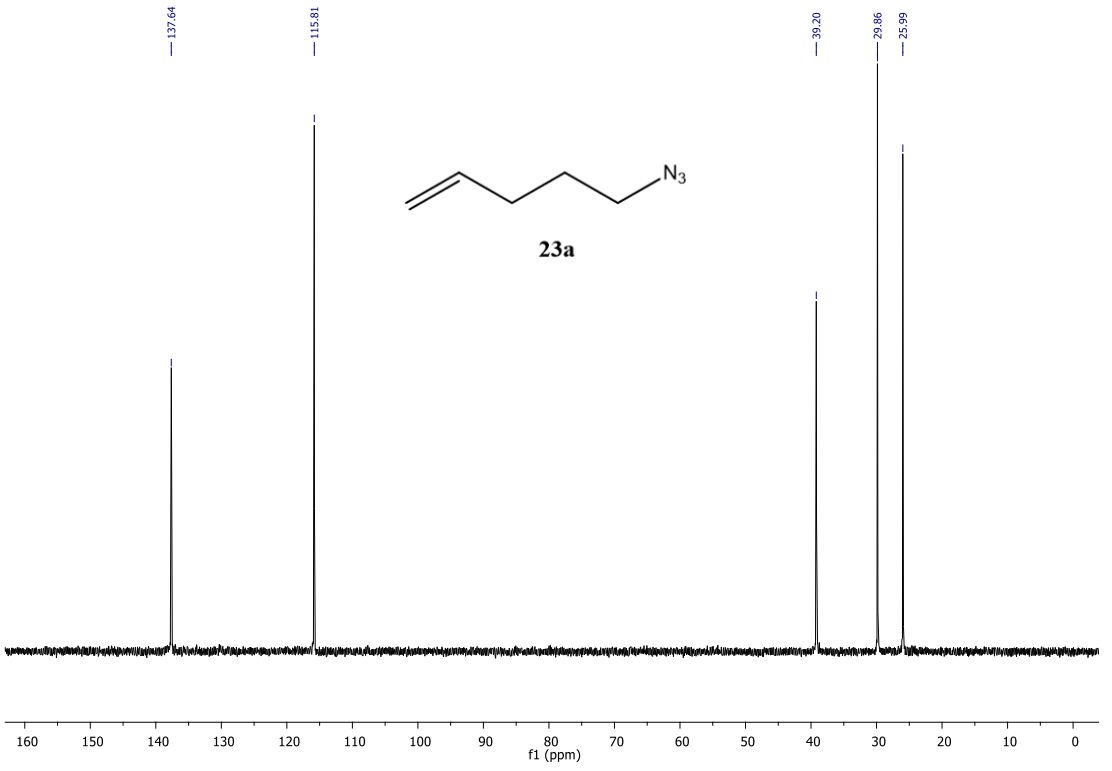

Figure 43 – ^{13}C-NMR spectrum of compound **23**.

The second reaction was the reduction of the azide function of compound **23** to amine. In this context, different strategies were studied. In a first moment, it was tried the reduction using a Ce-based catalytic system ($CeCl_3 \cdot H_2O$ (1,5 eq.) and NaI (9 eq.)), using acetonitrile as solvent (*Scheme 34*). Anyhow, from the chemical characterization, performed by FT-IR, ^{1}H-NMR and ^{13}C-NMR, the product **24** was not detected.

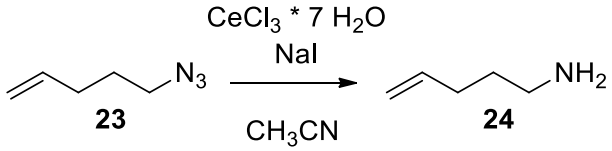

Scheme 34 – Synthesis of compound **24**.

Another reduction was performed in diethyl ether using triphenylphosphine (2 eq.), added carefully in portions, obtaining the corresponding ammonium chloride salt **27** (*Scheme 35*).

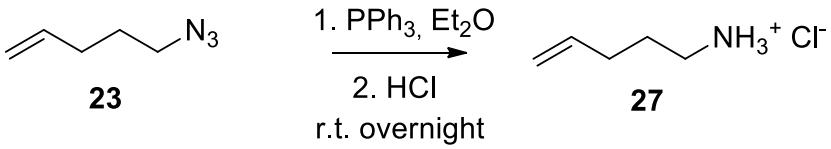

Scheme 35 – Synthesis of compound **27**.

Chemical characterization

Product **27** was characterized by FT-IR, ^{1}H-NMR and ^{13}C-NMR analysis. From the FT-IR spectrum (*Figure 44*), the peaks at 3000 cm^{-1} (N-H stretching), 1600 cm^{-1} (N-H bending), 1250–1020 cm^{-1} and 910-665 cm^{-1} (C-N stretching and N-H wagging, respectively) confirm the formation of the amine.

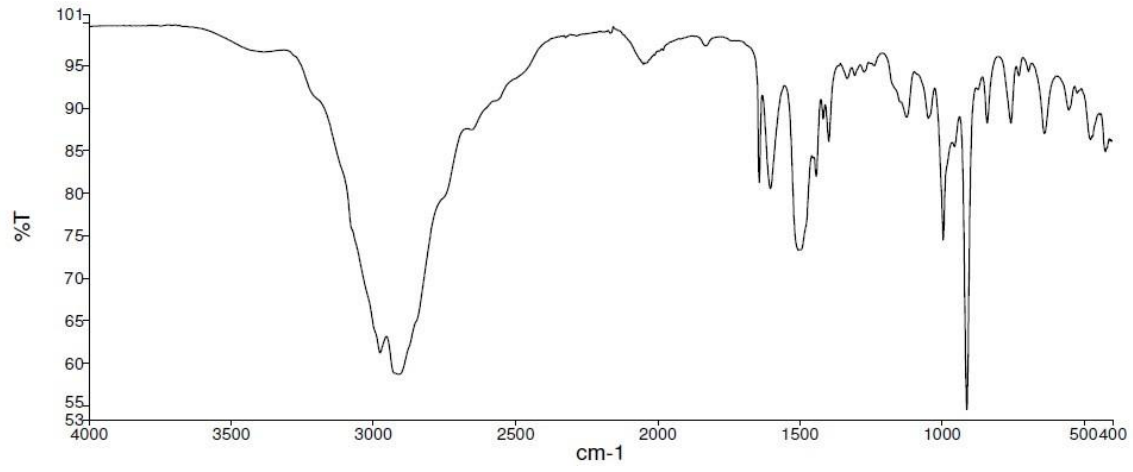

Figure 44 – FTIR spectrum of compound **27**.

Moreover, ^{1}H-NMR (*Figure 45*) and ^{13}C-NMR (*Figure 46*) analyses confirm the synthesis of compound **27**. In particular, from ^{1}H-NMR the signals at 5 and 5.8 ppm related to vinyl hydrogens are observed. The ^{13}C-NMR also confirm the presence of two vinyl carbons at 137 ppm and 115 ppm.

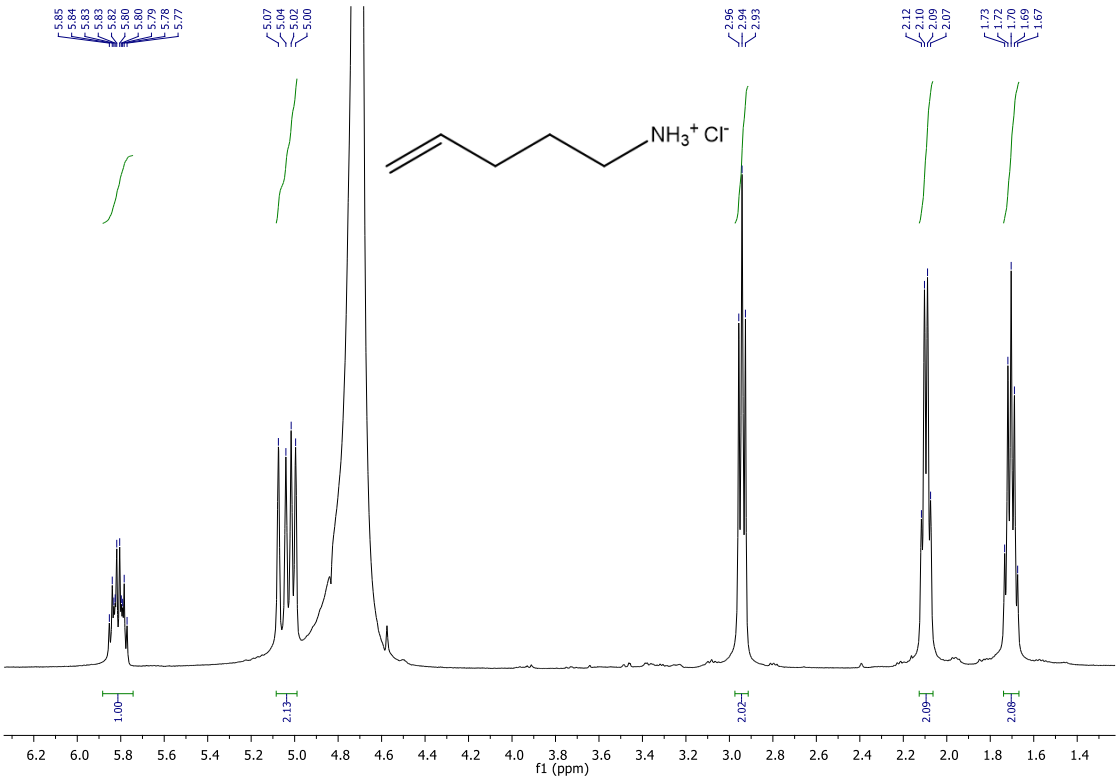

Figure 45 – ^{1}H-NMR spectrum of compound **27**.

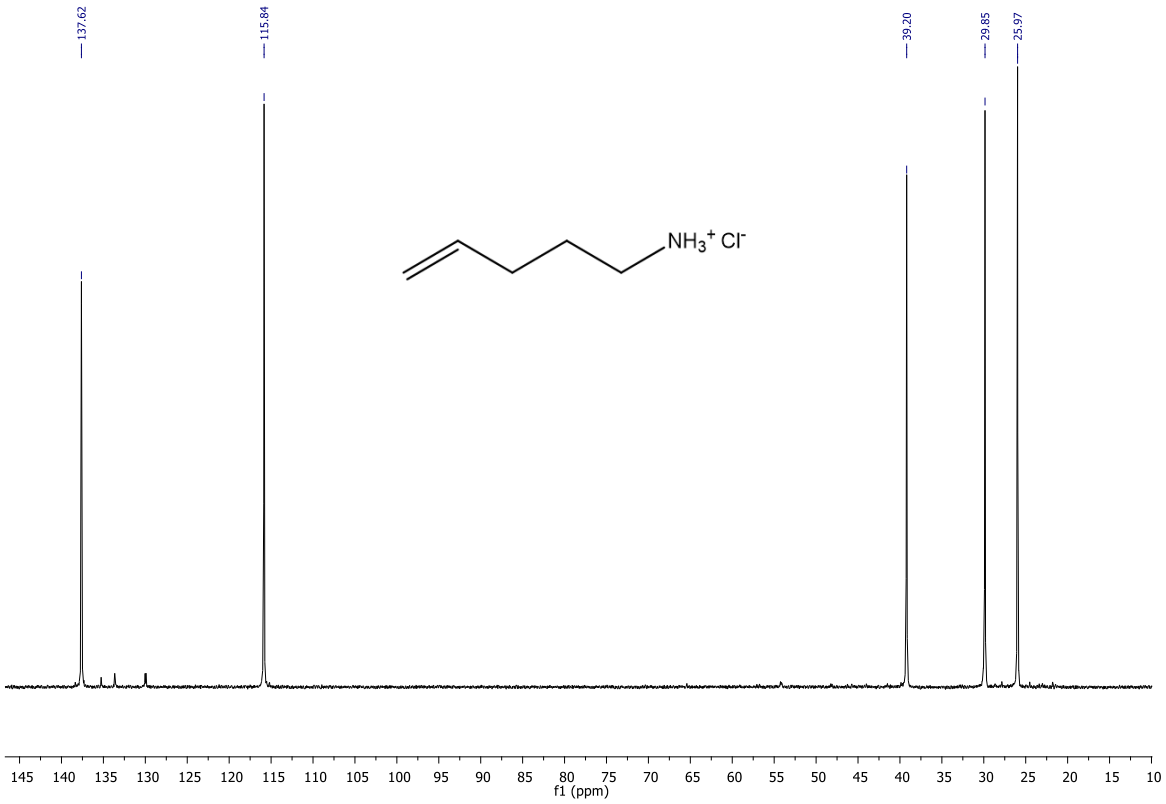

Figure 46 – ^{13}C-NMR spectrum of compound **27**.

At this point, it started the alkylation of the nitrogen atom of compound **27**. As shown in *Scheme 36*, after a base-treatment, it was firstly performed a dialkylation of the free amine group using a long-alkyl halide. The reaction was performed in an ethanolic solution heated at 90-95°C.

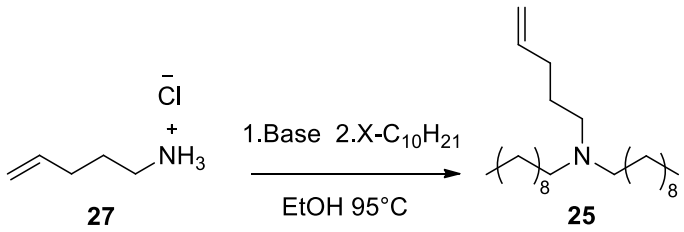

27 **25**

Scheme 36 – Synthesis of compound **25**.

The optimization of the reaction conditions is schematized in *Table 4*. The base Et_3N was added to the reaction mixture constituted by product **27** and the solvent and stirred overnight. The highest yield (45%, *Entry 4*) was obtained by keeping the reaction for 3 days, using 3 equivalents of Et_3N (3 eq.) and 1-iododecane **28**.

Table 4 – Optimization of reaction conditions for the synthesis of compound **25**.

Entry	Et_3N (eq.)	X (eq.)	Time (h)	Yield (%)
1	1,4	Br (3 eq.)	16	15
2	1,4	Br (5 eq.)	16	14
3	2	I (3 eq.)	16	16
4	3	I (3 eq.)	72	45

Chemical characterization

The reaction was characterized by ^{1}H-NMR (*Figure 47*) and ^{13}C-NMR analysis (*Figure 48*). In particular, the signals from 1.29 ppm to 1.34 ppm are related to aliphatic hydrogens in ^{1}H-NMR, while the peaks at 14 ppm, 22 ppm and 29 ppm are attributable to aliphatic carbons in ^{13}C-NMR. These results confirm the formation of product **25**.

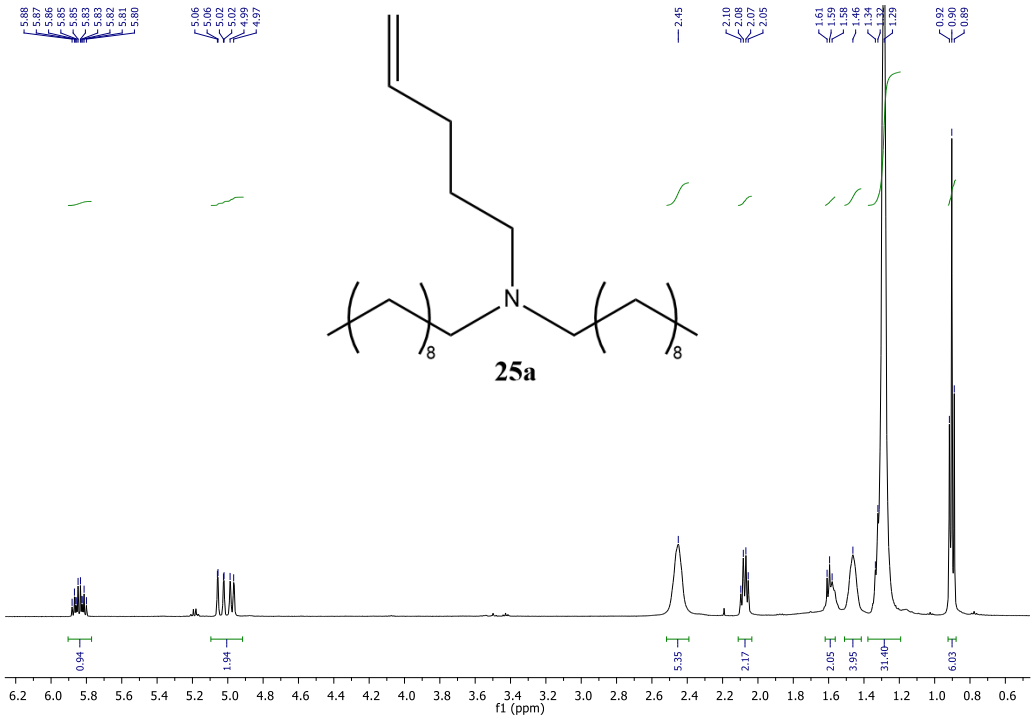

Figure 47 – ^{1}H-NMR spectrum of compound **25**.

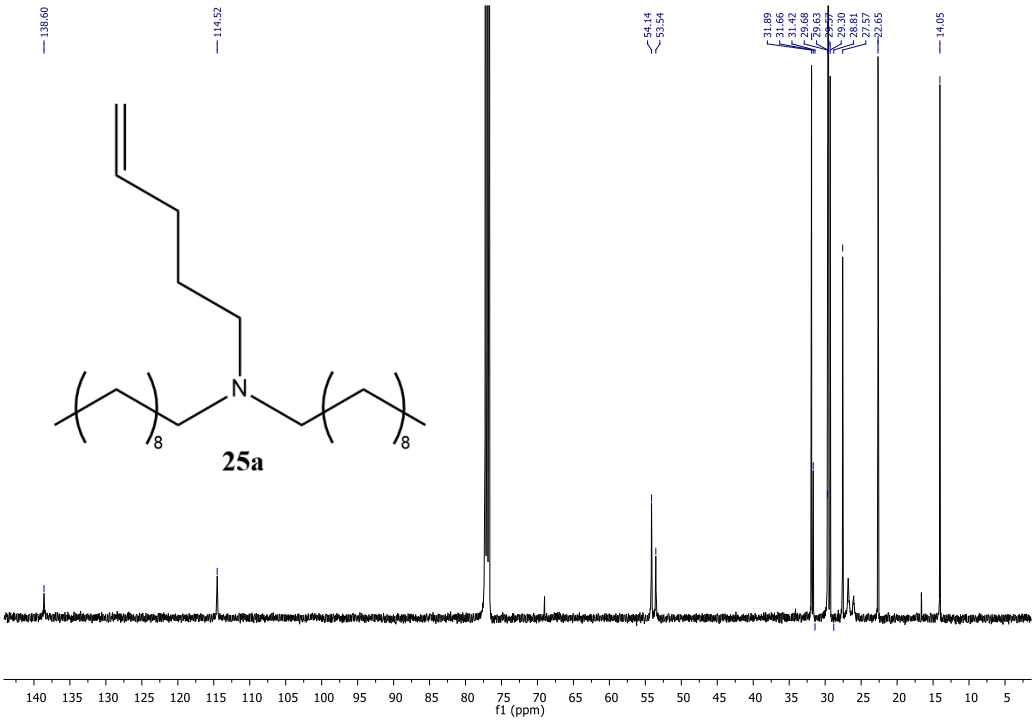

Figure 48 – ^{13}C-NMR spectrum of compound **25**.

The last step was the quaternarization of compound **25** with iodomethane **16** to the QAS, compound **26** (*Scheme 37*).

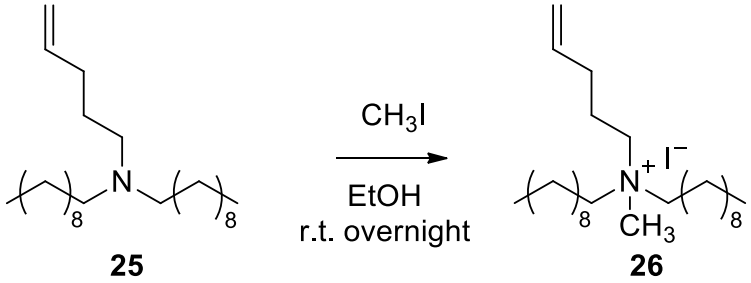

Scheme 37 – Synthesis of compound **26**.

The final product was characterized by ^{1}H-NMR and ^{13}C-NMR analyses which confirmed the presence of the product.

At this point, it is important to highlight that the double bond present in compound **26** gives the possibility to use this QAS in radical polymerization process. For example, this permits the synthesis of functionalized polyaddition polymers, such as PE, PP, PMMA and similar. Furthermore, the double bond can be further converted into a diol, making it suitable for the synthesis of PU, PUA or polyesters. A possible approach can be based on the formation of epoxide **29**, that in turn can be easily converted into the diol **30**, as resumed in *Scheme 38*.

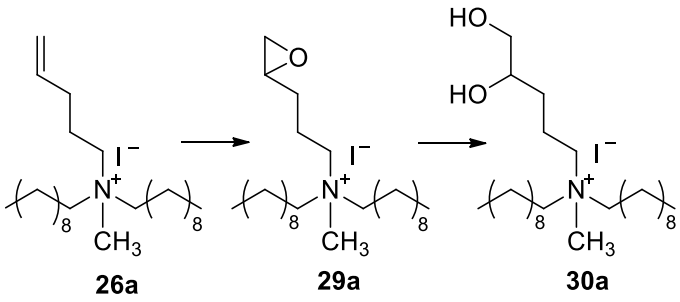

Scheme 38 – Possible synthesis of diol **30** from compound **26**.

The use of compound **26** for the functionalization of polymer materials is still in progress and further studies and experiments are required.

- **Antimicrobial activity of synthesized QASs**

The antimicrobial activity of the salt was checked by measuring the MIC. The Minimal inhibitory concentration (MIC) is the lowest concentration of an antimicrobial agent (such as antibiotics, antifungals, or antivirals) that inhibits the growth of a specific microorganism under specific conditions. MIC testing is commonly used in microbiology to determine the effectiveness of antimicrobial agents against bacteria, fungi, and other microorganisms. MIC testing is used in research and development of new antimicrobial drugs and agents.

This measure helps healthcare providers determine the most effective antimicrobial treatment for infections. Knowing the MIC of a specific drug and bacterium can guide medical professionals in choosing the most appropriate antimicrobial agent and its dosage.

Monitoring MIC values over time helps in detecting changes in the susceptibility of microorganisms to specific antimicrobial agents. This information is crucial for understanding the development of antibiotic resistance.

MIC testing involves exposing the microorganism to different concentrations of the antimicrobial agent and observing the growth. The lowest concentration at which there is no visible growth of the microorganism is considered the MIC. These values are interpreted based on established clinical breakpoints. Clinical breakpoints are concentrations set by organizations like the Clinical and Laboratory Standards Institute (CLSI) or the European Committee on Antimicrobial Susceptibility Testing (EUCAST). These breakpoints categorize bacteria as susceptible, intermediate, or resistant to a specific antimicrobial agent.

It is important to note that MIC values can vary based on the testing method, the growth conditions, and the specific strain of the microorganism being tested. Therefore, MIC results should be interpreted in the context of established guidelines and the specific testing conditions used.

The salt **19** showed a MIC in the rage of 0.24-0.48 mg/mL, a very high value compared to the MIC of chlorhexidine 0.48 mg/mL used as reference value.

The antimicrobial activity of the product **26** was tested, the ammonium salt showed a MIC of 15.6 mg/mL.

2.5. Experimental protocols

2.5.1. Materials and methods

All the reagents were of analytical grade and purchased from Merck. As first treatment, all solid reagents were dried at 50 °C under vacuum for 24 hours and in the case of reactions performed under nitrogen atmosphere, the glassware was oven dried at 100 °C for more than 2 hours prior to use.

Synthesis of poly(urethane acrylate) (PUA, 8)

In a 25 mL two-necked round bottom flask, 1 g of PEG 400 (2.5 mmol; 1 eq.; 380-420 g/mol,) was mixed with 0.83 g of IPDI (3.75 mmol; 1.5 eq.; 222.3 g/mol) and $InCl_3$ (0.1% wt). The system was heated at 70 °C for 15 minutes and, then, the formed oligomer **4** was cooled down to 50 °C. At this point, HEMA (50 wt%) was added dropwise to the reaction mixture, achieving the complete end-capping of **4** to UAO **5** after 4 hours at 50°C. Finally, the reaction was cooled down to room temperature and the product was isolated after solvent evaporation under vacuum. Afterwards, benzophenone (1.5 wt%) and methyl diethanolamine (1.5 wt%) were added to **5**. The reaction mixture was deposed in a small glass plate and it was exposed to the UV-lamp in order to obtain a film of polyurethane-acrylate.

Synthesis of N-decyl-N-(2,3-dihydroxypropyl)-N-methyldecan-1-amonium iodide (QAS, 19)

In a 25 mL two-necked round bottom flask, 0.1 g of 3-aminopropan-1,2-diol (1.1 mmol, 1 eq., 91.1 g/mol) was dissolved in an appropriate amount of solvent and, then, 5 eq. of 1-bromodecane (1.22 g; 5.5 mmol, 221.2 g/mol) were added. The reaction was heated at 90 °C and placed to react overnight. After that, the complete quaternization to QAS was ensured by reacting 3 eq. of iodomethane (0.468 g, 3.3 mmol, 141.9 g/mol), achieving so the white/pale yellow solid (compound **19**).

Synthesis of QAS-functionalized poly(urethane acrylate) (QAS-PUA, 21)

In a 25 mL two-necked round bottom flask, 1 g of PEG 400 (2.5 mmol, 1 eq., 380-420 g/mol) was firstly mixed with a small amount of compound **19**. Then, this mixture was placed to react with IPDI (0.83 g; 3.75 mmol; 1.5 eq.; 222.3 g/mol) and $InCl_3$ (0.1 wt%). The system was heated at 70 °C for 15 minutes and, after the cooling down to 50 °C, HEMA (50 wt%), achieving the end-capping to UAO **20** after 4 hours at 50°C. Finally, the reaction was cooled down to room temperature and benzophenone with methyl diethanolamine were added. The reaction mixture was deposed in a small glass plate and was exposed to the UV-lamp in order to obtain a film of poly(urethane acrylate) functionalized with QAS.

Synthesis of compound 23

Anhydrous DMF solution (1 mL) of sodium azide (2 eq.) and 5-bromo-1-pentene (1 eq.) were stirred under N_2 at 30 °C for 18 h. After that, water and n-pentane were added to the mixture. The organic layer was separated and washed twice with water, then it was filtered through a short pad of silica gel (3 cm) and using n-pentane. Due to the high volatility of 5-azido-pent-1-ene, the solution was carefully evaporated in vacuo (200 mbar/20 °C) to obtain a stock solution, containing ca. 4% of the product (based on NMR), which was further used in the successive steps. An aliquot was further evaporated in vacuo for the chemical analysis.

Synthesis of compound 24, I

The reaction was performed under microwave irradiation (100°C, 10 W, 20 minutes; at medium absorption). Subsequently separation was performed with HCl 4N and diethyl ether, after Na_2SO_4 was added to the organic phase and then it was filtered.

Synthesis of compound 24, II

The reduction was performed in diethyl ether using triphenylphosphine (2 eq.). The mixture was stirred at room temperature overnight. The reaction was quenched with HCl 2 M (1 eq.) in stirring for 1 hours, and then was added another eq. of HCl 2 M and stirred again for 15 minutes. The aqueous layer was washed three times with ethyl acetate and collected. Water was removed and the product was obtained after precipitation in $MeOH/Et_2O$ as white solid, the reaction was quantitative.

Synthesis of compound 25

The starting material was added in a round bottom flask with EtOH and a base. Solution was stirred for 30 min at room temperature, then an alkyl halide (X-$C_{10}H_{21}$) was added, and the temperature was increased at 95°C.

Synthesis of compound 26

Reaction was performed in a closed vial with EtOH as solvent. CH_3I (4 eq.) was added to the starting material and the solution was stirred overnight at room temperature. Reaction has quantitative yields.

Fourier transform infrared spectroscopy (FTIR-ATR)

FT-IR spectra were recorded with a Perkin-Elmer FT-IR Spectrum Two UATR spectrometer, equipped with ZnSe crystal. The measurements were performed in a range of 400-4000 cm^{-1} with a resolution of 2 cm^{-1}, 4 scans and the data were processed by the software Perkin-Elmer manager (Spectrum).

Thermogravimetric analysis (TGA)

TGA analysis was carried out using a Perkin-Elmer STA 6000, equipped with Al_2O_3 crucibles. About 15 mg of sample were analyzed in an inert atmosphere in a temperature range from 25 ºC to 900 ºC with a heating rate of 10 ºC/min.

NMR analysis

The ^{1}H-NMR and ^{13}C-NMR spectra were obtained using a Varian Mercury 400 (400 MHz or 100 MHz, respectively). Chemical shifts are reported in ppm. The deuterated solvents used were $CDCl_3$ (7.26 ppm for ^{1}H and 77.0 ppm for ^{13}C), DMSO-d6 (2.50 ppm for ^{1}H and 39.5 ppm for ^{13}C) and D2O (4.65 ppm for ^{1}H).

GPC analysis

GPC analysis was performed using an Agilent 1260 Infinity II Multi Detector Suite (MDS). The mobile phase consisting of THF contains 250 ppm of BHT (butylhydroxytoluene) and the flow rate is 1.0 ml/min. Two columns in series (PLgel MIXED-C and PLgel MIXED-D) preceded by a precolumn (Agilent GPC/SEC Guard Column) were used. Agilent GPC/SEC Software is used for the acquisition of chromatograms. The standards used for the calibration line are polystyrene with a range of Mp between 580-283,800 g/mol.

2.5.2. Characterization

Compound 3

^{1}H NMR: (400 MHz, $CDCl_3$) δ_H = 4.19-4.17, 3.63, 3.00, 1.74-1.67, 1.23-1.20, 1.09-1.01,0.94- 0.89. *^{13}C NMR*: (100 MHz, $CDCl_3$) δ_C = 155.81, 122.00, 70.77, 69.84, 64.03, 57.23, 46.80, 46.30, 44.83, 41.73, 36.74, 35.16, 32.07, 27.76, 23.59. *FT-IR* (neat, cm^{-1}): 3327, 2922, 2254, 1715, 1531, 1461, 1304, 1237, 1102, 1050, 855, 777, 578.

Compound 5

^{1}H NMR: (400 MHz, $CDCl_3$) δ_H = 6.14, 5.59, 4.30-4.28, 4.18, 3.88-3.85, 3.64, 2.91, 1.95, 1.85-1.69, 1.24-1.17, 1.05, 0.92- 0.87. *^{13}C NMR*: (100 MHz, $CDCl_3$) δ_C = 167.79, 136.23, 126.26, 70.76, 69.84, 66.63, 63.97, 61.55, 55,12, 46.49, 44.85, 42.05, 36.58, 35.27, 32.05, 27.84, 23.42, 18.54. *FT-IR* (neat, cm^{-1}): 3346, 2923, 1715, 1634, 1534, 1365, 1298, 1239, 1165, 1098, 944, 815, 484.

Compound 8

FT-IR (neat, cm^{-1}): 3330, 2869, 1689, 1536, 1460, 1303, 1238, 1099, 1040, 949, 865, 638.

Compound 23

^{1}H NMR: (400 MHz, $CDCl_3$) δ_H = 5.89, 5, 3, 2.20, 1.72. *^{13}C NMR*: (100 MHz, $CDCl_3$) δ_C = 137, 115, 39, 30, 26.

Compound 27

^{1}H NMR: (400 MHz, $CDCl_3$) δ_H = 5.89, 5, 3, 2.20, 1.72. *^{13}C NMR*: (100 MHz, $CDCl_3$) δ_C = 137, 115, 39, 30, 26. *FT-IR* (neat, cm^{-1}): 3000, 1621, 1537, 1461, 1256, 1011, 990, 667.

Compound 25

^{1}H NMR: (400 MHz, $CDCl_3$) δ_H = 5.89, 5, 2.42, 2.11, 1.6-1.45, 1.3, 0.9. *^{13}C NMR*: (100 MHz, $CDCl_3$) δ_C = 138.6, 114.5, 54.3, 53.9, 31.9, 31.4, 29.7, 29.5, 29.3, 18.8, 17.5, 22.8, 14.66. 39, 30, 26.

2.6. Conclusions

The development of suitable and effective antimicrobial polymers is a key point to fight the issues of antibiotic resistance and environmental pollution caused by the overuse of traditional drugs. In particular, polymers with QASs can be used as antimicrobial coating for many surfaces and facilities.

Differently from the surfaces treated with traditional antimicrobial agents, the use of antimicrobial polymers can ensure a series of advantages. First of all, the presence of QAS in the whole polymer matrix guarantees the retaining of antimicrobial activity, not only in the external layer, but also in its bulk. For this reason, a polymer functionalized with QASs can show antibacterial ability also after long term period and after eventual damages. Additionally, the UV-curing of coating is an economical and facile polymerization technique, especially for coating applications.

In this way, the proposed work was focused on the synthesis of different quaternary ammonium salts and their incorporation in a polymeric matrix, such as polyurethane and polyurethane-acrylate. The antimicrobial activity of synthesized salts was tested: compound **19** showed a very low MIC (0.24-0.48 mg/mL), while for compound **26** was measured higher MIC values (15.6 mg/mL).

After that, the incorporation of QAS in polymer materials was widely investigated. Starting from isoserinol, it was conducted a synthetic approach based on an initial Boc-protection of the amine function, the successive reaction of the N-protected diol with a difunctional isocyanate and, after the deprotection, the final quaternization to QAS. In this route, the main observations were the preference of MDI rather than IPDI; the effectively deprotection of the amine after the integration in the PU system but, also, the impossibility to determine the effective quaternization at the end of the process. In order to overcame this problem, an alternative route was based on an initial QAS formation through a stepwise reaction with an excess of 1-iododecane and iodomethane. The synthesized QAS **19** was effectively characterized through NMR analysis and it was used as a minor component during the synthesis of PUA. In this way, it was possible to cast a PUA film functionalized with compound **19**.

Moving to the second QAS, compound **26**, its structure is suitable for many functionalization of polymer systems. For this reason, further studies are necessary to test its applicability for the production of antimicrobial polymers.

Bibliography

[1] Cowan, M. M. *Clin Microbiol Rev.* **1999**, *12(4),* 564–582.

[2] Medici, S.; Peana, M. F.; Nurchi, V. M.; Zoroddu, M. A. *J. of Med. Chem*. **2019**, *62*, 5923−5943.

[3] Kardos, N.; Demain, A. *Appl. Microbiol. Biotechnol.* **2011**, *92*, 677–687.

[4] Bentley, R.; Bennett, J. W. *Adv. Appl. Microbiol.* **2003**, *52*, 303-327.

[5] Jomah, S.; Asdaq, S. M. B.; Al-Yamani, M. J. *J. Infect. Public Health.* **2020**, *13*, 1187-1195.

[6] Sortino, M.; Delgado, P.; Juàrez, S.; Quiroga, J.; Abonìa R.; Insuasty, B.; Nogueras, M.; Rodero, L.; Garibotto, F. M.; Enrize, R. D.; Zacchino, S. A. *Bioorg. Med. Chem*. **2007**, *15*, 484–494.

[7] Shin, H.; Cho, S. *J. Antimicrob. Chemother.* **2013**, *4*, 72-75.

[8] Talbot, G. H.; Bradley, J.; Edwards Jr., J. E.; Gilbert, D.; Scheid, M.; Bartlett, J. G. *Clin. Infect. Dis.* **2006**, *42*, 657–668.

[9] Cozad, A.; Jones, R., *Am. J. Infect. Control.* **2003**, *31 (4)*, 243-54.

[10] Cardote, T.; Barata, J.; Amador, C.; Alves, E.; Neves, M.; Cavaleiro, J.; Cunha, Â.; Almeida, A.; Faustino, M. *An. Acad. Bras. Cienc.* **2018**, *90*, 1175-1185.

[11] McDonnell, G.; Russell, A. D. *Clin. Microbiol. Rev.* **1999**, *12*, 147–179.

[12] Speight, S.; Moy, A.; Macken, S.; Chitnis, R.; Hoffman, P.; Davies, A.; Bennett, A.; Walker, J. *J. Hosp. Infect.* **2011**, *79*, 18-22.

[13] Kyzioł, A.; Khan, W.; Sebastián, V.; Kyzioł, K. *J. Chem. Eng.* **2020**, *385*, 123888.

[14] Elsabee, M. Z.; Abdou, E. S. *Mater. Sci. Eng. C Mater. Biol. Appl.* **2013**, *33*, 1819–1841.

[15] Chattopadhyay, S.; Heine, E.; Keul, H.; Möller, M. *Macromol. Biosci.* **2014**, *14*, 1116-24.

[16] Ergene, C.; Palermo, E. *Biomacromolecules* **2017**, *18(10),* 3400-3409.

[17] Knetsch, M. L. W.; Koole, L. H. *Polymers* **2011**, *3*, 340-366.

[18] Gottenbos, B.; Mei, H.; Klatter, F.; Nieuwenhuis, P.; Busscher, H. *Biomater*. **2002**, *23*, 1417-1423.

[19] Xue, Y.; Xiao, H.; Zhang, Y. *Int. J. Mol. Sci.* **2015**, *16*, 3626-3655.

[20] Lichter, J. A.; van Vliet, K. J.; Rubner, M. F. *Macromol.* **2009**, *42*, 8573–8586.

[21] Jellali, R.; Campistron, I.; Pasetto, P.; Laguerre, A.; Gohier, F.; Hellio, C.; Pilard, J.; Mouget, J. *Prog. Org. Coat.* **2013**, *76*, 1203-1214.

[22] Ikeda, T.; Ledwith, A.; Bamford, C.H.; Hann, R.A. *Biochim. Biophys. Acta. Biomembr.* **1984**, *769*, 57-66.

[23] Stuparu, M.C.; Khan, A. *J. Macromol. Sci. A* **2022**, *59*, 2-10.

[24] Ganewatta, M.S.; Tang, C. *Polymer*. **2015**, *63*, 1-29.

[25] Gabriel, G.; Maegerlein, J.; Nelson, C.; Dabkowski, J.; Eren, T.; Nüsslein, K.; Tew, G. *Chem*. **2009**, *15(2)*, 433-9.

[26] Buffet-Bataillon, S.; Tattevin, P.; Bonnaure-Mallet, M.; Jolivet-Gougeon, A. *Int. J. Antimicrob. Agen.* **2012**, *39*, 381-389.

[27] Zhang, J.; Zheng, Y.; Yu, P.; He, L.; Wang, H.; Wang, R. *J. Surfactants Deterg.* **2010**, *13*, 155-158.

[28] Lv, X.; Liu, C.; Song, S.; Qiao, Y.; Hu, Y.; Li, P.; Li, Z.; Sun, S. *RSC Adv.* **2018**, *8*, 2941 – 2949.

[29] Luo, Y.S.; Fang, B.; Yong, Y.J. *Oil Field Chem.* **2018**, *35*, 545–549.

[30] Ma, X.; Mu, H.; Hu, Y.; Yang, S. *Colloid. and Surf. A: Physicochem. and Eng. Asp.* **2021**, *626*, 127013.

[31] Singh, A.; Goel, N. *J. Mol. Model.* **2014**, *20*, 1-6.

[32] Dangerfield, E.; Plunkett, C.; Win-Mason, A.; Stocker, B.; Timmer, M. *J. Org. Chem.* **2010**, *75*, 5470-5477.

[33] Senthamarai, T.; Murugesan, K.; Schneidewind, J.; Kalevaru, N.; Baumann, W.; Neumann, H.; Kamer, P.; Beller, M.; Jagadeesh, R. *Nat. Commun.* **2018**, *9*, 1-12.

[34] Chiappe, C.; Pieraccini, C. *Green Chem.* **2003**, *5*, 193-197.

[35] Asensio, G.; Mello, R.; Boix-Bernardini, C.; Gonzalez-Nunez, M. E.; Castellano, G. *J. Org. Chem*. **1995**, *60*, 3692-3699.

[36] Dwamena, A.K. *Separations* **2019**, *6*, 9-11.

[37] Kushnick, T.; Randles, C. I.; Gray, C. T.; Brikeland, J. M. *Science* **1947**, *106*, 587-588.

[38] Massi, L.; Guittard, F.; Géribaldi, S.; Levy, R.; Duccini, Y. *Int. J. Antimicrob. Agents* **2003**, *21*, 20-6.

[39] Gilbert, P.; Moore, L.E. *J. Appl. Microbiol.* **2005**, *99*, 703-705.

[40] Nadagouda, M.N.; Vijayasarathy, P. *Med. Chem. Res.* **2022**, *31*, 1663–1678.

[41] Furi, L.; Ciusa, M. L.; Knight, D.; Di Lorenzo, V. *Antimicrob. Agents Chemother*. **2013**, *57*, 3488–3497.

[42] Bureš, F. *Top. Curr. Chem.* **2019**, *14*, 377.

[43] Xu, W.; Gao, G.; Kadla, J., *Cellul.* **2013**, 20, 1187-1199.

[44] Okeke, C.U.; Snyder, C.R.; Frukhtbeyn, S.A. *Molecules* **2019**, *24*, 1464.

[45] Guiqian, L.; Dingcai, W.; Ruowen, F. *React. Funct. Polym.* **2007**, *67*, 355-366.

[46] Bekir Dizman, B.; Elasri, M. O.; Mathias, L. J. *Macromolecules* **2006**, *39*, 5738-5746.

[47] Sha, D.; Yang, X.; Wang, B.; Liu, X. *ACS Appl. Polym. Mater.* **2020**, *11*, 4936 – 4942.

[48] Vaara, M. *Microbiol. Rev.* **1992**, *56*, 395–411.

[49] Sharma, S. K.; Chauhan, G. S.; Gupta, R.; Ahn, J. H. *J. Mater. Sci. Mater. Med.* **2010**, *21*, 717–724.

[50] Pinnaratip, R.; Bhuiyan, M. S. A.; Meyers, K.; Rajachar, R. M.; Lee, B. P. *Adv. Healthc. Mater.* **2019**, *8*, 1-17.

[51] Czachor-Jadacka, D.; Pilch-Pitera, B. *Prog. Org. Coating* **2021**, *158*, 106355–106369.

[52] Decker, C. *Macromol. Rapid Commun.* **2002**, 26, 1067–1093.

[53] Jenkins, A.; Kennedy, J.; Ferguson, J.; Sparrow, D.; Walton, J. *J. Chem. Educ.* **1981**, *58*, 49-76.

[54] Islam, M. R.; Beg, M. D. H.; Jamari, S. S. *J. Appl. Polym. Sci.* **2014,** *131*, 40787.

[55] Bengtstrom, L.; Salden, M.; Stec, A. A. *Fire Sci. Rev.* **2016**, *5*, 1–23.

[56] Das, A.; Mahanwar, P. *Adv. Ind. and Eng. Polym. Res.* **2020**, *3*, 93-101.

[57] Petrović, Z. S. *Polym. Rev.* **2008**, *48*, 109-155.

[58] Lu, Q. W.; Macosko, C. W. *Polymers* **2004**, *45*, 1981-1991.

[59] Dumont, M.; Kharraz, E.; Qi, H. *Ind. Crops Prod*. **2013**, *49*, 830-836.

[60] Delebecq, E.; Pascault, J.-P.; Boutevin, B.; Ganachaud, F. *Chem. Rev.* **2013**, *113*, 80-118.

[61] Thirumal, M.; Khastgir, D.; Singha, N. K.; Manjunath, B. S.; Naik, Y. P. *J. Appl. Polym. Sci.* **2008,** *108*, 1810-1817.

[62] Jaudouin, O.; Robin, J.J.; Lopez-Cuesta, J.M.; Perrin, D.; Imbert, C. *Polym. Int.* **2012**, *61*, 495-510.

[63] García-Pacios, V.; Costa, V.; Colera, M.; Martín-Martínez, J. M. *Prog. Org. Coat.* **2011,** *71*, 136-146.

[64] Wang, Y.; Chen, R.; Li, T.; Ma, P.; Zhang, H.; Du, M.; Chen, M.; Dong, W. *Ind. Eng. Chem. Research* **2020,** *59*, 458-463.

[65] Park, D.; Larson, A.M.; Klibanov, A.M. *Appl. Biochem. Biotechnol.* **2013**, *169*, 1134–1146.

[66] Zhuo, S.; Zhang,G.; Feng, X.; Jiang, H.; Shi, J.; Liua, H.; Li, H. *RSC Adv.* **2016**, *6*, 50581-50586.

[67] Zhang, L.; Brostowitz, N. R.; Cavicchi, K. A.; Weiss, R. A. *Macromol. React. Eng.* **2014**, *8*, 81-99.

[68] Liao, F.; Zeng, X.; Li, H.; Lai, X.; Zhao, F. *J. Cent. South Univ.* **2012,** *19*, 911-917.

[69] Kunwong, D.; Sumanochitraporn, N.; Kaewpirom, S. *Songklanakarin J. Sci. Technol.* **2011**, *33*, 201–207.

[70] Tanzi, M. C.; Verderio, P.; Lampugnani, M. G.; Resnati, M.; Dejana, E.; Sturani, E. *J. Mater. Sci. Mater. Med.* **1994**, *5*, 393–396.

[71] Maurya, S. D.; Kurmvanshi, S. K.; Mohanty, S.; Nayak, S. K. *Polym. Plast. Tech. Eng.* **2018**, *57*, 625-656.

[72] Decker, C. *Macromol. Rapid Commun.* **2002**, *23*, 1067.

[73] Scaiano, J. C.; Stamplecoskiew, K. G.; Hallett-Tapleyw, G. L. *Chem. Commun.* **2012**, 48, 4798.

[74] Yagci, Y.; Jockusch, S.; Turro, N. J. *Macromolecules* **2010**, *43*, 6245.

[75] Pastore, G.; Gabrielli, S.; Giacomantonio, R.; Lupidi, G.; Capodaglio, S.; Stella, F.; Leone, E.; Compagnucci, T.; Marcantoni, E. *Results in Materials* **2022**, *15*, 100294.

[76] Shufen, L.; Zhi, J.; Kaijun, Y.; Shugiu, Y.; Chow, W. K. *Polym. Plast. Technol. Eng.* **2006**, *45*, 95-108.

Chapter 3: Development of thermo-reversible systems in innovative materials

3.1. Introduction to click chemistry

Click chemistry, as first articulated by Sharpless and colleagues in 2001, was ideated from the will to increase the power of molecular assembly.[1] The logic behind click chemistry is simple: the traditional carbonyl (aldol) chemistry has limited thermodynamic driving force and it often requires harsh conditions and the use of catalyst. Even if in natural processes new bonds and complex structures are formed through a small number of good carbonyl (aldol) reactions, many biosynthetic pathways frequently require a unique enzyme for each step, hence the mimic of the enzyme-control strategy in synthetic approaches often necessitate a heavy investment of time and resources for catalyst development.

From this initial point, a list of considerations has emerged. Among them, the most important is the necessity of new molecular properties, that can emerge from the joining of small molecular building blocks. In this context, chemical methods exist, and more can be developed, that make molecular connections easily.

The "click" term refers to the type of convenience and satisfaction afforded by snapping objects together, applying a kind of connection similar to a luggage strap connector (*Figure 1*).

Figure 1 – Click-chemistry and schematization as luggage strap connector.

In other words, with a click-like reaction, two pieces having adequate ends rapidly react, making a linkage. Therefore, from the idea that the reactivity does not depend on the type of the pieces, but just on the click-connecters, an enormous range of investigations was boomed out in many fields, including materials science, surface science, analytical chemistry, chemical biology, and drug development.

The foundational reactions of click chemistry were all ones in the history of organic synthesis, including conjugate addition, strained ring opening, acylation/sulfonylation, aldehyde capture by α-effect nucleophiles, and cycloadditions. Since click reactions are usually characterized by high energy

content in one or more reactants, building in such driving force is often the difficult step. Although the click-chemistry philosophy for drug discovery is very appealing, the medicinal chemists in this field has been hesitant for a long time. Interestingly, applications of click reactions in polymer sciences are warmly welcomed, as like as in biomedical applications and in pharmaceutical sciences.

Finally, implicit but not explored in the original image of the click chemistry concept was also the ability to disconnect on command. This subject, often referred as "clip chemistry", is based on the fact that breaking bonds can be as important as making them.[2]

3.1.1. Click chemistry principles

The principles of click chemistry have been articulated in the landmark review of Sharpless and colleagues, more than 20 years ago now.[3] The main objective was to generate substances by joining small units together with heteroatom links (C-X-C). For this purpose, a set of stringent criteria have been postulated in order to define a click-reaction. These properties are:

- modular process;
- process wide in scope;
- very high yields of products;
- pure fusion processes: formulae of reactants should equal the formula of product;
- avoid the formation of harmful by-products;
- ease remotion of by-products;
- stereospecific reaction (but not necessarily enantioselective);
- simple reaction conditions (ideally, the process should be insensitive to oxygen and water);
- readily available starting materials and reagents;
- the use of no solvent or a solvent that is benign (such as water) or easily removed;
- simple product isolation;
- if required, purification should be by nonchromatographic methods;
- the product must be stable under physiological conditions.

It is important to highlight that a high thermodynamic driving force, usually greater than 20 kcal/mol, is normally necessary to fulfil most of these properties, achieving so a click reaction. Such processes proceed rapidly to completion and also tend to be highly selective for a single product, since these reactions are "spring-loaded" for a single trajectory.

The most common examples of click chemistry reactions are cycloadditions, such as 1,3-dipolar cycloaddition and the Diels-Alder family of transformations; nucleophilic substitution chemistry, in

particular ring-opening reactions of strained heterocyclic electrophiles (epoxides, aziridines, aziridiniumions, and episulfoniumions); carbonyl chemistry of the "non-aldol" type (formation of ureas, thioureas, aromatic heterocycles, oxime ethers, hydrazones, and amides); additions to carbon-carbon multiple bonds, especially oxidative cases (epoxidation, dihydroxylation, aziridination, and sulfenyl halide addition) but also Michael additions of Nu-H reactants.

In this context, the olefin-based organic synthesis plays a fundamental role. The starting materials of petrochemical nature are "gifts prepared by the carbonyl-based syntheses of ancient organisms; in fossil oils are stored the energy of CO_2-based photosynthesis, and, more importantly, countless carbon-carbon bonds". These starting materials are largely made of long saturated hydrocarbons and, to be useful, a manipulation is required. Therefore, the process of cracking at high temperatures (850°C) is fundamental to create many reactive monomers, having new C-C π bonds and used to create a large number of materials. In other words, during the cracking, an exchange of C-C σ bonds for new C-C π bonds is ensured by the high temperature.

The new created C-C π bonds are highly reactive, having about 22-25 kcal/mol greater free energy content than a C-C σ bond.[4] Hence, part of the energy used in cracking is captured in the C=C linkage and used to create new C-C σ bonds at the expense of C-H bonds. This is apparent in processes such as the Diels-Alder reaction, where there is a gain of σ links by reorganizing π C=C links, without altering the total C-C bond count (*Scheme 1*).

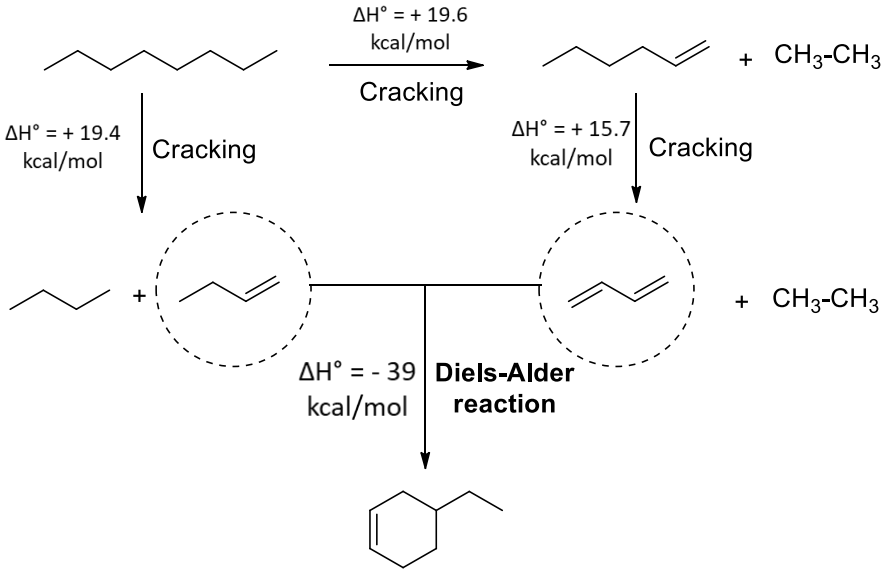

Scheme 1 – Formation of reactive olefins from the cracking of n-octane and their reaction to the thermodynamically favoured Diels-Alder adduct.

In conclusion, olefins are highly attractive starting materials and they are the starting materials for 90% by weight of all useful man-made organic compounds.[5] The simplest hydrocarbons (C_1-C_8 blocks, *Figure 2*) are accessible in large quantities and produced by the petrochemical industry on a large scale.

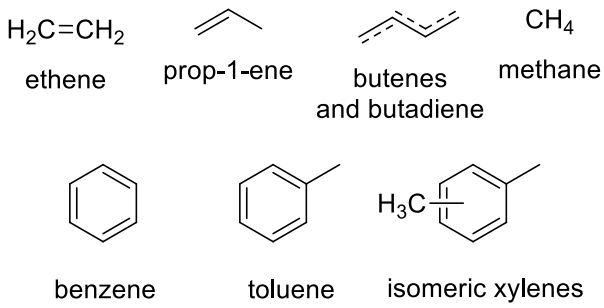

Scheme 2 –Small carbon building blocks from petroleum.

The importance of olefins is dramatically enhanced by their role as precursors of intermediates having even higher energy, such as epoxides, aziridines, episulfonium ions, and aziridinium ions. All these substrates are, in turn, highly suitable for click chemistry transformations and this sequence of oxidative creation/nucleophilic quenching of reactive electrophiles is at the heart of click chemistry. Indeed, the irreversible progression from system of high energy to ones of lower energy is the driving force of all the click-chemistry processes and it enables the generation of intermolecular connections. Common carbonyl compounds, by contrast, are quite thermodynamically stable relative to olefins.

3.1.2. Click chemistry reaction types

As first point, click chemistry reaction types can be divided into two classes: those in which protons must be shuffled about (epoxide ring opening, for example) and those in which no σ-bond connections are severed (cycloaddition reactions). The former tend to benefit dramatically from an aqueous environment, while the latter reveal little solvent dependence and are better overall in their adherence to click chemistry ideals. Besides that, the most important reactions are resumed in *Scheme 2*.

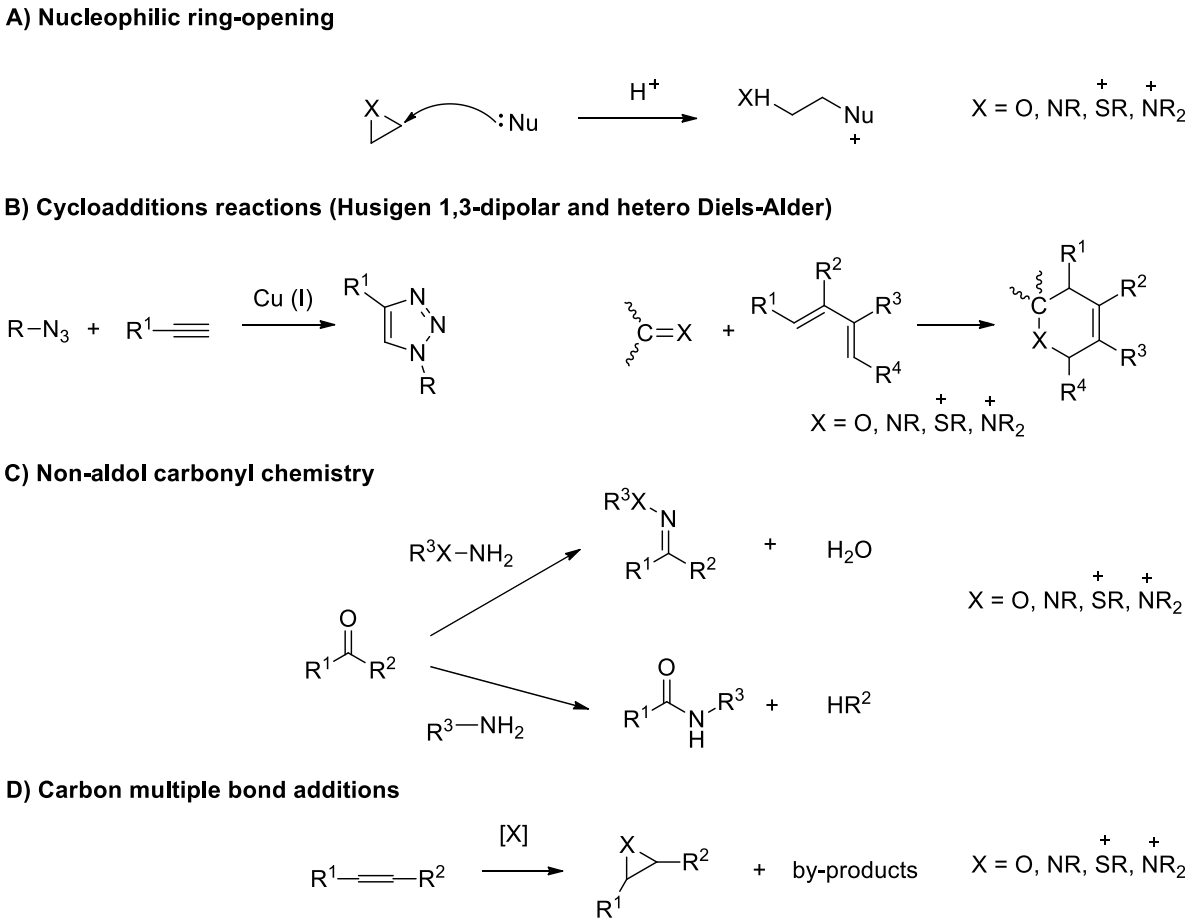

Scheme 2 – Click chemistry types of reaction.

For the purpose of this thesis, the discussion will include the nucleophilic opening of strained electrophilic rings and cycloaddition reactions.

A. Nucleophilic opening of heterocyclic rings:

The S_N2 ring opening reactions of three-membered heterocyclic electrophiles, such as epoxides, aziridines or aziridinium ions, are stereospecific, often highly regioselective, and nearly quantitative reactions. The advantage of nucleophilic attack to electrophilic three-membered rings relies on the strong disfavouring of elimination processes, which may result in high yields and facile product isolation.[6] Moreover, they are fusion events, and most of them can be performed in absence or in green solvents (water, alcohol or water/alcohol mixtures).

In a number of cases, the regioselectivity can be controlled by the choice of solvent. A perfect example is shown in *Scheme 3*.[7]

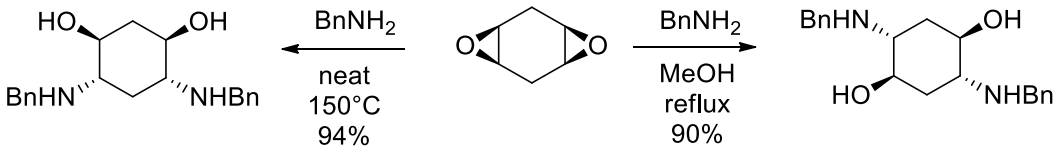

Scheme 3 – Regioselectivity control in the reaction of *cis*-cyclohexadiene diepoxide with benzylamine by varying the environment (neat VS protic solvent).

In the absence of solvents, the *cis*-cyclohexadiene diepoxide reacts with amines to give the amino alcohol, in which the entering nucleophiles are 1,3-related. When protic solvents are added, the same reactant give a different regioisomer, with nucleophiles in the 1,4-relationship. In both cases, the diamino diol products were isolated in pure form by direct crystallization from the crude reaction solution, which enabled the scalability of the reactions even at industrial scale.

Regioselectivity is similarly well-controlled for the ring opening of the *trans* diepoxide, as shown in *Scheme 4*.[8]

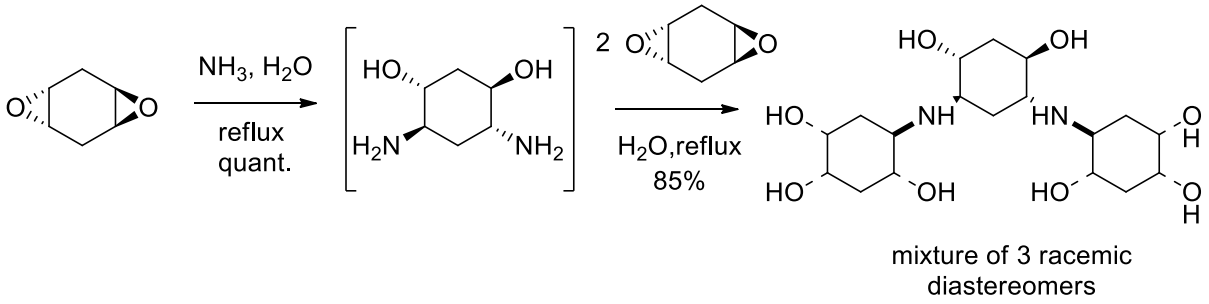

Scheme 4 – One pot reaction of ammonia with three equivalents of *trans*-cyclohexadiene diepoxide.

In this case, the one-pot reaction of three diepoxide units with two of ammonia resulted in the formation of a polycyclic structure, as a mixture of three possible racemic diastereomers.

Another interesting type of highly activated three-membered rings is the aziridinium ion. This system can be easily generated *in situ* starting from amino alcohols, β-halo amines and related compounds. All these substitutions are stereospecific and proceed with double inversion of configuration. Therefore, there will be a net retention of configuration in the cases where the nucleophilic attack on the aziridinium electrophile occurs at the centre bearing the leaving group, or with inversion of both centers when the amino group undergoes a 1,2-shift.[9]

Aziridinium systems are promising both for the broad reactivity and their easy synthesis from the corresponding epoxides. These features make the aziridinium ion as a perfect candidate for the rapid generation of building blocks and combinatorial libraries. An interesting example is the preparation of a 1,5-benzodiazepine derivative, depicted in *Scheme 5*.[10]

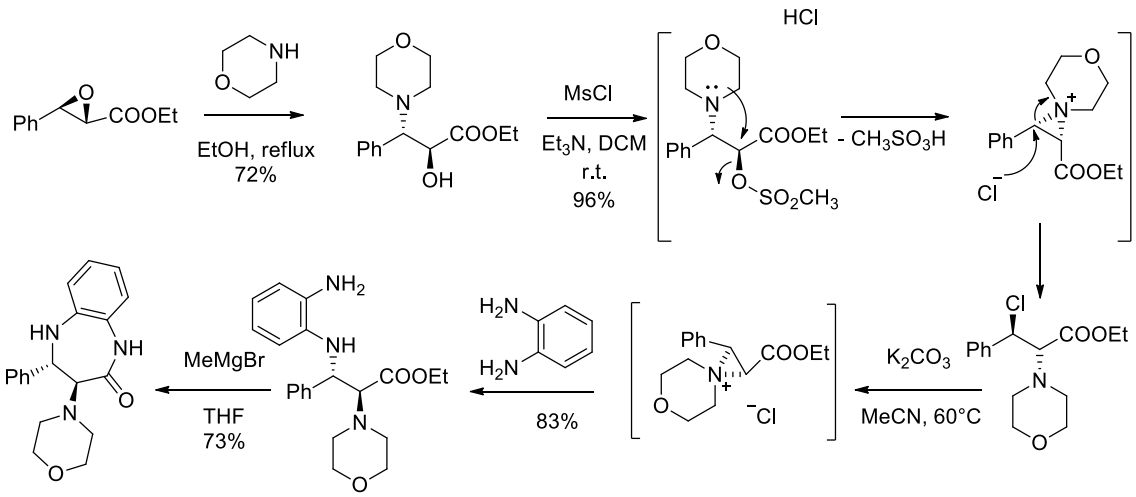

Scheme 5 – Efficient assembly of a benzodiazepine via an aziridinium intermediate.

B. Cycloaddition reactions:

Hetero Diels-Alder and 1,3-dipolar cycloadditions are nice examples of click chemistry ideals, since they provide a fast transformation through a modular fusion reaction.[11] Another appealable feature related to cycloadditions is the effective formation of heterocycles (six- and five-membered, respectively), providing so a fast access to many fundamental heterocyclic molecules by the reaction of acyclic reactants.[3]

The Cu (I)-catalysed Huisgen 1,3-dipolar cycloaddition of azides and terminal alkynes to form 1,2,3-triazoles fulfils all of the criteria of click chemistry almost perfectly, and it is extremely reliable and easy to use. Indeed, this reaction is regiospecific, leading to the exclusively formation of 1,4-substituted products, and it can be typically performed over a wide range of temperatures (0–160°C), in a variety of solvents (including water), and over a wide range of pH values (5-12).[12] Furthermore, this transformation enables a list of additional benefits: starting from the reactants, the reaction conditions permit a strong tolerance toward a wide number of substituted primary, secondary, tertiary, and aromatic azides. The same suitability has been proven for the acetylene component.[13] Moreover, azides and terminal alkynes are fairly easy to install and they are stable at standard conditions, tolerating common organic synthesis conditions in a large number of solvents and pHs. Additionally, the reaction is unaffected by steric factors and the purification of product is commonly performed with filtration.[14]

Finally, the role of Cu (I) catalyst is prominent, since the cycloaddition proceeds as much as 107 times faster than the uncatalyzed version. In this view, it is interesting to point out that, despite the general concerted mechanism of cycloadditions, experimental kinetic data and molecular modelling performed on the Huisgen 1,3-dipolar cycloaddition reaction seem to favour a stepwise reaction

pathway.[15] It has been calculated that the activation barrier for a catalysed concerted reaction is actually greater than that for an uncatalyzed concerted reaction (27.8 kcal/mol vs. 26 kcal/mol in one particular reaction using density functional theory calculations). Furthermore, a stepwise-catalysed reaction has an activation barrier 11 kcal/mol lower than a concerted catalyzed reaction.[12] Based on experimental evidence and by the fact that Cu(I) can readily insert itself into terminal alkynes (e.g.; in Sonogashira coupling),[16] the proposed mechanism is shown in *Scheme 6*.

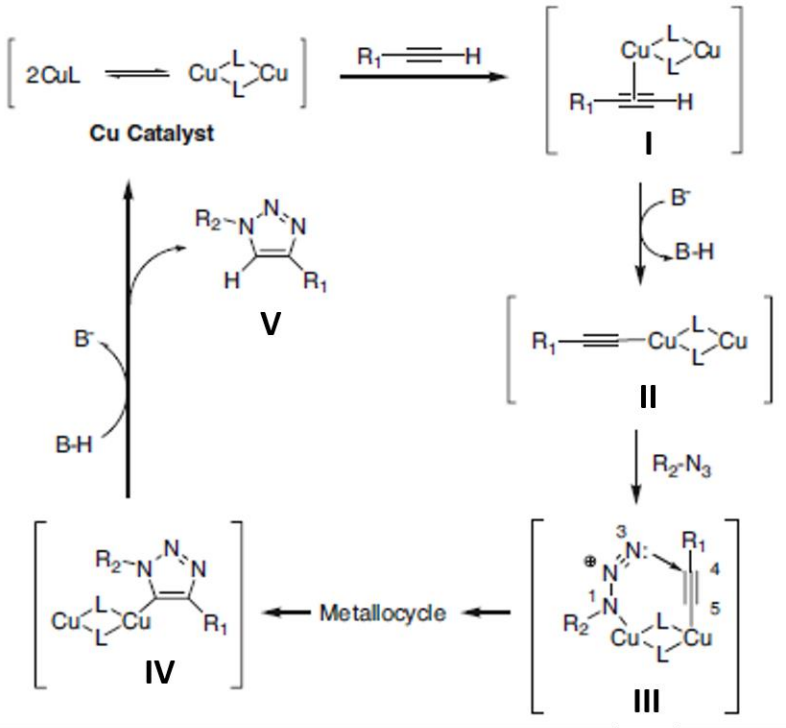

Scheme 6 – Proposed mechanism for the Huisgen 1,3-dipolar cycloaddition. L = ligands of catalyst; B = base.

It was envisioned that the first step of the reaction involves π complexation of a Cu(I) dimer to the alkyne (**I** in *Scheme 6*). After that, the deprotonation of the terminal hydrogen occurs to form a Cu-acetylide. There are actually several different kinds of Cu-acetylide complexes that can form, depending on the reaction conditions utilized; structure **II** represents just one possibility. The π complexation of Cu(I) lowers the pKa of the terminal alkyne, allowing deprotonation to occur in an aqueous solvent without the addition of a base. If a non-basic solvent (such as acetonitrile) is used, then a base would have to be added. In the following step, N(1) displaces one of the ligands from the second Cu in the Cu-acetylide complex to form structure **III**. In turn, this "activates" the azide for nucleophilic attack. Due to proximity and electronic factors, N(3) can now easily attack C(4) of the alkyne, leading to a metallocycle (not shown for simplicity). The metallocycle then contracts when the lone pair of electrons of N(1) attacks C(5) to form the respective triazole **IV**. Once the triazole is formed, the attached Cu dimer immediately complexes to a second terminal alkyne. However, this

second alkyne cannot undergo a cycloaddition due to the unfavorable structure of the complex, and it dissociates upon protonation to reform **IV**. One final protonation releases the Cu (I) catalyst from the 1,2,3-triazole product **V**, to undergo a second catalytic cycle with different substrates. Both of these protonations are most likely the result of interactions with protonated external base and/or solvent.

3.1.3. Connection and disconnection: "clip chemistry"

In the two decades since the introduction of the click chemistry concept, its toolbox has continually expanded. In click reactions, covalent bond tends to be formed, allowing for the efficient synthesis of functional (bio)(macro)molecules and materials.

Anyhow, in many cases, the control of chemical reactivity in complex environments requires efficient covalent bond cleavage, rather than or in addition to bond formation. Protecting group strategies provide a perfect example: synthetic organic chemistry was transformed by the development of selective functional group protection/deprotection methods that allow one to precisely cleave bonds in complex molecules.

Therefore, in comparison to the novelty introduced by the click chemistry, the advances provided by selective and efficient covalent bond breaking reactions in synthetic transformations are at the basis of the recent formulation of the "clip chemistry" concept.[2] The aim of clip chemistry is to offer new opportunities to tailor the compositions and structures of complex (bio)(macro)molecular systems with exquisite control. Working in concert, click chemistry and clip chemistry should offer powerful methods to address next-generation challenges across the chemical sciences.

In reverence to the concepts of click chemistry, the "clip" terminology has been introduced in order to unify the diverse types of covalent bond cleavage processes under a single terminology. Hence, "clip" chemistry can be defined as a covalent bond breaking reaction that is modular and wide in scope. It must give very high yields and generate inoffensive byproducts ideally in a stereo- and regio-specific manner. The process should involve simple reaction conditions and readily available starting materials and reagents.

Lastly, Sharpless and co-workers motivated click chemistry through comparisons to biological systems, which heavily rely on carbon-heteroatom bond forming processes with high thermodynamic driving forces (i.e., "spring-loaded" reactions). Similarly, Johnson *et al.* noted that precise bond cleavage reactions are also ubiquitous in biological systems, as perhaps best recognized recently in the discovery and rapid adoption of gene editing tools.[2]

In their review, Johnson and co-workers have identified six types of clip reactions:

- Stoichiometric clip reactions (*Figure 3*): they require the stoichiometric addition of another reagent to trigger bond cleavage (e.g., phosphine reducing agent for disulfide reduction). Silyl ether-fluoride cleavage is another powerful clip reaction, which is most notably known for its role in the protection/deprotection of alcohols.[17].

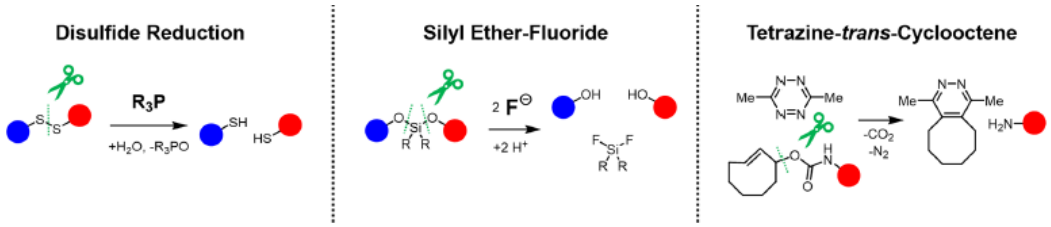

Figure 3 – Examples of stoichiometric clip reactions.

- Catalytic clip reactions (*Figure 4*): they require the presence of an added catalyst to induce bond cleavage. In this sense, Pd-catalysed deallylation is a notable example. Allyl carbamates and carbonates are quite stable in the presence of water. By contrast, upon addition of a palladium catalyst, alkene-coordination activates the carbamate to nucleophilic attack and subsequent cleavage.[18]

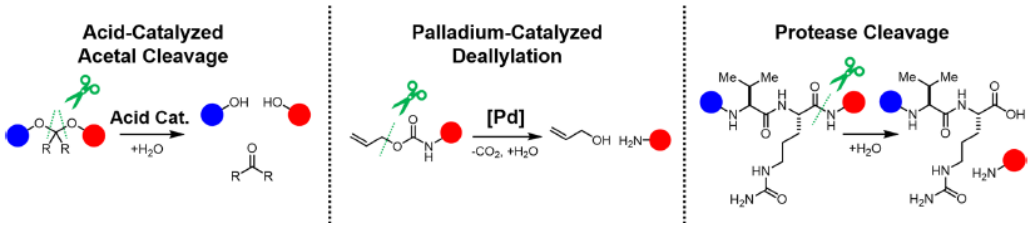

Figure 4 – Examples of stoichiometric clip reactions.

- Electron-transfer mediated clip reactions (*Figure 5*): these reactions utilize single electron transfer (SET) to drive covalent bond cleavage. The source of the electrons may be from an electrode, a stoichiometric reductant or oxidant, or through photoinduced electron transfer, for example, from a photocatalyst (i.e., photoredox catalysis). A classic example of SET-mediated clip reactions involves the electrochemical removal of protecting groups. For example, 4-pyridylmethyl protecting groups undergo efficient clip reactions at the benzylic position following single electron reduction, which enables the efficient release of functional groups such as thiols.[19]

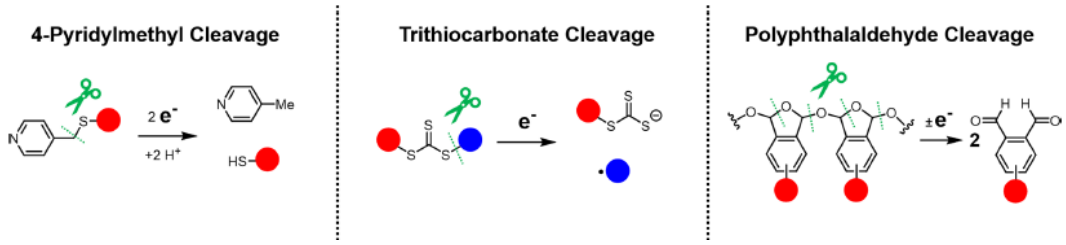

Figure 5 – Examples of electron-transfer mediated clip reactions.

- Light-mediated clip reactions (*Figure 6*): they use the energy from a photon to access high-energy intermediates, that ultimately undergo bond cleavage reactions. In some instances, these processes can involve direct bond photolysis, as observed in the homolysis of disulfides to thiol radicals, which can further abstract hydrogen atoms to form thiols. Anyhow, more commonly, light is used to excite caging groups bearing conjugated π-systems, which then undergo selective bond cleavage reactions of an adjacent single bond. Examples include the photocleavage of o-nitrobenzyl and coumarin derivatives and the photochemical cycloelimination of anthracene dimers.[20]

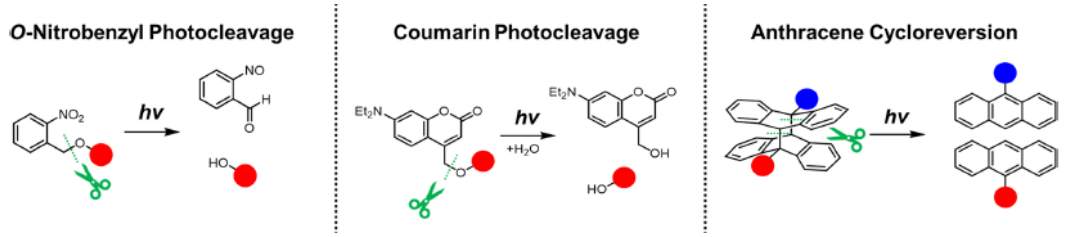

Figure 6 – Examples of light mediated clip reactions.

- Thermally mediated clip reactions (*Figure 7*): they involve bond dissociation upon changes in temperature. While the vast majority of chemical transformations are accelerated by heating, including many of the clip reactions listed above, the thermally mediated clip reactions discussed here, from a practical perspective, involve no addition of other reagents, catalysts, or energy sources. For example, furan-maleimide adducts are commonly explored for thermally reversible linkages. These adducts undergo near-quantitative reversion under much milder conditions than many other Diels–Alder adducts.[21] Thus, the ability to click and clip the furan-maleimide Diels–Alder adduct in a working temperature range (Diels–Alder at ~60 °C, retro Diels–Alder at ~100 °C) has led to its wide adoption in the synthesis of advanced materials.[22]

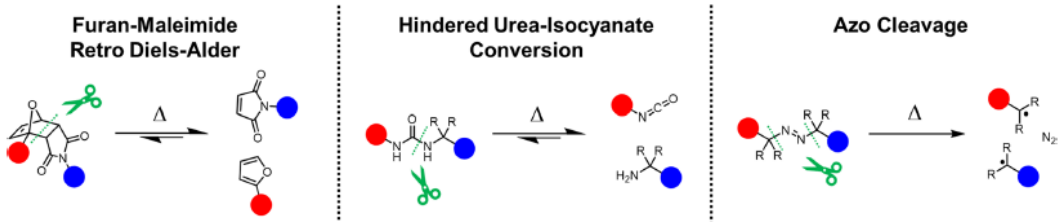

Figure 7 – Examples of thermally mediated clip reactions.

- Force mediated clip reactions (*Figure 8*): they utilize mechanical force to drive the scission of covalent bonds. Traditional mechanical degradation of materials leads to unselective bond scission reactions; however, new classes of tailored molecules, known as "mechanophores", have been developed in recent years to achieve selective force-induced transformations. Key examples include the formal retro-cycloadditions of cyclobutanes, the electrocyclic ring opening of dichlorocyclopropanes, and the ring opening of spiropyrans.

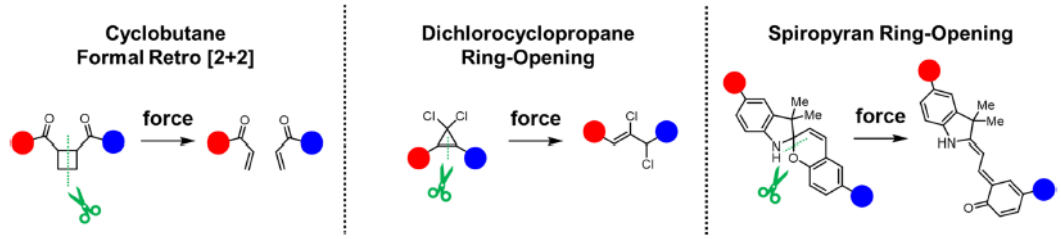

Figure 8 – Examples of force mediated clip reactions.

3.2. Triazolinediones (TADs): from the synthesis to the applications

4-Substituted 1,2,4-triazoline-3,5-dione ("triazolinedione" or TAD) was first reported at the end of the XIX century, by Thiele and Stange.[23]

The general structure of a TAD is reported in *Figure 8*.

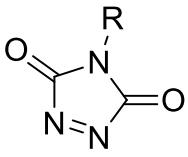

Figure 9 – General chemical structure for 4-substituted 1.2.4-triazoline-3,5-dione.

Moving in time, in the '20s, Diels *et al.* published the pioneering work based on the bond-forming reactivity of azodicarbonyl derivatives toward "unreactive" unsaturated hydrocarbon substrates.[24] In this way, they developed the famous Diels–Alder reaction, based on the spontaneous reaction of

diethyl azodicarboxylate (DEAD) and cyclopentadiene to spontaneously form a quantitative 1:1 adduct, at room temperature and without the need for additives or catalysts (*Scheme 7*).

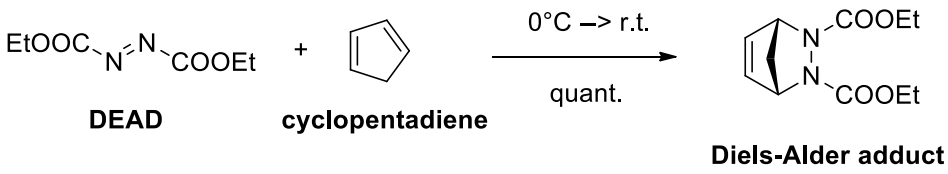

Scheme 7 – Diels-Alder reaction between DEAD and cyclopentadiene.

In this context, *cis* or cyclic (like TADs) azodicarbonyl derivatives are even more reactive than DEAD and perfect candidates for many cycloaddition reactions; however, they were excluded from these initial studies, as a result of the problematic synthesis and purification of TAD compounds.

The boost for the applications of TADs in synthetic processes and, more in particular, as a dienophile in the Diels–Alder reaction, was not established before the 1960s, when Cookson *et al.* obtained pure crystalline 4-phenyl-TAD (also known as Cookson's reagent) for the first time.[25] Moreover, they effectively tested the strong dienophile activity of this compound, as shown in *Scheme 8*.

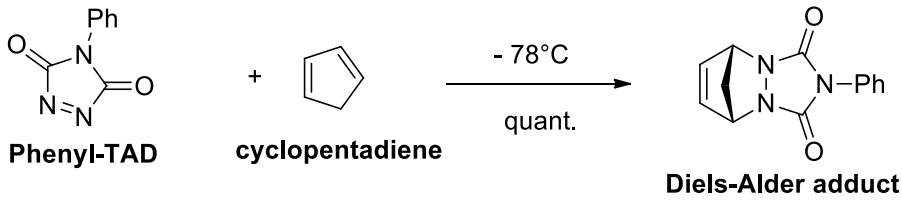

Scheme 8 – Diels-Alder reaction between phenyl-TAD and cyclopentadiene.

Cookson's procedure is considered as a major innovation in the field of TAD chemistry, as it was followed by a wide range of investigations into the reactivity and the synthetic applications of TAD-bearing compounds. The reactivity of TADs toward Diels-Alder reaction is 30,000 and 1,000 times faster than that of DEAD and tetracyanoethylene, respectively.

In this way, triazolinediones are generally considered as the most reactive bench-stable dienophiles and enophiles.[26] Moreover, their reactivity depends to a certain extent on the nature of the 4-substituent. Hence, electron-poor substituents can even further increase the electrophilicity, up to the point that some TAD reagents (e.g., 4-(4-nitrophenyl)-TAD), become too reactive to be isolated.[27] Nevertheless, once isolated, most TADs are generally easy to handle and stable for prolonged periods, when stored in a cold environment (i.e., -18 °C) in the absence of light and moisture. TADs and relative reactive compounds are shown in *Figure 10*.

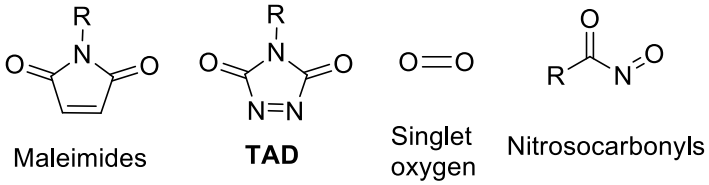

Figure 10 – TADs and related reactive compounds.

TAD reagents have a strong similarity in chemical structure with the well-established class of maleimides, which are widely used in a large number of applications, including in click chemistry.[28] Their modes of reactivity show some important similarities; anyhow, TADs can be involved in cycloaddition reactions with a wider range of substrates (even with simple olefins) and much faster than maleimides. This feature is due to higher intrinsic thermodynamic driving force: so, while maleimide-based conjugations are often reversible processes, most of the TAD-based reaction are irreversible. A consequence of that is also the relative lack of controlled reactivity of TADs toward typical nucleophiles, like amines and thiols.

In accordance to its strong reactivity, TAD compounds have been compared with singlet oxygen, since they show a high preference for pericyclic reactions toward more or less the same range of electron-rich or nonpolarized olefins.[29] This similarity can also be related to a sort of correspondence in the frontier orbitals (HOMO and LUMO), having both a filled and an empty π-type orbital of very similar energy.[30] Besides the similar preference for orbital-controlled reactions, the most relevant difference between TAD and singlet oxygen is their lifetime. Indeed, singlet oxygen normally has a half-time of few microseconds in many organic solvents; conversely, many TADs can be isolated and store for prolonged periods. Additionally, singlet oxygen is just effective in oxygenations, while many functionalities (depending on the R group) can be installed using TAD compounds. A reagent that is in the middle of TADs and singlet oxygen are the nitrosocarbonyl compounds. These also have very limited lifetimes and need to be generated *in situ* just like singlet oxygen, but they can be used to introduce different substituents.[31]

Although the synthesis and chemistry of simple TAD reagents is well-understood, in more recent applications, as in click chemistry and/or modern polymer chemistry, functional or "tailored" TAD reagents are often required to harness the full potential of the exceptional TAD reactivity.[32] In this way, the use of such functional TAD compounds enables unprecedented applications. However, the main limitation is the moderate synthetic accessibility of TAD compounds, even by actual standards.

3.2.1. Cookson's procedure for the synthesis of TADs

For the synthesis of TADs, the most important precursor is unequivocally recognized is the class of 4-substituted 1,2,4-triazolidine-3,5-diones (or urazoles).

The first efficient synthetic scheme for urazoles was reported in 1961 by Zinner and Deucker. The authors proposed the synthesis of 4-phenyl- and 4-butylurazole through the cyclization of the 4-substituted (ethoxycarbonyl)semicarbazide (or, simply, semicarbazide), which only requires mild reaction conditions.[33] The approach is shown in *Scheme 9*.

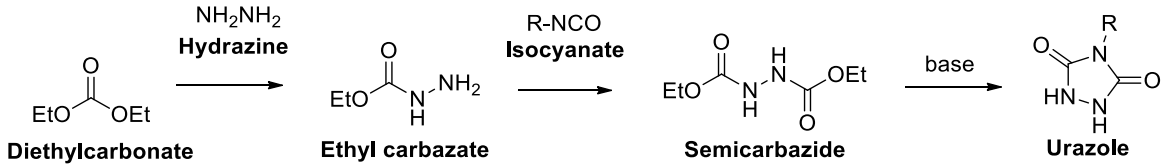

Scheme 9 – Zinner-Deucker synthesis of 4-substituted urazole *via* semicarbazide.

Significantly, ethyl carbazate was synthesized by the condensation reaction of cheap reagents and it was directly used to generate the semicarbazide, just by the mixing with a reactive isocyanate. Hence, by varying the isocyanate, it is possible to synthesize an important library of 4-substituted urazoles.

At this point, it is important to highlight that Cookson and coworkers were the first to use a urazole precursor for the synthesis of TADs.[34] For this purpose, they exploited the same synthetic approach of Zinner-Deucker for the TAD synthesis, through the cyclization of the semicarbazide obtained by the reaction of hydrazine, diethyl carbonate, and phenyl isocyanate. Once the formation of the urazole, a final oxidation ensured the synthesis of bench-stable crystals of 4-phenyl-1,2,4-triazoline-3,5-dione.

As this sequence was widely adopted, it became generally known as the Cookson's method. Even if many synthetic strategies have been adopted over the years to obtain a functionalized semicarbazide, in this thesis it will be exclusively discussed the approach based on the reaction of ethylcarbazate with isocyanates.

As a result of the high reactivity of isocyanates, these reagents readily react at room temperature with ethylcarbazate to give the corresponding semicarbazide adducts in excellent yields (up to 100%), typically after stirring overnight. If the reaction mixture is heated, complete conversions can be achieved in a matter of hours. The role of the solvent is not critical, but as the semicarbazide products tend to precipitate from hydrophobic solvents such as toluene, the use of such solvents vastly simplifies the workup to the point that after collecting and drying the solids, there is generally no need for a further purification step.

The substrate scope, with corresponding yields, for the synthesis of semicarbazides from isocyanates is resumed in *Figure 11*.

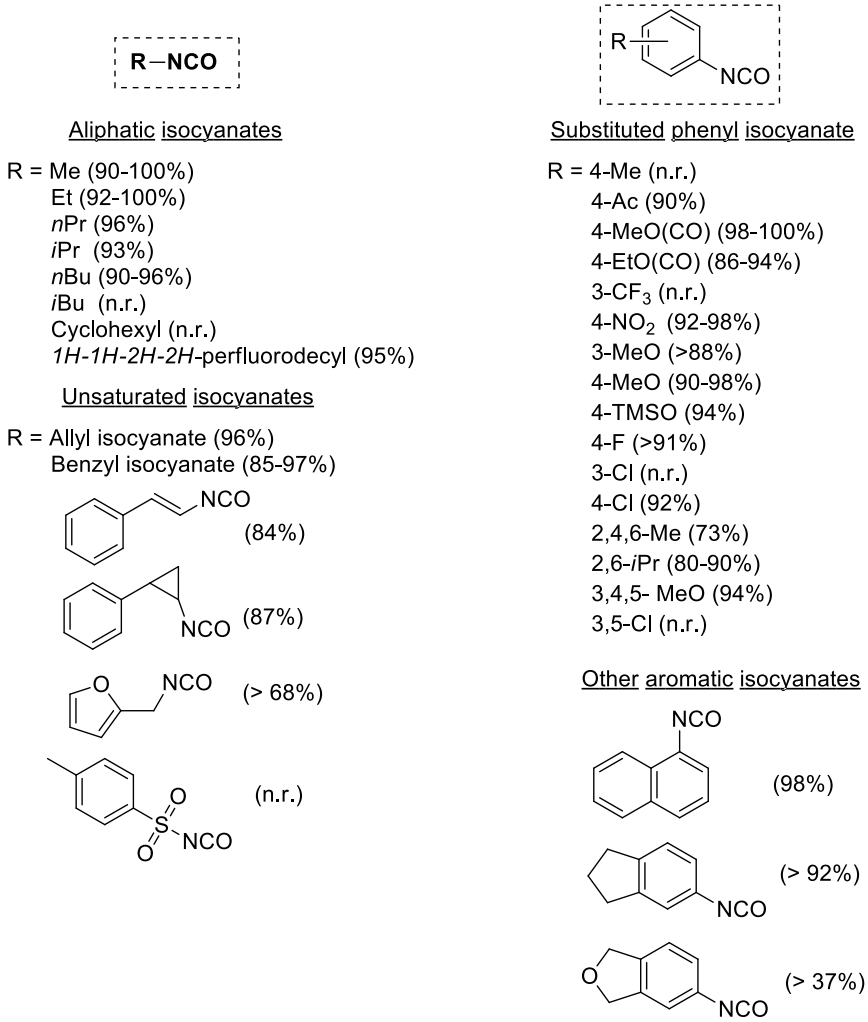

Figure 11 – Cookson's method: substrate scope with corresponding yield for the synthesis of semicarbazides from isocyanates. N.r. = yield non reported.

An analysis of *Figure 11* reveals that the structural variations in the obtained semicarbazides are heavily limited by the availability and reactivity of the isocyanates themselves. This means semicarbazides bearing a chemical functionality for further modifications are not easily accessible by this strategy, because of the general incompatibility with isocyanates.

However, important exceptions are reported in literature. For instance, Yamada and Shimizu reported the synthesis of (3-chloropropyl)semicarbazide, in which the alkyl chloride can be used as a functional handle to introduce various nucleophilic groups;[35] likewise, Read and Richardson have reported the synthesis of a semicarbazide bearing a carboxybenzyl-protected amine, which, after deprotection, can be derivatized by various electrophilic groups.[36]. On the matter of (industrial)

scalability, Chandrasekhar *et al.* have prepared nearly 4 kg of 4-phenylurazole in one batch with an overall yield exceeding 90%.[37]

Additionally, when the corresponding diisocyanate is used, the Cookson method can be used for the preparation of *bis*-semicarbazides. The possibility to convert bulk chemicals used in polyurethane synthesis, such as 4,4'-methylenediphenyl diisocyanate (MDI), into the corresponding bivalent triazolinedione (bisTAD) reagents obviously attracted the interest of polymer chemists. In this sense, reports by Wald and Wamhoff, as well as Butler and co-workers, triggered the development of a wide range of difunctional semicarbazides (and TAD reagents), as depicted in *Figure 12*.[38] These bivalent compounds also attracted attention in the patent literature, with reports on the transformation of some of the industrially relevant diisocyanates.[39]

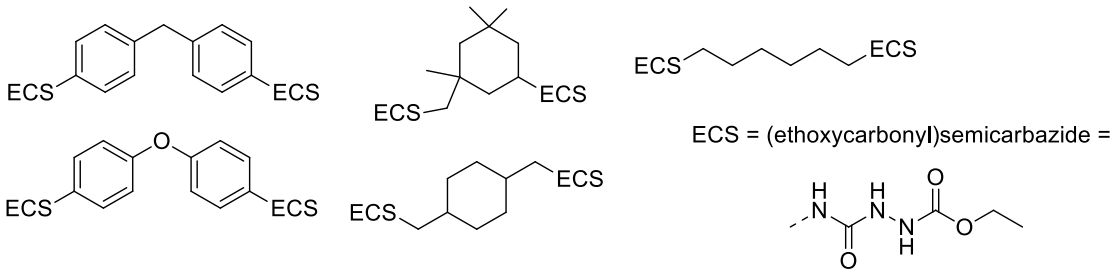

Figure 12 – Divalent semicarbazides created by combining ethyl carbazate with the corresponding diisocyanate.

Besides the formation of the urazole precursor, the formation of the corresponding TAD can be obtained by many oxidation processes. An important remark is that, although urazoles are readily oxidized by most oxidants, sometimes these reactions are hard to perform because of two interrelated issues, as the chemoselectivity of the oxidant and the reactivity of the resulting TAD compounds. Furthermore, the isolation of TAD reagents from reaction mixtures can be challenging.

Ideal oxidation methods should thus be highly chemoselective, give one single TAD reaction product, and generate no waste products or only waste products that are readily removed. Neither the oxidant nor its reduced forms should react with the TAD compound.

The common procedures to generate TADs are based on N-containing oxidants. In early work, nitric acid was used as a general large-scale oxidant (i.e., a few tens of grams) for nonfunctional urazole components. However, only moderate yields are obtained under these strongly acidic and oxidative conditions, which also have a severe impact on the stability of the generated TADs.

In order to greatly facilitate the workup, heterogeneous oxidants such as NO_2/N_2O_4 are highly preferred from a practical point of view. Hence, gaseous NO_2/N_2O_4 quickly gained popularity as a heterogeneous acid-free alternative to effect urazole oxidations. Consequently, this protocol can nowadays be regarded as the method of choice to convert a wide range of (functional) urazole

substrates in a traceless manner. Nevertheless, practical and safety considerations must be made when handling these gaseous and toxic reagents, especially in laboratory environment. Moreover, as a result of possible competitive electrophilic aromatic substitution, N_2O_4-based oxidation methods should not be used in the presence of electron-rich aromatic substrates or other nucleophilic species.

The laborious handling of toxic and gaseous reagents led to the development of solid-based heterogeneous systems. For example, silica-supported nitric acid can be used as a heterogeneous nitrogen (IV) oxide alternative for oxidations on a scale of hundreds of milligrams, and it has the ability to oxidize a broad substrate scope. DABCO−Br, on the other hand, generates a mild active halogen species in situ and is typically used on a multigram scale.

Finally, for highly sensitive (functionalized) urazoles, *in situ* oxidation in the presence of or just prior to adding the TAD coupling partner is recommended. Here, the choice for a mild oxidant such as NBS or DBH can also be required, since they are compatible with many functions. Nevertheless, such "one-pot" approaches can be very efficient for many applications.

3.2.2. TAD reactivity in pericyclic reactions

The most important cycloaddition reactions involving TADs are the Diels-Alder, the Alder-ene and the [2+2] cycloaddition reactions.

- Diels-Alder (DA) reaction:

The Diels-Alder (DA) reaction is a highly atom economical, efficient and applicable bond-forming reaction, where two new σ-bonds are gained. Moreover, up to four new stereocenters, with very pronounced and predictable levels of chemo-, stereo-, and regioselectivity, are generated.[40] Generally, the reaction requires elevated temperatures, but many DA reactions can also be affected at low temperature by using catalysts.

Theoretically, the bond-forming process can be reversed, giving a retro Diels-Alder (rDA) reaction that releases the original reaction partners. This dynamic feature of the DA/rDA reaction has been used in a range of interesting applications: in organic synthesis, it was used as temporary protection of dienes or to capturing and releasing transient reaction intermediates.[41] In polymer chemistry, the rDA reaction has been used to design covalently adaptable materials that show interesting properties, such as healing and remendability.[42]

In this context, the exceptional reactivity of TADs can be appreciated by the fact that the reaction with "good" Diels-Alder dienes is almost instantaneous and quantitative even at quite low temperatures (-78 to -50 °C, e.g.). Anyway, exciting examples of Diels-Alder reactions involving

TADs are surely the ones with less reactive dienes. In this sense, the reaction between anthracene and TADs is very fast at room temperature, but it is also one of the few DA reactions that shows reversibility at room temperature (*Scheme 10*).[43]

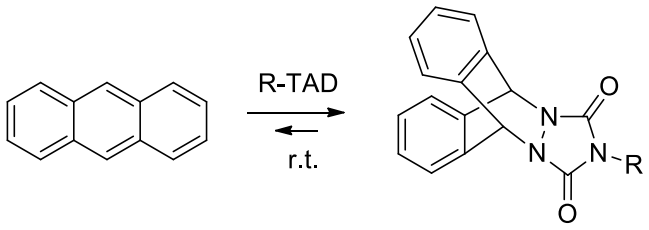

Scheme 10 – Diels-Alder reaction of TADs with anthracene.

In the case of styrene, it does normally not react with dienophiles even at elevated temperatures. Anyhow, a 1:2 adduct *via* a highly reactive diene intermediate (that cannot be isolated) is quantitatively formed when 2 equivalents of TADs are placed to react with 1 equivalent of styrene; by using 1 equivalent of TAD, half of the styrene is converted into the bis-adduct with TAD (*Scheme 11*).[44]

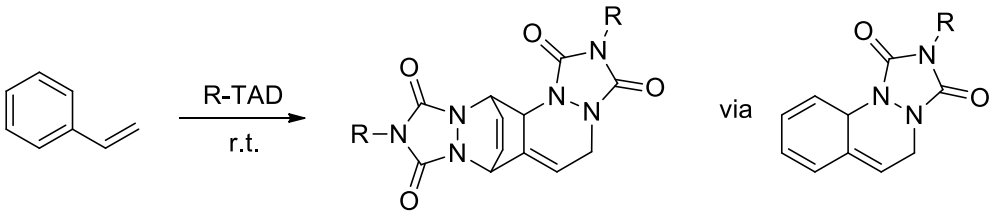

Scheme 11 – Double Diels-Alder reaction of 2 molecules of TADs with 1 of styrene.

Finally, other researchers have found that, while benzene, naphtalene, and phenantrene do not readily react with TAD compounds, Diels–Alder adducts of these compounds can be obtained by a photochemical Diels–Alder reaction or with the aid of an acid catalyst (*Scheme 12*).[45]

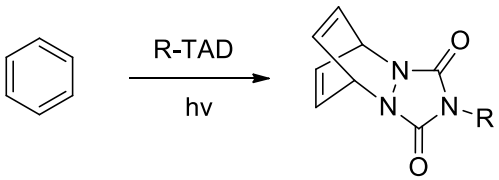

Scheme 12 – Photochemical Diels-Alder reaction of TADs with benzene.

- Alder-ene (AE) reaction:

The AE reaction (or just ene reaction) can be defined as the reaction of an alkene bearing an allylic hydrogen (the ene) with an electrophilic double bond (enophile). The general scheme is depicted in *Scheme 13*.

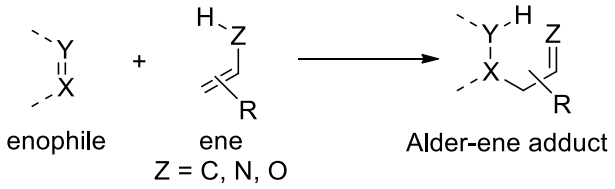

Scheme 13 – General representation of the Alder-ene reaction.

It belongs to the general class of pericyclic reactions and it comprises the migration of a σ-bonded hydrogen atom, the formation of a new C–C σ-bond at the expense of a C–C π-bond, and the displacement of the initial π-bond.[46]

Despite the great potential in organic synthesis of the Alder-ene reaction, its applications have been limited as compared to the DA reaction. One reason could be the unfavourable activation entropy and enthalpy, since the AE reaction is related to highly ordered transition state with relatively poor orbital overlap, resulting so in slow reaction rates. Therefore, this transformation often requires extreme conditions (high pressure and temperature), especially in the case of intermolecular reactions. A possible boost could be the use of Lewis acid catalysts, that can ensure enhanced reaction rates at lower temperature; anyhow, serious regioselectivity issues can emerge, especially when more than one allylic hydrogen is present in the ene substrate.[47]

All these features have limited the AE reaction mostly to intramolecular applications. However, the use of highly reactive enophiles (i.e., TADs) has been fundamental to achieve reliable and even selective intermolecular reactions. In this sense, the reactivity of TADs as enophile is prominent and many examples of Alder-ene reactions of TADs with simple alkenes have been reported to happen at room temperature, giving N-allylurazole adducts in quantitative yields, as shown in *Scheme 14*.

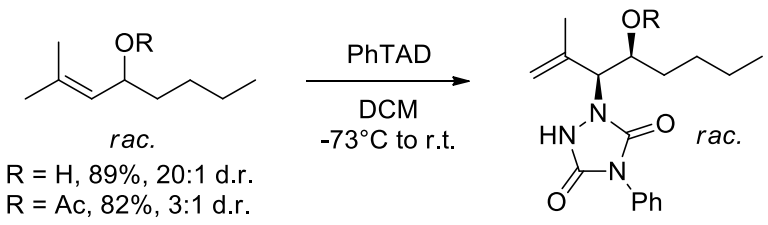

Scheme 14 – Regio- and diastereo-selective Alder-ene reaction of 4-phenyl-TAD with chiral allylic alcohols.

The mechanism of TAD-based AE reactions has been a matter of debate for a long time. The six-electron concerted pericyclic process, commonly indicated as the major mechanism for Alder-ene processes, has been initially proposed. Anyhow, experimental and thermodynamical data have indicated as the more probable mechanism the stepwise route involving the formation of the zwitterion aziridinium imide (AI), as depicted in *Scheme 15*.[48]

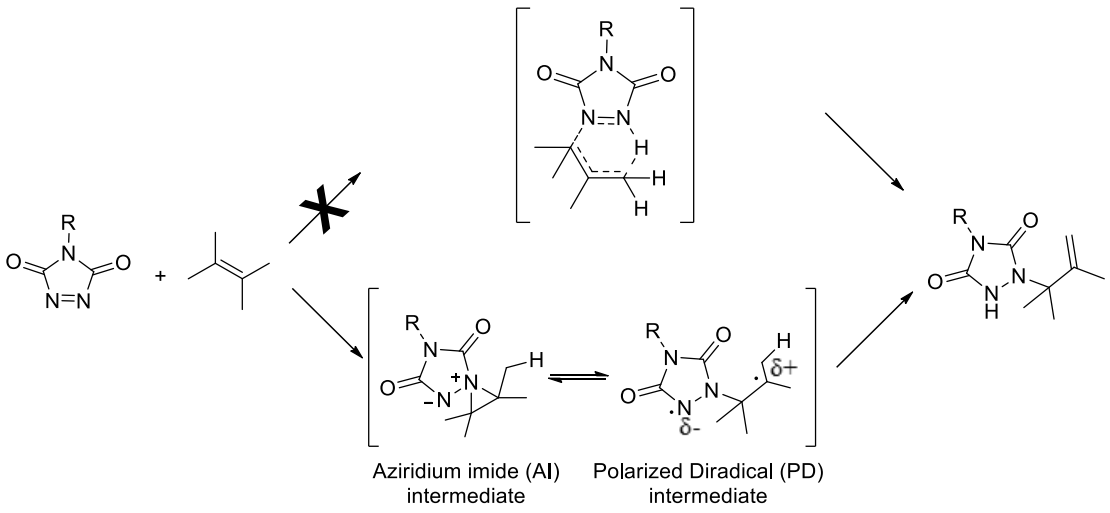

Scheme 15 – Stepwise route of the Alder-ene reaction of TADs with alkenes.

The exact mechanism for subsequent hydrogen transfer is not completely clear. A possible interpretation has been suggested by Squillacote and co-workers, where an open polarized diradical (PD) intermediate is formed; moreover, they assess a solvent-dependence in this mechanism.

Finally, likewise the Diels-Alder reaction, even for the Alder-ene transformation the retro-reaction is theoretically possible and it largely depends on the activation barriers for these reactions. Briefly, it could be roughly summarized that the higher the activation barriers for a reaction, the lower the tendency to give the retro-reaction. In this way, since the (very) high activation barriers for typical Alder-ene reactions, it is not unexpected that the retro Alder-ene (rAE) reaction has only rarely been observed in comparison to the retro-DA reaction.[49] Indeed, most of the described thermoreversible AE reactions require pyrolysis-type conditions and are thus of limited value in synthetic applications. Anyhow, on the basis of the much higher kinetic reactivity of TAD compounds as enophiles, one might expect to find AE reactions with these reagents that can be reversible in reasonable temperature intervals.[40] However, so far only one example has been reported in literature and it will be discussed in *Chapter 3.2.3*.

- [2+2] cycloadditions:

In classical pericyclic reactions, [2+2]-cycloadditions usually require π-bonds to approach each other in an antarafacial way, that is sterically impossible. Hence, in the large number of cases, this cycloaddition is a thermally forbidden process, achievable with other processes like photochemical conditions. However, when the reaction is performed with more sterically accessible two-electron π-systems, such as ketenes, an antarafacial addition mode is possible and orbital symmetry-allowed thermal concerted [2+2]-cycloadditions can occur.[50]

In this context, TADs allow an orbital symmetry for antarafacial additions, so they are optimal candidates for a thermal [2+2]-cycloaddition. Although a concerted thermal [2+2]-cycloaddition cannot be excluded for reasons of orbital symmetry, even in this pericyclic reaction an aziridinium imide intermediate is probably involved, as suggested by Seymour et al., and a stepwise reaction is preferred rather than the classical concerted pattern. In this context, after the AI intermediate formation, it rearranges to the neutral diazetidine ring, as shown in *Scheme 16*.[51]

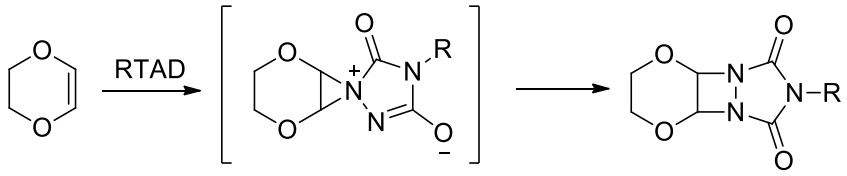

Scheme 16 – TAD-involving (2+2) cycloaddition, through AI intermediate.

Especially, electron-rich alkenes are good substrates for [2+2]-cycloaddition involving TADs. Anyhow, a mandatory requirement for the substrates is the absence of allylic hydrogens, since they will be transferred to give the thermodynamically preferred AE-type adducts.

3.2.3. TAD reactivity toward activated aryl systems

In electrophilic aromatic substitution (EAS) reactions, TAD compounds act as suitable electrophiles for highly activated aryl systems. Suitable substrates include dialkoxy- and trialkoxy-substituted aryls, as well as electron-rich nitrogen containing aryls, such as various aniline derivatives and indoles. The formation of charge-transfer complexes has also been observed in these reactions, although it is unclear if they are involved in the reaction pathway. Quite recently Breton was able to expand the substrate range for less-activated aryl substrates (including some dialkyl-substituted benzenes) by using trifluoroacetic acid as a catalyst or by simply shining visible light on the reactions.[52]

From a mechanistic point of view, it is interesting to point out again that an aziridinium imide (AI) intermediate is probably involved. This outcome arises from the consideration that both reactants are neutral, so the expected carbocationic intermediates of EAS are actually zwitterions that can also exist as an AI intermediate, as shown in *Scheme 17*.[40]

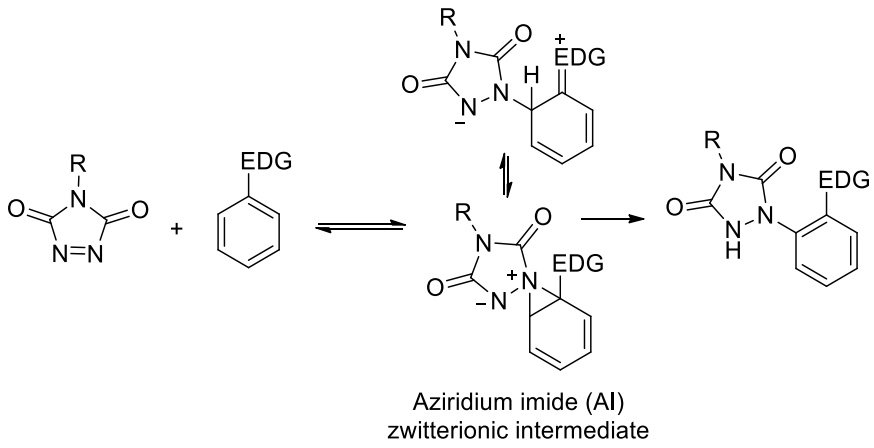

Scheme 17 – TAD-involving EAS, through AI intermediate.

The initial addition intermediate needs to undergo a proton transfer, that yields a 1-aryl-substituted urazole compound. Although this TAD reactivity mode can be quite pronounced, surprisingly, only a moderate number of studies have been reported.[53]

One of the most important examples of TAD reactivity with activated aromatic system is the reaction of TADs with "hindered" indoles, first proposed by Baran *et al.* in 2003. In this work, the authors used a volatile TAD (4-methyl-TAD) to thermo-reversibly protect a 2,3-disubstituted indole, as shown in *Scheme 18*.[54]

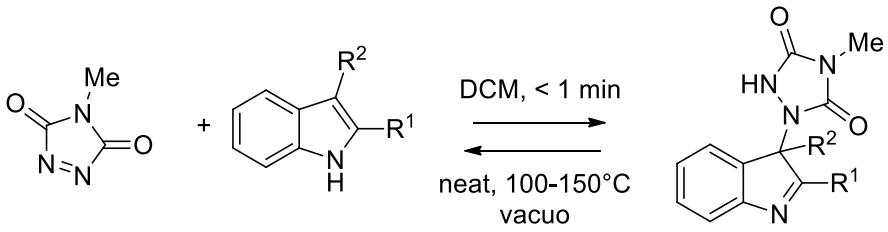

Scheme 18 – Thermo-reversible reaction of TADs and 2,3-disubstituted indoles.

The formed product is formally the Alder-ene adduct, resulting from the dearomatization of the indole functionality, where the indole N-H proton is transferred and the result is the stabilization of the AE adduct. Anyhow, the tendency to rearomatization can be used as a thermodynamic driving force to achieve the retro-reaction: this is the basis of the thermo-reversibility of the reaction of TADs and indoles. So, by simply heating the AE adduct, a retro-AE will take place, allowing the removal of the volatile TAD reagent and giving so the free indole moiety.

At this point, it is important to note that the reaction of 2,3-disubstituted indoles can also be considered as an "aborted" or shunted EAS reaction of TAD with an indole substrate, wherein the rearomatization step is prevented. In this context, the presence of a hindered group (i.e., *tert*-butyl) at position 2 of the indole ring and the presence of an alkyl group in position 3 have been proven to be fundamental to prevent the rearomatization, obtaining so the AE rather than the EAS product.

The dynamic high temperature reaction of the TAD–indole adduct formation was not only found to be a very clean and reliable transformation, it was also discovered that the liberated TAD moiety could be reacted (*in situ*) with another substrate, such as a conjugated diene, in a highly orthogonal way (*Scheme 19*).

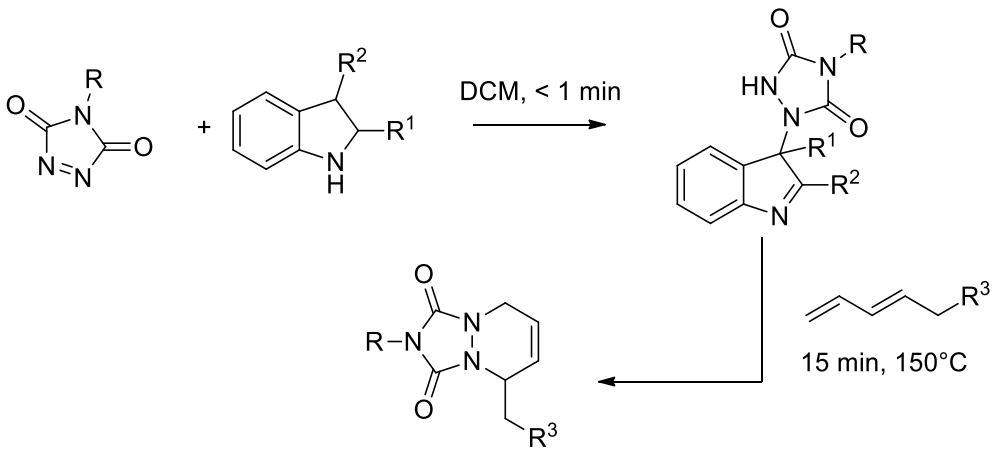

Scheme 19 – Thermal liberation of TADs from TAD-indole adducts an orthogonal reaction with conjugated dienes.

Trying to generalize the remarkable dynamic behaviour in exchanging 'clickable' TAD group between two different molecules (indole and conjugated diene), it was coined the concept of a 'transclick' reaction.[55] A transclick reaction has been defined as "any covalent linking process that can subsequently be triggered to form a new bond with an alternative or orthogonal reaction partner, and at the same time release one of the original binding partners, in which both bond forming steps meet the usual requirements for click reactions".

Finally, it is relevant to highlight the similar reactivity of TADs with indoles and phenols. Indeed, even the TAD reactions with phenols could be considered as an Alder-ene reaction followed by a keto-enol tautomerization to restore aromaticity.[56] The phenolic proton indeed seems to be implicated in the EAS reaction with TAD, as simple monoalkoxyaryls are much less reactive substrates, while phenols are excellent substrates, especially in an aqueous medium, that give selective and rapid formation of arylurazoles (*Scheme 20*).

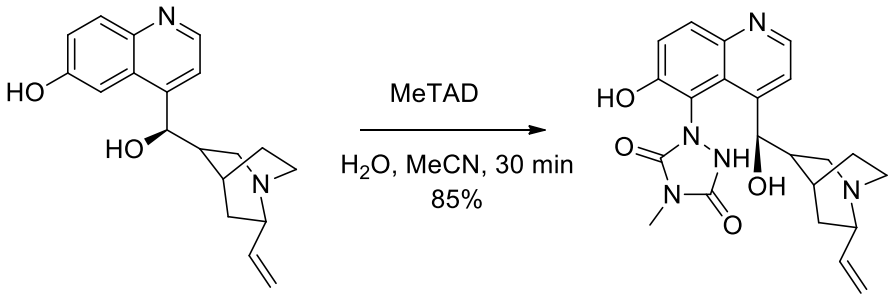

Scheme 20 – Selective arylurazoles synthesis in phenol-containing compounds.

3.3. TADs in macromolecular context

Besides the use of TADs as versatile synthetic tool, their use in polymer materials and in macromolecular context is probably the most important field of applicability.

The attention on TADs as versatile chemical in polymer applications started from the early stage, so from the development of the Cookson's procedure. Most of the early literature appeared in the 1970s and mainly dealt with the modification of polydienes. Nevertheless, the use of TADs in polymer chemistry has been further explored in other cases, such as for the homo- and hetero-polymerization of TADs or their use in surface modification of polymer materials.

Anyhow, the high reactivity of TADs is very important also for the click-like modification of other macromolecules, such as peptides, proteins, plant oils and others.

All these topics will be discussed in the following chapters.

3.3.1. Homo- and co-polymeryzation of TADs

The direct homo-polymerization of TAD compounds is a somewhat exotic field and only few numbers of examples have been reported. For instance, in 1970, Pirkle and Stickler investigated the direct polymerization reaction of TAD-based molecules to obtain polymers with all-nitrogen backbone, as reported in *Scheme 21*.[57]

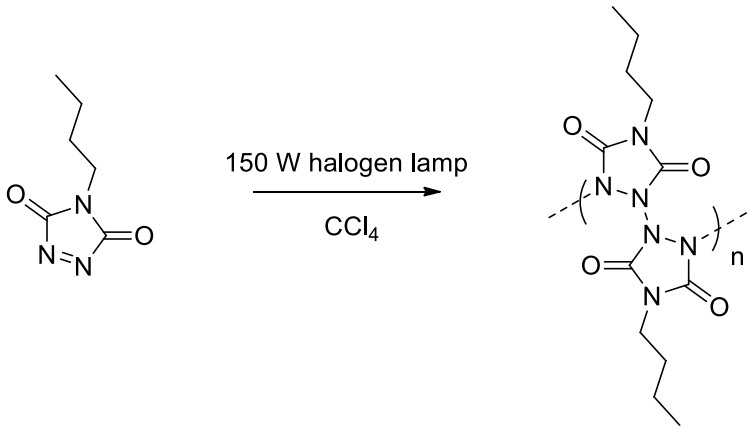

Scheme 21 – Direct homo-polymerization of mono-functionalized TADs.

In this report, a 0.3 M carbon tetrachloride solution of 4-butyl-1,2,4-triazoline-3,5-dione (BuTAD) was irradiated with a halogen lamp for 8 min, giving a colorless polymer with an average molecular weight of 4,200 g/mol (around 20 monomer units). However, the obtained polymer had a very limited lifetime in the original CCl_4 solution and the depolymerization slowly occured within a time frame of 30 min to a few days. Moreover, the polymer was fully degraded within minutes in the presence of trace amounts of pyridine. The same experiments did not give polymers when aromatic TAD components were used.

An alternative approach to directly polymerize TAD compounds is the homopolymerization of bifunctional TADs (or bisTADs).[58] In the presence of catalytic amounts of pyridine, a solution of a bifunctional TAD molecule (3,3'-dimethyl-4,4'-bis(1,2,4-triazoline-3,5-dione)diphenyl) in 1,2-dichloroethane can be gradually converted to a polymeric structure over the course of 30 min to 1 h. The obtained polymers were fully characterized by IR and NMR to support the assigned structure, shown in *Figure 13*, and were also shown to have a remarkable thermal stability (decomposition around 300 °C).

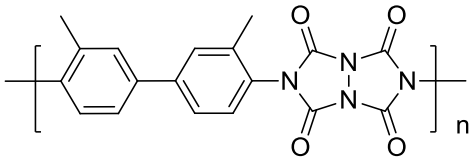

Figure 13 – Chemical structure of polymer obtained by the homo-polymerization of bisTAD.

Moving to more interesting hetero- and copolymerization examples involving TADs, the intriguing reactivity of TADs toward a wide range of relatively simple reaction partners has been used as possible tools for a copolymerization. For instance, exploiting the powerful electron-acceptor activity of TADs, Butler *et al.* have showed that 4-phenyl-1,2,4-triazoline-3,5-dione (PhTAD) could react

with a variety of electron-donating alkenes to yield alternating copolymers. An example could be the combination with vinyl ethers.[59] The reaction of PhTAD with ethyl vinyl ether in dichloromethane (DCM) resulted in a copolymer with a rather low Mn (up to 2,400 g/mol). In this mechanism, it is most likely involved a cationic ring opening-type polymerization of the initially formed zwitterionic aziridinium-type adducts, as depicted in *Figure 14*.

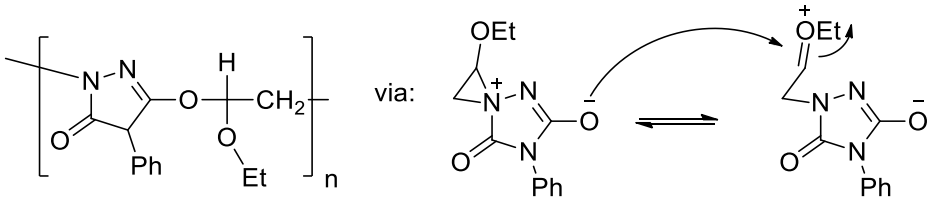

Figure 14 – Copolymer of PhTAD and ethyl vinyl ether.

Another pronounced reactivity, very useful in polymer applications, is the one as dienophiles and/or enophiles. In this context, bisTAD molecules, such as 4,4'-methylenebis(1,4-phenylene)-di-1,2,4-triazoline-3,5-dione (MDI-bisTAD), has been used to form polymers in a stepwise manner via an AA−BB monomer approach.[60]

Additionally, consecutive Diels-Alder and/or Alder-ene reactions have been explored. A very interesting example can be found in the work of Butler and co-workers, where bisTAD molecules have been combined with styrene.[59] TAD can react with styrene in an initial slow Diels−Alder reaction, in which the aromaticity of styrene is lost. The resulting 1:1 adduct, however, undergoes a faster second reaction. Careful investigations showed that, in this second reaction, a 1:2 ratio is obtained for respectively the Diels−Alder and the Alder-ene adduct. This cascade-type reaction of styrene with bisTAD has been used as a propagation mechanism in the copolymerization of polymers with molar masses up to 36,000 g/mol (*Scheme 22*).[61]

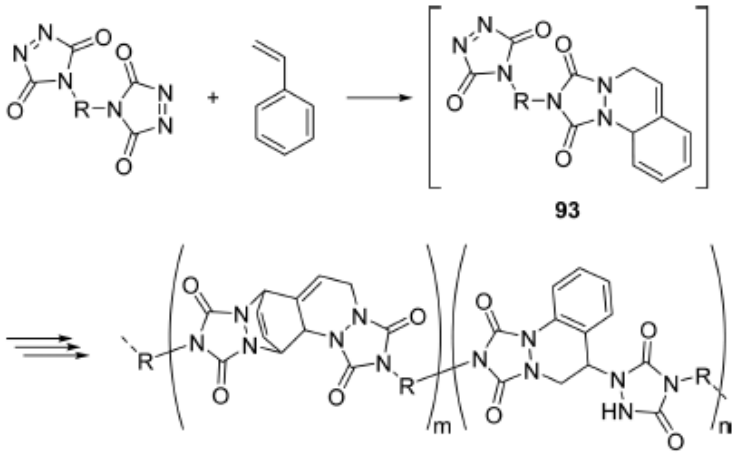

Scheme 22 – Copolymerization of styrene and bisTAD molecules.

A similar reactivity was observed in the reactions of TAD molecules toward β-dicarbonyl components. In particular, since these compounds were found to react with two TADs via two consecutive Alder-ene reactions on the enol form, hence bisTAD compounds have been effectively used as monomers in a number of copolymerizations with β-dicarbonyl compounds, as shown in *Scheme 23*.[62]

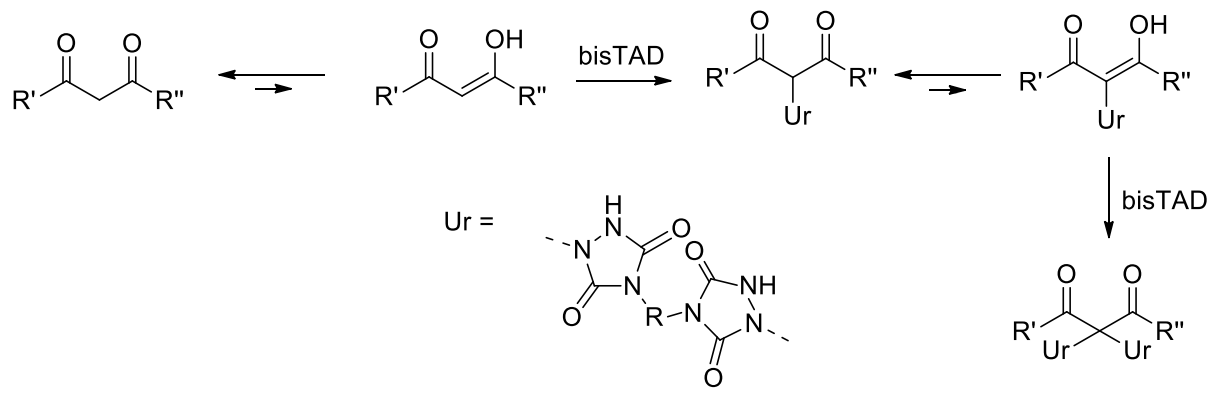

Scheme 23 – Copolymerization of β-dicarbonyl components and bisTAD molecules.

Although the low molecular weight model studies for the double Alder-ene reaction showed promising results, all acquired polymers had very low molar masses, as a result of precipitation of oligomers in the reaction medium.[63]

3.3.2. Functionalization of polymer matrices with TADs

The major application of triazolinediones in polymer science, so far, lies in the low-temperature modification of polydienes, both in academic and industrial context.[64] The alkene-TAD reaction is very versatile and gives an atom-efficient and site-selective way to functionalize substrates quite hard to chemically modify in a reliable way (*Scheme 24*).

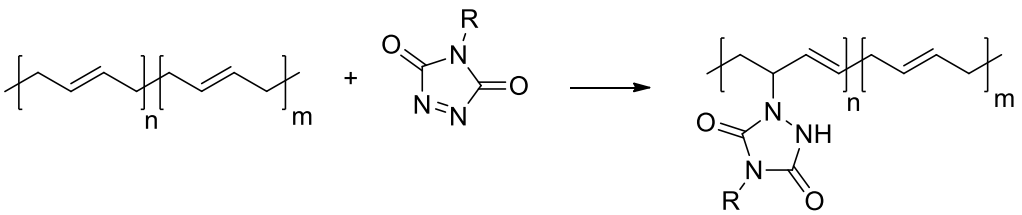

Scheme 24 – Functionalization of polydienes with TADs.

A wide range of polydienes (polybutadiene, polyisoprene, random styrene-butadiene copolymer, and a 1:1 alternating copolymer of furan and maleic anhydride) were modified with monofunctional TAD molecules. Although, theoretically, it is possible to add 4 mol of reactant per repeating unit (i.e., four "active" C−H bonds), the solubility of the obtained polymers plays a significant role, and the subsequent reactions are usually kinetically disfavoured. Polymers with modification degrees ranging from 5 to 100% can be obtained, in which the polymers with lowest conversion demonstrated elasticity, which was an indication for possible secondar supramolecular cross-linking reactions (higher conversion led to rigid amorphous polymers with high Tg).

Successive studies on TAD-functionalized polydienes have highlighted prominent cross-linking, supporting the hypothesis that the highly polar pendant urazole groups have pronounced inter- and intramolecular hydrogen-bonding interactions, which can be related to properties such as elasticity, changes in solubility character, thermal behaviour, and tensile strength.[65] Because the attached urazole groups contain a quite acidic proton (pKa ≈ 5), further modifications of this strong hydrogen bond donor are relatively straightforward. Following a simple acylation reaction that "caps" this acidic N-H group, polymers with a wider range of properties can be obtained by using different acid chloride modifiers, while the supramolecular self-associating behaviour is also blocked (*Figure 13*).[66]

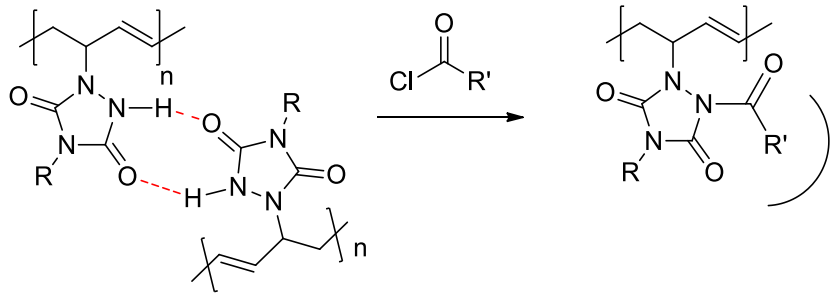

Figure 15 – Secondary cross-linking of a polybutadiene functionalized with PhTAD and the acylation of acidic urazole proton, blocking the self-associating behaviour.

Next to alkenes, electron-rich aromatic rings can also be included in simple linear polymers as reaction partners for TAD. On the one hand, vinyl-type (co)monomers, having an activated aromatic ring, can be easily synthesized and incorporated into linear polymer chains, which can then be functionalized or cross-linked with suitable TAD reagents, as illustrated in *Figure 16*.[67]

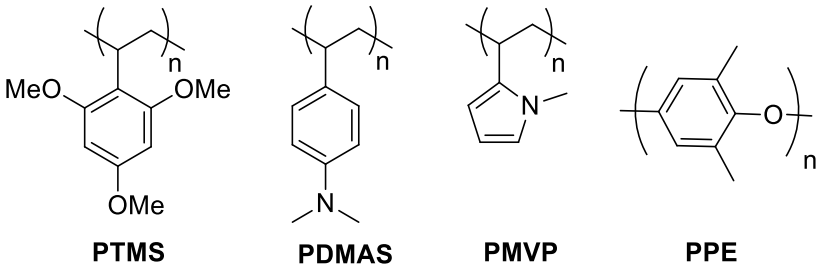

Figure 16 – Synthesized polymers for modification with TAD via EAS: poly(2,4,6-trimethoxystyrene), poly[4-(N,N-dimethylamino)-styrene], poly(N-methyl-2-vinylpyrrole), and poly(oxy-2,6-dimethyl-1,4-phenylene).

Poly(2,4,6-trimethoxystyrene) (PTMS) reacts only very slowly with PhTAD (10 days at room temperature, 2 days in boiling DCM) while the reactions with poly(4-(N,Ndimethylamino) styrene) (PDMAS) and poly(N-methyl-2-vinylpyrrole) (PMVP) were much faster. For the latter two materials, the TAD functionalization reactions proceed readily at room temperature and resulted in, respectively, 90% and 97% incorporation of PhTAD.[68]

On the other hand, a whole range of new polymer blends containing poly(oxy-2,6-dimethyl-1,4-phenylene) (PPE) were investigated for different applications at the end of the 1980s. As the repeating unit in these materials is actually a rather activated aromatic ring, these polymers can be directly modified using the EAS reaction with TAD at room temperature, as reported in the work Stadler and coworkers.[69] By addition of the highly polar urazole groups, physical linkages to other polymers and improved adhesion were achieved. With the goal to modify commercial blends, mixtures of polystyrene (PS) and PPE were functionalized with TAD to various extents. It was shown that PS and PPE, modified with up to 10% PhTAD, were still miscible, making this a valuable synthesis route for the modification of PPE blends.

Finally, the surface modification of polymers with TADs has been investigated. For instance, Cutts *et al.* has been treating surfaces of elastomers with TAD components (both mono- and bifunctional).[70] In this way not only the adhesion could be improved but also resistance to peeling with flexible paints was improved while the surface tack of the elastomers was reduced. This proved to be an advantageous method over the prior one (chlorination and halogen donor techniques), particularly because the applied triazolinediones are relatively mild and noncorrosive.

3.3.3. Click-like applications of TADs in macromolecules

Barbas and co-workers were the first to explicitly report on TAD reagents as useful tools for click chemistry, in their 2010 paper on a "click-like" conjugation strategy for natural peptide and protein

substrates. Herein, Barbas explored the use of TADs as an efficient tyrosine bioconjugation strategy.[71]

Although TAD molecules are known to react slowly with phenol substrates via an EAS pathway, Barbas observed that this reaction is greatly accelerated in aqueous medium. Conversely, a similar EAS or AE-type reaction with tryptophane side chains (indole core) is not accelerated, offering a way to site-selectively label tyrosine residues in natural peptide and protein substrates (*Scheme 25*).

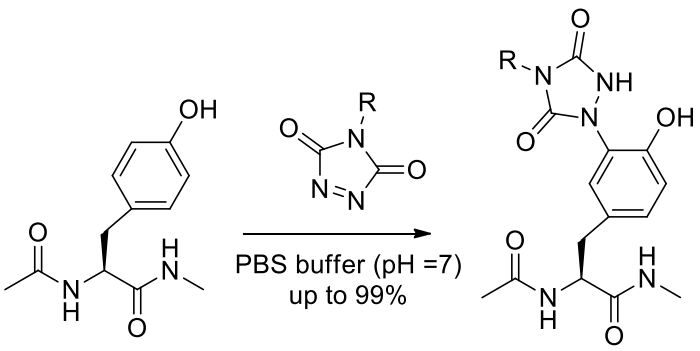

Scheme 25 – TAD-mediated bioconjugation of tyrosine.

Following the initial report, Barbas and co-workers showed the true potential of this tyrosine bioconjugation with a range of additional experiments and a systematic study of TAD orthogonality toward different amino acid side chains.[72]

In this way, they used a synthetic decapeptide with unprotected side chains, containing all of the potentially reactive amino acids, Trp, Ser, Glu, Lys, Arg, and His, as a stringent chemoselectivity test. Even when 3 equiv of a TAD reagent was applied, this peptide was site-selectively functionalized at the tyrosine residue (*Scheme 26*).

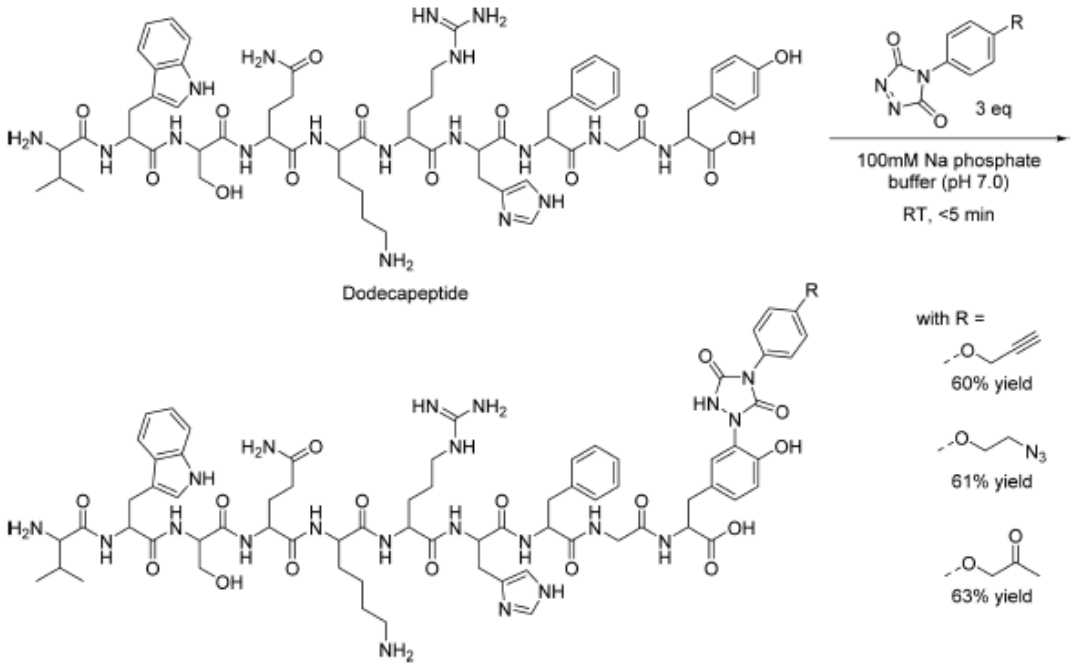

Scheme 26 – Tyrosine click reaction of a model decapeptide, including all possible TAD-reactive side chain residues, demonstrating the chemoselectivity and efficiency of the reaction.

As reactions with primary amines are typically hard to avoid, the success of this click-like tyrosine conjugation method can also be explained by the use of a buffered medium (pH 7 phosphate buffer), which will keep most of the free amines (on the lysine and N-terminal residue) in their unreactive protonated form. Purification by using reversed-phase HPLC yielded pure labelled peptides in approximately 60% yield.

Another important point of click chemistry is that it can bring the power of chemical synthesis to unprecedented or unsuspected applications in "unusual" contexts. In this context, the use of TAD-based click chemistry was expanding, Du Prez and coworkers showed interest in natural plant oils as complementary partners for TAD reagents.[73] Although most plant oils contain a large number of olefinic bonds, only very limited chemical transformations can be affected on these natural synthetic handles, often requiring catalysts and/or harsh reactions conditions. In contrast with this tendency, the initial study of simple unsaturated fatty acid methyl esters showed a specific and selective reactivity toward TAD reagents.[74] As a result of the nature of the Alder-ene reaction with isolated olefins, the fatty acid unsaturations actually remain present in the TAD-modified lipid tails and can even be used in a second, markedly slower Alder-ene reaction with a TAD reagent (*Scheme 27*).

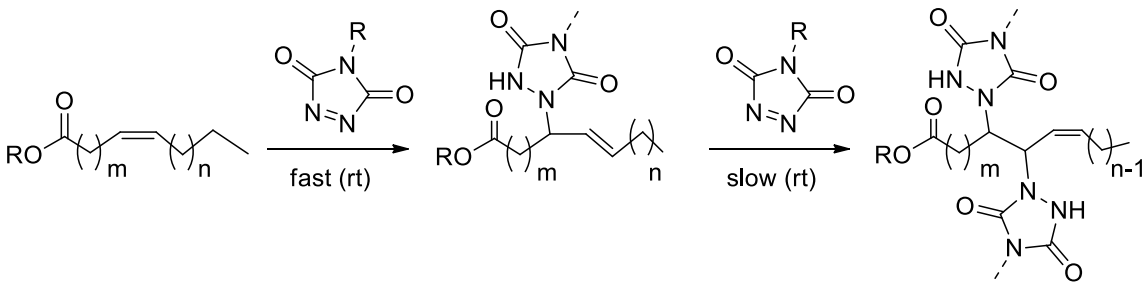

Scheme 27 – Clicking lipids: unsaturated fatty acid derivatives react selectively and specifically with TADs.

The versatility of this click reaction for unsaturated fatty acids was then demonstrated by cross-linking crude plant oils with bifunctional TAD molecules. By studying the gelation times (occurring within minutes at room temperature) and determining the thermal properties of the obtained cross-linked materials, a general trend in plant oil reactivity could be perceived, showing that a higher percentage of polyunsaturation resulted in both shorter gelation times and a higher Tg of the obtained plant oil network.

Another example of TAD-based chemistry as a versatile platform for click chemistry applications, mainly in a macromolecular context, is in clicking and unclicking reactions.[73] As an initial demonstration of dynamic TAD-click reactions, Du Prez and Winne reported a linear indole-functionalized polyurethane, making use of an indolediol, which was then cross-linked with a bifunctional TAD reagent. The resulting PU-network, containing TAD-indole cross-links, could be molded, recycled, and processed at elevated temperatures without loss of material properties. In one illustrative test, the stiff cross-linked material was broken into small fragments and then put into a mold under pressure for 30 min at 120 °C. A pristine sample was retrieved from the mold after cooling (*Figure 17*). While this last test was repeated seven times, a similar storage modulus was achieved each time.

Figure 17 – Thermo-reversible PU materials, having TAD-indole cross-links.

Concerning the unclicking step, the most important case is the already reported TAD-indole system. Anyhow, it should be considered that the fully "reversion" of this click reaction is feasible only in the case of volatile reagents, because the indole and TAD reagents will re-form the adduct quantitatively at room temperature.[40] However, by adding an alternative reaction partner for TAD, which is known

to result in an irreversible adduct formation, the TAD−indole adduct can be completely unclicked, while another substrate is now clicked onto the TAD reagent: this kind of transformations is also known as “trans-click” reaction and it is shown in *Scheme 28*.

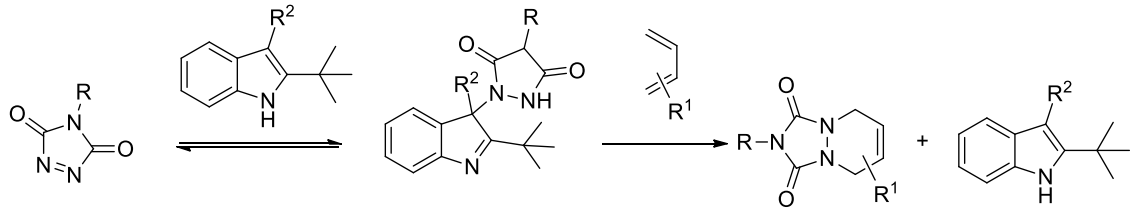

Scheme 28 – Transclick reaction of TAD-indole adduct, in presence of a diene.

Indeed, a TAD and an indole react in an equimolar ratio to afford the TAD-indole AE adduct. When this adduct is heated in the presence of 1 equiv of a conjugated diene, the TAD molecule is completely and selectively transferred to this diene, resulting in a new Diels−Alder adduct and the release of the original indole compound without any side reactions. In a recent work, the newly introduced “transclick” concept was used to develop rewritable polymer brush micropatterns.[75] For this, indole-functionalized surfaces were first patterned with a TAD-tagged atom transfer radical polymerization initiator, which was subsequently used in a surface-initiated polymerization. As a result of the dynamic nature of the TAD−indole connection at elevated temperature, (polymer) patterns could be erased, leaving the regenerated indole substrate ready for the printing of new patterns (*Scheme 29*). The robustness of this rewritable method was demonstrated by four repetitions on the same surface. In principle, this concept could be further expanded to selective and “programmed” transclick reactions from one substrate to another.

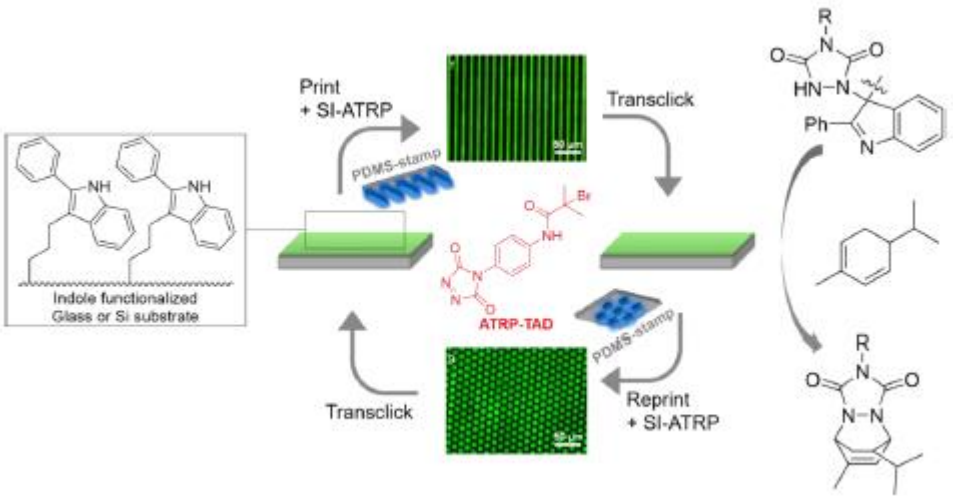

Scheme 29 – Rewritable surfaces: heterogeneous TAD click and transclick chemistry with indole-functionalized substrates.

3.4. Results and discussions

Since the introduction of the click-chemistry, un incalculable number of research has focused their attention on finding and development innovative approaches that are in line with the principles of the click-chemistry. In this context, a "process-chemistry" point of view is fundamental to achieve a successful process, since the most important goal of organic synthesis should be: "(..) not production of new compounds, but production of properties" (George S. Hammond, Norris Award Lecture, 1968).[3]

Additionally, it is important to use facile methods of synthesis and purifications, trying both to avoid harsh reaction conditions and to ease the product separation (e.g., by precipitation or distillation). Therefore, a perfect transformation is a modular reaction involving high-energy reactants (in turn, obtained through "smart" approaches), exploiting a thermodynamic driving force to achieve the formation of products with high regio- and stereo-selectivity.

With this view, triazolinediones (TADs) are promising reactants in many click-like processes, such as cycloadditions (in particular, Diels-Alder and Alder-ene reactions), bio-conjugation of peptides and proteins, clicking-unclicking processes and others. TAD reagents are highly reactive electrophiles, dienophiles and enophiles, showing a strong preference for orbital-controlled reactions with electron-rich partners having a delocalized π-cloud, including simple alkenes. Moreover, they are known as the most reactive dienophile and enophile bench-stable, with lifetime several times higher respect to comparable reagents, like singlet oxygen and nitrosocarbonyl compounds.

In the proposed work, made during my semester as exchange PhD student at University of Ghent (UGent) in the research group of prof. Johan Winne, it has been deepening the reactivity of TADs with phenolic substrates. From the literature, the most important examples are the tyrosine bioconjugation modifications in natural peptides and proteins with TADs. In this context, it is widely proven that the modification results in an *ortho*-substitution of the tyrosine residue with an urazole moiety.

Anyhow, the reactivity of TADs with *ortho*-disubstituted phenols is almost unexplored, in particular with substrates having the Butylated Hydroxy Toluene (BHT, **1**) scaffold (*Figure 18*).

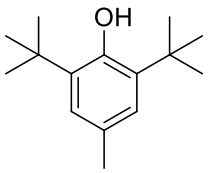

1

Figure 18 – Chemical structure of BHT **1**.

After the initial trials, it was surprisingly noted that the reaction of a model TAD with phenolic substates having the BHT scaffold led to the relatively fast formation of a thermo-reversible Alder-ene product. This intriguing reactivity is very similar to the one proposed by Baran and colleagues for the formation of indole-TAD adducts,[54] that formally are thermo-reversible Alder-ene products completely similar to phenol-TAD adducts proposed in this work. The most relevant similarities are the presence of hindered groups (i.e., *tert*-butyl, at position 2 of the indole ring and at positions 2,6 in the BHT scaffold). Moreover, the EAS is somewhat "shunted" in both cases, since the presence of substituents in position 3 (for indole) and in position 4 (for phenol). Hence, the presence of an alkyl substituent in position 4 in the BHT scaffold enables the dearomatization of the phenol ring, obtaining so the similar shunted EAS reaction observed in the indole-TAD case, wherein the rearomatization step is prevented. This feature it is at the basis of the thermal reversibility of synthesized adducts, since a source of heat can effectively promote the thermodynamic favoured rearomatization of the phenol ring to the detriment of the Alder-ene adduct.

In conclusions, TAD reactivity with phenol compounds was initially studied with model reactions and using small molecular weight compounds. The reactions were performed at room temperature and without catalysts, and some optimizations were based on finding suitable and non-harmful solvents for these reactions. All the adducts were examined through NMR, LC-MS and FTIR analyses; additionally, the thermo-reversibility of the adduct reactions were tested with "trans-click" reactions through off-line ^{1}H-NMR analysis.

After that, this particular reactivity was exploited in polymer applications. In particular, it was developed the synthesis of novel AA-BB polymers, made by the reaction of polyfunctional TADs and BHT-like phenols. These polymers were analysed through NMR, GPC, FTIR, DSC and TGA analyses, and the thermo-reversibility evaluated with "trans-click" reactions. Finally, it was tested the use of phenol-TAD adducts as "masked" cross-linker agent in the formation of polymer material starting from vegetable natural oil, using a strategy also known as "from oil to soil" approach.

3.4.1. Model reactions of TADs and phenols

At this stage, the reactions were performed by using low molecular weight reagents and at least one of the two reactants was mono-functionalized. The reactions can be divided in 3 sets:

- Reactions of TADs with *ortho*-substituted phenols (*Scheme 30*):

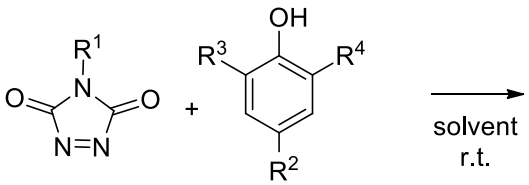

comp. **2** = R^1 = Ph
comp. **1** = R^2 = Me; R^3 = R^4 = *t*-Bu
comp. **3** = R^2 = H; R^3 = R^4 = *t*-Bu
comp. **4** = R^2 = R^3 = R^4 = Me
comp. **5** = R^2 = R^3 = Me; R^4 = *t*-Bu
comp. **6** = R^2 = Br; R^3 = R^4 = *t*-Bu

Scheme 30 – Model reactions of PhTAD **2** with *orto*-substituted phenols.

The model TAD reagent was 4-phenyl-1,2,4-triazoline-3,5-diones (PhTAD, **2**), while the phenolic substrates were BHT **1**, 2,6-di-*tert*-butylphenol **3**, 2,4,6-trimethylphenol **4**, 2-*tert*-butyl-4,6-dimethylphenol **5** and 4-bromo-2,6-di-tert-butylphenol **6**. Reactions outcome is schematized in *Figure 19.*

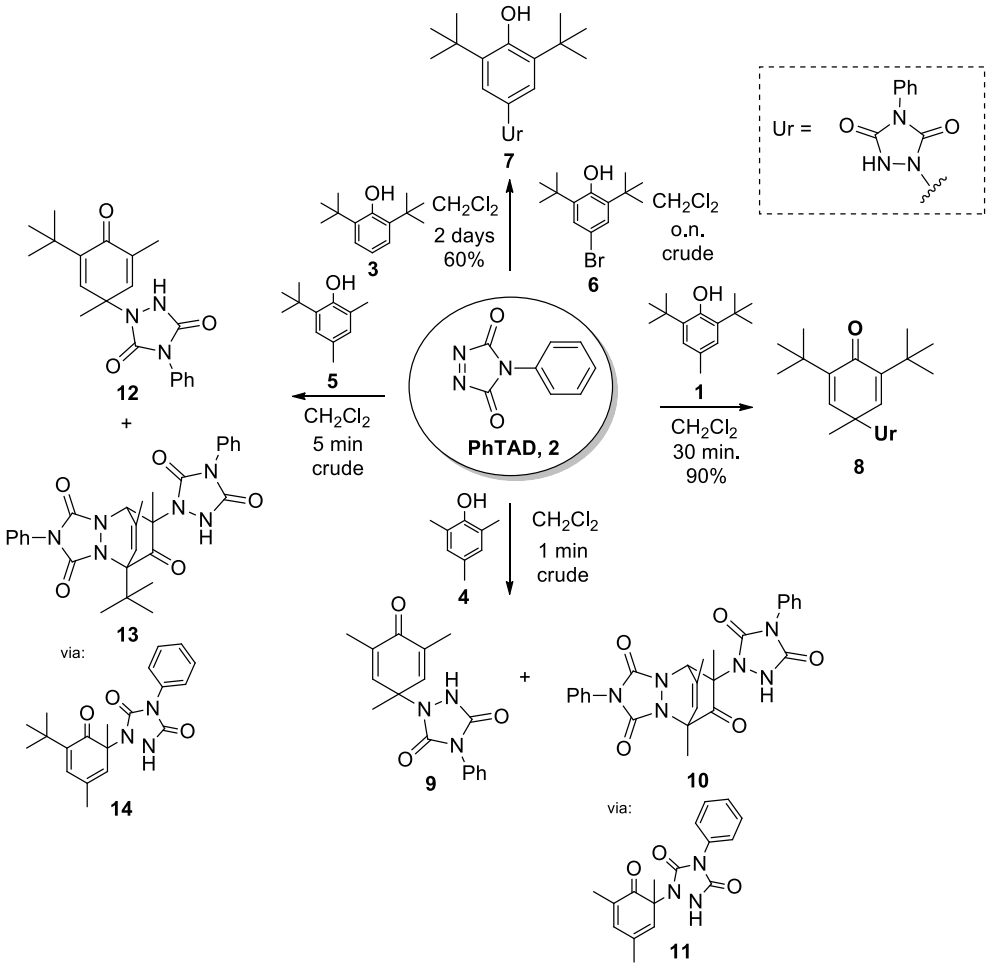

Figure 19 – Results obtained by the reaction of PhTAD **2** with phenols **1**,**3**,**4**,**5**,**6**.

When the phenolic substrate possessed hindered *orto* substituents and no substituent in *para* position (compound **3**), the reaction with PhTAD is slow and the main product was isolated through column chromatography with a yield of 60% and identified as the expected arylurazole formed by EAS in *para* position (**7**). The same product **7**, shown in *Figure 20*, has been identified when a bromide substituent is present in *para* position (compound **6**), as demonstrated by NMR analyses of the reaction crude.

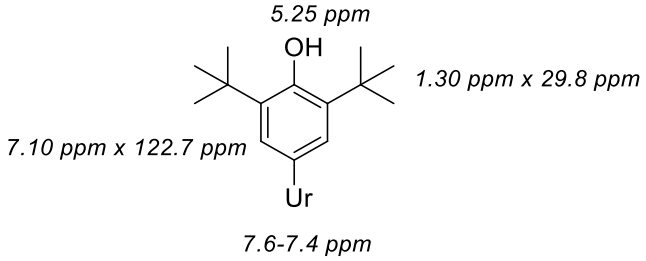

Figure 20 – Chemical structure of product **7** and the most relevant NMR signals (proposed through the interpretation of HSQC and HMBC 2D-NMR spectra).

Anyhow, the situation surprisingly changes when an alkyl substituent is present in *para* position, such as in the reaction of PhTAD **1** with BHT **2**. Indeed, in this case, the reaction was concluded within 30 minutes when dichloromethane was used as solvent. Moreover, the main product was isolated through column chromatography with an excellent yield (close to 90%) and fully characterized. In this sense, the coupling of ^{1}H-NMR, ^{13}C-NMR and 2D-NMR (HSQC and HMBC) have proven the formation of the Alder-ene adduct **8**, deriving by a shunted EAS transformation in which the rearomatization step is prevented by the presence of the methyl group in position 4 (*Figure 21*).

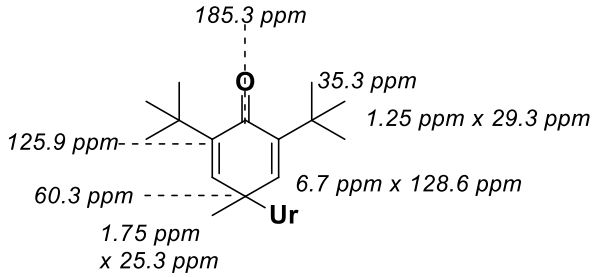

Figure 21 – Chemical structure of product **8** and the most relevant NMR signals (proposed through the interpretation of HSQC and HMBC 2D-NMR spectra).

In accordance to the literature of TAD-involving cycloadditions and EAS reactions, the formation of an aziridinium imide (AI) zwitterionic intermediate is more plausible than a direct pericyclic process and the possible mechanism for the synthesis of adduct **8** is depicted in *Scheme 31*.

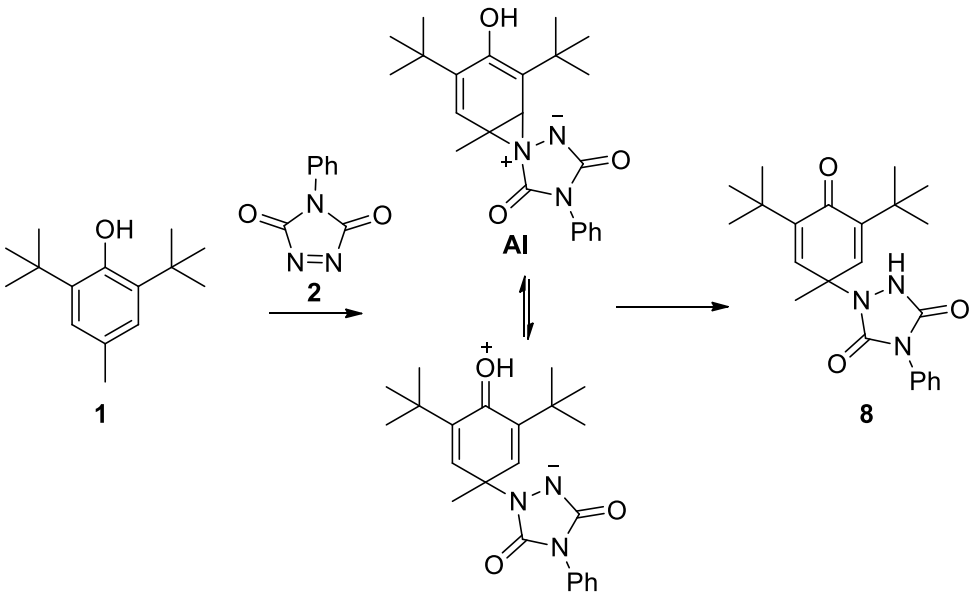

Scheme 31 – Reaction of BHT **1** with PhTAD **2** and plausible reaction mechanism.

In order to widen the substrate scope, it was chosen to explore the reactivity with phenolic substrates having a methyl substituent in *para* position and different *ortho*-substituents than the hindered *tert*-butyl group. Thus, PhTAD **1** was placed to react with compounds **4** and **5**, having two and one "small" alkyl group (i.e., methyl group) in *ortho* positions, respectively.

In this context, even faster reactions were surprisingly observed, since the TAD reagent completely disappeared in a few minutes using dichloromethane as solvent. Anyhow, the product isolation was hampered by the low stability of products during purification and the products identification was possible only by performing the reactions in deuterated solvents and directly analysing the reaction crude through NMR and LC-MS analysis. In this way, two major products were identified in both reactions (compounds **9** and **10**, from **4**; compounds **12** and **13**, from **5**). The plausible mechanism for the formation of compounds **9** and **10** is reported in *Scheme 32*. The identical mechanism could be proposed for the formation of **12** and **13**, starting from **5**.

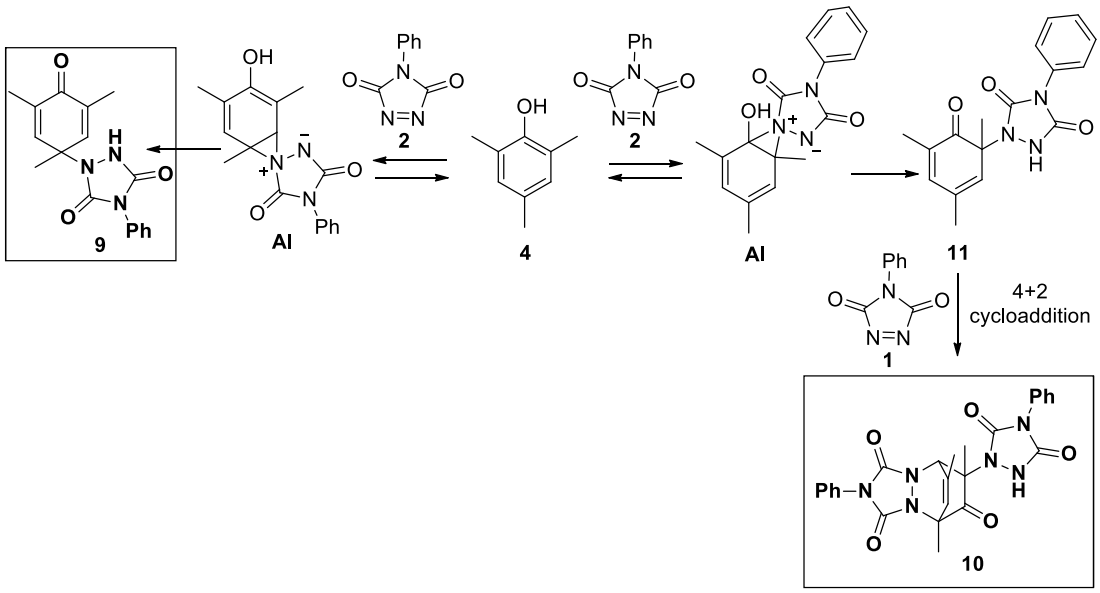

Scheme 32 – Reaction of 2,4,6-trimethylphenol **4** with PhTAD **2** and plausible reaction mechanism.

By NMR analyses, it was possible to identify one product as the Alder-ene adduct in *para* position (compound **9**), formally identical to the adduct formed in the reaction with BHT **2**. This statement was mostly supported by the presence of a peak (6.63ppm in deuterated DCM and 6.9ppm in deuterated DMSO, integrated as 2H) that is coupled with carbon signals (141.66ppm from HSQC, 186.40ppm from HMBC; solvent = CD_2Cl_2), that are the almost identical observations made for the adduct **8**. Instead, compound **10** was characterized by (solvent = CD_2Cl_2): 3 methyl protons (HSQC: 1.53 x 21.26; 1.86 x 14.07; 1.94 x 20.49; 3H each), 1 methenyl (HSQC: 5.29 x 58.63; 1H) and 1 alkenic (HSQC: 5.88 x 127.57; 1H); moreover, from HMBC, it was demonstrated the connection of

these protons with 1 more methenyl carbon (^{13}C = 66.11ppm), 1 alkenic (^{13}C = 144.56ppm) and 1 identified as carbonyl carbon (^{13}C = 194ppm). By these data and the literature, it was proposed the formation of a 2:1 adduct (2 PTAD x 1 phenol; compound **10**).

Resuming, even with compounds **4** and **5** there is a certain tendency to form the Alder-ene in *para* positions but, at the same time, the reaction can also happen in *orto* positions. In accordance to the common reactivity of phenols, it is possible to predict a major tendency to react in *orto*-position, hence the formation of compound **11** tends to be competitive to the detriment of the formation of compound **9**. Anyhow, in compound **11**, the dearomatization of phenol ring leads to the formation of a very reactive diene, that (reasonably) almost instantaneously reacts with a second TAD molecule through Diels-Alder (4+2) cycloaddition, forming compound **10**. From the consideration that the TAD reagent is rapidly involved in a 1:1 (compound **9**) and 2:1 (compound **10**) reactions, so it is quite easy to rationalize the faster reaction time of these transformations. The 2:1 adduct **10** formation is also supported by the fact that compounds **4** and **5** were abundantly present at the end of the reaction, even if only 1.1 equivalents of phenol were used.

From NMR spectra, the ratio between products **9** and **10** was estimated. Many spectra of reaction crudes were recorded: i) reaction in CH_2Cl_2, using 1.1 equivalents of phenol and $CDCl_3$ as NMR solvent; ii) reaction in CD_2Cl_2, using 1,1 equivalents of phenol; iii) reaction in CD_2Cl_2, using 2 equivalents of phenol; iv) reaction in DMSO-*d*6, using 1.1 equivalents of phenol. These trials are resumed in the *Table 1*.

Table 1 – Tested reaction conditions for the formation of products **9** and **10**.

Entry	Reaction Solvent	NMR Solvent	Equiv. of compound 4	NMR ratio between 9:10
I	CH_2Cl_2	$CDCl_3$	1.1	1 : 2.5
II	CD_2Cl_2	CD_2Cl_2	1.1	1 : 1.1
III	CD_2Cl_2	CD_2Cl_2	2	1: 1.35
IV	DMSO-*d*6	DMSO-*d*6	1.1	1 : 0.65

Using dichloromethane as reaction solvent, the main product was the bis adduct **10**. This is more evident when a larger amount of starting material **4** was used, as clear by comparing the NMR ratio observed in *Entry II* and *III*. The result of *Entry I* seems somewhat discordant with this interpretation; anyhow, it could be explained in the low thermal stability of the Alder-ene adduct **9**. Indeed, after the reaction, the solvent was removed with reduced pressure at 40°C and, considering the thermo-reversibility of this adduct, a retro Alder-ene can be hypothesized, favouring so a greater formation of bis adduct **10**. By contrast, in DMSO-*d*6 (*Entry IV*), the ratio is inverted and a higher amount of

Alder-ene adduct **9** was observed. This outcome is in accordance with the longer reaction time (1 minute in DCM; 30 minutes in DMSO); moreover, this study finds evidence of the solvent-dependency of these transformations.

- Reactions of TADs with BHT-like phenols (*Scheme 33*):

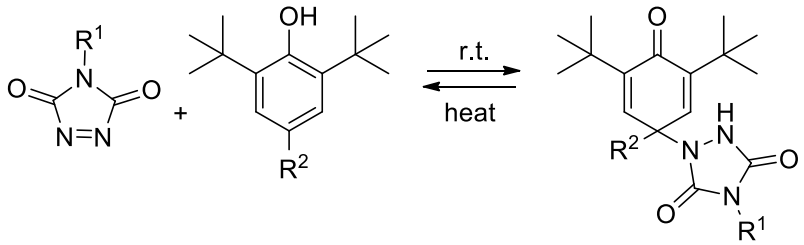

Scheme 33 – Model reactions of TADs with orto-hindered-para-substituted phenols. At least one reactant is monofunctionalized.

In this set of reactions, it was studied the reactivity of mono- and bis-functional TADs with mono-, bis-, and tetra-functional phenols having the BHT scaffold. At this stage, one reactant was monofunctional, while the other was mono- or poly-functional. The model reactants are resumed in *Table 2*.

Table 2 – Reactants used for model reactions.

	TADs	BHT-like phenols
Mono functional	PhTAD (**2**) 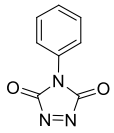	BHT (**1**) 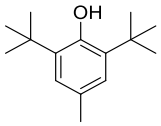
Di functional	IPDI-bisTAD (**15**) 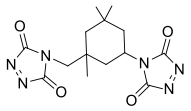	Bis-BHT (**17**) 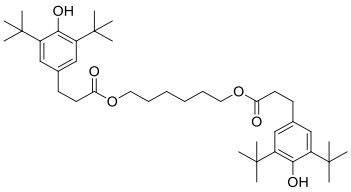
	MDI-bisTAD (**16**) 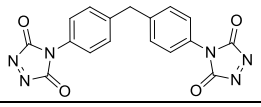	
Poly functional		Tetra-BHT (**18**) 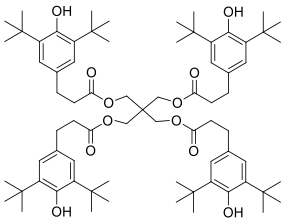

From these reactions, it was proven the tendency of BHT-like phenols to (almost) selectively react with TAD reagents, forming the corresponding Alder-ene (AE) adducts. Additionally, it was checked the reactivity of polyfunzionalized TADs and phenols, with a view with the successive polymer applications. The most relevant experiments are resumed in *Table 3*.

Table 3 – Results from model reactions.

Entry	TAD	Phenol	Solvent and reaction time	Product and yield (%)
V	PhTAD (**2**)	BHT (**1**) 1.05 eq.	DCM, 30 min	Comp. **8** 90%
VI	PhTAD (**2**)	BHT (**1**) 1.05 eq.	MeCN, 2 h	Comp. **8** 79%
VII	IPDI-bisTAD (**15**)	BHT (**1**) 2.1 eq.	MeCN, o.n.	Comp. **19** 60%
VIII	MDI-bisTAD (**16**)	BHT (**1**) 2.1 eq.	MeCN, o.n.	Comp. **20** 72%
IX	PhTAD (**2**)	Bis-BHT (**17**) 0.55 eq.	MeCN, o.n.	Comp. **21** 69%
X	PhTAD (**2**)	Tetra-BHT (**18**) 0.27 eq.	MeCN, o.n.	Comp. **22** 55%

The reaction of PhTAD **2** with BHT **1** was performed in a solvent different than dichloromethane, since the toxicity and environmental issues related to halogenated solvents. Therefore, acetonitrile was chosen as alternative solvent. In a similar way to the reaction of **2** with **4** performed in DMSO, even in this case it was observed a longer reaction time and a slightly lower yield performing the reaction in a solvent different than DCM (*Entry V*: 30 min; 90%; *Entry VI*; 2h: 80%). Anyhow, these deficiencies are not limiting and, for further reactions, it was preferred to continue the investigation using acetonitrile as solvent.

This choice was determined also by the results of *Entries VII* and *VIII*, where the bis-AE adducts **19** and **20** were obtained as insoluble solid with satisfactory yields, after the stirring of reactants in acetonitrile at room temperature for at least 10 hours. This aspect was crucial to facilitate the purification step, since a simple filtration was used to separate these products. This was not the same in *Entries IX* and *X*, where the column chromatography was required to isolate the products, obtaining moderate to satisfactory yields.

The structure of Alder-ene adducts **19**-**22**, confirmed through NMR, LC-MS and FT-IR analyses, are reported in *Figure 22*.

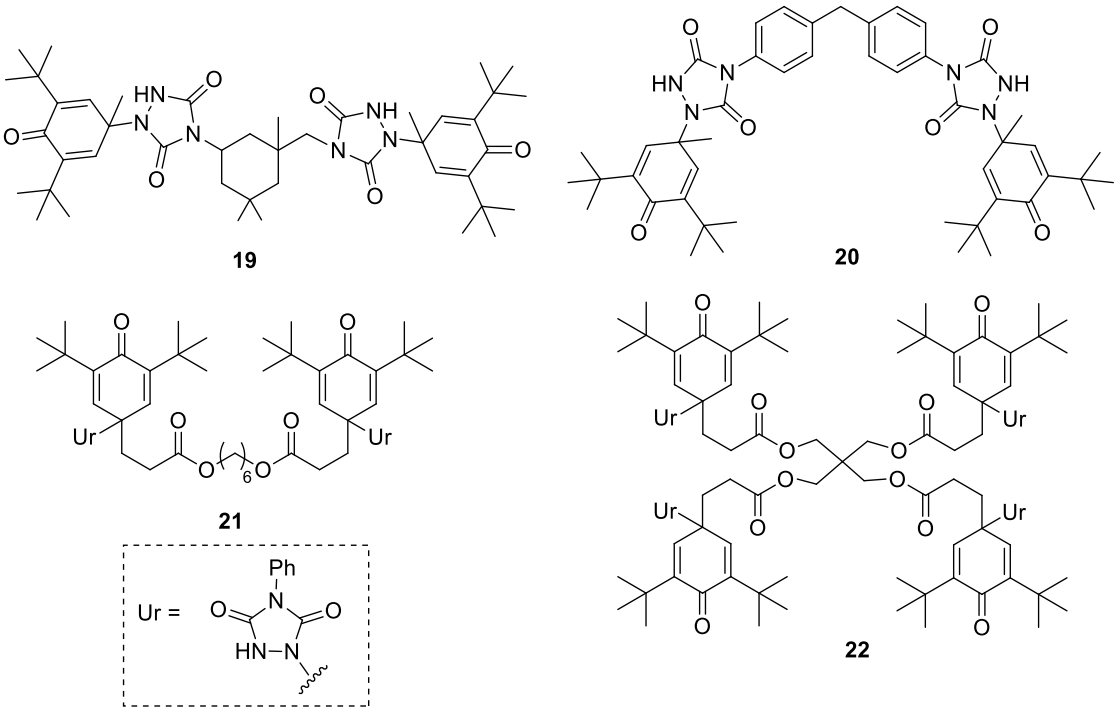

Figure 22 – Chemical structure of products **19-22**.

In conclusion, the change from mono- to poly-reactants causes longer reaction times and lower yields. Anyhow, it was effectively proven the reaction efficiency with poly-functionalized reactants, that is fundamental for the polymer applications. Additionally, the non-solubility of adducts **19** and **20** in acetonitrile was an additional benefit for the process development.

- Transclick-like reactions (*Scheme 34*):

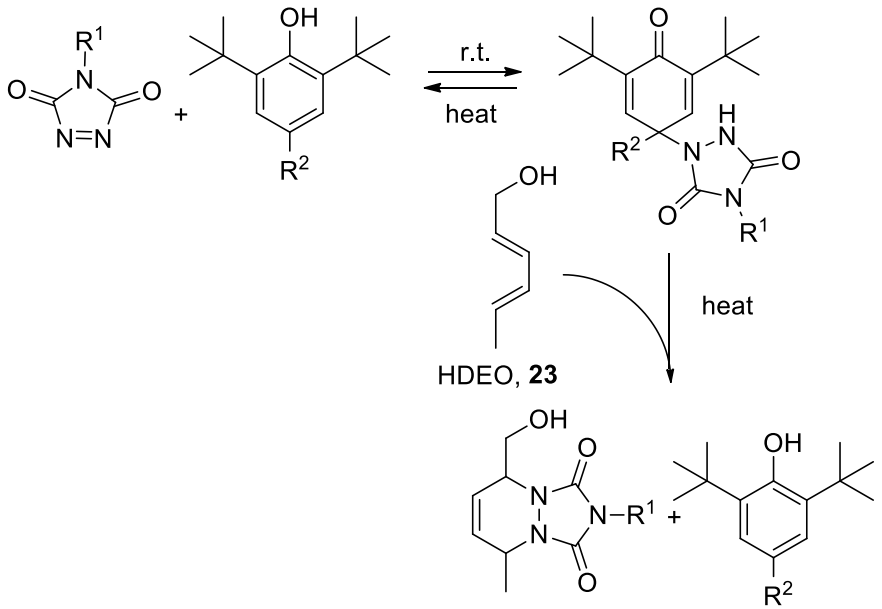

Scheme 34 – Thermo-reversibility reactions of synthesized AE adducts through transclick-like reaction.

In order to study the thermo-reversibility of synthesized compounds, AE adducts **8** and **19-22** were dissolved in DMSO-*d*6, together with an adequate quantity of an electron-rich conjugated diene (HDEO **23** = E,E-2,4-hexadien-1-ol diene) and the "trans-click" reaction was performed. In other words, the thermo-reversibility of the covalent bond created in AE adducts was exploited to liberate the TAD moiety and to obtain the orthogonal "transclick" reaction *in situ* with HDEO, that acts as kinetic and thermodynamic trap, forming the irreversible Diels-Alder adducts with the liberated TAD partner. In this way, the solution was placed to heat and the process was monitored through off-line ^{1}H-NMR analysis at regular intervals.

Until now, this kind of reactivity was exclusively reported for Alder-ene adducts formed by the reaction of TADs and 2,3-disubstituted indoles. Anyhow, in this work, it was proven the efficiency of AE adducts **8** and **19-22** in trans-click reactions, as evident in *Figure 23*, where there are reported the NMR spectra of the process conducted with adduct **8**, recorded before the reaction (t_0) and after 15, 30 and 60 minutes, using DMSO-*d*6 as solvent and a heating temperature of 80°C.

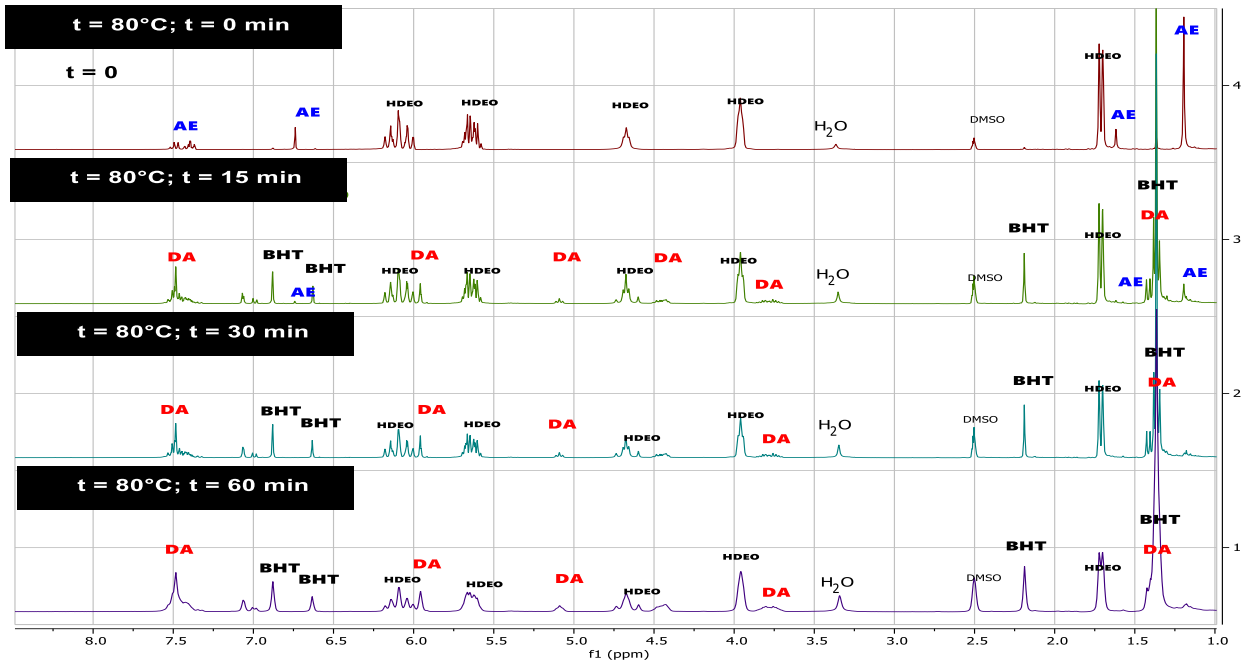

Figure 23 – Off-line ^{1}H-NMR spectra for the transclick reaction of adduct **8** (T=80°C).

Reagents and products of this specific transclick reaction are reported in *Figure 24*.

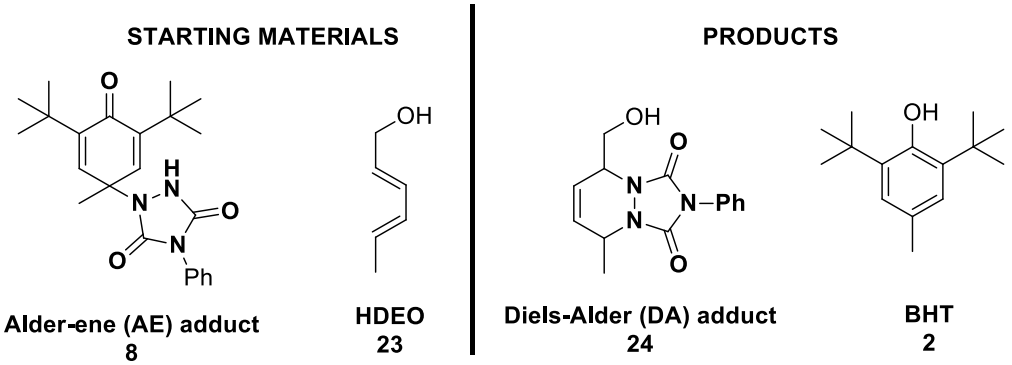

Figure 24 – Reagents and products for the proposed transclick reaction.

From *Figure 23*, it is possible to appreciate the presence of AE adduct **8** and HDEO **23** before the transformation (the latter was present in excess respect to **8**). After 15 minutes of heating, the signals of AE adduct were almost disappeared and, within 30 minutes, they were completely absent. Meanwhile, new signals, relative both to the Diels-Alder adduct (TAD-HDEO, compound **24**) and to the liberated BHT **2**, strongly arose.

The trans-click reaction at 80°C was performed also with Alder-ene adducts **19**-**22**. Assuming the disappear of signal linked to Alder-ene adducts (in particular the signal at 6.7-6.8ppm) as the end of the reaction, so the time needed for a complete transclick reaction were:

- adduct **8** = 30 min;
- adduct **19** = 1h;
- adduct **20** = 2h;
- adduct **21** = 30 min;
- adduct **22** = 15 min.

Finally, after the transclick reactions, it was observed the formation of small signals belonging to unknown compounds (10.9 ppm, 10.4 ppm, 7.1-6.9 ppm, 1.4-1.35 ppm). These signals are more intense when the reaction was performed at higher temperatures (100, 120 and 140°C) or when the heating was performed without the HDEO partner. Assuming that HDEO acts as an instantaneous trap for the liberated TAD in the transclick reaction, hence the unknown by-products should be mostly linked to side reactions of the liberated BHT. According to the literature, the most probable reaction occurring at high temperature under air atmosphere is the thermal oxidation of BHT.[76] This oxidation reaction is divided into three steps: firstly, peroxides are formed; then, the peroxide decompose, generating a large number of free radicals, which in turn triggered more complex oxidation reactions leading to many oxidation products (some of them are shown in *Figure 25*); finally, free radicals could combine to generate polymers or dimers of BHT.

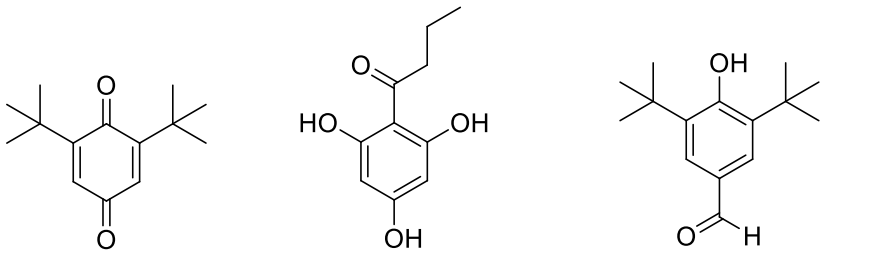

Figure 25 – Possible oxidation products obtained during the thermal oxidation of BHT.

3.4.2. Use of Alder-ene adducts in polymer applications

After the examination of the innovative process with low molecular weight reactants, the reactivity was exploited to develop new polymer materials. In this way, the work could be divided in two main arguments:

- Development of thermo-reversible AA-BB copolymers (*Scheme 35*):

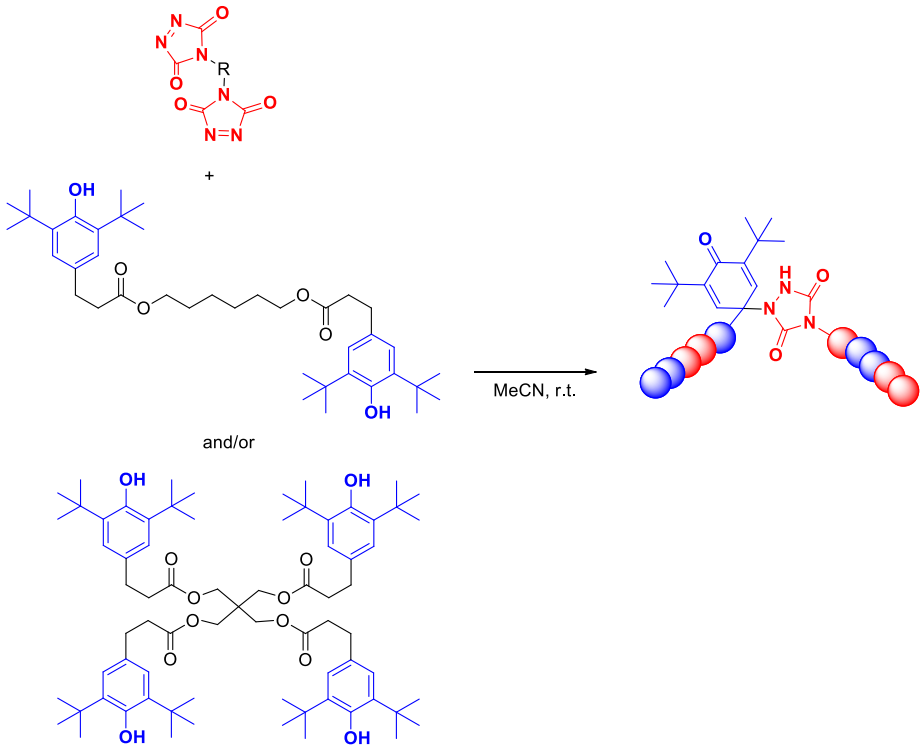

Scheme 35 – Synthesis of AA-BB polymers.

The reactants were the same of the model reactions. However, in this case, only poly-functionalized starting materials were used. The most important experiments are resumed in *Table 4*.

Table 4 – Reactants used for the synthesis of AA-BB polymers.

Entry	TAD	Phenol	Solvent and reaction time	Results
XI	IPDI-bisTAD (**15**)	Bis-BHT (**17**)	MeCN, o.n.	Linear polymer **P1** Low yield
XII	MDI-bisTAD (**16**)	Bis-BHT (**17**)	MeCN, o.n.	Linear polymer **P2** High yield
XIII	IPDI-bisTAD (**15**)	Tetra-BHT (**18**)	MeCN, o.n.	Polymer network **P3** No polymer formation
XIV	MDI-bisTAD (**16**)	Tetra-BHT (**18**)	MeCN, o.n.	Polymer network **P4** High yield
XV	MDI-bisTAD (**16**)	Bis-BHT (**17**) + Tetra-BHT (**18**)	MeCN, o.n.	Cross-linked polymers **P5-8** High yields

The polymerization of bisTAD **15** and **16** with bis-BHT **17** led to the formation of linear polymers **P1-2**, as confirmed by solubility test in different solvents (DMSO, THF, DCM). Anyhow, it is important to note that these materials were insoluble in the reaction solvent (acetonitrile), hence the purification of products was done with a simple filtration.

The solubility of these materials enabled the chemical characterization through NMR and GPC analyses. From the ^{1}H-NMR, ^{13}C-NMR and 2D-NMR (HSQC and HMBC) analyses, it was possible to confirm the formation of AE adducts even in macromolecules; moreover, the "transclick" reactions was successfully performed, demonstrating the thermo-reversibility of the synthesized polymers. In this regard, in *Table 5* are resumed the NMR signals monitored for the transclick reaction of **P2**; while, in *Figure 26*, the NMR spectra (after 30 min, 1 h, 2h and 12h) of the reaction at 80°C.

Table 5 – NMR signals monitored during the transclick reaction of **P2**.

REAGENTS		PRODUCTS	
Alder-ene (AE) polymer P2	**HDEO 23**	**Diels-Alder (DA) adduct 25**	**Bis-BHT 17**
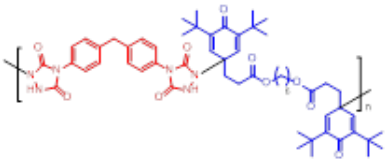 Monitored signals: **6.6ppm** **1.35ppm**	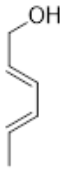	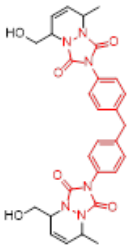 Monitored signals: **5.95ppm**	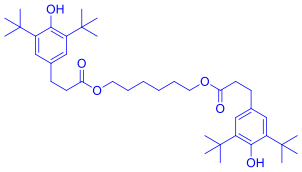 Monitored signals: **6.9ppm** **6.7ppm** **1.4-1.3ppm**

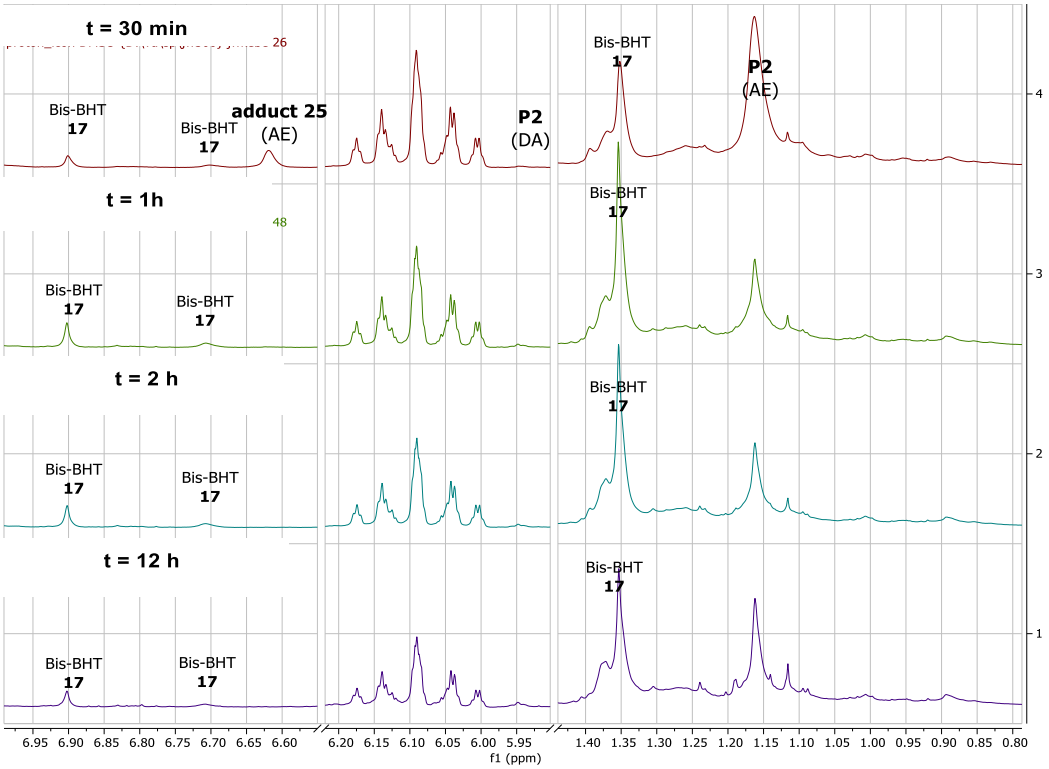

Figure 26 – Off-line ^{1}H-NMR spectra for the transclick reaction of adduct **P2** (T=80°C).

From *Figure 26*, it is possible to conclude that, for linear polymer **P2**, the "transclick" reaction is concluded within 1 hour.

Through the GPC analysis, it was possible to determine the molecular weight of obtained products (*Table 6*). For polymer **P1**, the GPC analysis was performed directly after the polymerization. Instead, for **P2**, the analysis was repeated also after purification through dissolution/precipitation in solvent (CH_2Cl_2) and non-solvent (n-hexane) repeated 2 times.

Table 6 – Results of GPC analysis.

Polymer	M_n (g/mol)	M_w (g/mol)	M_z (g/mol)	M_{z+1} (g/mol)	PD
P1	2,353	3,820	5,846	8,315	1.6
P2	1,953	2,722	3,608	4,453	1.4
P2, after purification	3,297	5,237	7,429	9,684	1.6

Moreover, these polymers were thermal characterized through DSC and TGA analyses. From TGA, three degradative steps were noticed (*Table 7*), while, from the DSC analysis, it was possible to assess a very high glass-transition temperature for polymer **P2** (Tg (midpoint) = 140°C in cooling step; 128°C in second heating).

Table 7 – Results of TGA analysis.

Polymer	T_{on}^{I} (°C)	T_{on}^{II} (°C)	T_{on}^{III} (°C)	W_{loss}^{I} (%)	W_{loss}^{II} (%)	W_{loss}^{III} (%)
P1	139	275	390	8	57	25
P2	127	250	360	19	36	37
P2, after purification	137	257	379	5	37	54

Moving to the formation of pure polymer networks (entries **XIII** and **XIV**), it was possible to obtain an efficient transformation only with MDI-bisTAD **16**. The 3D-network nature of **P4** was confirmed by dissolution tests, that were in all cases negative, and only a prominent swelling process was observed. Moreover, FT-IR analysis was used to check the chemical structure of this material. Instead, the solid product of entry **XIII** was soluble in THF and other solvents. For this reason, it was assumed the lack of formation of polymer **P3**, and successive trials have been performed using only MDI-bisTAD.

In this way, it was finally examined the formation of cross-linked polymers **P5-8** (entry **XV**) by using variable amounts of bis- and tetra-BHT (*Table 8*).

Table 8 – Trials for the formation of cross-linked polymers.

Polymer	Molar % of bis-BHT 17	Molar % of tetra-BHT 18
P5	90%	5%
P6	80%	10%
P7	60%	20%
P8	20%	40%

Even in this case, the cross-linked nature of these polymers was confirmed by dissolution tests, that were in all cases negative, and only an important swelling process was observed. After that, the FT-IR and TGA were performed. The results of the latter analysis are resumed in *Table 9*.

Table 9 – Results of TGA analysis.

Polymer	T_{on}^{I} (°C)	T_{on}^{II} (°C)	T_{on}^{III} (°C)	W_{loss}^{I} (%)	W_{loss}^{II} (%)	W_{loss}^{III} (%)
P6	135	252	410	7	33	48
P7	146	254	436	6	33	53

Finally, it was performed a thermal-induced dissolution of polymer **P6**, in order to check the transclick reaction in macromolecular context. In this way, it was possible to dissolve **P6** in DMSO-*d*6 by using an ultrasound bath heated at 50-60°C; after that, the trans-click reaction at 80°C was considered concluded within 1 hour from the beginning of the stirring of dissolved polymer with HDEO.

- Cross-linking of vegetable natural oil to develop renewable polymer materials (*Scheme 36*):

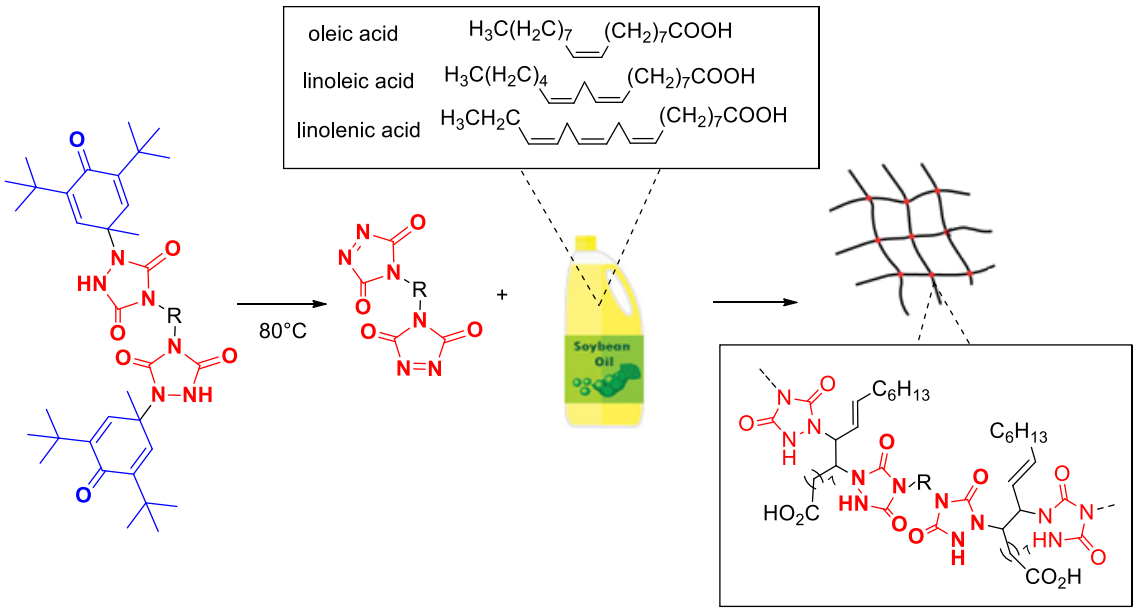

Scheme 36 – Use of AE adducts as heat-triggered cross-linker for the formation of polymer materials from vegetable oil.

Most vegetable oils contain a large number of unsaturated fatty acids, free or more commonly as triglycerides. These carbon-carbon double bonds offer a site for directed chemical transformations, even if the number of reactions involving these double bonds is quite limited. Among them, a previous work reported the use of the TAD chemistry in combination with plant oils for the formation of polymeric plant foil via an additive-free preparation under ambient conditions. The "from oil to foil" approach was based on the use of bis-TAD, able to react with unsaturated fatty acids via Alder-ene reactions. In this way, the fatty acid unsaturation remains (shifted) in the molecule and it can be used in a second modification, that create the 3D network of the forming polymer material through cross-linking.[40]

Herein, it was tested the possibility to use the Alder-ene adducts formed by the reaction of bis-TADs and BHT as "masked" cross-linker for the formation of plant foils. One of the main advantages is the storage: since the high reactivity of TADs, it is not possible to storage free TADs for prolonged time and it is preferred the more stable reduced form (the urazole). In the previous work, it was necessary to generate the bis-TAD by the oxidation of the urazole; instead, in this work, the Alder-ene adducts can easily liberate the free-TAD by heating. Furthermore, an antioxidant, (BHT) is released during the heating, with a consequent increase of stability toward oxidative deterioration in the formed polymer material.

In these experiments, it was first tested the thermo-reversibility of adducts **19** and **20** in a suitable solvent. For this regard, it was chosen dimethylcarbonate (DMC) because it is a quite safe solvent and it enabled the heating of adducts at temperature over than 70°C. After the heating of the solution, the distinctive red coloration of liberated TAD is evident, as shown in *Figure 27*.

Figure 27 – Distinctive red-colour of TAD, liberated after the heat-treatment.

In accordance to the results obtained by transclick reactions, the heating was ensured for more than 10 minutes; after that, the vegetable oil was added and quickly mixed. In particular, it was used soybean oil, since it is formed for more than 80% of mono- and poly-unsaturated fatty acids (like linoleic oil, oleic oil and linolenic oil) and it was proven its high reactivity in the "from oil to foil" approach. Finally, the solution was poured in a mold, observing the formation of a gel after just few minutes. The solvent was removed in a vacuum oven and the polymer films, obtained by this heat-triggered cross-linking of vegetable natural oil, are reported in *Figure 28*.

Figure 28 – Pictures of polymer materials obtained by the cross-linking of soybean oil.

From this work, it was observed a greater suitability of adduct **19** rather than **20**, since the latter was related to a poor solubility in the DMC solution, resulting in an inhomogeneous mixing of liberated bisTAD and fatty acids and, so, in an inefficient formation of the polymer foil.

3.5. Experimental protocols

3.5.1. Materials and methods

All the reagents were of analytical grade and purchased from Merck or TCI (Tokyo Chemical Industries) and used as received. In the case of bisTADs, they were obtained by the oxidation of urazole precursors. These urazoles were previously synthesized and their purity (> 99%) was checked by NMR analysis. In the case of reactions performed under nitrogen atmosphere, the glassware was oven dried at 100 °C for more than 2 hours prior to use.

Reactions of PhTAD 2 with phenols 3-6

The reaction was performed in a closed vial, using CD_2Cl_2 as solvent and using 1.1 equivalents of phenol. The reaction was considered concluded when the distinctive bright red coloration of PhTAD turned to yellow. The reaction crude was directly characterized by NMR and LC-MS analyses.

Reaction of PhTAD 2 with BHT 1

In a 50 mL round-bottom flask, 500 mg of 4-phenyl-1,2,4-triazoline-3,5-dione (PhTAD; purity = 97%; 2.77 mmol; 1 eq.; 175.14 g/mol) and 640.9 mg of 2,6-di-tert-butyl-4-methylphenol (BHT; 2.91 mmol; 1.05 eq.; 220,36 g/mol) were dissolved in 20 mL of CH_2Cl_2. The flask was covered from the sunlight with an aluminium foil and the reaction was stirred at room temperature with a magnetic stirring bar. The reaction was considered concluded when the distinctive bright red coloration of PhTAD turned to yellow. In this way, the reaction was concluded within 30 minutes. Then, the solvent was removed in vacuo and the residue was chromatographed through a column filled with silica gel (n-hexane/EtOAc 9:1 to 6:4) to furnish 980 mg (2.48 mmol, 89.5% yield) of adduct **8**.

Reaction of IPDI-bisTAD 15 with BHT 1

In a 50 mL round-bottom flask, 1g of 4-((5-(3,5-dioxo-1,2,4-triazolidin-4-yl)-1,3,3-trimethylcyclohexyl)methyl)-1,2,4-triazolidine-3,5-dione (IPDI-urazole; 2.96 mmol; 1 eq.; 338.36 g/mol) was dissolved in 20 mL of CH_3CN. Afterwards, 0.67 equivalents of oxidant trichloroisocyanuric acid (TCICA, 1.98mmol; 460.17mg; 232.41g/mol) was added. The flask was

covered from the sunlight with an aluminium foil and the reaction was stirred for 2 hours. Then, the mixture was filtered with cotton over a glass filter and the residue was washed with 5-10mL acetonitrile. The filtrate was collected in a 100mL one-neck round bottom flask, resulting in a pink IPDI-bisTAD solution. At this point, the filtrate could be concentrated under reduced pressure, resulting in the pink solid IPDI-bisTAD with an oxidation reaction yield of 90-95%. Alternatively, it was added solvent directly to the filtrate reaching 50mL of reaction mixture in total and, then, 5.92mmol of BHT (1.3g; 2.1eq.; 220.36g/mol). The flask was covered from light and the reaction was stirred overnight. The day after, the solution turned to pale yellow and it was observed the formation of a white solid. After filtration, 1.31g (1.69mmol, 60% yield) of adduct **19** was obtained.

Reaction of MDI-bisTAD 16 with BHT 1

In a 50 mL round-bottom flask, 1 g of 4,4'-(methylenebis(4,1-phenylene))bis(1,2,4-triazolidine-3,5-dione) (MDI urazole; 2.73 mmol; 1 eq.; 366.33 g/mol) was dissolved in 20 mL of CH_3CN. Afterwards, 0.67 eq. of oxidant trichloroisocyanuric acid (TCICA, 1.83 mmol; 425.31 mg; 232.41 g/mol) were added. The flask was covered from the sunlight with an aluminium foil and the reaction was stirred for 2 hours. Then, the mixture was filtered over a glass filter and the residue was washed with 5-10 mL acetonitrile. The filtrate was collected in a 100 mL one-neck round bottom flask, resulting in a bright red MDI-bisTAD solution. At this point, the filtrate could be concentrated under reduced pressure, resulting in the red solid MDI-bisTAD with an oxidation reaction yield of 90-95%. Alternatively, it was added solvent directly to the filtrate reaching 50mL of reaction mixture in total and, then, also 5.44 mmol of BHT (1.2 g; 2.1 eq.; 220.36 g/mol). The flask was covered from light and the reaction was stirred overnight. The day after, the solution turned to pale yellow and it was observed the formation of a white solid. After filtration, 1.56 g (1.94 mmol, 72% yield) of adduct **20** was obtained.

Reaction of PhTAD 2 with bis-BHT 17

In a 25 mL round-bottom flask, 106.5 mg of 4-phenyl-1,2,4-triazoline-3,5-dione (PTAD; purity = 97%; 0.59mmol; 1eq.; 175.14g/mol) and 338.6 mg of hexane-1,6-diyl bis(3-(3,5-di-*tert*-butyl-4-hydroxyphenyl)propanoate) (bis-BHT; 0.31 mmol; 0.53 eq.; 638.92 g/mol) were dissolved in 10 mL of CH_3CN. The flask was covered from light and the reaction was stirred overnight. The day after, the solution coloration turned from bright red to pale yellow. Then, the solvent was removed in vacuo and the residue was chromatographed through a column filled with silica gel (n-hexane/EtOAc 9:1 to 2:3) to furnish 201.3 mg (0.20 mmol, 69% yield) of adduct **21**.

Reaction of PhTAD 2 with tetra-BHT 18

In a 25 mL round-bottom flask, 118.5 mg of 4-phenyl-1,2,4-triazoline-3,5-dione (PhTAD; purity = 97%; 0.66 mmol; 1 eq.; 175.14 g/mol) and 216.3 mg of pentaerythritol tetrakis(3,5-di-*tert*-butyl-4-hydroxyhydrocinnamate) (tetra-BHT; purity = 98%; 0.18 mmol; 0.27 eq.; 1177.63 g/mol) were dissolved in 10 mL of CH_3CN. The flask was covered from light and the reaction was stirred overnight. The day after, the solution coloration turned from bright red to pale yellow. Then, the solvent was removed in vacuo and the residue was chromatographed through a column filled with silica gel (n-hexane/EtOAc 9:1 to 2:3) to furnish 170.9 mg (0.09 mmol, 55% yield) of adduct **22**.

Synthesis of polymer P1

In a 50 mL round-bottom flask, 372.2 mg of 4-((5-(3,5-dioxo-1,2,4-triazolidin-4-yl)-1,3,3-trimethylcyclohexyl)methyl)-1,2,4-triazolidine-3,5-dione (IPDI urazole; 1.1 mmol; 1 eq.; 338.36 g/mol) was dissolved in 20 mL of CH_3CN. Afterwards, 0.67 equivalents of oxidant trichloroisocyanuric acid (TCICA, 0.74 mmol; 171.4 mg; 232.41 g/mol) was added. The flask was covered from the sunlight with an aluminium foil and the reaction was stirred for 2 hours. Then, the mixture was filtered with cotton over a glass filter and the residue was washed with 5-10 mL acetonitrile. The filtrate was collected in a 200 mL beaker, resulting in a pink IPDI-bis-TAD solution, with an oxidation reaction yield of 90-95%. After that, it was added solvent to reach 50 mL in total. Then, 1.1 mmol of hexane-1,6-diylbis(3-(3,5-di-*tert*-butyl-4-hydroxyphenyl) propanoate) (bis-BHT; 700mg; 1.05eq.; 638.92g/mol) was added and the stirring was kept overnight covering the beaker from the sunlight with an aluminium foil. The day after, the solution coloration turns to pale pink, a sign that probably some traces of TAD were present; however, leaving the reaction for 2 days did not cause any change. Anyhow, it was also observed the formation of a yellow sticky solid not soluble in solution. After the collection and 3 washes with fresh solvent, 100 mg of polymer **P1** was obtained.

Synthesis of polymer P2

In a 50 mL round-bottom flask, 403 mg of 4,4'-(methylenebis(4,1-phenylene))bis(1,2,4-triazolidine-3,5-dione) (MDI urazole; 1.1 mmol; 1 eq.; 366.33 g/mol) was dissolved in 20mL of CH_3CN. Afterwards, 0.67equivalents of oxidant trichloroisocyanuric acid (TCICA, 0.74mmol; 171.4mg; 232.41g/mol) was added. The flask was covered from the sunlight with an aluminium foil and the reaction was stirred for 2 hours. Then, the mixture was filtered with cotton over a glass filter and the residue was washed with 5-10 mL acetonitrile. The filtrate was collected in a 200 mL beaker, resulting in a red MDI-bis-TAD solution, with an oxidation reaction yield of 90-95%. After that, it was added solvent to reach 50 mL in total. Then, 1.1 mmol of hexane-1,6-diyl bis(3-(3,5-di-*tert*-butyl-4-

hydroxyphenyl)propanoate) (bis-BHT; 700mg; 1.05eq.; 638.92g/mol) was added and the stirring was kept overnight covering the beaker from the sunlight with an aluminium foil. The day after, the solution coloration turns to yellow and it was also observed the formation of a yellow sticky solid not soluble in solution. After the collection and 3 washes with fresh solvent, 400 mg of polymer **P2** was obtained.

Synthesis of polymer P4

In a 50 mL round-bottom flask, 1 g of 4,4'-(methylenebis(4,1-phenylene))bis(1,2,4-triazolidine-3,5-dione) (MDI urazole; 2.73 mmol; 1 eq.; 366.33 g/mol) was dissolved in 20 mL of CH_3CN. Afterwards, 0.67equivalents of oxidant trichloroisocyanuric acid (TCICA, 1.83 mmol; 425.31 mg; 232.41 g/mol) was added. The flask was covered from the sunlight with an aluminium foil and the reaction was stirred for 2 hours. Then, the mixture was filtered with cotton over a glass filter and the residue was washed with 5-10 mL acetonitrile. The filtrate was collected in a 200 mL beaker, resulting in a red MDI-bis-TAD solution, with an oxidation reaction yield of 90-95%. After that, it was added solvent to reach 50 mL in total. Then, 0.67 mmol of pentaerythritol tetrakis(3,5-di-*tert*-butyl-4-hydroxyhydrocinnamate) (tetra-BHT; purity = 98%; 805 mg; 0.26 eq.; 1177.63 g/mol) was added and the stirring was kept overnight covering the beaker from the sunlight with an aluminium foil. The day after, the solution coloration turns to pale red, a sign that probably some traces of TAD were present. Therefore, 805 mg of tetra-BHT was readded after 1 day and the reaction stirred for one more day. Leaving the reaction for 2 days results in a yellow coloration and the formation of a yellow solid not soluble in solution. After the collection and 3 washes with fresh solvent, 1.5 g of **P4** was obtained.

Synthesis of polymers P5-8

In a 50 mL round-bottom flask, 403 mg of 4,4'-(methylenebis(4,1-phenylene))bis(1,2,4-triazolidine-3,5-dione) (MDI urazole; 1.1 mmol; 1 eq.; 366.33 g/mol) was dissolved in 20 mL of CH_3CN. Afterwards, 0.67 equivalents of oxidant trichloroisocyanuric acid (TCICA, 0.74 mmol; 171.4 mg; 232.41 g/mol) was added. The flask was covered from the sunlight with an aluminium foil and the reaction was stirred for 2 hours. Then, the mixture was filtered with cotton over a glass filter and the residue was washed with 5-10 mL acetonitrile. The filtrate was collected in a 200 mL beaker, resulting in a red MDI-bis-TAD solution, with an oxidation reaction yield of 90-95%. After that, it was added solvent to reach 50mL in total. Then, different amount of hexane-1,6-diyl bis(3-(3,5-di-*tert*-butyl-4-hydroxyphenyl)propanoate) (bis-BHT; 638.92 g/mol) and pentaerythritol tetrakis(3,5-di-*tert*-butyl-4-hydroxyhydrocinnamate) (tetra-BHT; purity = 98%; 1177.63 g/mol) were added and the stirring was kept overnight covering the beaker from the sunlight with an aluminium foil. The day

after, the solution coloration turns to yellow and the formation of a yellow solid not soluble in solution was observed: after the collection and 3 washes with fresh solvent, polymers **P5-8** were obtained.

General procedure for "trans-click" reaction

The "trans-click" reaction was studied through off-line ^{1}H-NMR analyses. Firstly, a 4M stock solution of HDEO in DMSO-*d*6 (0.88 g = 8.95 mmol of HDEO in 2.25 mL of DMSO-*d*6) was prepared. Meanwhile, in glass vials, 30mg of AE adducts were dissolved in 0.75mL of DMSO-*d*6. Then, the HDEO stock solution was properly added into the glass vials, in order to have a ratio 1 : 1.5 equivalents between adducts and HDEO. The resulting solution is continuously stirred and heated at 80°C, recording NMR spectra at different times (15 min, 30 min, 1 h, 2 h, 4 h, 12 h).

General procedure for the "from oil to foil" approach

Firstly, two distinct solutions were prepared: solution A was made by dissolving 286.3 mg of adduct **19** in 2 mL of DMC (dimethylcarbonate), in order to have 125 mg of "free" IPDI-bisTAD; solution B by dissolving 250 mg of soybean oil in 2 mL of DMC. Solution A was stirred and heated at 80°C in a glass vial for 10 minutes, observing a red coloration during the heating. After that, solution B was added in the same glass vial and the overall solution was stirred for 1 minute and then placed in a plastic lid. The cross-linking starts immediately, observing gelation after 5-30 minutes. Hence, the lid is placed in vacuum oven at 40°C overnight, in order to remove the solvent in excess, finally gaining a solid plant-based foil.

Fourier transform infrared spectroscopy (FTIR-ATR)

FTIR spectra were recorded with a Perkin-Elmer FT-IR Spectrum Two UATR spectrometer, equipped with ZnSe crystal. The measurements were performed in a range of 400-4000 cm^{-1} with a resolution of 2 cm^{-1}, 4 scans and the data were processed by the software Perkin-Elmer manager (Spectrum).

Thermogravimetric analysis (TGA)

TGA analysis was carried out using a Mettler-Toledo TGA/SDTA 851e apparatus. Samples (5 to 10 mg) were heated in a nitrogen atmosphere with a heating rate of 10 K/min going from 25°C to 600°C. For the analysis of the thermograms, the STARe software of Mettler-Toledo was used.

Nuclear Magnetic Resonance (NMR) analysis

The ^{1}H-NMR and ^{13}C-NMR spectra were obtained using a Bruker Advance 400 FT-NMR spectrometer (400 MHz or 100 MHz, respectively). Chemical shifts are reported in ppm. The deuterated solvents used were $CDCl_3$ (7.26 ppm for ^{1}H and 77.0 ppm for ^{13}C), DMSO-d6 (2.50 ppm for ^{1}H and 39.5 ppm for ^{13}C) and CD_2Cl_2 (5.32 ppm for ^{1}H and 54.0 ppm for ^{13}C).

Liquid Chromatography – Mass spectroscopy (LC-MS) analysis

LC-MS analysis was performed analyses on an Agilent Technologies 1100 series LC/MSD system with a diode array detector (DAD) and a single quad MS. Analytical reversed phase HPLC-analyses were performed with a Phenomex Luna C18 (2) column (5 μm, 250 mm × 4.6 mm) and a solvent gradient (0-100 % acetonitrile in H_2O in 15 min). The eluted compounds were analysed via UV detection (214 nm).

Gel-permeation chromatography (GPC) analysis

GPC analysis was performed using an Agilent 1260 Infinity II Multi Detector Suite (MDS). The mobile phase consisting of THF contains 250 ppm of BHT (butylhydroxytoluene) and the flow rate is 1.0 ml/min. Two columns in series (PLgel MIXED-C and PLgel MIXED-D) preceded by a precolumn (Agilent GPC/SEC Guard Column) were used. Agilent GPC/SEC Software is used for the acquisition of chromatograms. The standards used for the calibration line are polystyrene with a range of Mp between 580-283,800 g/mol.

Differential Scanning Calorimetry (DSC) analysis

DSC thermograms were recorded using a TA Instruments Q2000 DSC with autosampler option and Refrigerated Cooling System (RCS). Nitrogen gas was used as purge gas. The samples were studied in TAi Tzero Hermetic aluminium sample pans and at a scan rate of 10 K/min.

3.5.2. Characterization

Compound 7

^{1}H NMR: (400 MHz, CD_2Cl_2) δ_H = 8.43 (s, 1H), 7.55-7.3 (m, 5H), 7.04 (s, 2H), 5.21 (s, 1H), 1.28 (s, 18H). *^{13}C NMR*: (100 MHz, CD_2Cl_2) δ_C = 155.1, 155, 153.41, 136.83, 131.25, 129.24, 128.51, 127.17, 126.14, 122.72, 34.33, 29.78. *HSQC*: 7.54 x 126.14, 7.45 x 129.24, 7.37 x 128.51, 7.04 x 127.72, 1.28 x 29.78. *ESI-MS* (m/z): 382.159 ($[M+H]^+$; 100%).

Compound 8

^{1}H NMR: (400 MHz, $CDCl_3$) δ_H = 8.51 (s, 1H), 7.55-7.31 (m, 5H), 6.67 (s, 2H); 1.78 (s, 3H), 1.21 (s, 18H). *^{13}C NMR*: (100 MHz, $CDCl_3$) δ_C = 185.29, 154.18, 153.42, 148.56, 137.47, 130.66, 129.26, 128.61, 125.88, 60.34, 35.30, 29.28, 25.26. *HSQC*: 7.43 x 129.26, 7.39 x 128.61, 7.36 x 125.88, 6.58 x 137.47, 1.69 x 25.26, 1.12 x 29.28. *FTIR* (neat, cm^{-1}): 3236 (w), 2962 (m), 2364 (w), 1776 (s), 1696 (s), 1650 (m), 1515 (m), 1422 (m), 1364 (w), 1337 (w), 1247 (w), 1167 (w), 1075 (w), 1017 (w), 882 (w), 771 (w). *ESI-MS* (m/z): 396.220 ($[MH]^+$; 78,4%), 340.168 ([M-55]; 100%).

Compound 9

^{1}H NMR: (400 MHz, CD_2Cl_2) δ_H = 8.40 (s, 1H), 7.40-7.05 (m, 5H), 6.67 (s, 2H), 1.77 (s, 6H), 1.64 (s, 3H). *^{13}C NMR*: (100 MHz, CD_2Cl_2) δ_C = 186.40, 154.86, 154.36, 141.66, 136.25, 129.67, 129.14, 128.60, 125.94, 60.05, 24.32, 15.70. *HSQC*: 6.67 x 141.66, 1.77 x 15.70, 1.64 x 24.32. *HMBC*: 6.67 x 15.70, 24.32, 60.05, 141.66 186.40; 1.77 x 24.32, 136.25, 141.66, 186.40; 1.64 x 60.05, 141.66. *ESI-MS* (m/z): 312.094 ($[M+H]^+$; 100%).

Compound 10

^{1}H NMR: (400 MHz, CD_2Cl_2) δ_H = 8.40 (s, 1H), 7.40-7.05 (m, 5H), 5.93-85 (m, 1H), 5.31-5.26 (m, 1H), 1.94 (s, 3H), 1.86 (s, 3H), 1.53 (s, 3H). *^{13}C NMR*: (100 MHz, CD_2Cl_2) δ_C = 194.80, 153.92, 153.35, 151.86, 151.11, 144.56, 130.44, 130.10, 129.09, 129.07, 128.46, 128.20, 127.57, 125.90, 125.88, 66.11, 63.08, 58.63, 21.26, 20.49, 14.07. *HSQC*: 5.88 x 127.57, 5.29 x 58.63, 1.94 x 20.49, 1.86 x 14.07, 1.53 x 21.26. *HMBC*: 5.88 x 14.07, 20.49, 58.63, 66.11; 5.29 x 20.49, 63.08, 127.57, 144.56, 194.80; 1.94 x 58.63, 127.57, 144.56; 1.86 x 66.11, 127.57, 144.56; 1.53 x 58.63, 63.08, 194.80. *ESI-MS* (m/z): 487.113 ($[M+H]^+$; 100%).

Compound 12

^{1}H NMR: (400 MHz, CD_2Cl_2) δ_H = 8.78 (s, 1H), 7.40-7.05 (m, 5H), 6.63-6.58 (m, 2H), 1.73 (s, 3H), 1.61 (s, 3H), 1.08 (s, 6H). *^{13}C NMR*: (100 MHz, CD_2Cl_2) δ_C = 185.16, 154.35, 153.34, 146.44, 140.21, 139.51, 137.56, 129.89, 128.69, 128.41, 126.07, 60.19, 34.64, 28.77, 24.77, 15.97. *HSQC*: 6.62 x 139.51, 6.59 x 140.21, 1.73 x 15.97, 1.61 x 24.77, 1.08 x 28.77. *HMBC*: 6.63-6.58 x 15.97, 24.77, 34.64, 139.51, 140.21, 185.16; 1.73 x 137.56, 185.16; 1.61 x 60.19, 140.21, 1.08 x 28.77, 34.64, 146.44. *ESI-MS* (m/z): 354.154 ($[M+H]^+$; 100%).

Compound 13

^{1}H NMR: (400 MHz, CD_2Cl_2) δ_H = 8.78* (s, 1H), 7.40-7.05* (m, 5H), 6.19-6.13 (m, 1H), 5.27-5.20 (m, 1H), 1.94 (s, 3H), 1.53 (s, 3H), 1.47 (s, 3H), 1.23 (s, 3H), 1.20 (s, 3H). *^{13}C NMR*: (100 MHz, CD_2Cl_2) δ_C = 192.98, 154.10, 153.30, 151.56, 150.48, 145.21, 131.61, 129.96, 128.92, 128.32, 128.78, 128.55, 126.03, 125.91, 125.70, 76.08, 64.08, 55.72, 33.26, 28.14, 26.56, 24.39, 21.54, 20.49. *HSQC*: 6.16 x 125.91, 5.23 x 55.72, 1.93 x 20.49, 1.53 x 24.39, 1.47 x 21.54, 1.23 x 26.56, 1.20 x 28.14. *HMBC*: 6.16 x 20.49, 33.36, 55.72, 76.08, 192.98; 5.23 x 20.49, 64.08, 125.91; 1.93 x 55.72, 125.91, 145.21, 192.98; 1.53 x 26.56, 28.14, 33.36, 76.08; 1.47 x 55.72, 64.08, 192.98; 1.23 x 24.39, 28.14, 33.36, 76.08. 1.20 x 24.39, 26.56, 33.36, 63.08, 76.08. *ESI-MS* (m/z): 529.139 ($[M+H]^+$; 100%).

Compound 19

^{1}H NMR: (400 MHz, DMSO-d6) δ_H = 10.24 (s, 1H), 10.22 (s, 1H), 6.65-6.56 (m, 4H), 4.01 (tt, 12.9, 3.4 Hz, 1H) 3.14 (s, 2H), 2.02-1.86 (m, 2H), 1.57 (s, 3H), 1.51 (s, 3H), 1.39-1.32 (m, 1H), 1.30-1.23 (m, 1H), 1.18 (s, 2H), 1.17 (s, 18H), 1.16 (s, 18H), 0.99 (s, 3H), 0.96 (s, 3H), 0.90 (s, 3H). *^{13}C NMR*: (100 MHz, DMSO-d6) δ_C = 185.93, 157.15, 155.93, 155.90, 154.78, 146.31, 146.24, 146.16, 146.03, 139.80, 139.60, 59.90, 59.70, 52.25, 45.42, 41.18, 40.60, 39.34, 38.05, 35.24, 34.91, 31.96, 29.56, 29.49, 27.50, 25.76, 25.72, 23.31. *HSQC*: 6.63 x 139.80, 6.59 x 139.60, 4.01 x 45.42, 3.14 x 52.25, 1.97 x 38.05, 1.92 x 41.18, 1.57 x 25.76, 1.51 x 25.72, 1.35 x 41.18, 1.28 x 38.05, 1.18 x 31.96, 1.17 x 29.56, 1.16 x 29.49, 0.99 x 27.50, 0.96 x 23.31, 0.90 x 34.91. *FTIR* (neat, cm^{-1}): 3240(w), 2958(m), 2362(w), 1776(m), 1700 (s), 1670 (s), 1649 (s), 1439 (s), 1388 (m), 1364 (w) 1247 (w), 1167 (w), 1075 (w), 1027 (w), 882 (w), 773 (w). *ESI-MS* (m/z): 775.327 ($[MH]^+$; 1%), 792.430 ($[M+NH_4]^+$; 100%).

Compound 20

^{1}H NMR: (400 MHz, DMSO-d6) δ_H = 10.64 (s, 2H), 7.40-7.25 (m, 8H), 6.71 (s, 4H), 4.03 (s, 2H), 1.59 (s, 6H), 1.17 (s, 36H). *^{13}C NMR*: (100 MHz, DMSO-d6) δ_C = 185.91, 154.54, 153.82, 146.11, 141.61, 139.78, 129.74, 129.69, 126.86, 59.85, 40.61, 34.95, 29.54, 25.87. *HSQC*: 7.35 x 129.74, 7.28 x 126.86, 6.71 x 139.78, 4.03 x 40.61, 1.59 x 25.87, 1.17 x 29.54. *FTIR* (neat, cm^{-1}): 3234(w), 2961(m), 2518(w), 1776(m), 1696 (s), 1668 (s), 1649 (s), 1422 (s), 1364 (m), 1364 (w) 1246 (w), 1152 (m), 1074 (w), 1017 (w), 881 (w), 763 (w). *ESI-MS* (m/z): 820.358 ($[M+NH_4]^+$; 100%).

Compound 21

^{1}H NMR: (400 MHz, $CDCl_3$) δ_H = 8.88 (s, 2H), 7.55-7.32 (m, 10H), 6.58 (s, 4H), 3.99 (t, J = 6.4 Hz, 4H), 2.38-2.30 (m, 4H), 2.28-2.17 (m, 4H), 1.62-1.45 (m, 4H), 1.33-1.2 (m, 4H), 1.13 (s, 36H). *^{13}C NMR*: (100 MHz, $CDCl_3$) δ_C = 185.72, 173.31, 154.35, 154.19, 149.47, 135.50, 130.58, 129.34, 128.64, 125.79, 64.86, 62.75, 35.24, 32.75, 29.36, 28.76, 28.05, 24.95. *HSQC*: 7.48 x 129.34, 7.43 x 128.65, 7.42 x 125.79, 6.58 x 135.50, 3.99 x 64.86, 2.38-2.30 x 32.75, 2.28-2.17 x 28.76, 1.62-1.45 x 28.08, 1.33-1.32 x 24.95, 1.13 x 29.36. *FTIR* (neat, cm^{-1}): 3245(w), 2960(m), 2362(w), 1776(m), 1696 (s), 1668 (s), 1648 (s), 1515 (m), 1421 (s), 1364 (m), 1365 (w) 1246 (w), 1153 (m), 1073 (w), 1017 (w), 881 (w), 768 (w). *ESI-MS* (m/z): 989.303 ($[MH]^+$; 1%).

Compound 21

^{1}H NMR: (400 MHz, $CDCl_3$) δ_H = 8.76 (s, 4H), 7.43-7.26 (m, 20H), 6.51 (s, 8H), 4.10-3.97 (m, 8H), 2.26-2.16 (m, 16H), 1.13 (s, 72H). *^{13}C NMR*: (100 MHz, $CDCl_3$) δ_C = 185.63, 172.38, 154.23, 154.08, 149.69, 135.24, 130.56, 129.95, 128.73, 125.93, 62.66, 60.85, 43.32, 35.24, 32.43, 29.35, 28.36. *HSQC*: 7.40 x 125.93, 7.33 x 129.95, 7.28 x 128.73, 6.51 x 135.24, 4.04 x 60.85, 2.22 x 32.43, 2.19 x 28.36, 1.13 x 29.35. *FTIR* (neat, cm^{-1}): 3250(w), 2961(m), 2362(w), 1796(m), 1696 (s), 1668 (s), 1649 (s), 1515 (m), 1422 (s), 1364 (m), 1365 (w) 1246 (w), 1153 (m), 1074 (w), 1017 (w), 881 (w), 763 (w).

Polymer P1

^{1}H NMR: (400 MHz, DMSO-d6) δ_H = 10.24 (s), 10.22 (s), 6.52 (s), 6.50 (s), 4.07 – 3.99 (m), 3.98 – 3.90 (m), 3.14 (s), 2.41 – 2.34 (m), 2.31-2.24 (m), 2.02-1.86 (m), 1.55 – 1.47 (m), 1.39-1.32 (m), 1.37-1.33 (m), 1.28-1.25 (m), 1.15 (s), 0.99 (s), 0.96 (s), 0.89 (s). *^{13}C NMR*: (100 MHz, DMSO-d6) δ_C = 186.61, 172.46, 157.34, 156.22, 148.38, 137.72, 64.52, 63.03, 52.64, 47.08, 45.42, 42.42, 38.04, 35.10, 31.94, 31.18, 29.46, 29.41, 28.35, 27.48, 25.46, 23.26. *FTIR* (neat, cm^{-1}): 3240(w), 2960(m), 2362(m), 1776(m), 1700 (s), 1670 (s), 1649 (s), 1439 (s), 1388 (m), 1364 (w) 1247 (w), 1167 (w), 1075 (w), 1027 (w), 882 (w), 773 (w).

Polymer P2

^{1}H NMR: (400 MHz, DMSO-d6) δ_H = 10.64 (s), 7.4-7.25 (m), 6.61 (s) 4.03 (s), 3.99 – 3.91 (m), 2.41 – 2.34 (m), 2.18-2.06 (m), 1.55 – 1.47 (m), 1.28-1.25 (m), 1.17 (s). *^{13}C NMR*: (100 MHz, DMSO-d6) δ_C = 185.97, 172.48, 154.82, 153.98, 150.42, 148.03, 141.64, 137.65, 129.75, 129.64, 126.89, 64.56, 62.99, 35.15, 31.37, 30.85, 29.46, 28.34, 25.45. *FTIR* (neat, cm^{-1}): 3240(w), 2960(m), 2362(m),

1776(m), 1707 (s), 1646 (m), 1514 (m), 1418 (s), 1366 (m), 1248 (w), 1168 (w), 1064 (w), 1019 (w), 882 (w), 762 (w).

Polymer P4

FTIR (neat, cm^{-1}): 3240(w), 2960(m), 2362(m), 1780(s), 1707 (s), 1662 (s), 1649 (s), 1514 (m), 1418 (s), 1366 (w) 1247 (w), 1140 (w), 1047 (w), 1020 (w), 882 (w), 766 (w).

Polymer P6

FTIR (neat, cm^{-1}): 3236(w), 2953(m), 2362(m), 2203 (w), 1777(w), 1706 (s), 1662 (m), 1646 (m), 1514 (m), 1420 (s), 1366 (w) 1248 (w), 1141 (m), 1060 (w), 1018 (w), 882 (w), 760 (w).

3.5. Conclusions

In this work, it is proposed a novel reactivity of TAD compounds toward activated aryl systems. More in detail, it is first proposed the synthesis of thermo-reversible Alder-ene adducts by the catalyst-free reaction of TADs and *ortho*-hindered-*para*-substituted phenols, at room temperature and using acetonitrile as solvent.

In order to (almost) exclusively form the Alder-ene product, it was found as mandatory the presence of an alkyl group (e.g.,methyl) in position 4 and hindered groups (i.e., *tert*-butyl) in position 2 and 6 of the phenol ring.

Instead, it was observed the slow EAS in *para* position when any or bromine substituent was present. Furthermore, in presence of "small" alkyl groups in *ortho* positions, it was surprisingly observed a cascade-type reaction, where, besides the Alder-ene adduct in para position, another major product was formed, reasonably made by the addition of two molecules of TAD through an Alder-ene reaction in orto position, followed by an instantaneous Diels-Alder reaction.

After these initial experiments, it was chosen BHT **1** and PhTAD **2** as model reactants and, then, the attention moved on the study of the reactivity with poly-functionalized reactants. In this way, many Alder-ene adducts were effectively formed and characterized, while the thermo-reversibility of these compounds was checked by "trans-click reactions, finding a complete transformation within 15 min – 2 hours of heating at 80°C (depending on the type of adduct).

From these results, it was tried to use the explore the reactivity in polymer applications. In this way, a large number of AA-BB copolymers were synthesized and analysed, checking also in this case the reversibility through "transclick" reaction. Moreover, by using tetra-functionalized monomers, it was effectively produced both cross-linked polymers and pure polymer networks. Even if the quite

low molecular weight of these polymers, it is important to highlight that the proposed polymers can be considered as an analogous of PU materials, as depicted in *Scheme 37*.

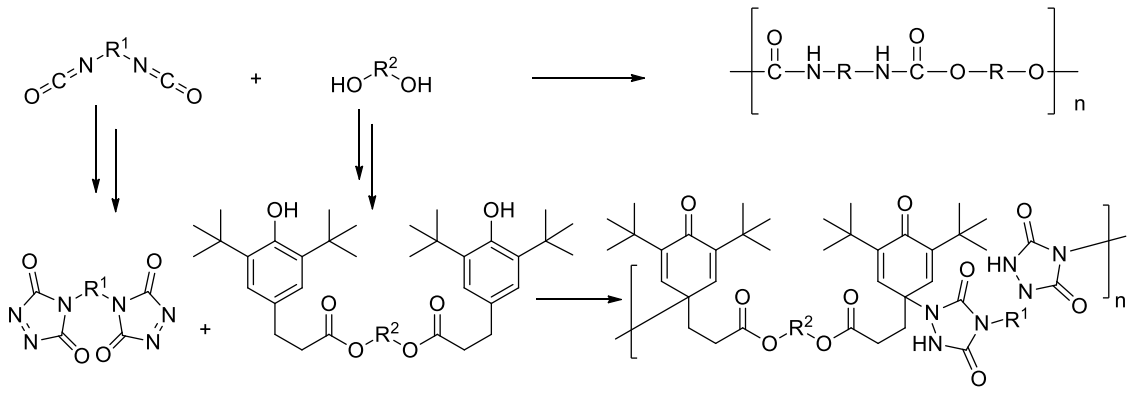

Scheme 37 – Similarity between synthesized polymers and PUs.

Indeed, polyurethane reagents are diisocyanates, like methylene diphenyl diisocyanate (MDI) or isophorene diisocyanate (IPDI), and di- or polyols, like 1,6-hexanediol. From these substrates, it is possible to effectively obtain the reagents for the Alder-ene polymerization: for TADs, diisocyanate are already used in the Cookson procedure, so problems of feeding are not present at all; while the reaction of 3-(3,5-di-*tert*-butyl-4-hydroxyphenyl)propionic acid chloride with suitable diols or polyols is an effective way to synthesize bis- or poly- phenols with the BHT-like structure.[77]

Finally, it was demonstrated the efficiency of adduct **20** to act as thermal-triggered cross-linker in the formation of polymer films starting from natural vegetable oil, showing so the use of TADs as an effective chemical to generate new materials starting from a renewable feedstock.

Bibliography

[1] Devaraj, N. K. *Chem. Rev.* **2021**, *121*, 6697−6698.

[2] Shieh, P.; Hill, M. R.; Zhang, W.; Kristufek, S. L.; Johnson, J. A. *Chem. Rev.* **2021**, *121*, *12*, 7059–7121.

[3] Kolb, H. C.; Finn, M. G.; Sharpless, K. B. *Angew. Chem., Int. Ed.* **2001**, *40*, 2004−2021.

[4] Benson, S. W. *Thermochemical Kinetics, 2nd ed.*, Wiley, New York, **1976**.

[5] Wittcoff, H. A.; Reuben B. G., in *Industrial Organic Chemicals*, Wiley, New York, **1996.**

[6] Seebach, D.; Aebi, J. D.; Gander-Coquoz, M.; Naef, R. *Helv. Chim. Acta* **1987**, *70*, 1194-1216.

[7] Kavadias, G.; Droghini, R. *Can. J. Chem.* **1979**, *57*, 1870-1876.

[8] Suami, T.; Ogawa, S.; Uchino, H.; Funaki, Y. *J. Org. Chem.* **1975**, *40*, 456-461.

[9] a) De Sousa, S. E.; O'Brien, P.; Poumellec, P. *J. Chem. Soc. Perkin Trans. 1* **1998**, 1483-1492; b) Grieco, P. A.; Carroll, W. A. *Tetrahedron Lett.* **1992**, *33*, 4401-4404.

[10] Chuang, T.-H.; Sharpless, K. B. *Org. Lett.* **1999**, *1*, 1435-1437.

[11] a) Tietze, L. F.; Kettschau, G. *Top. Curr. Chem.* **1997**, *189*, 1-120; b) Gothelf, K. V.; Jorgensen, K. A. *Chem. Rev.* **1998**, *98*, 863-909.

[12] Hein, C. D.; Liu, X.-M.; Wang, D. *Pharm. Res.* **2008**, *25* (*10)*, 2216-2220.

[13] Rostovtsev, V. V.; Green, L. G.; Fokin, V. V.; Sharpless., K. B. *Angew. Chem., Int. Ed. Engl.* **2002**, *41*, 2596–2599.

[14] Himo, F.; Lovell, T.; Hilgraf, R.; Rostovtsev, V. V.; Noodleman, L.; Sharpless, K. B.; Fokin V. V. *J. Am. Chem. Soc.*, **2005**, *127*, 210–216.

[15] Bock, V. D.; Hiemstra, H.; Maarseveen. J. H.-V. *Eur. J. Org. Chem*. **2006**, *2006*, 51–68.

[16] Chinchilla, R.; Najera, C. *Chem. Rev.* **2007**, *107*, 874–922.

[17] Wuts, P. G. M. *Greene's Protective Groups in Organic Synthesis*, 5th ed.; John Wiley & Sons: Hoboken, NJ, **2014**.

[18] Jeffrey, P. D.; McCombie, S. W. *J. Org. Chem.* **1982**, *47*, 587−590.

[19] Montenegro, M. I. *Electrochim. Acta* **1986**, *31*, 607−620.

[20] a) Givens, R. S.; Rubina, M.; Wirz, J. *Photochem. Photobiol. Sci.* **2012**, *11*, 472−488;

[21] Kwart, H.; King, K. *Chem. Rev.* **1968**, *68*, 415−447.

[22] Gandini, A. *Prog. Polym.Sci.* **2013**, *38*, 1−29.

[23] Thiele, J.; Stange, O. *Justus Liebigs Ann. Chem.* **1894**, *283*, 1-46.

[24] Diels, O.; Blom, J. H.; Koll, W. *Justus Liebigs Ann. Chem.* **1925**, *443*, 242−262.

[25] Cookson, R. C.; Gilani, S. S. H.; Stevens, I. D. R. *Tetrahedron Lett.* **1962**, *3*, 615−618.

[26] Butler, G. B. *Polym. Sci. U.S.S.R.* **1981**, *23*, 2587−2622.

[27] Zolfigol, M. A.; Bagherzadeh, M.; Mallakpour, S.; Chehardoli, G.; Ghorbani-Choghamarani, A.; Koukabi, N.; Dehghanian, M.; Doroudgar, M. *J. Mol. Catal. A: Chem.* **2007**, *270*, 219−224.

[28] Pounder, R. J.; Stanford, M. J.; Brooks, P.; Richards, S. P.; Dove, A. P. *Chem. Commun.* **2008**, *2008*, 5158−5160.

[29] Bouas-Laurent, H.; Castellan, A.; Desvergne, J. P.; Lapouyade, R. *Chem. Soc. Rev.* **2000**, *29*, 43−55.

[30] Baran, P. S.; Guerrero, C. A.; Corey, E. J. *Org. Lett.* **2003**, *5*, 1999−2001.

[31] Leach, A. G.; Houk, K. N. *Chem. Commun.* **2002**, *2002*, 1243−1255.

[32] Adam, W.; Bottke, N.; Engels, B.; Krebs, O. *J. Am. Chem. Soc.* **2001**, *123*, 5542−5548.

[33] Zinner, G.; Deucker, W. *Arch. Pharm.* **1961**, *294*, 370−372.

[34] Cookson, R. C.; Gupte, S. S.; Stevens, I. D. R.; Watts, C. T. *Org. Synth.* **1971**, *51*, 121−127

[35] Yamada, S.; Shimizu, M. *Patent JP04005287,* **1992**

[36] Read, G.; Richardson, N. R. *J. Chem. Soc., Perkin Trans. 1* **1996**, *1996*, 167−174.

[37] Chandrasekhar, B.; Kumar, G. B.; Mallela, S.; Bhirud, S. B. *Org. Prep. Proced. Int.* **2004**, *36*, 469−472.

[38] a) Wald, K.; Wamhoff, H. *Chem. Ber.* **1978**, *111*, 3519−3523; b) Wagener, K. B.; Matyasjewski, K. A.; Butler, G. B. *J. Polym. Sci.,Polym. Lett. Ed.* **1979**, *17*, 129−137.

[39] Sowerby, R. L. *PatentWO8707892,* **1987**.

[40] De Bruycker, K.; Billiet, S.; Houck, H. A.; Chattopadhyay, S.; Winne, J. M.; Du Prez, F. E. *Chem. Rev.* **2016**, *116*, 3919−3974.

[41] a) Yakhimovich, R. I.; Fursaeva, N. F.; Pashinnik, V. E. *Chem. Nat. Compd.* **1985**, *21*, 98−103; b) Henderson, A. P.; Mutlu, E.; Leclercq, A.; Bleasdale, C.; Clegg, W.; Henderson, R. A.; Golding, B. *T. Chem. Commun.* **2002**, *2002*, 1956−1957.

[42] Chen, X.; Dam, M. A.; Ono, K.; Mal, A.; Shen, H.; Nutt, S. R.; Sheran, K.; Wudl, F. *Science* **2002**, *295*, 1698−1702.

[43] Roy, N.; Lehn, J.-M. *Chem. – Asian J.* **2011**, *6*, 2419−2425.

[44] Cookson, R. C.; Gilani, S. S. H.; Stevens, I. D. R. *J. Chem. Soc. C* **1967**, *1967*, 1905−1909.

[45] a) Kjell, D. P.; Sheridan, *J. Am. Chem. Soc.* **1984**, *106*, 5368−5370; b) Hamrock, S. J.; Sheridan, R. S. *Tetrahedron Lett.* **1988**, *29*, 5509−5512.

[46] Alder, K.; Pascher, F.; Schmitz, A. *Ber. Dtsch. Chem. Ges. B* **1943**, 76, 27−53.

[47] Hayashi, Y.; Shibata, T.; Narasaka, K. *Chem. Lett.* **1990**, *19*, 1693−1696.

[48] Squillacote, M.; Mooney, M.; De Felippis, J. *J. Am. Chem. Soc.* **1990**, *112*, 5364−5365.

[49] Hoffmann, H. M. R. *Angew. Chem., Int. Ed. Engl.* **1969**, *8*, 556−577.

[50] Hall, J. H.; Krishnan, G. *J. Org. Chem.* **1984**, *49*, 2498−2500.

[51] Seymour, C. A.; Greene, F. D. *J. Am. Chem. Soc.* **1980**, *102*, 6384−6385.

[52] Breton, G. W.; Hoke, K. R. *J. Org. Chem.* **2013**, *78*, 4697−4707.

[53] a) Ban, H.; Gavrilyuk, J.; Barbas, C. F. *J. Am. Chem. Soc.* **2010**, *132*, 1523−1525; b) Ban, H.; Nagano, M.; Gavrilyuk, J.; Hakamata, W.; Inokuma, T.; Barbas, C. F. *Bioconjugate Chem.* **2013**, *24*, 520−532; c) Wilson, R. M.; Chantarasiri, N. *J. Am. Chem. Soc.* **1991**, *113*, 2301−2302.

[54] Baran, P. S.; Guerrero, C. A.; Corey, E. J. *Org. Lett.* **2003**, *5*, 1999−2001.

[55] Houck, H. A.; De Bruycker, K.; Billiet, S.; Dhanis, B.; Goossens, H.; Catak, S.; Van Speybroeck, V.; Winne, J. M.; Du Prez, F. E. *Chem. Sci.* **2017**, *8*, 3098.

[56] Breton, G. W. *Tetrahedron Lett.* **2011**, *52*, 733−735.

[57] Pirkle, W. H.; Stickler, J. C. *I. J. Am. Chem. Soc.* **1970**, *92*, 7497−7499.

[58] Lai, Y.-C.; Butler, G. B. *J. Macromol. Sci., Chem.* **1985**, *22*, 1443−1461.

[59] Butler, G. B.; Guilbault, L. J.; Turner, S. R. *J. Polym. Sci., Part B: Polym. Lett.* **1971**, *9*, 115−124.

[60] Mallakpour, S.; Rafiee, Z. *Polymer* **2007**, *48*, 5530−5540.

[61] Wagener, K. B.; Matyasjewski, K. A.; Butler, G. B. *J. Polym. Sci., Polym. Lett. Ed.* **1979**, *17*, 129−137.

[62] Williams, A. G.; Butler, G. B. *J. Polym. Sci., Polym. Lett. Ed.* **1980**, *18*, 313−316.

[63] Williams, A. G.; Butler, G. B. *J. Org. Chem.* **1980**, *45*, 1232−1239.

[64] a) Butler, G. B. Polym. Sci. U.S.S.R. **1981**, *23*, 2587−2622; b) Baumgartner, E. Patent *EP0390028A2*, **1990**; c) Ostermayer, B. *EP0412414A2*, **1990**; d) Blackborow, J. *EP0728766A2*, **1996**.

[65] Leong, K.-W.; Butler, G. B. *J. Macromol. Sci., Chem.* **1980**, *14*, 287−319.

[66] Mallakpour, S.; Rafiemanzelat, F.; Sheikholeslami, B. *Iran. Polym. J.* **1997**, *6*, 235−241.

[67] Mallakpour, S. E.; Butler, G. B. *J. Polym. Sci., Part A: Polym. Chem.* **1989**, *27*, 125−138.

[68] Stock, J.; Stadler, R. *Polym. Bull.* **1989**, *21*, 319−326.

[69] Stadler, R.; de Araujo, M. A.; Kuhrau, M.; Rosch, J. *Makromol. Chem.* **1989**, *190*, 1433−1443.

[70] Cutts, E.; Knight, G. T. *US3966530*, **1974**.

[71] Ban, H.; Gavrilyuk, J.; Barbas, C. F. *J. Am. Chem. Soc.* **2010**, 132, 1523−1525.

[72] Ban, H.; Nagano, M.; Gavrilyuk, J.; Hakamata, W.; Inokuma, T.; Barbas, C. F. *Bioconjugate Chem.* **2013**, *24*, 520−532.

[73] Billiet, S.; De Bruycker, K.; Driessen, F.; Goossens, H.; Van Speybroeck, V.; Winne, J. M.; Du Prez, F. E. *Nat. Chem.* **2014**, *6*, 815−821.

[74] Turunç, O.; Billiet, S.; De Bruycker, K.; Ouardad, S.; Winne, J.; Du Prez, F. E. *Eur. Polym. J.* **2015**, *65*, 286−297.

[75] Roling, O.; De Bruycker, K.; Vonhören, B.; Stricker, L.; Korsgen, M.; Arlinghaus, H. F.; Ravoo, B. J.; Du Prez, F. E. *Angew. Chem., Int. Ed.* **2015**, *54*, 13126−13129.

[76] Dai, S.; Yu, C.; Liang, M.; Cheng, H.; Li, W.; Lai, F.; Maa, L.; Liu, X. *Arabian J. of Chem.* **2023**, *16*, 104932.

[77] Raghunanan, L.; Yue, J.; Narine S. S. *J. Am. Oil Chem. Soc.* **2014**, *91*, 349–356.